A KINETIC AND FLUORESCENCE STUDIES OF THE INTERACTION OF p21^{ras} WITH THE GUANINE NUCLEOTIDES AND THE GTPase ACTIVATING PROTEINS, p120-GAP AND NF1-GAP.

A Thesis Submitted to London University In Partial Fulfilment

of the Requirements for the Degree of Doctor of Philosophy

by

KEITH J.M. MOORE

Division of Physical Biochemistry,
National Institute for Medical Research,
Mill Hill, London, NW7 1AA.

and

Department of Physiology,
University College London,
University Street,
London, WC1E 6JJ

SEPTEMBER 1992

ProQuest LLC.
789 East Eisenhower Parkway
P.O. Box 1346
Ann Arbor, MI 48106 – 1346

TO MY FAMILY

The Road goes ever on and on
Down from the door where it began,
Now far ahead the road has gone,
And I must follow if I can,
Pursuing it with eager feet,
Until it joins some larger way,
Where many paths and errands meet,
And whither then ? I cannot say.

J.R.R Tolkien, "Lord of the Rings" .

INDEX OF CONTENTS

INDEX OF FIGURES and TABLES

ABBREVIATIONS

The abbreviations used are those described in the Journal of Biological Chemistry except the following. Three letter codes for individual amino acids have been used. Forward and reverse rate constants are quoted as k_{+i} and k_{-i} for a step i in a given scheme.

ATB: anti-thrombin-benzamidine agarose

Buffer A: 50 mM TrisHCl, pH 7.5, 50 mM NaCl, 10 mM $MgCl_2$, 10 mM DTT.

Buffer B: 50 mM TrisHCl, pH 7.5, 100 mM NaCl, 10 mM $MgCl_2$, 10 mM DTT.

Buffer C: 20 mM TrisHCl, pH 7.5, 1 mM $MgCL_2$, 0.1 mM DTT.

Buffer D: 10 mM TrisHCl, pH 7.5, 50 mM NaCl, 0.1 mM EDTA, 1 mM PMSF.

Butyl-PBD: 5-(4-biphenyl)-2-(4'-t-butylphentl)-1oxa-3,4-diazole.

C-terminal: carboxy terminus.

CC: cysteine - cysteine

CNBr: cyanogen bromide.

CXC: cysteine -any amino acid - cysteine.

coumarinGDP: 2'(3')-O-[N-(7-dimethylamino-4-methylcoumarin-3-yl)carbamoyl-GDP. Other coumarin derivatives are similarly abbreviated.

DANSYL: dimethylamoninaphthalene sulphonyl.

DMPOPOP: dimethyl-p-Bis-(2-(5-phenyloxazolyl))benzene.

DTT: DL-dithiothreitol.

DEAE: diethylaminoethyl.

E.coli: *Esherichia coli.*

ED-GTP: 2'(3')-O-(N-(2-aminoethyl)carbamoyl-guanosine 5' triphosphate. Other ED- derivatives of guanine nucleotides are similarly abbreviated.

EDTA: ethylenediamine tetraacetic acid.

EF-Tu: bacterial elongation factor Tu.

fluoresceinGDP: the thiourea conjugate between fluorescein isothiocyanate and ED-GDP.

FRET: Non-radiative fluorescence resonance energy transfer (Forsters theory).

GAP: GTPase Activating Protein.

GAP_{365}: residues 683 - 1047 of human p120-GAP.

GAP_{344}: residues 704 - 1047 of human p120-GAP.

GDS: guanine nucleotide dissociation stimulatory protein.

GDI: guanine nucleotide dissociation inhibitory protein.

GSH: glutathione

GST: glutathione transferase.

GppNHp: guanylylimido 5'diphosphate

GTPase: guanosine 5'-triphosphatase.

GNRP: guanine nucleotide release protein.

HMDA: hexamethylenediamine.

HPLC: high performance liquid chromatography.

I: Ionic strength.

IAA: 3ß-indole acrylic acid.

IC_{50}: Concentration of an inhibitor required to reduce the observed effect to 50% of the starting value.

IPTG: ß-isopropylthiogalactoside.

k_{cat}: steady state GTPase rate constant (in s^{-1}).

k_{2a}': maximally activated rate of the conformational change in the ternary complex with a GAP.

K_d: equilibrium dissociation constant.

$K_{1'}$: $[GAP]_{344}$ required to obtain half k_{2a}'.

K_I: competitive inhibitor equilibrium dissociation constant.

k_{obs}: observed rate constant.

M: modulation, the effective amplitude of the emitted sine function.

mantGDP: 2'(3')-[O-[N-methylanthraniloyl]-guanosine 5' diphosphate.
Mant-derivatives of other guanine nucleotides are similarly abbreviated.

MESG: methylthioguanosine (2-amino-6-mercapto-7-methyl-purine ribonucleoside.

4-MeU: 4-methylumbelliferone.

MTPBS buffer: 16 mM NaH_2PO_4, 4 mM NaH_2PO_4, 150 mM NaCl, pH 7.3.

NATA: N-acetyltryptophanamide.

NBS: N-bromosuccinimide.

neurofibromin: protein product of the neurofibromatosis type 1 (NF1) gene.

NF1-GRD: p120-GAP related domain of neurofibromin (termed "NF1" in this thesis).

NF1-GST: fusion protein between NF1-GRD and glutathione transferase.

ϕ: absolute phase delay of the fluorescence (lifetime analysis).

$\delta\phi$: phase difference between parallel and perpendicular components (correlation time analysis).

p120-GAP: residues 1 - 1047 of human GAP.

PIP_2: phosphatidyl inositol 4,5, bisphosphate.

PL-C: phospholipase C.

PK-C: protein kinase C.

PNPase: bacterial purine nucleoside phosphorylase.

r_o: limiting anisotropy (when the orientation of the excited state dipoles are preserved during the lifetime of the excited state).

r_{obs}: observed anisotropy.

SAX: strong anion exchange.

τ_L: fluorescence lifetime.

τ_c: rotational correlation time (subscripts 1 and 2 refer to multiple decay models).

TEAB: triethylammonium bicarbonate.

TEMED: N, N, N', N' tetramethylethylene diamine.

tRNA: transfer RNA.

$v_{initial}$: initial rate of an enzyme catalysed reaction at a given [~~enzyme~~ substrate] (in moles s^{-1})

V_{max}: maximal initial rate of an enzyme catalysed reaction (at saturating [~~enzyme~~ substrate]) in moles s^{-1}.

Y: ratio of the modulation of the AC values for parallel and perpendicular components (correlation time analysis).

X^2: reduced chi-squared of the fit.

ABSTRACT

The protein products of the *ras* proto-oncogenes, $p21^{ras}$, are 21 KDa guanine nucleotide binding proteins which possess a slow intrinsic GTPase activity. These proteins are thought to be involved in the regulation of cell growth and differentiation, and some single point mutations in the *ras* genes lead to cell transformation. The biological signal mediated by $p21^{ras}$ is determined by the *in vivo* concentration of the $p21^{ras}$.GTP complex since only when bound to GTP are these proteins thought to be biologically active. Nucleotide exchange of bound GDP for cytoplasmic GTP leads to the reformation of the $p21^{ras}$.GTP complex. Two proteins (GAPs) have been identified which accelerate the rate of GTP hydrolysis by wild type $p21^{ras}$ but not by oncogenic $p21^{ras}$ mutants.

The kinetic mechanism of the $p21^{ras}$.GTPase in the presence of the catalytic-domains of two GAPs, p120-GAP and neurofibromin, has been investigated. The studies are based primarily on the use of a fluorescent GTP analogue, 2'(3')-O-(N-methylanthraniloyl)-GTP (mantGTP), which shows changes in fluorescence intensity during several elementary steps in the GTPase mechanism.

The experimental results are compatible with a mechanism where the intrinsic hydrolysis of GTP by $p21^{ras}$ is preceded, and controlled, by a protein conformational change in the $p21^{ras}$.GTP complex. p120-GAP accelerates the overall rate of GTP cleavage by promoting this rate limiting conformational change.

The binding of p120-GAP to $p21^{ras}$.GTP is a rapidly reversible reaction (equilibrium dissociation constant, K_d = 20 μM at $I \approx$ 20 mM). p120-GAP accelerates the rate of the subsequent conformational change in $p21^{ras}$.GTP by a factor of 10^5 compared to the rate of the equivalent reaction in the absence of p120-GAP. A similar extent of activation was observed with neurofibromin although the affinity for $p21^{N\text{-}ras}$.GTP was 20-fold higher than that of p120-GAP. In contrast to p120-GAP, the binding reaction with neurofibromin may not be rapidly reversible. For both proteins, increasing ionic strength lead to a marked increase in the K_d ; the rate constant of the conformational change being essentially unaltered.

The binding of p120-GAP and neurofibromin to the $p21^{ras}$.mantGTP complex is associated with an increase in fluorescence intensity, anisotropy and energy transfer (from tryptophan residues in the GAP proteins). These fluorescence signals can be used to determine the equilibrium dissociation constants for the binding of GAP proteins to $p21^{ras}$.

The intrinsic GTPase activity of the Gly 12 → Pro mutant of $p21^{ras}$ is only weakly accelerated by either p120-GAP or neurofibromin although both GAPs bind with an affinity similar to that with the wild type $p21^{ras}$ protein. An explanation for the weakly transforming phenotype of this mutant compared to other Gly 12 mutants is offered. One consequence of this interpretation is that the *in vivo* rate of GAP-activated GTP hydrolysis and nucleotide exchange may be slower than generally assumed.

Finally, the hydrodynamic properties of $p21^{ras}$ proteins have been investigated using time resolved fluorescence techniques combined with a range of fluorescent guanine nucleotide analogues. In all cases, the rotational correlation time of $p21^{ras}$ is consistent with a dimeric structure for these proteins in solution.

CHAPTER ONE :

GENERAL INTRODUCTION

"If ever there was a structure in search of a function, it is *ras* p21."

(Grand and Owen, 1991).

1.1 The ras Proto-Oncogene

1.1.1 *The ras Gene Family.*

The mammalian ras gene family was initially discovered when two of its members were the found to be the transforming principles of the acutely transforming Harvey and Kirsten strains of rat sarcoma retroviruses viruses (Harvey, 1964 ; Kirsten and Mayer, 1967). These genes were given the acronym "*ras*" from rat sarcoma virus, and subsequently discovered to be the transduced cellular genes (proto-oncogenes) H-ras-1 and K-ras-2 (DeFeo et al ; 1981, Ellis et al., 1981). Approximately 30 % of human malignancies contain an activated ras oncogene, which is capable of transformation in NIH 3T3 cells (e.g Der et al., 1982 ; Hall et al., 1983 ; Marshall, 1986 ; Barbacid, 1987 ; Vousden et al., 1986 ; Bos et al., 1987 ; Bos, 1988, 1989).

The mammalian ras proto-oncogene family is known to consist of at least 3 genes (reviewed in detail by Barbacid, 1987). The two genes initially identified from the rat sarcoma viruses are termed H-ras-1 and K-ras-2 and are usually abbreviated to H-ras and K-ras respectively. The third mammalian ras gene, N-ras, has no viral equivalent and was first identified in a human neuroblastoma cell line (Hall et al., 1983 ; Hall and Brown, 1985). Two inactive pseudogenes, termed H-ras-2 and K-ras-1 have also been characterised (Hall, 1984). The chromosomal location of all five genes has been determined (O'Brien et al., 1983).

The three functional ras genes encode closely related protein products with a molecular weight of 21,000 and hence have been termed $p21^{ras}$ or p21 (Shih et al., 1979). These protein products are all 188-189 amino acids in length and are derived from 4 exons (Barbacid, 1987). Although there are two alternative splicing products of the K-ras-2 gene transcript (using either exon 4A or 4B), in mammalian cells, only exon 4B is used. Despite the similarity between the final protein products of the three genes, the introns between coding regions vary enormously in size.

1.1.2 *Primary Sequence Domain Structure of ras Proteins.*

The primary structures of the H-ras, K-ras, and N-ras gene products are very similar within species (for example, human N-, K-, and H-ras proteins have more than 80% of their amino acid sequence in common) with the N-terminal halves of these proteins (residues 1-85) being identical (detailed amino acid sequence data are given by Barbacid, 1987). The amino acid residues 86 - 166 comprise a second primary structure domain with 85% identity between any pair of human ras proteins. The three mammalian ras genes are *least* similar in the C-terminal region of the protein, from residues 167 - 185. This hypervariable region may be involved in defining the selective interaction between a given $p21^{ras}$ gene product and one or more cellular components specific for that ras protein. However, unequivocal supportive evidence for this hypothesis is not yet available. The C-terminal four residues comprising the so-called "CAAX box" (see section 1.3) are conserved in all ras proteins, and are involved in post-translational modification and membrane localisation.

The ras genes have been found in a large number of species and are highly conserved throughout evolution (Barbacid, 1987). A comparison of the primary sequence of these proteins with the mammalian counterparts indicate that three domains in particular are highly conserved (Marshall, 1986, section 1.4). Strikingly, mammalian ras genes can complement non-viable $RAS1^-$ $RAS2^-$ yeast mutants whilst mammalian cells can be transformed by mutant yeast RAS genes (DeFeo-Jones et al., 1985). As well as the *bona fide* ras genes, a large number of ras-related proteins have been identified (reviewed by Hall, 1990a, section 1.8). Briefly, it is convenient to divide these polypeptides into three groups based on their

similarity to mammalian H-ras ; (1) the ras family - greater than 50% similarity, (2) the rho family - with about 30% similarity, and (3) the rab family - also with about 30% similarity to H-ras. All of these proteins probably exhibit common structural and biochemical features which are likely to be involved in guanine nucleotide binding and hydrolysis. The key role of these ligands in regulating $p21^{ras}$ activity is discussed below.

1.2 Biochemical Properties of $p21^{ras}$ Proteins.

Early biochemical studies of $p21^{ras}$ proteins indicated that they were able to bind the guanine nucleotides GDP and GTP with high affinity (e.g Scolnick et al., 1979) and possessed a slow intrinsic GTPase activity (e.g Gibbs et al., 1984). These properties, along with the ability to exchange bound GDP for cytoplasmic GTP, are thought to be vital to the regulatory functions of these proteins (for reviews see Barbacid., 1987, Bollag and McCormick., 1992, Grand and Owen., 1991, Santos and Nebrada., 1989 ; McCormick, 1992). Based on these three biochemical properties, the ras proteins have been included within the large and diverse family of GTPases, whose functional and structural properties have recently been reviewed (Bourne et al., 1990, 1991 ; Hall, 1990a, 1992b ; Downward, 1990, 1992).

The essential feature of all these proteins, including $p21^{ras}$, is their ability to cycle or "switch" between GDP- and GTP-bound forms. The basic cycle of GTP binding and hydrolysis has been harnessed by several GTPase proteins to direct a diverse range of cellular functions (Bourne et al., 1990, 1991). A third conformation, that of the nucleotide-free state, may serve as a transient intermediate during the replacement of GDP by GTP in the guanine nucleotide binding site of the GTPase. Alternatively, the nucleotide - free state of $p21^{ras}$ may exist only when bound to accessory proteins (guanine nucleotide release proteins, GNRPs, see section 1.7.3). Such a model has been proposed for another GTP-binding protein, bacterial elongation factor Tu (EF-Tu), which forms a complex with elongation factor Ts (EF-Ts) to form a Tu.Ts complex in the nucleotide - free state of EF-Tu (Eccleston, 1984). Whether this situation is also applicable to $p21^{ras}$ is unknown, although Mistou et al., (1992) have proposed such a mechanism despite little evidence. The GTP hydrolysis reaction catalysed by $p21^{ras}$ proteins is essentially irreversible and therefore makes the GTPase cycle unidirectional.

The switching functions of each individual GTPase is determined by the differing abilities of its conformational states to interact with different macromolecules. For example, we describe the GTP-bound and GDP-bound forms of transmembrane signalling G-proteins as "active" and "inactive" respectively because the former activates effector enzymes, such as adenylyl cyclase, whereas the latter does not. Similarly, the GTP-bound form of elongation factor Tu can bind aminoacyl tRNA whereas the GDP-bound form cannot. It is important at this stage to be aware of the possible confusion that may arise when the terms "active" and "inactive" are used. One must distinguish between the GTPase protein being "active" in terms of a biological and cellular function (as used above) and "catalytically active" in the GTP-bound form with respect to the mechanism of GTP hydrolysis at the enzymological level.

For most GTPases, the fraction of protein molecules in the "biologically active" conformation - that is with GTP-bound - depends on the relative rates of two reactions: (a) the dissociation of GDP from the active site of the protein.GDP complex and (b) the hydrolysis of bound GTP. The detailed kinetics of the interaction of guanine nucleotides with GTPases, and specifically the $p21^{ras}$ proteins, will be discussed in section 1.6. Briefly, however, the relative proportion of protein in the active GTP-bound state can be increased either by accelerating the rate of GDP dissociation or by reducing the rate of GTP hydrolysis (or both). For many GTPase proteins, specific protein ligands regulate these two rate constants. Those that modulate the GDP dissociation rate are called guanine nucleotide exchange proteins or release proteins (GNRPs, section 1.7.3). These proteins are further subdivided depending on whether they possess stimulatory (GDS) or inhibitory (GDI) effects on the nucleotide exchange rate. The second major group of regulatory proteins are the GTPase activating proteins (GAPs) accelerate the rate of GTP hydrolysis (see section 1.7.1).

1.3 Post-translational Modifications and Subcellular Localisation of $p21^{ras}$.

$p21^{ras}$ expressed in eukaryotic cells undergoes a number of post-translational modifications to ensure the membrane localisation of $p21^{ras}$. These reactions can be divided into 2 sets (Figure 1.1). In the first set, three irreversible modifications occur that are triggered by the presence of a COOH-terminal CAAX sequence (where C = cysteine, A = any aliphatic amino

Figure 1.1 : Post-translational Modifications of $p21^{H\text{-}ras}$.

The post-translational modifications that occur to $p21^{H\text{-}ras}$ are shown. These reactions are divided arbitrarily into two sets as discussed in the text. The amino acid sequences of the C=-terminal nine amino acids and the enzymes responsible for catalysing these reactions are shown.

(Modified from Grand and Owen, 1991).

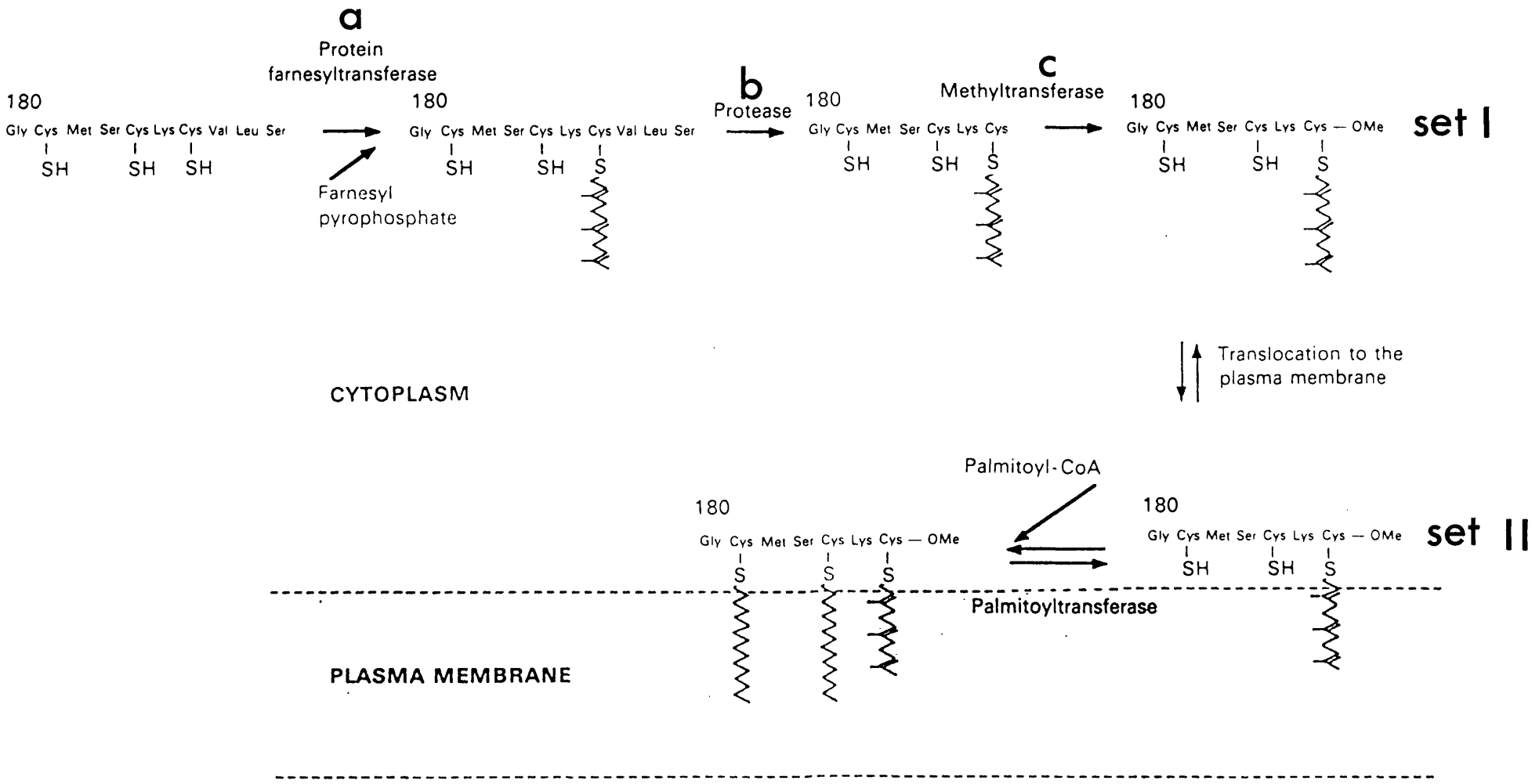
a
Protein
farnesyltransferase
180
Gly Cys Met Ser Cys Lys Cys Val Leu Ser
SH SH SH
Farnesyl
pyrophosphate
180
Gly Cys Met Ser Cys Lys Cys Val Leu Ser
SH SH S
b
Protease
180
Gly Cys Met Ser Cys Lys Cys
SH SH S
c
Methyltransferase
180
Gly Cys Met Ser Cys Lys Cys — OMe
SH SH S
set I
Translocation to the
plasma membrane
CYTOPLASM
Palmitoyl-CoA
180
Gly Cys Met Ser Cys Lys Cys — OMe
S S S
180
Gly Cys Met Ser Cys Lys Cys — OMe
SH SH S
set II
Palmitoyltransferase
PLASMA MEMBRANE

acid, but usually Ser, Met or Ala, and X = any amino acid). (a) Farnesylation of Cys 186 by a cytoplasmic protein farnesyltransferase using farnesyl pyrophosphate as a cosubstrate (Hancock et al., 1989 ; Reiss et al., 1990 ; Manne et al. 1990). (b) Cleavage of the C-terminal three amino acids (AAX) by a membrane localised protease (Hrycyna and Clarke, 1990 ; Gutierrez et al., 1989) and (c) carboxylmethylation of the alpha-carboxyl group of the C-terminal cysteine by a methyltransferase bound to the plasma membrane (Schafer et al., 1989 ; Clarke et al., 1988 ; Gutierrez et al., 1989). In the second set of reactions, either or both of the cysteine residues close to the C-terminus (residues 181 and 184 in H-ras) are palmitoylated by an acyltransferase. Such reactions do not occur for the K-ras-B protein since these Cys residues are absent from the C-terminus. Palmitoylation of ras proteins is a very dynamic event, with a very high rate of lipid turnover *in vivo* (half life of protein-bound palmitate $\approx$ 20 min, Magee et al., 1987).

Within a eukaryotic cell, a large proportion of the ras proteins are associated with the inner surface of the plasma membrane (Willingham et al., 1980). The first set of reactions are not sufficient to ensure *bona fide* membrane localisation of H-ras and N-ras gene products (Hancock et al., 1989, 1990), although they do appear to create a C-terminus on p21 which is hydrophobic enough to interact weakly with the plasma membrane. For the K-ras-B protein, "set one" processing is essential and sufficient for tight association with the cell membrane (Hancock et al., 1989, 1990). The explanation for this observation has been attributed to the presence of an extremely basic region just upstream of the C-terminus in K-ras-B (Barbacid, 1987 ; Casey et al., 1989 ; Jackson et al., 1990).

The site directed mutagenesis work of Willumsen et al (1984) demonstrated that mutation of Cys 186 → Ser negated the transforming ability of activated mutants of $p21^{ras}$. It has become clear that it is membrane localisation (by whatever mechanism) that is required for transformation rather than the post-translational modifications of the CAAX sequence, triggered by Cys 186 (Buss et al., 1988). Thus, the palmitoylation sites and the polybasic domain potentiate the transforming ability of mutant proteins by increasing the fraction of $p21^{ras}$ associated with the cell membranes. However, proteins in which Cys 186 has been mutated are completely inactive. Thus, the post-translational modifications of the CAAX motif are

essential for transforming activity, but the second signals (which combine with them for targeting to the plasma membrane with high affinity) are not (Hancock et al., 1990).

1.4 Structural Studies of $p21^{ras}$ Proteins

1.4.1 *X-ray Crystallographic Studies of Wild Type and Mutant $p21^{ras}$ Proteins.*

(a) Secondary Structure and the Guanine Nucleotide Binding Site.

From the work of two laboratories, the overall backbone structure of p21 has been described (de Vos et al., 1988 ; Tong et al., 1989a, 1991 ; Pai et al., 1989, 1990 ; Milburn et al., 1990 ; Krengel et al., 1990 ; Schlichting et al., 1989, 1990a,b ; Figure 1.2.a). There is general agreement that the protein as crystallised comprises 5 alpha-helices, 1 six-stranded beta-sheet and 10 interconnecting loops although there are some discrepancies in the precise dimensions of the different sheet, loop and helix regions described by the two groups (Pai et al., 1990., c.f Tong et al., 1991).

Two areas of the protein, comprising residues 116 - 119 and 145 - 147 are highly conserved in all ras molecules and are involved in the binding of the purine base of the guanine nucleotide (Figure 1.2.b). Asn 116 makes hydrogen bonds with three elements of the nucleotide binding site. Hydrophobic interactions also take place between the guanine ring and the phenyl group of Phe 28 and with the alkyl group of Lys 117. These amino acids form a "deep narrow groove" into which the guanine base binds with great specificity (Tong et al., 1991).

There are a large number of interactions formed between the gamma and/or beta phosphate groups of GDP or GTP and $p21^{ras}$ (Figure 1.2.b). These interactions, in addition to those with the guanine base, probably account for the increase in stability of nucleotide-bound $p21^{ras}$ compared to the apo-protein (Feuerstein et al., 1987 ; John et al., 1990). The paucity of hydrogen bonds to the alpha-phosphate compared to the beta and gamma groups explains why the affinity of $p21^{ras}$ for GMP is approximately six orders of magnitude less than that for GDP (John et al., 1990). The beta-phosphate group is hydrogen bonded to the main chain

Figure 1.2: X-ray Crystallographic Structure of Truncated (residues 1 - 166) $p21^{H\text{-}ras}$.

Panel A: Ribbon diagram showing the major secondary structure components. The 10 interconnecting loops are numbered L1 → L10 and the residues containing within each loop are shown in brackets. Loop 1 is the phosphate binding (P) loop containing Gly12 and Gly 13 ; loop 2 is the "effector loop", which is a site of interaction of $p21^{ras}$ with GAP, contains residues Thr 35 and Ile 36 ; loop 4 contains residues proposed to be involved in the mechanism of GTP hydrolysis (see Figure 1.3.b) and it the site of the Gln 61 → Leu mutation.

(Taken from Wittinghofer and Pai, 1991).

Panel B: Schematic diagram of the interaction of the GTP analogue, GppNHp, with residues at the active site of $p21^{H\text{-}ras}$. Broken lines indicate hydrogen bonds (< 3.4 A). The Mg^{2+} ion is indicated. mc : main chain ; side chains are shown. With respect to chapter 8, note especially Phe 28 and Thr 35 which interact with the guanine base and the Mg^{2+} ion respectively. Note also that whilst the 2' hydroxyl of the ribose moiety interacts with the main chain of Val 29, no interactions occur between the 3' hydroxyl and $p21^{ras}$.

(Taken from Wittinghofer and Pai, 1991).

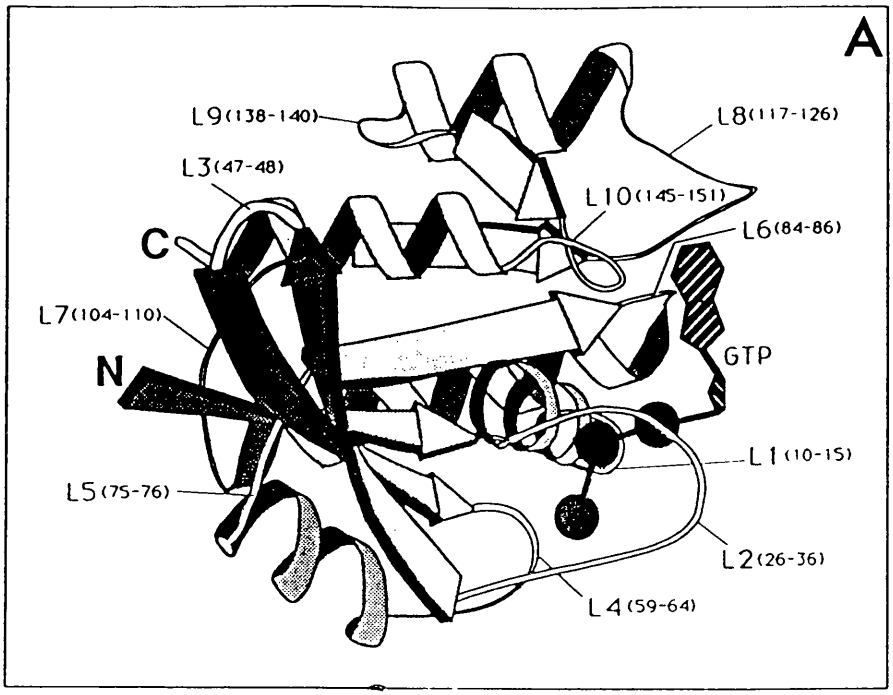
A
L9(138-140)
L8(117-126)
L3(47-48)
L10(145-151)
C
L6(84-86)
L7(104-110)
GTP
N
L1(10-15)
L5(75-76)
L2(26-36)
L4(59-64)

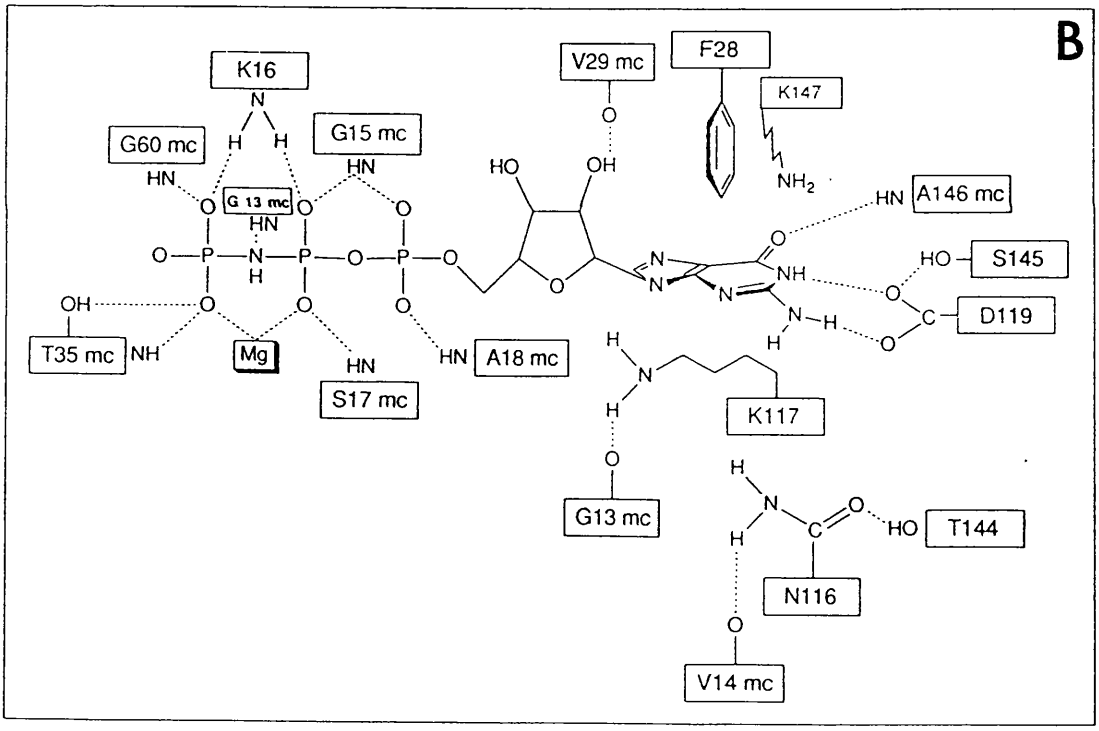
B
K16
V29 mc
F28
K147
G60 mc
G15 mc
G 13 mc
A146 mc
S145
D119
T35 mc
Mg
S17 mc
A18 mc
K117
G13 mc
T144
N116
V14 mc

amino groups of residues 13 - 17, all of which point towards the phosphate group creating a polarised local electrostatic field (Pai et al., 1990). The gamma-phosphate is also extensively hydrogen bonded to Thr 35, Tyr 32, and Gly 60.

(b) The Mg^{2+} Ion Binding Site.

A single Mg^{2+} ion is known to be bound at the active site of $p21^{ras}$, with six ligands arranged in an octahedral co-ordination, although there is some discrepancy between the reports of the precise nature of the Mg^{2+} binding site. In the GTP-bound form, the Mg^{2+} ion is co-ordinated by 2 oxygen atoms (from the beta and gamma phosphates), 2 hydroxyl groups (from Ser 17 and Thr 35), and 2 water molecules (Pai et al., 1989, 1990 ; Milburn et al., 1990 ; Tong et al., 1991). Originally, it was proposed that in the GDP-bound form the interaction with the gamma-phosphate oxygen is lost and is replaced by a direct co-ordination between the Mg^{2+} ion and the carboxyl side chain of Asp 57. The interaction with Thr 35 is also lost in the GDP-bound form and is replaced by a water molecule (Schlichting et al., 1990).

An alternative structure for the Mg^{2+} binding site of the GDP-bound form has been proposed by Milburn et al., (1990) and Tong et al., (1991). In this model, the six interactions derive from the beta-phosphate (1), Ser 17 (1) and 4 water molecules (the direct interaction with Asp 57 is replaced by an additional water molecule). Indeed, data from electron spin resonance investigations of the $p21^{ras}.Mn^{2+}$.GDP complex support this assignment (Smithers et al., 1990 ; Latwesen et al., 1992). A recent article (Pai and Wittinghofer, 1991) from which Figure 1.3.a is taken, shows such a co-ordination. For the GTP-bound form, there is agreement between the two models.

(c) Structural Differences Between $p21^{ras}$.GTP and $p21^{ras}$.GDP.

Mutational and deletion analyses of $p21^{ras}$ have been performed to identify residues in $p21^{ras}$ that are required for the interaction of $p21^{ras}$ with GTPase activating proteins (GAPs, e.g Schaber et al., 1989, see also section 1.7.1). These studies have identified a sequence comprising residues 32 - 40, termed the effector region or switch 1 region, which may repre-

Figure 1.3 : Changes in Mg^{2+} Co-ordination During the Hydrolysis of GTP by $p21^{ras}$ and A Possible Chemical Mechanism.

Panel A: Schematic diagram of the changes in Mg^{2+} co-ordination that are proposed to occur upon GTP hydrolysis. In the GTP bound state, the side chains of both Ser 17 and Thr 35 interact with the Mg^{2+} ion, whilst in the GDP bound form, the interactions with Thr 35 and the oxygen of the terminal phosphate are lost. Despite original suggestions that Asp 57 replaced the gamma-phosphate in the co-ordination sphere (Schlichting et al., 1990b), more recent results suggest the structure shown in the Figure. The loss of the interaction with Thr 35 is proposed to trigger the conformational changes in loop 2, the effector loop.

(From Wittinghofer and Pai, 1991).

Panel B: (a) Representation of the proposed catalytically active conformation of residues in loop 4 (Pai et al., 1990 ; Krengel et al., 1990). (b) Formal representation of a possible reaction mechanism.

(From Goody et al., 1992).

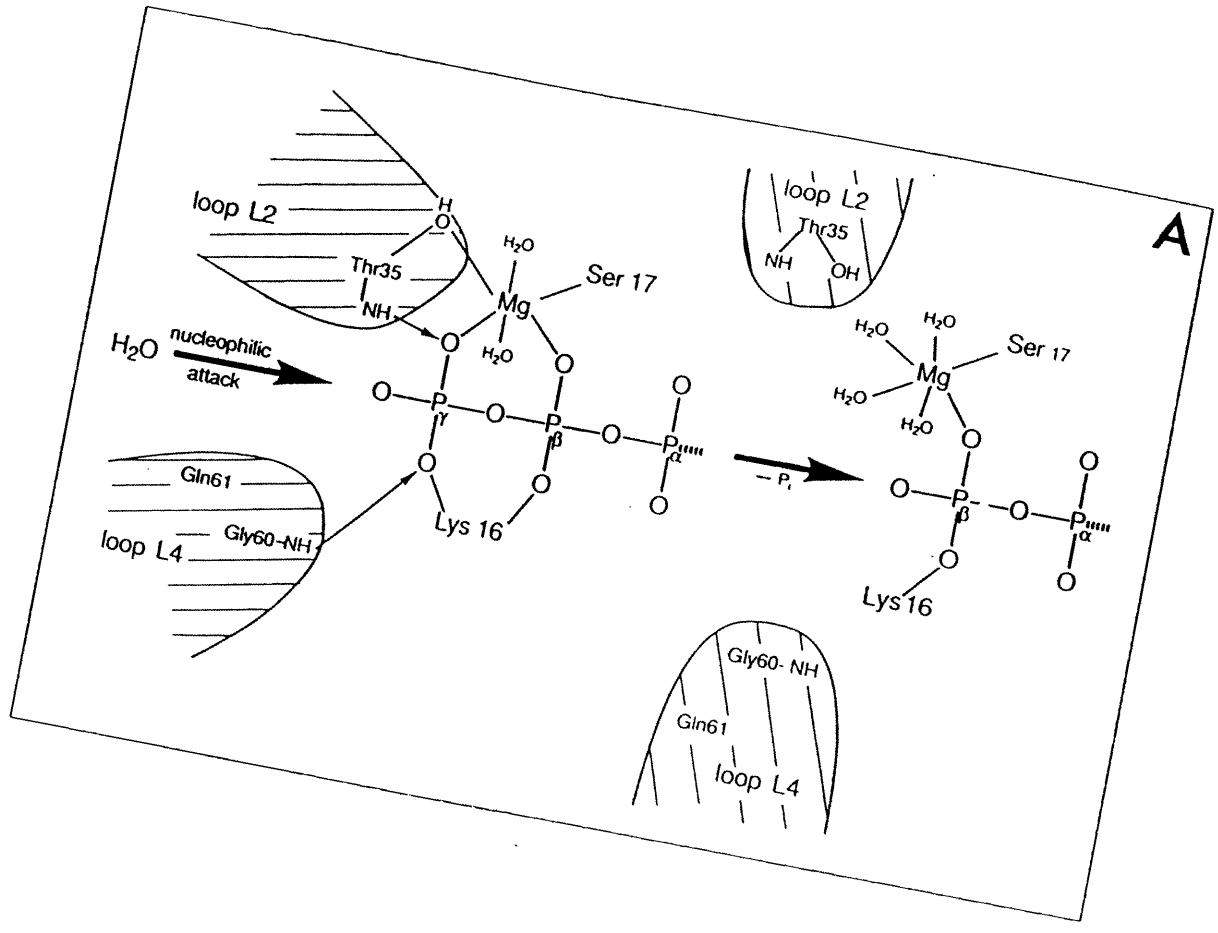
A
loop L2
Thr35
NH
H
O
H2O
Mg
Ser 17
H2O
nucleophilic
attack
Gln61
loop L4
Gly60-NH
Lys 16
loop L2
Thr35
NH
OH
H2O
H2O
Ser 17
Mg
H2O
H2O
− Pi
Lys 16
Gly60- NH
Gln61
loop L4

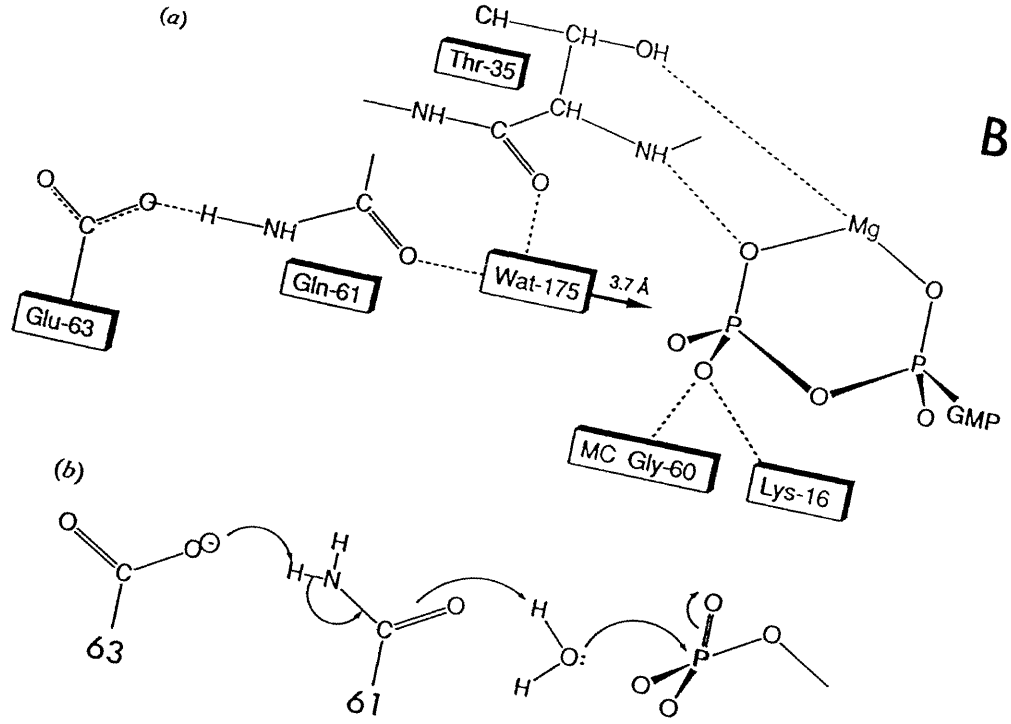
(a)
B
Thr-35
Glu-63
Gln-61
Wat-175
3.7 Å
MC Gly-60
Lys-16
GMP
(b)
63
61

sent part of the binding site for GAP. This area, which mainly comprises loop 2, is exposed on the surface of $p21^{ras}$ and is therefore available for the binding of the large GAP polypeptide (de Vos et al., 1988). A comparison of the GTP- and GDP-bound forms of $p21^{ras}$ indicate that differences between the two proteins are most marked in this area (Schlichting et al., 1990a ; Milburn et al., 1990). The implication from these observations is that GAP binding to $p21^{ras}$ will be determined by the conformation of this area of the protein and therefore on the nucleotide status of $p21^{ras}$. Differences in the structures of the GDP- and GTP-bound forms of $p21^{ras}$, other than in the effector region, have also been observed. The change in Mg^{2+} ion co-ordination has been described in (b) above whilst the loop 4 region (residues 60 - 65, Milburn et al., 1990) has a well defined structure in the presence of GDP but not GTP.

Based on the refined crystal structure of p21 bound to the non-hydrolysable GTP analogue, GMP.PNP, a mechanism for the hydrolysis of GTP has been proposed (Pai et al., 1990 ; Krengel et al., 1990, Figure 1.3.b). It has been suggested that a water molecule (Wat 175) is activated for a nucleophilic reaction with the gamma-phosphate by the carbonyl group of the side chain of Gln 61. Furthermore, the proximity of the carboxylate group of Glu 63 to the amido group of Gln 61 will favour nucleophilic attack by orientating Gln 61 correctly and increasing proton withdrawal (Pai et al., 1990). An increase in the hydrophilicity of the gamma-phosphate and the acidity of the leaving group is achieved by the interactions of the beta- and gamma-phosphates with the Mg^{2+} ion and with Lys 16. All of these effects have been proposed to promote the hydrolysis of bound GTP.

1.4.2 *Quaternary Structure of $p21^{ras}$ Proteins.*

In contrast to the detailed tertiary structural information outlined above, the quaternary structure of $p21^{ras}$ proteins has been little studied and is often assumed to be monomeric. However, a few experiments have addressed the issue. Santos et al., (1988) have used radiation inactivation to study the oligomeric structure of $p21^{ras}$ both *in vivo*, and with bacterially expressed and purified protein, *in vitro*. In both cases, the results gave a target size consistent with the protein being a dimer or higher oligomer. Addition of high concentrations of dithiothreitol (DTT) in the solution of purified protein gave identical results, thus excluding the

possibility of disulphide bond formation being the cause of the dimer formation.

John et al., (1989) also found evidence that $p21^{ras}$ could aggregate. Gel filtration of the full length $p21^{ras}$ protein gave an apparent molecular mass of 25 kDa although the truncated protein (residues 1 - 166) gave a molecular mass of 18.5 kDa - the expected value from its amino acid composition. These data suggested that the C-terminal tail of full length $p21^{ras}$ (which is absent from the protein used for X-ray crystallography) is involved in the oligomerisation process. Takai and co-workers (Takai et al., 1992) have used gel filtration and sucrose gradient ultracentrifugation to study the oligomerisation of the $p21^{ras}$ related proteins smg25A, rab3, rap1B, and rhoB. In all cases, the data were consistent with oligomeric structures for these proteins, but on forming complexes with accessory proteins (guanine nucleotide exchange factors), they bound as monomeric proteins with a 1:1 stoichiometry.

We have made time resolved fluorescence measurements to determine the rotational correlation time of complexes of $p21^{ras}$ with a range of fluorescent guanine nucleotide analogues (chapter 9). In all the complexes studied, the rotational correlation times measured are more compatible with those expected of a dimeric structure of $p21^{ras}$.

1.5 Biochemical Effects of Ras Mutations

Ras genes with point mutations are found in approximately 30% of human tumours and are therefore the most common oncogenes associated with human carcinogenesis (Barbacid, 1987 ; Bos, 1988, 1989). Analysis of $p21^{ras}$ mutants isolated *in vivo* have identified mutations at residues 12, 13 and 61, with residue 59 implicated from studies with viral ras oncogenes). However, use of *in vitro* mutagenesis approaches has revealed many other sites where mutations give rise to a transforming phenotype. In light of the X-ray crystallographic information, it has become possible to propose explanations for the transforming phenotype of many mutants in molecular terms.

1.5.1 *Mutations leading to altered nucleotide binding properties.*

Mutants that have a decreased affinity for nucleotides are frequently found as transforming mutants. These proteins exchange GDP faster than wild type proteins and consequently have a higher proportion of GTP bound at the active site. Such mutations are found within those residues involved in nucleotide binding (Asp 116, Lys 117, Thr 144 and Asp 119) leading to a 10 - 5000-fold increase in nucleotide exchange rates (Der et al., 1986 ; Feig et al., 1986 ; Sigal et al., 1986 ; Walter et al., 1986 ; Clanton et al., 1986). However, mutations which completely abolish nucleotide binding (such as some Gly 13 mutants) have no transforming activity (Clanton et al., 1986).

The substitution of Lys 16 → Asn leads to a reduction in nucleotide affinity, but not specificity (Sigal et al., 1986). However, mutation of Lys 16 also has other implications. For example, it also increases the hydrophilicity of the gamma-phosphate of GTP and the acidity of the leaving group during hydrolysis (Pai et al., 1990). Furthermore, by hydrogen bonding with residues 10 and 11, Lys 16 also stabilises the secondary structure of the protein. Substitution of Lys 16 by other residues can also have steric effects on Ser 17, which is itself involved in the binding of the beta- and gamma-phosphates. The effect of a mutation at one residue affecting the conformation of other residues in the protein applies equally well to other point mutations. The other residue critical for nucleotide binding is Phe 28, which binds the base through aromatic : aromatic interactions. Phe 28 is itself held in place by a similar interaction with Lys 147. Mutations at either of these sites (for example, Phe 28 → Leu, Reinstein et al., 1991) increases the rate of nucleotide exchange dramatically and leads to a transforming phenotype.

1.5.2 *Mutations leading to altered GTPase activity.*

Many groups have reported a decrease in the rate of GTP hydrolysis associated with oncogenic variants of $p21^{ras}$ (for example, McGrath et al., 1984 ; Temeles et al., 1985 ; Manne et al., 1985 ; Trahey et al., 1987). Such mutations are usually found at positions 12 and 61 (Seeburg et al., 1984 ; Fasano et al., 1984 ; Bizub et al., 1988). The molecular model for GTP

hydrolysis by $p21^{ras}$ outlined above (section 1.4, Pai et al., 1990 ; Krengel et al., 1990) has been used to provide possible explanations for the altered phenotype of these mutants. However, it should be noted that a more recent structural report (Prive et al., 1992) has questioned the validity of some of the earlier interpretations made by Krengel et al., (1990). Oncogenic substitutions of Leu and His at position 61 cannot activate WAT 175 due to side chain differences (Krengel et al., 1990) - specifically the Leu side chain is chemically unable to polarise the water molecule and the His side chain occupies the position of WAT 175 itself. Interestingly, elongation factor Tu (EF-Tu) has a His at the equivalent of position 61 in $p21^{ras}$ whilst the ras related rap proteins have a Thr at codon 61. Both of these proteins have a lower GTP cleavage rate than $p21^{ras}$. Interestingly, mutation of Thr 61 to Gln in rap increases the GTP cleavage rate to the level of $p21^{ras}$ (Frech et al., 1990). Mutational analysis of various substitutions at position 61 has been undertaken (Der et al., 1986) and 17 mutations giving rise to a decreased GTPase activity have been described. Glu 61 is not an activating mutation, presumably because this residue can supply the necessary groups for polarisation of WAT 175 (Milburn et al., 1990).

Other commonly found activating mutations are at position 12. The crystal structures have been obtained for both the Arg 12 and Val 12 mutants. The side chain of Arg 12 has the same effect as that of His 61 - to displace WAT 175 from the binding site. The hydrophobic side chain of Val 12 pushes Gln 61 and WAT 175 too far apart for them to interact. In contrast, Pro 12, which is only weakly activating and does not have a reduced GTP cleavage rate, causes no distortion of the protein at this position (Wittinghofer and Pai, 1991). Codon 13 mutants (except for Pro 13) are also transforming (Bos et al., 1985) because such mutations distort the otherwise rigid loop 1 structure and prevent GTP hydrolysis (Tong et al., 1991).

Several other mutants have altered GTP cleavage reactions and most are postulated to be due to an alteration in the orientation of the residues involved in catalysis. Thus, substitution of Glu 63 → Lys 63 leads to a transforming phenotype and reduced GTP cleavage rate (Fasano et al., 1984), presumably because this residue can no longer stabilise the side chain of Gln 61 in a catalytically active conformation. Similarly, mutation of Gly 60 (which normally interacts with the gamma-phosphate of GTP) probably leads to misalignment of the sub-

strate in the hydrolytic reaction. Viral $p21^{ras}$ has a Ala 59 → Thr 59 substitution, and this residue is now sufficiently close to the gamma-phosphate to become a site for autophosphorylation. Since the rate of autophosphorylation is slower than the wild type rate of GTP hydrolysis, this mutation effectively increases the half life of the active $p21^{ras}$.GTP bound state (John et al., 1988).

(d) Mutations of $p21^{ras}$ In the Effector Loop.

Mutations in residues 32 - 40 critically affect GAP binding to $p21^{ras}$.GTP. For example, a Thr 35 → Ala 35 mutation reduces the affinity of $p21^{ras}$ for GAP. The explanation for this effect is that Ala 35 can no longer interact correctly with the gamma-phosphate or the Mg^{2+} ion, and therefore cannot orientate the effector loop in the correct conformation to allow high affinity GAP binding. Mutations at both positions 36 and 38 also abolish GAP binding (Cales et al., 1988 ; Adari et al., 1988) although they are not always transforming. For example with Asp 38 mutants, although the $p21^{ras}$.GTP concentration is increased, changes in the effector region also prevent interaction of $p21^{ras}$.GTP with downstream effector molecules.

1.6 Preliminary Kinetic Studies of the Interaction of Guanine Nucleotides with $p21^{ras}$

In the study of the biochemical properties of $p21^{ras}$, focus has been primarily based on its ability to bind and hydrolyse guanine nucleotides. These kinetic studies provide the basis for investigating which steps in the intrinsic GTPase mechanism of $p21^{ras}$ are modulated by interaction with macromolecules (such as GAPs and GNRPs) acting both upstream and downstream of $p21^{ras}$ in the signal transduction pathway. When purified after expression in bacterial or eukaryotic systems, $p21^{ras}$ contains 1 mole of tightly bound guanine nucleotide per mole of protein (Poe et al., 1985, mainly GDP). Early kinetic studies of the interaction of guanine nucleotides with $p21^{ras}$ used an assay developed by Manne et al (1984) to follow the binding of radiolabelled GTP and GDP. Subsequent studies of the rate of nucleotide exchange with $p21^{ras}$ (Hattori et al., 1985 ; Hall and Self., 1986 ; Sigal et al., 1986) were limited by the rate of the dissociation of the nucleotide already bound tightly to the active site of $p21^{ras}$.

The steady state (i.e multiple turnover) GTPase rate (k_{cat}) for $p21^{ras}$ has been estimated by incubating $p21^{ras}$.GDP (purified from E.coli) with an excess of GTP and the rate of conversion of GTP to GDP was monitored with time (Der et al., 1986 ; Gibbs et al., 1984 ; McGrath et al., 1984). More recently, experiments to measure the multiple turnover steady state GTPase activity of $p21^{ras}$ (which is dependent on the rates of several reactions, described below), have been replaced by those of the elementary rate constant for the cleavage of protein bound GTP. From these studies, a general trend has emerged whereby the GTP cleavage rate of transforming mutant proteins is lower than that of the wild type protein.

1.7 Interactions of $p21^{ras}$ With Other Proteins

1.7.1 *GTPase Activating Proteins*

In 1987, Trahey and McCormick reported a cytoplasmic protein in *Xenopus oocytes* that stimulated the hydrolysis of GTP by wild type $p21^{ras}$ at least 200-fold but had no effect on the Asp 12 or Val 12 $p21^{ras}$ mutants. Thus, this GTPase activating protein (GAP) serves as a negative regulator of $p21^{ras}$, catalysing the conversion of $p21^{ras}$.GTP to the inactive $p21^{ras}$.GDP form. Its ability to interact with, but not stimulate the hydrolysis of, oncogenic mutants was proposed to explain their oncogenic potential (Trahey and McCormick, 1987 ; McCormick, 1989 ; Figure 1.4). GAP activity has also been observed in other tissues, and is widely distributed (Trahey et al., 1988 ; Adari et al., 1988, Gibbs et al., 1988). It has become apparent that a family of GAP molecules exist, each interacting with its own target within the ras gene superfamily. Thus, RasGAP will bind to $p21^{ras}$ and stimulate its intrinsic GTPase activity, and while it will bind to other ras related proteins, it does not necessarily accelerate their GTP cleavage rates. RhoGAP and RapGAP, amongst others, have been identified and will be discussed with their related proteins (section 1.7.1.6).

1.7.1.2 Identification and Biochemical Properties of ras GAPs

The GAP protein identified by Trahey and McCormick, (1987) was subsequently purified (Gibbs et al., 1988, Halenbeck et al., 1990) and cloned (Trahey et al., 1988 ; Vogel et al.,

Figure 1.4 : Simple Negative Regulator Model for the Function of GAP.

In this model, proposed by McCormick (1989), the binding of GTP by $p21^{ras}$ induces the binding of GAP, and consequently the translocation of GAP from the cytosol to the plasma membrane. GAP bound to $p21^{ras}$.GTP is then able to bind an unidentified downstream effector ("X") which transduces the biological signal mediated by $p21^{ras}$.

(A) In a normal cell, containing wild type $p21^{ras}$, the duration of the signal output from the effector X is limited by the GAP-mediated hydrolysis of GTP to GDP, the product of which does not bind to GAP.

(B) In a cell containing an activated $p21^{ras}$ protein (such as Gly 12 → Val or Gln 61 → Leu mutants), GAP still binds to the GTP-bound state although the intrinsic rate of GTP hydrolysis is not accelerated by this interaction. Thus, the duration of the signal output from X is greater than that observed for the wild type cell.

(Taken from McCormick, 1989).

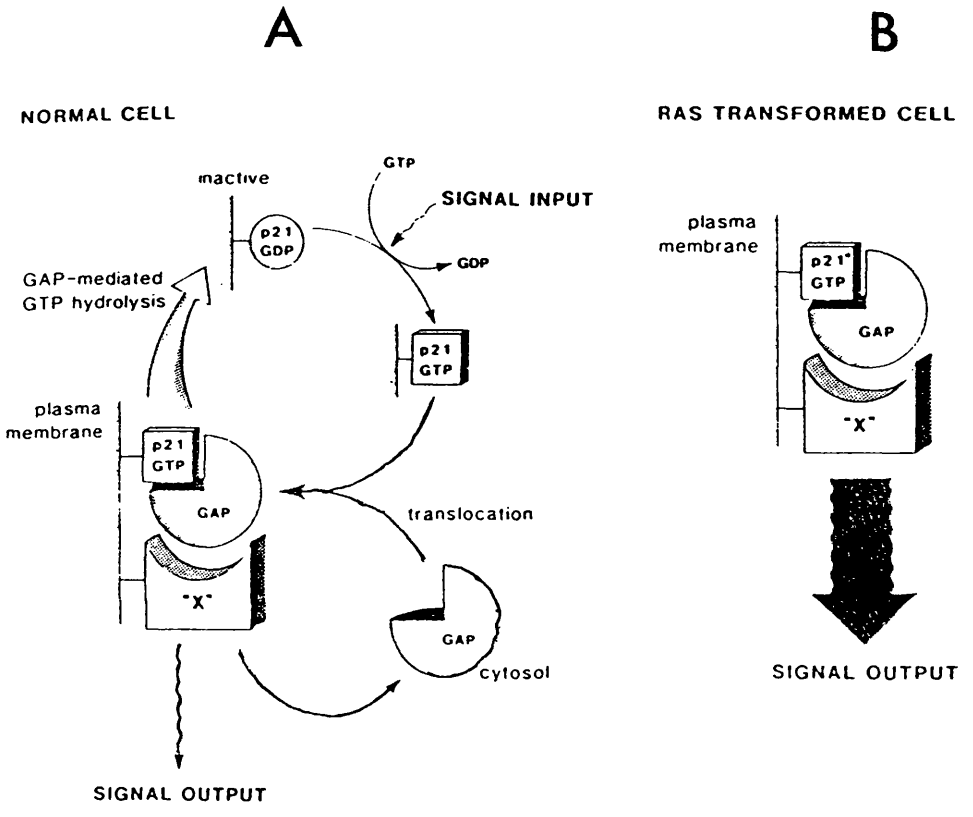
A
B
NORMAL CELL
RAS TRANSFORMED CELL
inactive
GTP
SIGNAL INPUT
p21
GDP
GDP
GAP-mediated
GTP hydrolysis
p21
GTP
plasma
membrane
p21
GTP
GAP
"X"
translocation
GAP
cytosol
SIGNAL OUTPUT
plasma
membrane
p21*
GTP
GAP
"X"
SIGNAL OUTPUT

1988). This protein exists in 2 forms: a 120 kD form and an alternatively spliced 100 kD form (Trahey et al., 1988 ; Vogel et al., 1988 ; Halenbeck et al., 1990). These GAP proteins have been termed p120-GAP and p100-GAP respectively. Inspection of the predicted amino acid sequence of GAP revealed two regions referred to as SH2 sites. These regulatory sequences are found in non-receptor tyrosine kinases, phospholipase C, and the crk oncogene (for review see Koch et al., 1991). An SH3 region was noticed more recently. SH2 and SH3 sequences are thought to be involved in interactions of GAP with tyrosine phosphoproteins, as discussed below. However, only the carboxy-terminal one-third of the protein is required for catalytic activity (Marshall et al., 1989 ; Skinner et al., 1991). Whilst p120-GAP is ubiquitously distributed in human tissues, p100-GAP has thus far only been identified in human placental tissue (Trahey et al., 1988) The p120-GAP proteins from human, murine and bovine cells share 95% sequence homology. GAP is primarily a cytosolic protein (Trahey and McCormick, 1987 ; Gibbs et al., 1988), although in response to stimulation by PDGF, a significant amount of GAP is found in the membrane fraction.

Other GAPs for ras have since been discovered. In the yeast, *Saccharomyces serevisiae*, two genes encoding GAP activity, IRA1 and IRA2, down-regulate RAS function by stimulating the RAS.GTPase (Tanaka et al., 1989). Human p120-GAP can replace both of these genes (Ballester et al., 1989 ; Tanaka et al., 1990) whilst human $p21^{ras}$ proteins are not substrates for the IRA proteins (Adari et al., 1988 ; Tanaka et al., 1991). More recently, sequencing of the neurofibromatosis type 1 gene (NF1) has revealed 30 % sequence homology with the catalytic domain of p120-GAP, as well as more extensive sequence homologies with the IRA genes (Ballester et al., 1990 ; Buchberg et al., 1990 ; Xu et al., 1990b). The catalytic domain, which is homologous in all of these proteins, encompasses only a small region of about 300 amino acids. The SH2 and SH3 domains (src homology domains 2 and 3, see above), which are found in only p100-GAP and p120-GAP, are thought to be involved in binding to other proteins (see section 1.7.1.4).

1.7.1.3 Biochemical Characterisation of ras GAPs

p120-GAP has a number of properties that may be shared with other ras GAPs.

(a) p120-GAP is specific for ras proteins and is inactive on all other guanine nucleotide binding proteins tested thus far, with the exception of the ras homologue R-ras (section 1.8.1, Garrett et al., 1989).

(b) While p120-GAP is capable of binding to oncogenic mutants of $p21^{ras}$ (Vogel et al., 1988), it does not significantly accelerate their intrinsic GTP hydrolysis rates (Trahey and McCormick, 1987). Some mutants of $p21^{ras}$ (notably the Gln 61 → Leu mutant) bind GAP with higher affinity than does wild type $p21^{ras}$.

(c) Mutants of $p21^{ras}$ with changes in the region encompassing amino acids 32 - 40 have been shown to affect binding to the (as yet unidentified) effector proteins (Sigal et al., 1986a). p120-GAP binds weakly to these effector mutants (Vogel et al., 1988 ; Schaber et al., 1989) and only poorly catalyses their GTPase activity (Cales et al., 1988 ; Adari et al., 1988). These data suggest that GAP binds at the effector site, and that GAP may itself be part of the effector complex (section 1.9.2). The ability of GAP to stimulate the GTPase activity of R-ras and yeast RAS proteins supports the idea that the 32 - 40 region is necessary for GAP action since this region is highly conserved amongst all these proteins (Barbacid, 1987). Antibodies against the 32 - 40 region block GAP interaction (Rey et al., 1989). Furthermore, the conformation of this region is highly dependent on whether GTP or GDP is bound to $p21^{ras}$ (see section 1.4.3) : GAP binding to $p21^{ras}$ is similarly nucleotide-sensitive.

(d) p120-GAP binds tightly to the product of the K-rev-1 gene, a ras homologue rap 1 (see section 1.7.1.7), with an affinity $\approx$ 100-times higher than that of $p21^{ras}$. However, it fails to catalyse the hydrolysis of GTP by this protein (Frech et al., 1990 ; Hata et al., 1990). Overexpression of rap1A protein suppresses the transformation caused by activated ras oncogenes (Kitayama et al., 1989). rap1A may be a potent inhibitor of GAP since it binds GAP more tightly than $p21^{ras}$ and this binding is not terminated by GTP hydrolysis. It seems unlikely however that the true biological function of rap1A in the cell is to deprive $p21^{ras}$ of GAP. It is difficult to reconcile the observation that both rap1A and the oncogenic Leu 61 mutant of $p21^{ras}$ bind GAP with similar affinities, and yet these two proteins have opposite effects on cell behaviour. Clearly, there are many *possible* reasons for this apparent discrepancy, al-

though at present there is no clear explanation.

(e) Binding of the anti-ras monoclonal antibody Y13-259, blocks the action of p120-GAP on $p21^{ras}$ (Trahey and McCormick, 1987). Mutants of $p21^{ras}$ in the region to which this antibody binds (residues 63 - 73) also fail to interact with GAP and destroy biological activity of the $p21^{ras}$ protein (Srivastava et al., 1989). These data support an essential role for GAP in ras function. This region is also one which undergoes conformational changes upon GTP hydrolysis (section 1.4.3) and in three dimensions is very close to the 32 - 40 effector region.

Whilst the binding of NF1-GAP to rap1 has not yet been examined, all of the other properties listed above apply to NF1-GAP as well as to p120-GAP (Xu et al., 1990 ; Martin et al., 1990 ; Ballester et al., 1990 ; Bollag and McCormick, 1991), albeit with some slight differences. For example, NF1-GAP binds to $p21^{ras}$.GTP with a 30-fold higher affinity than does p120-GAP (Martin et al., 1990) whilst the maximally activated rate of GTP hydrolysis by $p21^{ras}$ in the presence of NF1-GAP has been reported to be 30-fold lower than that of p120-GAP (Bollag and McCormick, 1991). In addition, NF1-GAP has been reported to be primarily associated with the membrane fraction of cells, and is apparently differentially regulated by lipids (Bollag and McCormick, 1991).

1.7.1.4 Tyrosine Phosphorylation of ras GAPs

Much attention has focused on the interaction of p120-GAP with tyrosine kinases. Among the growth factor receptors shown to phosphorylate p120-GAP are those for platelet derived growth factor (PDGF, Molloy et al., 1989 ; Kaplan et al., 1990), epidermal growth factor (EGF, Ellis et al., 1990, Margolis et al., 1990) and colony stimulating factor 1 (CSF-1, Reedijk et al., 1990). In addition, the tyrosine kinase oncogenes, v-src, v-fps, and v-abl, are also able to phosphorylate p120-GAP on tyrosine (Ellis et al., 1990). However, when it has been measured, the stoichiometry of phosphorylation is low ($\leq$ 10 %) and this modification has no apparent modification to the activity of p120-GAP. p120-GAP binds to many of these kinases but only when they have been activated. In addition, the activated PDGF and CSF-1 receptors form complexes with p120-GAP which can be mimicked using only the SH2 domains of

p120-GAP (Kaplan et al., 1990 ; Reedijk et al., 1990). However, the bulk of cellular p120-GAP does not enter these complexes, although that which does it presumably translocated to the plasma membrane.

The isolated SH2 domains derived from p120-GAP are sufficient to direct binding to phosphotyrosine containing proteins, including p62 and p190 (Bouton et al., 1991 ; Ellis et al., 1990) as well as to autophosphorylated tyrosine kinases (Anderson et al., 1990 ; Moran et al., 1990). However, not more than 10 % of the total cellular p62 interacts with p120-GAP. In contrast, in EGF-stimulated (but not unstimulated) fibroblast cells, up to 50% of the cytoplasmic p120-GAP is complexed with p190. Indeed, the p190 / p120-GAP complex has a reduced GTPase stimulating activity, suggesting that p190 may act upstream of $p21^{ras}$ by inhibiting p120-GAP activity.

1.7.1.5 Regulation of ras GAPs

Whilst it is clear that GAPs regulate the activity of $p21^{ras}$, it is the regulation of GAP activity that is apparently the target of extracellular signals since the accumulation of $p21^{ras}$.GTP in T-lymphocytes, at least, has been attributed to an inhibition of GAP activity. In response to T-cell activation, the activity of GAP is inhibited, thus leading to the activation of $p21^{ras}$ (Downward et al., 1990a). This effect apparently proceeds via protein kinase C activation since the independent activation of PK-C with phorbol esters also inhibits GAP activity. However, inhibition of PK-C, using a pseudosubstrate for this enzyme, was ineffective in blocking the CD3 dependant accumulation of $p21^{ras}$.GTP in these cells. In support of the hypothesis that there may be PK-C independent pathways for the inhibition of GAP, addition of insulin to fibroblasts over expressing the insulin receptor also leads to increased $p21^{ras}$.GTP concentrations via a PK-C independent pathway (Burgering et al., 1991).

In vitro assays have shown that phospholipids containing the arachidonate moiety at the *sn2* position are all capable of inhibiting rasGAP and rhoGAP activity in crude extracts (Tsai et al., 1989 a,b), and a cytoplasmic protein that may mediate these effects has been identified (Tsai et al., 1990). It appears that lipid inhibition primarily affects NF1-GAP (rather than

p120-GAP) activity and it has been claimed that lipids do not prevent the interaction of NF1-GAP with $p21^{ras}$.GTP (Bollag and McCormick, 1991).

Recently, it was found that cyclooxygenase metabolites of arachidonic acid actually *stimulate* p120-GAP activity (Han et al., 1991). While arachidonic acid inhibits both p120-GAP and NF1-GAP, the stimulation by these ecosanoids is specific for p120-GAP. This stimulation is also only observed for prostaglandins 9α-$PGF_{2\alpha}$ and PGA_2 but not with 9ß-$PGF_{2\alpha}$, $PGF_{1\alpha}$, or TX B_2.

1.7.1.6 GAPs for ras-Related Proteins.

Since the GAPs for ras proteins are extremely selective, it is expected that different GAPs exist for other small GTP-binding proteins with a low intrinsic GTPase activity (discussed in more detail in section 1.8). Most work has focused on the GAP protein specific for rap1 since rap1 has been shown to bind non-productively to p120-GAP (Frech et al., 1990 ; Hata et al., 1990). Both cytosolic (Kikuchi et al., 1989 ; Ueda et al., 1989) and membrane-bound (Polakis et al., 1990) forms of rapGAP have been described. The latter has a monomeric molecular weight of 88kD, is inactive towards all small guanine nucleotide binding proteins except rap1 (Polakis et al., 1990) and shows no significant homology to any of the rasGAPs (Rubenfield et al., 1991).

GAPs for other proteins have been identified although none have been purified to homogeneity or characterised to the same degree as for rasGAP and rapGAP. Thus, the partial purification of rhoGAP from human spleen (Garrett et al., 1991) and bovine brain (Yamamoto et al., 1990) has been reported, and a ral specific GAP has been identified in brain and testis cytosol (Emkey et al., 1991). Both cytosolic and membrane bound forms of a rab 3A specific GAP have been identified (Burstein et al., 1991). A GAP which interacts with the effector region of the ypt1 protein has been identified in porcine liver (Becker et al., 1991). Interestingly, the products of the bcr and n-chimerin genes are GAPs for rac proteins (Diekmann et al., 1991). It is likely that each small GTP-binding protein will have its own GAP or GAPs - the aim now is to understand which GAPs interact (productively and non-productively) with

which GTP-binding proteins.

1.7.2 *Guanine Nucleotide Release Proteins (GNRPs).*

1.7.2.1 Mammalian GNRPs.

The search for exchange factors (guanine nucleotide release proteins, GNRPs) has been prompted by the expectation that these factors would be directly upstream of ras in a signalling pathway. Thus far, three groups have reported factors with stimulatory exchange activity on mammalian $p21^{ras}$. West et al (1990) have described a membrane factor (native molecular weight 100 kDa) that promotes the release of GDP from recombinant $p21^{ras}$ by up to 40-fold. This factor, which has a subunit molecular weight of 35 kDa on SDS-PAGE, promotes the release of GDP from $p21^{ras}$, R-ras, rap1A, rap1B, and rho proteins (see below, Huang et al., 1990). It did not, however, promote the release of GDP from elongation factor Tu or from the alpha subunit of transducin. The protein described by Wolfman and Macara (1990) increased the GDP-dissociation rate to a similar degree (60-fold) and had a native molecular weight of 100 - 160 kDa. However, this protein was identified in the cytosol not in membrane fractions. Finally, Downward et al (1990b) described a cytosolic protein with an apparent molecular weight of 60 kDa which required the COOH-terminal sequences of $p21^{ras}$ for its effect. This observation may be significant in that the three ras gene products (N-, H-, and K-ras) differ dramatically in this region of their amino acid sequence (Barbacid, 1987). In addition to these exchange factors for ras, a GDP dissociation stimulator (GDS) for rap1A is also active on post-translationally modified Ki-ras (Mizuno et al., 1991). The GDP dissociation stimulator (GDS) and inhibitor (GDI) proteins that have been identified for other small guanine nucleotide binding proteins will be discussed in section 1.8. To date, there has been no report of a GDI protein specific for $p21^{ras}$.

1.7.2.2 Yeast GNRPs

In the yeast *Saccharomyces cerevisiae*, where the RAS effector is adenylate cyclase, genetic analysis has identified regulators of RAS function (Broach and Deschenes, 1990). Genetic

evidence initially identified a gene (CDC25) in yeast cells which was implicated as a GNRP. Subsequent biochemical analysis identified the CDC25 gene product as a membrane-associated protein of molecular weight 180 kDa (Garreau et al., 1990). This protein had the essential properties predicted for a GNRP : it accelerates the GTP-dependant activation of adenylate cyclase (Engelberg et al., 1990), and promotes GDP/GTP exchange on the yeast RAS proteins (Jones et al., 1991).

Genetic selection of genes that were able to suppress the effect of mutations in CDC25 identified a fragment of a gene with COOH-terminus homology to CDC25 called SDC25 (Crechet et al., 1990). After expression in *E.coli*, this protein catalysed the release of GDP (and to a lesser extent GTP) from yeast RAS and mammalian $p21^{ras}$ proteins (Crechet et al., 1990, Mistou et al., 1992). Interestingly, only the C-terminal fragment of SDC25 suppresses CDC25 mutations ; the intact gene does not (Damak et al., 1991). It has been shown that CDC25 : RAS interaction requires the C-terminal portion of yeast RAS proteins, a region which is unrelated to any part of the human $p21^{ras}$ proteins. It is therefore surprising that SDC25, which is homologous to CDC25 throughout its sequence, still acts on human $p21^{ras}$. It is possible therefore that SDC25 does not normally act on RAS proteins.

1.8 Ras Related Proteins

It has recently become clear that the ras genes are part of a larger superfamily of genes. The protein products of these genes can be divided into 3 main groups, based on their similarity to human $p21^{H\text{-}ras}$ (see section 1.1.2) - the ras, rho and rab families. All of these proteins are likely to contain common structural elements for the binding and hydrolysis of GTP. In this section, a brief description of the biochemical and biological properties of the major members of each group will be given. For a more complete survey see Grand and Owen (1991), Hall, (1990, 1992a,b), and Downward (1990, 1992).

1.8.1 *The Ras Family.*

In addition to the four different ras proteins described above (N-ras, H-ras, and K-ras-A and

-B), this family includes the 23 kDa human R-ras protein (Lowe and Goeddel, 1987 ; Garrett et al., 1989). Whilst RasGAP can interact with R-ras causing stimulation of the GTPase activity, the biological effects of R-ras and $p21^{ras}$ are quite different. For example, mutant H-ras proteins can cause transformation whilst R-ras cannot. Furthermore, their abilities to be stimulated by rasGAP are attenuated by different phospholipids (Tsai et al., 1989b). The sequence of the effector binding region in the ral proteins, (ralA and ralB) is quite different from that of $p21^{ras}$. Whilst it is known that RalA is non-transforming (Chardin, 1988), no function has yet been assigned to these proteins (Chardin and Tavitan, 1986).

This group also includes the products of the Krev-1 gene, termed rap1 (or smg p21). rap1A is apparently ubiquitous, has a molecular weight of 21 kDa (184 residues), has 50% homology to $p21^{ras}$, and has an effector loop (residues 32 - 40) which is identical to $p21^{ras}$ and R-ras. This suggests that all three proteins may bind the same (or similar) effector molecules. Rap 1A and 1B are post-translationally modified as described for $p21^{Ki\text{-}ras}$ (section 1.3) except that they are geranylgeranylated instead of being farnesylated (Buss et al., 1991). The rap proteins have a Thr residue at codon 61 ($p21^{ras}$ proteins have a Gln residue thought to be involved in the GTP hydrolysis reaction) and this difference may lead to a reduction in the intrinsic GTP cleavage rate of rap compared to $p21^{ras}$ and also to the insensitivity of the GTPase of rap to stimulation by p120-GAP. Indeed, mutation of this residue to Gln in rap1A yields a protein with GTPase activities similar to $p21^{ras}$ and which is now sensitive to stimulation by p120-GAP (Hart and Marshall, 1990). The presence of a Val 12 mutation in rap1A increases the ability of this protein to suppress transformation by oncogenic $p21^{ras}$ mutants (Kitayama et al., 1990).

Guanine nucleotide exchange proteins have been isolated which increase the rate of nucleotide exchange on the rap proteins, termed rap GDS (for review see, Takai et al., 1992). The rap GDS, (M_r = 61 kDa) is active not only on rap proteins, but also on $p21^{Ki\text{-}ras}$ and rho p21 proteins. However, rap GDS will only catalyse nucleotide exchange on post-translationally modified form of rap 1A and rap 1B. This requirement appears to be a general phenomenon for all the GNRPs (both GDS and GDI proteins for different small GTP-binding proteins) purified by Takai and co-workers (Takai et al., 1992). In contrast, the $p21^{ras}$ GDS proteins

and the CDC25 gene product from yeast (see section 1.7.3.1) are active even on the post-translationally unmodified form of $p21^{ras}$. Less well characterised are the rap specific GAPs, although two such proteins have been isolated termed rapGAP1 and rapGAP2. They have molecular weights of 250 - 400 kDa and 80 - 100 kDa respectively and seem specific to rap proteins since they are inactive on $p21^{ras}$, rho or rab proteins (Kikuchi et al., 1989 ; Polakis et al., 1991 ; Ueda et al., 1989).

1.8.2 *The Rho Family.*

The human Rho family of proteins (Rho A, B and C, M_r = 21 kDa) show approximately 30% similarity to $p21^{H\text{-}ras}$ (Yeramian et al., 1987 ; Chardin et al., 1988). They have a lower intrinsic GTP cleavage rate compared to $p21^{ras}$ since they have an Ala at the position equivalent to Gly 13 in $p21^{ras}$, and this corresponds to an activating mutation in $p21^{ras}$ (Garrett et al., 1989). Rho C is ADP-ribosylated by *Clostridium botulinum* exoenzyme C3 on the Asn residue at position 41, and this results in the disassembly of actin microfilaments, suggesting that Rho C may be involved in cytoskeletal control (Chardin et al., 1989). A GAP molecule for Rho A has been isolated in mammalian cells and *Xenopus* oocytes and has a molecular weight of $\approx$ 29 kDa (Garrett et al., 1989). Rho does not interact with rasGAP, probably due to Glu at position 40 (equivalent to Asp 38 in H-ras) which would be likely to destroy rasGAP interactions. RhoGAP is apparently ubiquitous and has been identified in the cytoplasm of all cell lines investigated. Whilst RhoGAP is unrelated in sequence to rasGAP, the amino acid sequence of RhoGAP does show homology with two proteins (Hall, 1992): the breakpoint cluster region protein, bcr, which has been identified in acute lymphocytic leukemia (Diekmann et al., 1991), and the brain protein, n-chaemerin. Whilst neither of these proteins had any GAP activity with Rho.GTP, they were active on $p21^{rac}$ (see below). GDS and GDI proteins have been identified or isolated for Rho (Paterson et al., 1990 ; Ohga et al., 1989 ; Hori et al., 1991 ; Isomura et al., 1990, Ueda et al., 1990) and appear to be specific for post-translationally modified forms of the protein.

Microinjection of activated Rho (Val 14) into Swiss 3T3 cells lead to a rapid (after 15 min) change in cell morphology : finger-like and bulbous projections are observed and the cell

contracts (Paterson et al., 1990). However, ADP-ribosylated Rho is incapable of mediating morphological changes which is consistent with the hypothesis that ADP-ribosylation of Asn 41 prevents effector binding. ADP-ribosylation does not affect the interaction with Rho GAP, suggesting that Rho has target molecules other than RhoGAP (Paterson et al., 1990). Injection of Val 14 Rho proteins into mutant cells with low amounts of actin filaments leads to actin polymerisation and restoration of the wild type cell morphology, suggesting that Rho proteins can induce actin polymerisation *in vivo*. The yeast RHO homologues (CDC42) are thought to be involved in the establishment of cell polarity and the localisation of budding (Bender et al., 1989). Interestingly, the establishment of cell polarity in yeast appears to be mediated by actin cytoskeleton (Novick and Botstein, 1985).

The rac 1 and rac 2 members of the Rho family have also been reported although at present there is no definite function ascribed to them (Didsbury et al., 1989, 1990). The rac 1 protein is the same as TC25, a gene isolated in a tetracarcinoma cell line (Menard et al., 1992). The rac proteins are ADP-ribosylated by exoenzyme C3 (see above) and are isoprenylated, localising them to particulate cell fractions. Interestingly, the Rac.GTP cleavage rate is accelerated not only by RhoGAP but also by bcr and n-chaemerin. Rac is found in large quantities in secreting neutrophils and monocytes, although at present there is no clear evidence that either the Rho or Ras family of proteins are involved in exocytosis (Adam-Visi et al., 1987). Recently, however, rac has been identified as the 3rd component for the superoxidase system in neutrophils (Abo et al., 1991). Microinjection of Val 12 Rac proteins leads to cell ruffling, the accumulation of large vesicles within the cytoplasm which flow from the cell to nuclear membranes. These observations have also implicated rac in control of cell morphology and of the cytoskeleton, suggesting that this may be the major function of the Rho family of GTP-binding proteins (Hall, 1992b ; Ridley and Hall, 1992).

1.8.3 *The Rab Family.*

The rab gene family of proteins differ from p21^{ras} in their C-terminal regions, possessing either a CC or CXC motif as the lipid modification / membrane association signal at the COOH-terminus. The first members of this family to be identified were the yeast proteins,

YPT1 (Gallwitz et al., 1983) and SEC4. YPT1 functions in the early stages of the secretory pathway in yeast, is associated with Golgi-like structures, and is also implicated in microtubule organisation (Segev et al., 1988) and Ca^{2+} regulation (Schmitt et al., 1988). SEC4 was isolated as a mutation in the yeast secretion pathway, causing a build up of *post-Golgi* vesicles (Salminen and Novick, 1987). It is thought to be involved in the *final* stages of secretion, specifically with the fusion of vesicles to the plasma membrane (Walworth et al., 1992).

Many mammalian homologues to these yeast proteins have been identified. Originally 4 YPT homologues were identified in a rat brain cDNA library (rab 1, 2, 3, and 4, Touchot et al., 1987), and the human homologues (H-rab-1, -2, -3A, and -4) have now been identified, along with 3 other human rab genes (Zahraoui et al., 1989). The localisation of rab proteins is apparently similar to that of the yeast YPT1 type proteins with different rab proteins localised in different cellular compartments (Charvier et al., 1990).

It is emerging that the ras-related gene family consists of a large number of small GTP-binding proteins, all of which are likely to have their own specific GAP, GDS and GDI molecules, which is indicative of a very complex series of interactions. These ras-related proteins are generally ubiquitous and are often absolutely required by the cell, although, as for $p21^{ras}$, the exact molecular targets of these proteins remains obscure in most cases.

1.9 Biological and Biochemical Functions of $p21^{ras}$ Proteins.

1.9.1 *Biological Effects of $p21^{ras}$.*

The importance of $p21^{ras}$ as a regulator of intracellular signalling pathways, particularly those controlling growth, has long been apparent, but its biochemical mechanism of action has remained obscure. The essential requirement for Ras in actively dividing normal cells has been demonstrated (Mulcahy et al., 1985), as has the ability of wild type or mutant $p21^{ras}$ to stimulate cell division (Stacey and Kung, 1984 ; Feramisco et al., 1984). If $p21^{ras}$ plays a role in signal transduction, it might be expected that ras-transfected cells should respond to one or more growth factors. Whilst the details of the role of $p21^{ras}$ in growth

factor responses are not clear, it has been shown to be involved in pathways by which the cell responds to a number of different stimuli. For example, in the rat phaeochromocytoma (PC12) cell line, $p21^{ras}$ is required for neurite outgrowth and c-fos expression in response to nerve growth factor (NGF) but not for outgrowth in response to cyclic AMP (Hagag et al., 1986 ; Stacey et al., 1987). The observation that inhibition of c-fos expression can negate many of the phenotypic characteristics of $p21^{ras}$-transformed cells (Ledwith et al., 1990) lends support to the proposal that c-fos acts downstream of $p21^{ras}$ in one or more signal transduction pathways. In addition, the maturation of *Xenopus oocytes* can be induced by microinjection of activated $p21^{ras}$ (Birchmeier et al., 1985) and the effect of insulin on maturation in these cells also appears to be mediated via a $p21^{ras}$-dependent pathway (Deshpande and Kung, 1987). Finally, the mitogenic response of quiescent mouse NIH 3T3 cells to PDGF in serum is associated with an increase in the $p21^{ras}$.GTP levels in these cells which may be important in the transmission of that signal (Satoh et al., 1988 ; 1990).

1.9.2 *Biochemical Targets of $p21^{ras}$ Proteins In Signal Transduction.*

If $p21^{ras}$ is involved in signal transduction it might be expected that it could be shown to exert an effect at one or more points in a second messenger system. Such an example was the demonstration that RAS proteins in yeast act as regulatory subunits for adenylate cyclase and thus regulate cyclic AMP (cAMP) levels (Toda et al., 1985 ; Kataoka et al., 1985). Unfortunately, no evidence has been presented that this function extends to higher eukaryotes (Birchmeier et al., 1985 ; Beckner et al., 1985). Since that time great effort has been invested in attempting to determine precisely where $p21^{ras}$ acts in signal transduction pathways. The results obtained have been equivocal and it is still far from clear how or where $p21^{ras}$ plays a role in second messenger systems.

1.9.2.1 p120-GAP and NF1-GAP as regulators and / or effectors of $p21^{ras}$ activity.

When the GTPase activating protein (GAP) was first discovered, the expectation was that it would act as a negative regulator of $p21^{ras}$ i.e converting the biologically active $p21^{ras}$.GTP complex to the inactive GDP-bound form (Trahey and McCormick, 1987). However, further

interest in GAP was stimulated when mutational analysis of $p21^{ras}$ (Cales et al., 1988 ; Adari et al., 1988, section 1.7.1.3 (c)) identified a region comprising residues 32 - 40 which was considered to be the site of interaction of $p21^{ras}$.GTP with effector molecules *in vivo* (Sigal et al., 1986a). Since it was possible to show independently that *in vitro* the GAP binding domain mapped to the same region (Vogel et al., 1988 ; Schaber et al., 1989), it was suggested that GAP may also mediate some of the biological functions of $p21^{ras}$.GTP - that is that it may be the downstream target effector molecule of $p21^{ras}$. More recently, it has been shown that NF1-GAP also binds to this region (Bollag and McCormick, 1991 ; McCormick, 1992). Unfortunately, one cannot unequivocally decide which if either of these molecules is an effector because both have the properties associated with both a negative regulator and effector of $p21^{ras}$ (Figure 1.5). One possibility, discussed by McCormick (1992) is that both proteins acts as effectors but they mediate different signals.

Several recent observations are consistent with the role of GAP as a negative (upstream) regulator of $p21^{ras}$. The activation of protein kinase C in T lymphocytes increases the amount of $p21^{ras}$ in the GTP form, apparently as a result of a reduction in GAP activity (Downward et al., 1990 ; section 1.7.1.5). A possible link between $p21^{ras}$ and growth factors has come from the observation that some membrane receptor and cytoplasmic tyrosine kinases phosphorylate GAP (section 1.7.1.4). Whilst it is tempting to speculate that the phosphorylation of GAP could lead to a reduction in GAP activity (and therefore lead to an accumulation of $p21^{ras}$.GTP) as has been shown for PK-C in T-lymphocytes (Downward et al., 1990), only a small fraction of GAP is phosphorylated and this does not appear to affect GAP activity. More convincing evidence for an upstream negative regulator role for GAP comes from the experiments described by Zhang et al, (1990) ; over-expression of GAP suppresses transformation by high levels of normal wild type $p21^{ras}$ but has no effect on oncogenic ras transformation. Thus, if GAP is considered to be a negative regulator, then it is able to prevent the mitogenic signal mediated by $p21^{ras}$.GTP by stimulating the hydrolysis of GTP and thus prevents transformation of these cells. In the model where GAP is the effector for $p21^{ras}$.GTP, it would be predicted that over-expression of GAP would actually increase the degree of transformation, and this is not the observed effect of over-expression (Zhang et al., 1990 ; 1992).

Figure 1.5 : Regulation of the Activity of $p21^{ras}$ by Guanine Nucleotide Exchange Factors, GAP, and NF1.

The exchange of bound GDP for GTP is catalysed by a guanine nucleotide exchange factor (GDS). Upstream activation of $p21^{ras}$ into the GTP-bound form may occur via stimulation of the GDS activity. The $p21^{ras}$.GTP complex interacts with a downstream effector, which may also be GAP and/or NF1, which mediates the downstream signal. The duration of the signal is determined by the stimulation of the intrinsic GTPase activity by either GAP or NF1. At least in T-lymphocytes, extracellular activation signals mediate their action through inhibition of GAP or NF1 activity, thus increasing the duration of the $p21^{ras}$.GTP bound state.

(Taken from Downward, 1992).

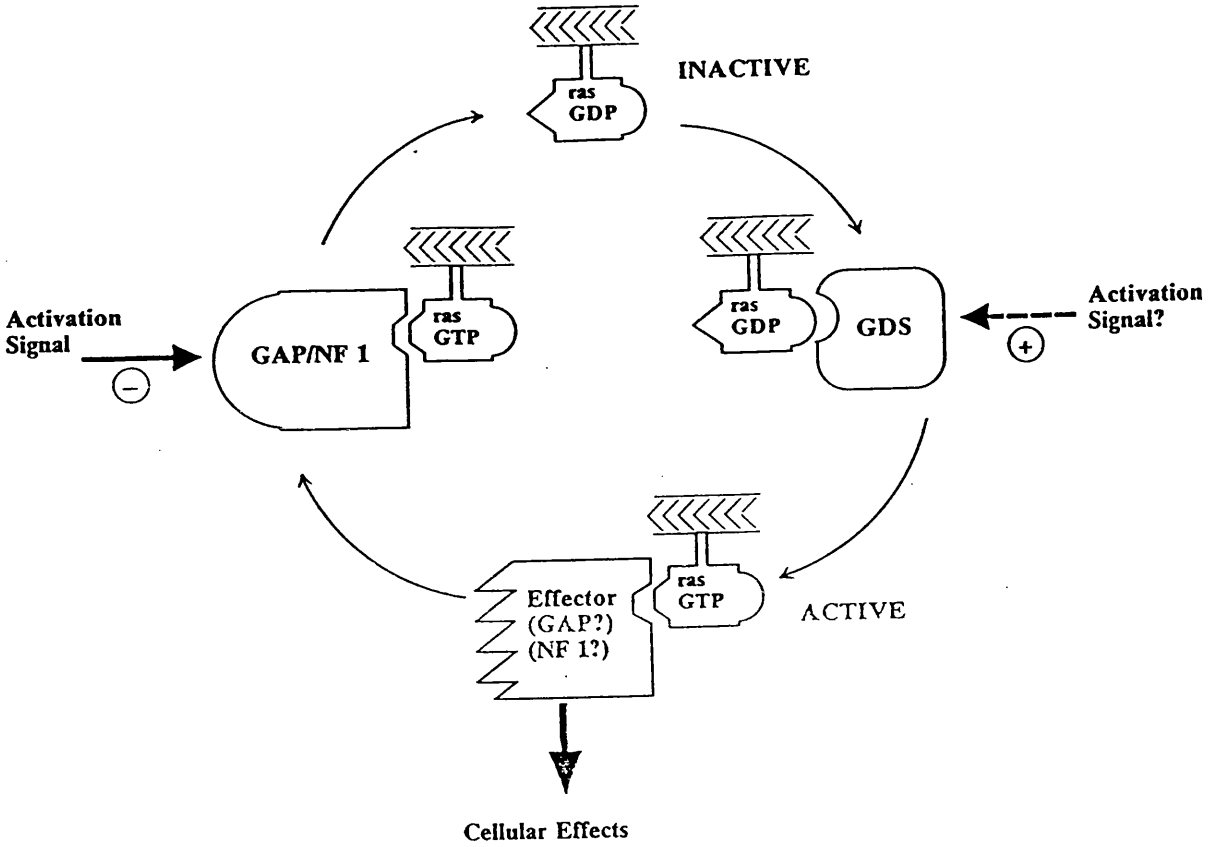
INACTIVE
ras
GDP
Activation
Signal
GAP/NF 1
ras
GTP
ras
GDP
GDS
Activation
Signal?
ras
GTP
Effector
(GAP?)
(NF 1?)
ACTIVE
Cellular Effects

In contrast to this data, there is also evidence in support of a model whereby GAP and NF1 act as possible effectors of $p21^{ras}$.GTP. Firstly, both GAP and NF-1 bind to the effector regions of $p21^{ras}$. However, this data could also be interpreted as showing that the true (unidentified effector) competes with the upstream negative regulator (GAP or NF-1) for $p21^{ras}$.GTP at the effector binding site. More direct support for an effector function of GAP comes from studies on the effects of $p21^{ras}$ and GAP on the opening of a muscarinic receptor coupled K^+ channel in atrial cell membranes (Yatani et al., 1990) which is coupled to its receptor by the G-protein, G_K. Addition of recombinant GAP or $p21^{ras}$.GTP rapidly blocked the current through these channels - the ras proteins mediate this effect in conjunction with endogenous GAP and *vice versa*. The conclusion from this work is that $p21^{ras}$ and GAP act *together* to transduce the biological signal and therefore that the $p21^{ras}$.GTP.GAP complex is responsible for blocking the channels. Whilst this effect can be overcome by pre-loading the cells with G_K bound to a non-hydrolysable GTP analogue (GTPgammaS), ras and GAP do not appear to affect the rate of GTP hydrolysis by G_K. Rather, they appear to either uncouple G_K directly from its upstream receptor or indirectly by inhibiting the binding of the α sub-unit of G_K to its ßg subunits. Whatever the precise mechanism of this effect (direct physical association of proteins or indirect signals produced by the $p21^{ras}$.GTP.GAP complex), these experiments raise the possibility that $p21^{ras}$ proteins may affect the activity of classical heterotrimeric G-proteins by uncoupling them from their receptor and producing free beta : gamma subunits (Hall, 1990a).

Further corroborating evidence that GAP may be an effector comes from experiments in which mutant $p21^{ras}$ or ras-related proteins which have an increased affinity for GAP have been shown to inhibit wild type $p21^{ras}$ function. Firstly, a COOH-terminally truncated yeast RAS mutant (Gln 68 → Leu, equivalent to Leu 61 in mammalian $p21^{ras}$), which is both cytosolic and predominantly bound to GTP, can inhibit $p21^{ras}$ activity *in vivo* and this block can be overcome by increasing the intracellular GAP concentration (Gibbs et al., 1990). A similar situation occurs with the rap1 proteins (section 1.8.1) which bind GAP more tightly than wild type proteins and can suppress oncogenic $p21^{ras}$ transformation (Kitayama et al., 1989). In both cases, one could envisage that these proteins compete with $p21^{ras}$ for GAP and hence reduce the effective concentration of GAP. If GAP is a negative regulator of $p21^{ras}$.GTP,

these proteins would be expected to potentiate the biological activity of wild type $p21^{ras}$, whilst the model with GAP as an effector is compatible with the experimental observations. It is possible however, that both proteins also bind the true effector with greater affinity although it does seem more than a coincidence that both these inhibitory proteins also bind GAP with a high affinity.

Whether GAP or NF1 are involved in the effector functions of $p21^{ras}$ is still unclear. Experiments which deplete the effective concentration of an effector will prevent transformation by oncogenic forms of $p21^{ras}$ (for example, see above) whilst depletion of negative regulators will lead to transformation of normal cells containing wild type $p21^{ras}$. In this regard, the experiments of Basu et al., (1992) and DeClue et al., (1992) are particularly interesting. In these experiments, a Schwann cell line which is defective in NF1 but has normal levels of p120-GAP was characterised. This cell line had increased levels of $p21^{ras}$ bound to GTP and were derived from a malignancy. These data suggest that, at least in these cells, NF1 is the major regulator of GTPase activity, and that p120-GAP is unable alone to completely down-regulate $p21^{ras}$.GTP.

The simple negative regulator model originally suggested for p120-GAP (Trahey and McCormick, 1987) now looks increasingly less likely. Whilst the experiments of Yatani et al (1990) suggest a biological role for the $p21^{ras}$.GTP.GAP complex, there is no report as yet that it can mediate the most striking biological activity of $p21^{ras}$ - that of stimulating cell proliferation. Until this has been demonstrated, one cannot rule out the possibility that the real downstream target of $p21^{ras}$.GTP remains unknown.

1.9.2.2 Downstream signalling events mediated by $p21^{ras}$.

Although the nature of the $p21^{ras}$: effector interaction is unclear, some of the downstream features of the signal transduction pathway have been elucidated. However, despite the vast amount of effort invested in dissecting the signal transduction pathway, the literature is full of inconsistencies, obtaining differing results when using different cell types or when using related, but different, techniques. For example, Birchmeier et al., (1985) have suggested that

injection of oncogenic forms of $p21^{H\text{-}ras}$ into *Xenopus oocytes* does not affect the intracellular concentration of cAMP. In contrast, Sadler and co-workers (Sadler and Maller, 1989 ; Sadler et al., 1990) observed that activated $p21^{ras}$ proteins activate cAMP phosphodiesterase. Whilst these experiments were performed in slightly different ways (and are therefore not directly comparable), a rational explanation for this apparent discrepancy will probably require a more complete understanding of $p21^{ras}$ activity than is available at present. This section summarises only some of the main areas of signal transduction and secondary metabolism in which $p21^{ras}$ has been implicated and about which there is probably the most widespread agreement.

The introduction of activated $p21^{ras}$ mutants into quiescent 3T3 cells rapidly leads to the activation of protein kinase C (PK-C, Morris et al., 1989) and this activation is known to be essential for $p21^{ras}$ - induced DNA synthesis (Morris et al., 1989 ; Lloyd et al., 1989a,b). In T-lymphocytes, the increase in $p21^{ras}$.GTP levels following receptor stimulation appears to be mediated by activation of PK-C which subsequently leads to an inhibition of GAP activity (Downward et al., 1990). The mechanism by which oncogenic $p21^{ras}$ activates PK-C is a matter of debate. Early studies suggested there may be an increase in PIP_2 breakdown in ras transformed cells (Fleischmann et al., 1986 ; Hancock et al., 1988). In contrast, other workers (Seuwen et al., 1988 ; Price et al., 1989) have been unable to detect differences in the rate of PI turnover after oncogenic transformation by $p21^{ras}$. Such apparent contradictions are not uncommon in the study of $p21^{ras}$ signal transduction ! Ras-transformed cells also show an increase in phosphatidyl choline (PC) breakdown (Lacal et al., 1987 ; Cabot et al., 1988). In NIH 3T3 cells at least, injection of PL-C can induce transformation (Smith et al., 1989) and $p21^{ras}$ probably acts as an upstream activator of PL-C (Smith et al., 1990).

The molecular basis for protein kinase C activation by $p21^{ras}$ remains obscure, but it does not seem likely that PK-C is constitutively activated in $p21^{ras}$ transformed cells (Wolfman and Macara, 1987). Finally, it appears that $p21^{ras}$ proteins are capable of producing responses through PK-C dependant and independent pathways (Cai et al., 1990, Downward et al., 1990). The PK-C independent pathway (activated by oncogenic $p21^{ras}$) will involve a kinase cascade, possibly including the Ser/Thr kinases products of the c-raf and c-mos proto-

oncogenes acting downstream of $p21^{ras}$ (Stacey et al., 1988 ; Feig and Cooper, 1988).

This brief survey of the considerable literature on the relationship between $p21^{ras}$ and the second messenger system gives some idea of the general air of confusion which seems to pervade the subject. Areas of agreement between different groups of workers seem to be rather limited, both in terms of general phenomena and in specific experiments. Activated $p21^{ras}$ in cells may have functions that are different, qualitatively and quantitatively, from those of the wild type protein in normal cells. It must be hoped that this is simply a reflection of the stimulation of the wild type, but not mutant, $p21^{ras}$.GTPase by the GTPase activating proteins.

1.10 The Kinetic Mechanism for the Intrinsic GTPase Activity of $p21^{ras}$.

A mechanism such as that shown in scheme 1.1 can be proposed to show the minimal number of steps for the GTPase activity, where nucleotide-free $p21^{ras}$ is represented by R (Neal et al., 1988).

$$R + GTP \overset{1}{\rightleftharpoons} R{\cdot}GTP \overset{2}{\rightleftharpoons} R{\cdot}GDP{\cdot}P_i \overset{3\ P_i}{\rightleftharpoons} R{\cdot}GDP \overset{4}{\rightleftharpoons} R + GDP$$

Scheme 1.1

Each step is numbered such that the forward and reverse rate constants for step i are k_{+i} and k_{-i} respectively. It should be noted that this scheme may be an over simplification of the GTPase mechanism since no conformational changes are included. The most likely mechanism for the hydrolysis of GTP is a direct in-line transfer of the terminal phosphate from GTP to water, and thus does not include a phosphoenzyme intermediate (Feuerstein et al., 1989 ; Webb, 1992). The rate of inorganic phosphate release (step 3 in scheme 1) is unknown. However, for the intrinsic GTPase mechanism, and for the GAP-activated mechanism up to GTP cleavage rates limited by manual mixing techniques ($\approx 0.05\ s^{-1}$) , then the rate of P_i

release is at least as fast as the rate of GTP cleavage (MR. Webb, A.E Nixon, unpublished results).

An important feature of the kinetic measurements performed by Neal et al (1988) and more recently by other groups is that individual elementary rate constants are measured by using single turnover conditions whereby stoichiometric 1:1 complexes of guanine nucleotides with $p21^{ras}$ are used. Under these conditions, the process of interest only occurs once on any given $p21^{ras}$ molecule, unlike multiple turnover experiments where the observed rate is a complex function of several individual rate constants.

In the absence of guanine nucleotides, $p21^{ras}$ is relatively unstable, being much more sensitive to thermal denaturation (Feuerstein et al., 1987a, but see Mistou et al., 1992). The association and dissociation rate constants have been measured using radiolabelled nucleotides and nitrocellulose filtration techniques (Feuerstein et al., 1987 ; Neal et al., 1988). Using these values, the equilibrium dissociation constant, K_d, has been calculated to be 7×10^{-13} M (0.7 pM) for GTP and 8×10^{-12} M (8 pM) for GDP at 37°C. These values are much higher than those estimated previously (10^{-7} - 10^{-9} M, Hattori et al., 1985 ; Sigal et al., 1986 ; Clanton et al., 1986 ; Feig and Cooper, 1988) although these early measurements were performed under conditions where the absolute value for the K_d could not be determined with accuracy (Goody et al., 1991). Whilst the kinetic approach to the measurement of equilibrium binding constants has its own limitations, when the experiments are performed carefully, it is generally superior to other equilibrium methods.

Using the fluorescent mant-derivatives of guanine nucleotides (Hiratsuka, 1983), the rate of nucleotide binding to $p21^{ras}$ has been investigated using stopped flow techniques (John et al., 1990). The most simple interpretation of the experimental results is that the binding of GTP and GDP occurs via a two-step mechanism ; an initial binding step followed by an irreversible protein conformational change. Based on a complex kinetic argument, the mechanism of nucleotide binding has been proposed to be even more complex than that described above (John et al., 1990) since the stopped flow data were incompatible with the filter binding studies. John et al., (1990) have proposed that nucleotide - free $p21^{ras}$ can exist in two con-

formations (R and R^*) where the stopped flow experiments preferentially monitor nucleotide binding to R whilst the filter binding experiments monitor nucleotide binding to R^*.

The elementary first order rate constant for the cleavage of GTP bound at the active site of $p21^{ras}$ is relatively slow ($\approx 10^{-4}$ s^{-1}, Neal et al., 1988) and at equilibrium, < 2% GTP is observed, suggesting that the equilibrium constant for the cleavage step is > 50. For single point mutants of $p21^{ras}$, the rate of GTP cleavage is usually significantly reduced, although the absolute rate depends on the particular mutant under study. For example, the GTP cleavage rate of the Asp 12 mutant is only 2-fold lower than that of the wild type protein (Neal et al., 1988), whilst the equivalent value for the Val 12 (Eccleston et al., 1991) and Leu 61 (Krengel et al., 1990) mutants of $p21^{ras}$ is 8-fold and 40-fold respectively. A well documented exception to this trend is that the Pro 12 mutant has a 2-fold *higher* GTP cleavage rate than the wild type protein (Colby et al., 1986 ; Gibbs et al., 1988) . A reduction in *intrinsic* GTPase activity is unlikley to be the sole determinant which defines the biological activity of the point mutants. The differential interaction of wild type and mutant $p21^{ras}$ proteins with upstream or downstream macromolecules (GAPs and exchange factors) are also likely to be affected by the point mutations.

These experiments measure only the rate of GTP cleavage and do not address the possibility of protein conformational changes in $p21^{ras}$ which may occur during the GTP cleavage reaction. Fluorescence spectroscopy has been used by several groups to probe for such conformational changes in solution. These experiments will be discussed in detail in chapters 4 and 10.

1.11 Experimental Approach and Aims of the Present Study.

The use of molecular biology, particularly site directed mutagenesis, has lead to the expression and purification of a wide range of mutant $p21^{ras}$ proteins. Some of these mutants have altered biological activities, notably with respect to their transforming potential *in vivo*. One of the main goals for the elucidation of the molecular basis for the observed phenotypes of these mutant proteins is to characterise them biochemically, both in terms of their structure and with respect to the mechanism and rate of their GTPase activities. The present study

will concentrate primarily on the second theme - the characterisation of the kinetic mechanism of the intrinsic- and GAP-activated $p21^{ras}$.GTPase for wild type and mutant proteins.

Whilst an investigation of the intrinsic GTPase of these proteins in the absence of other cellular factors (Neal et al., 1988) provides a basis for the kinetic experiments described here, they are unlikely to be directly applicable to the *in vivo* situation. A more complete understanding of the effect of point mutations *in vivo* requires an investigation of how the mutations affect not only the intrinsic kinetic properties of $p21^{ras}$ but also their effect on the interaction of $p21^{ras}$ with upstream (exchange factors) and downstream (GTPase activating proteins) modulators of $p21^{ras}$.

Based on these considerations the kinetic mechanism of the intrinsic and rasGAP activated GTPase of $p21^{ras}$ has been investigated. These studies aim to measure the rates of elementary processes and the equilibrium constants between successive steps in a pathway, and thus potentially allow the identification of the significant intermediates in the mechanism. The mechanism of the wild type protein is compared to that of several single point mutants of $p21^{ras}$, in order to identify differences that may correlate with the altered phenotype of these mutant proteins. These results of these studies will also be considered in light of the proposed model for the chemical mechanism of GTP hydrolysis based on X-ray crystallographic evidence. Finally, a comparison is made between the effect of NF1-GAP and p120-GAP on the intrinsic $p21^{ras}$ GTPase mechanism, since such studies may be able to provide further clues as to the *in vivo* function of these proteins and the relative importance of p120-GAP and NF1-GAP as negative regulators of $p21^{ras}$ function.

The main approach that has been used is fluorescence spectroscopy combined with single turnover kinetic procedures. This approach has the advantage that the kinetics of a specific step in the GTPase mechanism can be investigated (see sections 1.6.1 - 1.6.3). Due to the inherent sensitivity of fluorescence spectroscopy, changes in the environment of the fluorophore occurring during a particular step in the mechanism, which may be a result of a protein conformational change, can be monitored. This approach has proven useful in the study of the mechanism of other nucleoside triphosphatases such as the GTPase of elongation factor

Tu (Eccleston et al., 1981, 1985), and the ATPase of myosin subfragment 1 (Trentham et al., 1972, 1976). The overall aim of all of these studies is to determine how single point mutations within $p21^{ras}$ lead to the observed phenotype of these proteins, particularly with respect to their ability to lead to cell transformation.

CHAPTER TWO

MATERIALS AND METHODS

All of the reagents used were at least of Analar grade from Sigma or BDH unless otherwise stated.

2.1 Protein Purification

2.1.1 *$p21^{ras}$.GDP Proteins*

Wild type (Gly12) and mutant (Asp12 and Val 12) $p21^{N\text{-}ras}$ proteins were overproduced in an E.coli expression system (donated by Dr A. Hall, Chester Beatty Laboratories, Institute of Cancer Research, London. Hall et al., 1983 ; Hall and Brown, 1985) and initially purified as described (Hall and Self, 1986; Neal et al., 1988 ; Neal, 1989). However, the purification procedure was subsequently modified to improve the purity and yield of $p21^{ras}$ and is described in chapter 3.

Wild type (Gly12 Phe28) and mutant $p21^{Ki\text{-}ras\text{-}B}$ proteins (Gly 12 Trp 28; Val 12 Trp 28; Val 12 Phe 28; and Pro 12 Phe 28) were a generous gift from Dr P.Lowe (Department of Cell Biology, Wellcome Research Laboratories, Beckenham, Kent). These proteins were expressed in E.coli, truncated at the C-terminus (containing residues 1-166) and purified as described by Lowe et al (1991). Wild type (Gln 61) and double $p21^{H\text{-}ras}$ mutant (Ser 186 Leu 61) proteins were expressed and purified essentially as described for $p21^{N\text{-}ras}$ from expression systems donated by Dr Hall. Wild type truncated $p21^{H\text{-}ras}$ (residues 1 - 166) was a gift from Dr Lowe. Trp 35 and Trp 36 $p21^{H\text{-}ras}$ proteins (residues 1 - 167) were a gift from Dr S. Campbell-Burk (DuPont Chemical Company, Wilmington, USA).

2.1.2 *$p21^{ras}$ Apo-protein*

Nucleotide-free $p21^{N\text{-}ras}$ (apo-$p21^{ras}$) was prepared by hydrophobic interaction high performance liquid chromatography (HIHPLC) on a Spherogel TSK-Phenyl-5PW column (75 x 7.5 mm, Beckman) as described (Feuerstein et al., 1987a; Neal et al, 1988). The recovery of apo-p21 was only 10 - 15 % of the $p21^{ras}$.GDP loaded onto the column. Early preparations of $p21^{ras}$.GDP were also purified from other contaminant E.coli proteins using the same HIHPLC system except that the elution buffers contained 10 mM $MgCl_2$ rather than 10 mM EDTA.

2.1.3 *GTPase Activating Proteins*

2.1.3.1 The COOH - Terminal Fragment of p120-GAP.

Two p120-GAP constructs were used in these experiments, although both express only the COOH-terminal one third ($\approx$ 36 kD) of p120-GAP. This fragment of p120-GAP retains the ability to activate the $p21^{ras}$ GTPase mechanism (Marshall et al, 1989, Skinner et al., 1991).

(a) The first construct to be used (GAP_{365}, encoding residues 683 - 1047) was purified by Dr M. Webb (N.I.M.R) using a standard 2-column chromatography procedure from an E.coli expression system donated by Dr A. Hall as described (Moore et al., 1992b). The purification of this fragment required $\approx$ 5 days after which time it was typically 70 - 90 % pure and was available in relatively limited quantities (20 mg from a 4 L E.coli culture). This construct was used to prepare the GAP used for all of the kinetic measurements described in chapter 4.

(b) An alternative COOH - terminal GAP fragment (GAP_{344}, encoding residues 704-1047) was engineered to contain an additional tripeptide (Glu^{1048}-Glu-Phe^{1050}) at the COOH-terminus (expression system donated by Drs Skinner and Lowe, Wellcome Research Laboratories, Beckenham, Kent; Skinner et al., 1991). The additional tripeptide is the epitope for IgG (purified from ascites, Kilmartin et al, 1982) which has been attached to Sepharose by CNBr activation (Stammers et al, 1991) to produce an affinity column for this GAP construct

(Skinner et al., 1991). The GAP fragment was expressed in E.coli using a *tac* promoter (similar to that described by Lowe et al (1991)). 20 g wet weight of E.coli cells were sonicated in 25 mL of 10 mM Tris-HCl, pH 7.5, 50 mM NaCl, 0.1 mM EDTA, 1 mM PMSF (buffer D) and the cell debris removed by centrifugation at 40,000 rpm for 60 min in a 70.Ti rotor. The cell supernatant is diluted in buffer D to a protein concentration of 50 mg/mL (section 2.3.1), loaded onto a 15 mL Sepharose-anti-(Glu-Glu-Phe) affinity column (0.5 mL/min) and washed in buffer D (1 mL/min) either overnight or until the A_{280} of the eluent returned to a constant baseline value (typically < 0.1). GAP was eluted from the column in buffer D plus 10 mM Asp-Phe dipeptide (adjusted to pH 7.5 with NaOH) at 0.5 mL/min and was detected by SDS-PAGE (section 2.2) and dye binding protein assays (section 2.3.1). Pooled fractions were precipitated by the addition of ammonium sulphate to 78 % saturation at $4^{o}C$, centrifuged for 20 min at 10,000 rpm in a Sorvall RC5 rotor, and the pellet resuspended in 0.1 - 0.2 mL buffer C (20 mM TrisHCl, pH 7.5, 1 mM $MgCl_2$, 0.1 mM DTT), dialysed against 1000 mL of the same buffer overnight at $4^{o}C$ and stored at $-70^{o}C$. The whole purification procedure required only 24 hours. GAP_{344} was available in large quantities (typically 15 - 20 mg from 20 g E.coli cells) and was > 95 % pure by SDS-PAGE. The two preparations of GAP will be referred to as GAP_{344} or GAP_{365} throughout the thesis.

2.1.3.2 The p120-GAP Related Domain of NF1-GAP.

The gene encoding the fragment of NF1 which shows sequence homology to p120-GAP (the GAP related domain, residues 1195 to 1528, Marchuck et al., 1991) has been fused with the gene encoding glutathione transferase (GST) to form an NF1-GST fusion gene (expression system developed by Dr R. Skinner, Department of Cell Biology, Wellcome Research Laboratories, Beckenham, Kent). In addition, the Glu-Glu-Phe epitope (see above) was added at the COOH - terminus. This construct was inserted into E.coli and, in collaboration with Drs Skinner and Lowe, used to over-express the fusion protein, NF1-GST, which could subsequently be cleaved at the fusion site using thrombin to yield NF1 and GST.

The expression and purification of the GAP related domain of NF1 was achieved as described below. An E.coli starter culture was prepared by the inoculation of 6 mL of L-broth + ampi-

cillin (0.2 mg/mL) with ≈ 3 - 4 single colonies of E.coli cells containing the NF1-GST fusion gene which was grown overnight at 37°C with shaking at 200 rpm. 1 mL of this starter culture was added to 500 mL of the same medium and the cells grown in 2 L conical flasks at 37°C with shaking at 200 rpm. The A_{600} of the culture was monitored and when the O.D had reached 0.9 (≈ 4 hours), IPTG was added to each flask to a final concentration of 1 mM. These cells were grown overnight (17 hours) at 37°C with shaking (200 rpm), after which time the A_{600} was ≈ 1.8. The cells were pelleted by centrifugation for 20 min at 8000 rpm (Sorvall RC5) and resuspended in 25 mL of 50 mM TrisHCl, pH 7.5, 50 mM NaCl, 5 mM $MgCl_2$, 1 mM DTT, 1 mM PMSF. Approximately 7 g of cells were obtained using this growth procedure.

The cells were lysed by sonication at 4°C (Ultrasonics W-385, setting 7, 0.5" probe, 50% pulsing, 6 x 5 sec pulses) and after each sonication, 30 μL of the suspension was removed, spun for 1 min in a bench microfuge and 2 μL of the supernatant assayed for total protein concentration using the BIORAD assay (section 2.3.1). The concentration of protein in the supernatant reached a maximum value (≈ 45 mg/mL) after 4 sonication procedures, at which point cell lysis was considered to be complete. Cell debris was removed by centrifugation at 39,000 rpm for 70 min at 4°C in a Beckman 70 Ti rotor.

A 15 mL glutathione-sepharose column (700 mg, Sigma) was equilibrated at 4°C with 100 mL of MTPBS buffer (16 mM Na_2HPO_4, 4 mM NaH_2PO_4, 150 mM NaCl, pH 7.3) and the cell supernatant (≈ 25 mL) loaded at 0.3 mL/min. The column was washed with ≈ 50 mL of the same buffer at 0.5 mL/min. The concentration of protein in the fractions (fraction volume 3 mL) was determined using 1 μL of each fraction in the BIORAD total protein assay (section 2.3.1). After the protein concentration returned to baseline (<0.05 mg/mL), the NF1-GST fusion protein was eluted with 50 mL of 5 mM glutathione in MTPBS (corrected to pH 7.5 with NaOH) at 0.5 mL/min collecting 1.5 mL fractions. The protein concentration in each fraction was determined using 2 μL of each fraction as above. In addition, 10 μL of a 1:10 dilution of the fractions containing protein were analysed by SDS-PAGE (section 2.2).

The appropriate fractions containing the NF1-GST fusion protein were pooled (volume ≈ 10

mL) and 5 mM $CaCl_2$ plus 100 units of thrombin protease added to cleave the fusion protein to yield NF1 and GST. A white non-proteinaceous precipitate formed on the addition of the $CaCl_2$ which is likely to be due to the formation of the insoluble $Ca_3(PO_4)_2$. The cleavage reaction was performed at 30°C and followed either using SDS-PAGE or using the immunoprecipitation assay described below. The principle of this assay is that the fusion protein and free GST can be removed from the reaction solution with Sepharose-GSH whilst the NF1 released after cleavage with thrombin will be unaffected by this treatment. 2 μL of the reaction mixture ($\approx$ 18 μg protein containing 5 mM GSH) was diluted 350-fold into 700 μL of TMPBS buffer to give a final GSH concentration of $\approx$ 14 μM. 50 μL of packed Sepharose-GSH in 50 μL TMPBS buffer was added and mixed for $\approx$ 3 min, before centrifugation on a bench microfuge for 2 min. The supernatant (800 μL) was added to 200 μL of stock BIORAD protein assay reagent and the concentration of protein in the supernatant determined as described (section 2.4). This assay has the advantage that it can be performed in real time during the cleavage reaction since the assay requires only 5 min to perform. When the concentration of protein (predominately NF1) in the supernatant was unchanged with time (typically 160 - 180 min), the reaction mixture was spun at 6,000 rpm for 5 min in a Denby BS400 benchtop centrifuge. The supernatant ($\approx$ 11 mL) and the pellet were assayed for total protein by the BIORAD assay (section 2.3.1) which demonstrated that $\approx$ 97 % of the protein (132 mg) remained in the supernatant.

The thrombin was removed from the supernatant by immunoaffinity chromatography using an Anti-Thrombin / Benzamidine (ATB) agarose column. 100 mg of anti-thrombin was swollen in 2 mL of MTPBS buffer and added to 1 mL of Benzamidine - agarose matrix. The suspension was poured into a 4 x 60 mm column and washed in 30 mL of buffer C at 0.5 mL/min. The reaction supernatant was loaded onto and eluted from this column in the same buffer at 0.5 mL/min. The elution of protein from this column was followed with the BIORAD protein assay (2 μL fractions, section 2.3.1), and the appropriate fractions pooled (volume $\approx$ 16 mL, [protein] = 7 mg/mL).

The NF1 protein was purified from the reaction mixture of NF1 and GST by use of the Sepharose-GSH affinity column, to which only the cleaved GST will bind. For the GST to

bind to the GSH-affinity column, the concentration of free GSH in the protein sample (≈ 3.5 mM GSH) had to be significantly reduced. This was achieved by ammonium sulphate precipitation of the protein to 78 % saturation followed by centrifugation at 10,000 rpm for 10 min at 4°C (Sorvall, RC5 rotor), and resuspension of the pellet in 6 mL of buffer C. The estimated [GSH] in the resuspended pellet was << 0.1 mM whilst the protein concentration was measured to be ≈ 15 mg/mL by BIORAD assay. The sample (6 mL) was applied at 0.5 mL/min onto the Sepharose-GSH affinity column described above which have previously been equilibrated in buffer C. The column was washed with a further 20 mL of the same buffer at 0.5 mL/min, and 2 μL of each fraction (1 mL volume) assayed for total protein using the BIORAD assay. Appropriate fractions were pooled (volume ≈ 19 mL) and concentrated in an ultrafiltration cell (Amicon, 25 mm diameter YM10 membrane, 4°C, pressure = 4 bar) to 5 mL. BIORAD assays of the sample indicated a yield of ≈ 40 mg of NF1 from 7 g of cells.

2.2 SDS-Polyacrylamide Gel Electrophoresis.

Protein homogeneity was determined by polyacrylamide gel electrophoresis run in the presence of sodium dodecyl sulphate (SDS-PAGE, Laemmli, 1970). The resolving gels contained 15% w/v acrylamide, 0.087 % w/v N, N'-methylene bisacrylamide (bis acrylamide), 0.375 M TrisHCl, pH 8.8, 0.2 % w/v SDS, 0.03 % v/v TEMED, and 0.05 % w/v ammonium persulphate (APS). The stacking gel contained 5 % w/v acrylamide, 0.15 % w/v bis acrylamide, 0.21 M TrisHCl, pH 6.8, 0.1 % w/v SDS, 0.05 % v/v TEMED and 0.1 % w/v APS. The separation of constituent proteins in the sample was achieved by electrophoresis in 25 mM Tris base, 200 mM glycine and 0.1 % w/v SDS under constant current for ≈ 1 hr. Two alternative models of gel apparatus were used (Hoefer Scientific, San Fransisco, USA). The first used 0.5 x 90 x 94 mm gel plates and was run using the "Mighty Small" apparatus at a constant current of 16 ma per gel with tap water cooling. The alternative apparatus (model SE600 gel system) used 0.5 x 150 x 80 mm gel plates and was run at 65 ma per gel with thermostatically controlled water cooling at 4°C.

Samples were prepared by boiling for 5 minutes in sample buffer containing 2.5 mM TrisHCl, pH 6.8, 10 mM DTT, 2 % w/v SDS, 30% v/v glycerol and 0.005 % w/v bromophenol blue.

Typically, 15 μL of protein sample (containing 10 - 15 μg protein) was mixed with 50 μL of sample buffer, and after boiling $\approx$ 5 μg of protein loaded onto the gel. After electrophoresis, the gels were stained for 15 min at room temperature in 0.5 % w/v Coomassie Brilliant Blue R (Sigma), 10 % v/v acetic acid, and 50 % v/v methanol. The gel was then destained in 50 % v/v methanol, 10 % v/v acetic acid at room temperature or at 50^{o}C until the stained bands were clearly visible (typically 20 - 30 min at 50^{o}C). After destaining, the gels were stored in 10 % v/v glacial acetic acid, 10 % v/v methanol, 80 % v/v water. An estimation of the percentage purity of a given protein was achieved by scanning densitometry of the SDS-PAGE gel.

2.3 Protein Concentration Determination.

2.3.1 *The Bradford Technique.*

Total protein concentration was determined using a modified Bradford technique (Bradford, 1976) as described by Sedmark and Grossberg (1977) using bovine serum albumin (BSA) as standard. The Bradford assay reagent contained 0.06 % w/v Coomassie Brilliant Blue G250 in 3 % v/v perchloric acid and typically had an absorbance of $\approx$ 1.4 at 465 nm (the absorbance maximum for the leuko form of the dye). The absorbance maximum for the protein : dye complex was always 594 $\pm$ 1 nm. The concentration of BSA was determined spectrophotometrically since 1 mg/mL BSA has an absorbance of 0.66 at 280 nm. Individual assays contained 0.5 mL Bradford reagent and 0 - 100 μg of BSA in 0.5 mL of 0.85 % w/v NaCl. The solutions were left for 5 min at room temperature and the absorbance of each assay sample measured at 594 nm. The absorbance values varied approximately hyperbolically with the amount of BSA added. The sample of unknown concentration was treated in the same way as for the BSA standard and the absorbance readings for several dilutions of the stock sample were converted to an equivalent protein concentration using the BSA standard curve.

Alternatively, a commercially available Coomassie reagent (BIORAD protein assay reagent, BIORAD, USA) was used. In this assay, 0.2 mL of BIORAD reagent is mixed with 0 - 100 μg of protein standard (bovine serum albumin or bovine gamma-globulin) in water and made up

to a total volume of 1 mL with water. After 15 min at room temperature, the absorbance at 595 nm was determined, and was found to vary linearly with protein concentration up to ≈ 25 μg/mL. Using this assay, the colour yield with gamma-globulin is ≈ 1.8-fold greater than that with BSA. The concentration of the sample protein is determined exactly as described above in the previous paragraph.

2.3.2 *The Bicinchoninic Acid (BCA) Protein Assay.*

This assay utilises the ability of protein (at alkaline pH) to reduce Cu^{2+} to Cu^{1+} ions which can subsequently be detected with high sensitivity using the BCA reagent (Smith et al., 1985). The assay was performed using BSA as the standard and using the stock reagents supplied commercially (Pierce Chemical Co., Rockford, IL, USA). Incubations were typically performed for 2 hours at room temperature which gave a colour yield of ≈ 0.01 A_{562} / μg protein.

2.3.4 *Ultraviolet Absorption Spectroscopy.*

The protein samples (≈ 100 μL of 1 mg/mL) were applied to a PD-10 G25 Sephadex desalting column (Pharmacia) and eluted in the appropriate buffer, containing DTT which was added immediately prior to use. The absorbance of the fractions in the region 220 - 320 nm was determined using the fresh buffer as a blank. The absorbance readings were converted to protein concentrations using an extinction coefficient calculated from the absorbance of the constituent chromophoric amino acids (Phe, Tyr, and Trp) in the protein (Gill and von Hippel., 1989; Mach et al., 1992). At 276 nm, these values were 24 mM^{-1} cm^{-1} for wild type $p21^{N\text{-}ras}$, 15.55 mM^{-1} cm^{-1} for GAP_{344}, 19.32 mM^{-1} cm^{-1} for GAP_{365} and 31.72 mM^{-1} cm^{-1} for NF1.

2.3.4 *Quantitative Amino Acid Analysis.*

20 μL of $p21^{ras}$.GDP (containing ≈ 10 nmol of protein based on the Bradford assay) was hydrolysed in the gaseous phase by 6 M HCl at 110°C for 24 hours in a sealed tube, which

was subsequently opened and the sample evaporated to dryness at 110°C overnight. Quantitative amino acid analysis was performed according to the procedure of Moore and Stein (1948, 1954) on a Beckman 121MB analyser using ninhydrin derivatisation. The protein concentration was calculated from the known amino acid sequence using only the stable amino acids.

2.4 Assays For $p21^{ras}$.

2.4.1 *Total $p21^{ras}$ Concentration.*

The total protein concentration in the sample of $p21^{ras}$ was determined using the assays outlined in sections 2.3.1 - 2.3.3. For the simulated extinction coefficient of $p21^{ras}$ purified from E.coli, 1 mole of guanine nucleotide per mole of protein was assumed to be bound at the active site. The amino acid sequences of $p21^{N\text{-}ras}$ and $p21^{K\text{-}ras}$ quoted in Barbacid (1987) were used.

2.4.2 *Quantitative HPLC of $p21^{ras}$-Bound Nucleotides.*

The total concentration of guanine nucleotide in the sample of $p21^{N\text{-}ras}$ was determined by quantitative HPLC using an internal GTP standard of known concentration. The nucleotide was released from 100 μL of $\approx$ 0.5 mM $p21^{N\text{-}ras}$.GDP by acid precipitation using an equal volume of 10 % w/v perchloric acid and sample adjusted to pH 4.0 with 50 μL 4 M sodium acetate to stabilise the released nucleotide. The sample was spun for 3 min on a bench microfuge to remove denatured protein and 50 μL of the supernatant analysed for the released nucleotide (Webb and Eccleston, 1981). Nucleotides were eluted isocratically from a Whatman strong anion exchange column (SAX, 250 x 4.6 mm) at 1.5 mL/min with 0.5 M $(NH_4)H_2PO_4$ adjusted to pH 4.0 with HCl. The elution of guanine nucleotides was monitored by absorption at 254 nm, and under these conditions, GDP eluted with a retention time (RT) of $\approx$ 4 min and GTP had a RT $\approx$ 9 min. The areas of the peaks were calculated using a Hewlett-Packard 3390A integrator and compared to those from a sample of GTP co-loaded with the $p21^{N\text{-}ras}$.GDP sample to determine the concentration of nucleotide in the $p21^{N\text{-}}$

^{ras}.GDP. Corrections were made for the GTP in the sample of $p21^{N\text{-}ras}$.GDP ($\approx$ 15%) and for the GDP in the GTP standard ($\approx$ 3%). Since $p21^{ras}$ binds guanine nucleotides with a dissociation constant of $\approx 10^{-11}$ M (Neal et al., 1988 ; John et al., 1990), the total concentration of guanine nucleotide in the sample is expected to be equal to the total $p21^{ras}$ concentration. However, any other guanine nucleotide binding proteins present in the sample, such as E.coli elongation factor Tu, will give false positive readings in this assay.

2.4.3 *Active $p21^{ras}$ Concentration*

2.4.3.1 [^{3}H]GDP and [gamma-^{32}P]GTP Binding Assays for $p21^{ras}$.

The activity of $p21^{ras}$.GDP was determined from its ability to bind [^{3}H]GDP in a competitive binding assay described by Hall and Self (1986) but with several modifications. Briefly, 0.5 - 1 μM $p21^{N\text{-}ras}$.GDP was incubated with a 10-20 fold molar excess of [^{3}H]GDP (specific activity $\approx$ 1500 cpm/pmol, Amersham) in 50 mM TrisHCl, pH 7.5, 100 mM NaCl, 10 mM $MgCl_2$, 10 mM DTT (buffer B) for 180 min at 37^{o}C (reaction volume 50 μL). $p21^{N\text{-}ras}$.[^{3}H]GDP was separated from excess [^{3}H]GDP by either of two methods. Routinely, the sample was diluted to 0.85 mL with ice cold buffer A and filtered through nitrocellulose filters (0.45 μm pore size, HAWP Millipore), after which the filters were dried and counted in 0.5 % w/v Butyl-PBD in toluene. Alternatively, the undiluted sample (50 μL) was applied to Biogel P6 gel filtration column (20x0.9 cm) in buffer A, and 1.5 mL fractions were counted in 20 mL Beckman "Readysafe" scintillant. The counting efficiency of the [^{3}H]GDP was shown to be essentially the same as that counting in Butyl-PBD / Toluene. Ion exchange HPLC (section 2.4.2) of the sample of [^{3}H]GDP indicated that > 90% of the radioactivity eluted at the position expected for GDP. The [^{3}H]GTP binding assays were performed exactly as above.

A modification of this assay is to increase the rate of nucleotide exchange using EDTA and $(NH_4)_2S0_4$ (Hall and Self, 1986 ; Hoshino et al., 1987). The assays were performed as above except that the buffer contained 50 mM TrisHCl, pH 7.5, 20 mM EDTA, 200 mM $(NH_4)_2S0_4$, 10 mM DTT (fast exchange buffer), the incubation period was 5 min at room temperature, and the sample was made to 40 mM $MgCl_2$ after the exchange reaction was complete. Excess

nucleotide was removed by nitrocellulose or gel filtration as above.

The [gamma-^{32}P]GTP binding assay was performed essentially as described for the rapid exchange EDTA / $(NH_4)_2S0_4$ gel filtration assay except that the [^{3}H]GDP is replaced by [gamma-^{32}P]GTP ($\approx$ 400 cpm pmol^{-1}, Amersham).

2.4.3.2 p21^{ras} Assays Based on the Binding of Chromophoric GDP Analogues.

A novel assay for p21^{ras} was developed based on the binding of the chromphoric and fluorescent GDP analogue, 2'(3')-[O(-N-methylanthraniloyl)]-GDP (mantGDP, Hiratsuka, 1983). Mant-nucleotide analogues were prepared as described in section 2.5.1. A sample of p21^{ras}.GDP was stoichiometrically converted to the mantGDP complex by incubation of p21^{ras}.GDP for 5 min at room temperature with an equal volume of "2x fast exchange buffer" (100 mM TrisHCl, pH 7.5, 40 mM EDTA, 400 mM $(NH_4)_2S0_4$, 20 mM DTT) containing greater than a 20-fold molar excess of mantGDP over p21^{ras}. After the exchange reaction was complete, $MgCl_2$ was added to a final concentration of 40 mM and the complex separated from excess mantGDP by gel filtration on a PD-10 G25 Sephadex column in buffer B. The elution of the p21^{ras}.mantGDP complex could be monitored by visualisation of mant-nucleotide fluorescence under U.V light. The p21^{ras}.mantGDP peak was pooled in one fraction and the absorbance of the protein : nucleotide complex determined at 350 nm. Following the addition of excess GDP to a sample of p21^{ras}.mantGDP, there was no significant change in absorbance at 350 nm during the time course of mantGDP dissociation, suggesting that there is no change in extinction coefficient of the mant-chromophore at 350 nm upon binding to p21^{ras}. Consequently, the extinction coefficient of aqueous mantGDP at this wavelength (5.7 mM^{-1} cm^{-1}, Hiratsuka, 1983) was used to calculate the concentration of p21^{ras}.mantGDP. The concentration of the stock p21^{ras}.GDP was calculated from the ratio of the loading volume of the p21^{ras}.GDP to the eluting volume of the p21^{ras}.mantGDP (typically $\approx$ 800 μL) from the gel filtration column. Control experiments indicated > 95 % recovery of protein samples from the gel filtration column.

The limitation of this assay is the relatively low extinction coefficient of the mant chromophore (5.7 mM^{-1} cm^{-1} at 350nm), leading to a correspondingly low sensitivity of this assay. However, increased sensitivity can be achieved by measuring the concentration of the $p21^{ras}$.mantGDP sample down to $\approx$ 0.1 μM by the fluorescence intensity (excitation = 366 nm, emission = 442 nm) of the complex. In this procedure, the fluorescence intensity of the protein:nucleotide complex is compared to that of a standard curve of fluorescence intensity against $mantGDP_{(aq)}$ concentration, and the data are corrected for the 2.8-fold increase in fluorescence intensity of mantGDP upon binding to $p21^{ras}$ (Neal et al., 1990). This assay has also been used with mantGTP and mant-guanylylimidodiphosphate (mantGppNHp) and also with other chromophoric analogues of guanine nucleotides which have higher extinction coefficients than mant-nucleotides (section 2.5.2 - 2.5.3).

2.4.2.3 Phosphate Release Assays for Active $p21^{ras}$ Concentration.

The stochiometric binding of GTP by $p21^{ras}$ and its complete (>97%) hydrolysis to 1 mole of GDP and P_i per mole of $p21^{ras}$ provides the basis for this assay of $p21^{ras}$ concentration. Thus, determination of the concentration of P_i released during the hydrolysis of GTP should be equal to the *active* $p21^{ras}$ concentration since this assay requires the prior exchange of bound-GDP for exogenously added GTP. Since the intrinsic GTP hydrolysis rate is very slow (requiring $\approx$ 5 hours at 37°C to go to 95% completion), it is more convenient to accelerate the rate of GTP hydrolysis and P_i production using GAP.

Whilst there are several procedures for the measurement of inorganic phosphate (Fiske and Subbarow, 1925; de Groot et al., 1985; Banik and Roy, 1990), a novel continuous assay for P_i using absorbance spectrometry has recently been developed (Webb, 1992; Webb and Hunter, 1992). This assay is based on the reaction of a guanosine analogue, 2-amino-6-mercapto-7-methyl-purine ribonucleoside (methylthioguanosine, MESG), with inorganic phosphate catalysed by purine nucleoside phosphorylase (PNPase). The products of this reaction are ribose 1-phosphate and 2-amino-6-mercapto-7-methyl-purine, the latter of which shows an increased absorbance at 360 nm compared to that of the substrate, MESG in the pH range 6.5 - 8.5. At this wavelength, the change in extinction coefficient upon phosphorolysis is 11 mM^{-1}

cm^{-1} at pH 7.5 (Webb and Hunter, 1992). This assay is applicable only to $p21^{ras}$ proteins whose GTPase is stimulated by GAP since during the time course of the intrinsic GTP cleavage process, there is considerable spontaneous breakdown of the MESG substrate which also leads to an increase in absorbance.

The assay to measure wild type $p21^{ras}$ is as follows. The MESG used in this study was synthesised by Dr M.R Webb (N.I.M.R, Mill Hill, Webb, 1992). A solution of 2 - 20 μM $p21^{ras}$.GDP in 20 mM TrisHCl, pH 7.5, 1 mM EDTA is incubated with 6.3 mM GTP for 10 min at 30°C (total volume 100 μL, containing < 0.1 mM Mg^{2+} carried over with the $p21^{ras}$ solution). This step facilitates the stoichiometric exchange of protein-bound GDP for added GTP. The reaction is quenched by the addition of 0.1 M $MgCl_2$ to 2.5 mM and following the addition of 12.5 U/mL PNPase and 0.2 mM MESG, the absorbance is monitored at 360 nm. The GTP cleavage reaction is initiated by the addition of GAP to $\approx$ 1 μM and is typically complete within 5 min at room temperature. The concentration of $p21^{ras}$.GDP is calculated from the amplitude of the absorbance change during the reaction and using the change in extinction coefficient of 11 mM^{-1} cm^{-1} at 360 nm occurring upon phosphorolysis.

2.5 Preparation and Synthesis of Guanine Nucleotide Analogues.

2.5.1 *The 2'(3')-O-(N-methylanthraniloyl) Derivatives of Guanine Nucleotides.*

The 2'(3')-O-(N-methylanthraniloyl) (Mant) derivatives of GTP, GDP, GppNHp, and cGMP were prepared by direct acylation of the 2' and 3' hydroxyl groups of the ribose moiety with N-methylisatoic anhydride (Hiratsuka, 1983; Neal et al, 1990). The synthesis was performed as previously described (Hiratsuka, 1983; Neal et al., 1990) except that a 2-fold excess of N-methylisatoic anhydride (Molecular Probes, Oregon, USA) over guanine nucleotide was used. The crude reaction mixture was made to 0.2 M with triethylammonium bicarbonate, pH 7.2 (TEAB) and loaded onto a DEAE-Cellulose DE52 column (30 x 300 mm) equilibrated in the same buffer. The mant-nucleotides were eluted at 4°C with a linear gradient of TEAB (0.2 - 0.6 M, 3000 mL total volume) at 2 mL min^{-1}. Using this modified gradient system, the major impurities in the reaction mixture (unreacted guanine nucleotide and N-methylanthranilic

acid) eluted under the initial conditions of ionic strength (0.2 - 0.25 M TEAB). The mant-nucleotides were identified by absorption spectroscopy (A_{252} / A_{350} = 3.92) and ion exchange HPLC as described in section 2.4.2 except that the elution buffer contained 25% v/v MeOH. MantGDP and mantGTP eluted at ≈ 0.42 and ≈ 0.46 M TEAB respectively. The concentration of the mant-nucleotides was determined using the extinction coefficients determined by Hiratsuka (1983); ϵ_{252} = 22.3 mM^{-1} cm^{-1} ; ϵ_{350} = 5.7 mM^{-1} cm^{-1}. The original procedure which used a 1.5-fold excess of N-methylisatoic anhydride over guanine nucleotide gave yields of 35 - 40 % whilst using a 2-fold excess of anhydride, the yield of product was typically 60 - 70 %.

An additional by-product of these syntheses, 2', 3'-bis mant-nucleotides, containing a mant-moiety on both of the hydroxyl residues, eluted from the DE52 column at ≈ 0.55 M TEAB. These compounds had a higher retention time on ion exchange HPLC than the singly substituted nucleotides, and their A_{252} / A_{350} ratio was ≈ 2.7. In addition, they had a higher mobility (R_f) than mant-nucleotides on thin layer chromatography (see below). This by product was usually formed with ≈ 10 % yield, although became a considerable impurity (up to 40 %) when the ratio of N-methylisatoic anhydride over guanine nucleotide was increased to 3-fold.

Ion exchange HPLC analysis (see above) demonstrated that all of the mant-nucleotide analogues were > 98 % pure. This result was obtained when the elution was monitored at either 254 nm or 350 nm suggesting the absence of significant quantities of the parent guanine nucleotides in these samples. Alternatively, the parent nucleotides and their mant-derivatives were separated using the SAX ion exchange HPLC column and a linear gradient of MeOH from 0 - 25 % v/v in 0.5 M $NH_4H_2PO_4$, pH 4.0 at 1.5 mL min^{-1}. The mant-nucleotide samples were injected onto the column equilibrated in the phosphate buffer in the absence of MeOH and after 10 min the MeOH gradient was applied over 5 min. The parent nucleotides eluted before the onset of the gradient whilst the mant-derivatives eluted from the column in the presence of MeOH. No significant contamination (≈ 1%) of the parent nucleotides could be detected using this procedure. The analogues were further characterised by hydrolysis in 50 mM NaOH for 15 min at room temperature after which ion exchange

HPLC which demonstrated that they had been hydrolysed to the parent guanine nucleotide and N-methylanthranilic acid (identified by preparation of a standard by aqueous hydrolysis of N-methylisatoic anhydride).

The 2'- and 3'-isomers of mantGTP, -GDP, and -GMP were separated by reverse phase HPLC on a C18 Novapak (150 x 3.9 mm) column eluting isocratically at 2 mL/min with 100 mM potassium phosphate, pH 6.0, containing 4% v/v acetonitrile. Under these conditions, all of the 2' and 3' isomers of the mant-guanine nucleotides can be separated with near baseline resolution.

2.5.2 *2'(3')-O-(N-(2-aminoethyl)carbamoyl)Guanosine 5'-triphosphate.*

These ribose modified derivatives of guanine nucleotides provide the starting point for the synthesis of a range of different fluorescent nucleotides, which is based on work with adenine nucleotides (Cremo et al., 1990). This involves the formation of the 2'3' cyclic carbonate derivative of the nucleotide (Maeda et al., 1977) followed by reaction with an amine to yield the 2'(3')-O-carbamate derivative (Scheme 2.1). This derivative possesses a primary amino group separated from the ribose moiety by a spacer arm, which varies in length depending on the amine used. These derivatives allow the synthesis of a wide range of fluorescent nucleotide analogues by reaction with commercially available amine-reactive fluorophores.

The 2'(3')-O-(N-(2-aminoethyl)carbamoyl)- derivative of GTP (ethylene diamine GTP, ED-GTP) was prepared as follows. 520 μmole of the trisodium salt of GTP was applied to a DEAE-cellulose DE52 column converted to the bicarbonate form with TEAB, and after washing with $\approx$ 500 mL of water at 2 mL min^{-1}, the GTP was eluted with 0.6 M TEAB as the triethylammonium salt. The pooled fractions were evaporated to dryness *in vacou* at 35^{o}C and the sample washed with 3 x 100 mL MeOH to remove residual TEAB. Tributylamine (2 mmole, 0.48 mL) was added to convert the sample to the tributylammonium salt and was made anhydrous with three washes with $\approx$ 50 mL dry dimethylformamide (DMF). The nucleotide ($\approx$ 500 μmole, compound I in Scheme 2.1) was dissolved in 8 mL of dry DMF to which was added 2.5 mmole (0.405 g) of N,N'carbonyldiimidazole (CDI). This solution was

Scheme 2.1 : Synthesis of 2'(3')-O-(N-(2-aminoethyl)carbamoyl) guanosine 5'-triphosphate (ED-GTP).

The synthesis of ED-GTP (compound IV) was performed as described in the text.

Compound I : Guanosine 5'-triphosphate (GTP).

Compound II : : The phosphorylimidazolidate of the 2'3' cyclic carbonate derivative of GTP.

Compound III : The phosphoramidate derivative of ED-GTP.

Compound IV : 2'(3')-O-(-(2-aminoethyl)carbamoyl) guanosine 5'-triphosphate (ED-GTP).

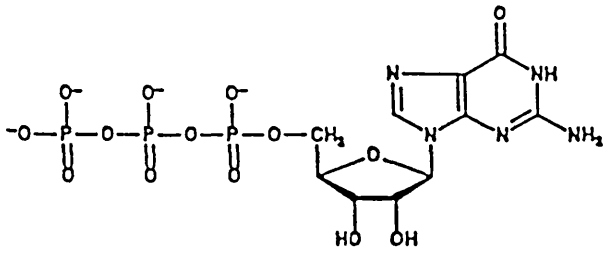

I

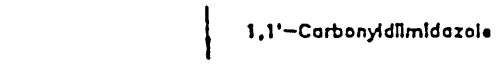

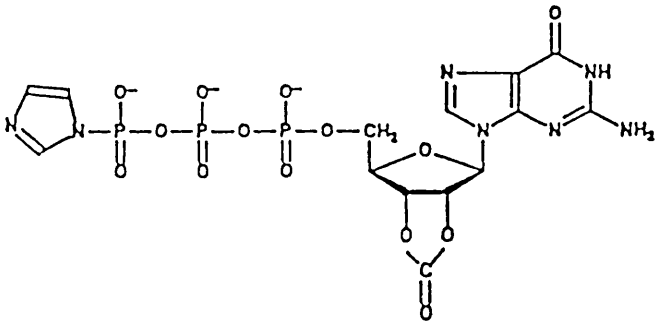

II

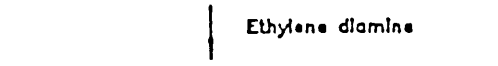

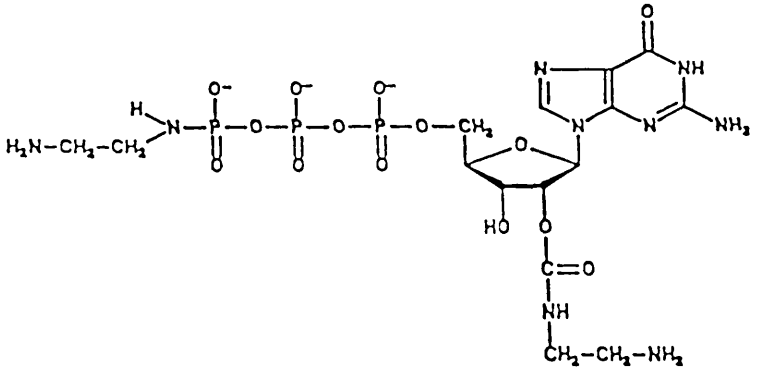

III

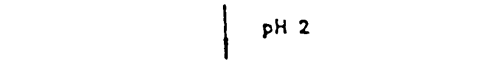

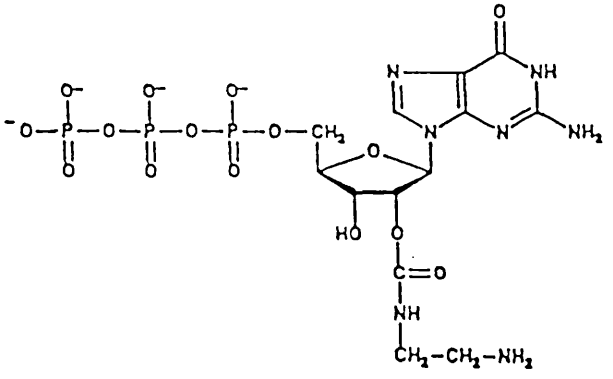

IV

stirred for 6 hours at $4^{o}C$ to yield the phosphorylimidazolidate of the 2'3'-cyclic carbonate derivative of GTP (compound II). Unreacted CDI was quenched with 3.6 mmole (144 μL) of absolute methanol, 2.5 mmole (167 μL) of ethylene diamine (diluted in 5 mL dry DMF) was added dropwise to this solution, and the reaction mixture left for 30 min at room temperature to form the phosphoramidate derivative of ethylene diamine GTP (compound III). The white precipitate which formed was obtained by centrifugation, washed 3 times with $\approx$ 20 mL dry DMF, and dissolved in 30 mL water. This sample was adjusted to pH 2.0 with concentrated HCl and left for 16 hours at $4^{o}C$ to displace the imidazole moiety of the terminal phosphate (compound IV). Ion exchange HPLC analysis (see section 2.5.1) showed that ED-GTP had been formed with a yield of $\approx$ 60 %. The product was purified by applying to a DE52 bicarbonate column (30 x 4 cm) eluting with a linear gradient of TEAB, pH 7.6 from 0.01 - 0.6 M (3000 mL total volume) at $4^{o}C$. ED-GTP eluted at $\approx$ 0.38 M TEAB, was identified by ion exchange HPLC, concentrated by rotoevaporation, washed with 3 x 50 mL MeOH, resuspended in water and stored at $-20^{o}C$.

Purified ED-GTP was found to elute from the HPLC column as a doublet of peaks (peak 1 comprising 60 % of the total A_{252}) which could be resolved with near baseline resolution by reducing the $NH_4H_2PO_4$ concentration to 0.3 M. The compounds eluting in these peaks were found to be stable by HPLC at pH 4.0 but both were converted to the starting mixture yielding 2 peaks on HPLC at higher pH ($t_{1/2}$ $\approx$ 4 hours at pH 7.0, $20^{o}C$). These observations suggest that the doublet represents the separation of the 2' and 3' isomers of ED-GTP, the re-equilibration of which is base catalysed.

The 5'-diphosphate ethylene diamine derivative (ED-GDP) was either prepared exactly as described for ED-GTP starting from GDP or by digestion of ED-GTP with myosin subfragment 1 in 20 mM TrisHCl, pH 7.5, 5 mM EDTA. In the latter case, the reaction was monitored using the HPLC system described above and when the reaction was deemed complete, the protein was removed by acid precipitation using Dowex-H^{+}, followed by centrifugation. The supernatant was made to 10 mM with TEAB and purified as described above for ED-GTP.

2.5.3 *Other Fluorescent 2'(3')-O-carbamoyl GTP Derivatives.*

The thiourea conjugate between fluorescein and the 2'(3')-O-(N-(2-aminoethyl)-carbamoyl) derivatives of GTP and GDP were prepared by Dr Eccleston using a general procedure developed for the synthesis of a range of ED-GTP analogues (K.M & JFE, unpublished syntheses). Briefly, 1 mM ED-GTP or ED-GDP in 20 mM $NaHCO_3$ was reacted with an equal volume of 5 mM fluorescein isothiocyanate (isomer 1, Molecular Probes) in acetone. After 3 hours at room temperature, thin layer chromatography [Merck Silica gel 60 F254, buffer: n-butanol, water, ammonia (70:20:10)] showed the formation of a new fluorescent spot which remained at the origin. The products were purified by DE52 bicarbonate chromatography at 4^oC as described above. The 2'(3')-O-[N-(7-dimethylamino-4-methylcoumarin-3-yl)carbamoyl derivative was prepared by Dr Eccleston using similar procedures. The 2'3' cyclic carbonate of GTP (section 2.5.2) was reacted directly with a 5-fold excess of 3-amino-7-dimethylamino-4-methylcoumarin (gift from Dr J.E.T Corrie, N.I.M.R; Corrie., 1990) in dry DMF for 3 days at 20^oC. TLC analysis and purification of the product was performed as described above. In addition to the ED-derivatives of GTP (described above), the hexamethylenediamine (HMDA) analogue (gift from Dr C Cremo, Washington State University, USA), which has a longer 6 carbon spacer arm between the ribose moiety and the primary amino group, was available. The fluorescein derivative of this analogue was synthesised by Mr C.Davis (N.I.M.R, Mill Hill, London) using the same procedure described for the ED-derivatives.

2.6 Preparation of $p21^{N\text{-}ras}$-Nucleotide Complexes.

The nucleotide state of $p21^{ras}$ was routinely changed by a direct exchange of bound GDP for exogenously added nucleotide in the presence of EDTA and $(NH_4)_2S0_4$ followed by gel filtration to remove excess nucleotide essentially as described for the Mant-assay. Alternatively, nucleotide-free $p21^{N\text{-}ras}$ was prepared by hydrophobic interaction HPLC (section 2.1.2) and a two-fold molar excess of the desired nucleotide added to the apo-protein. Unbound nucleotide was removed by gel filtration on a Biogel P6 column.

2.7 Measurement of the Relative Dissociation Constants of Nucleotides to $p21^{N\text{-}ras}$.

The binding affinity of nucleotide analogues to $p21^{N\text{-}ras}$ relative to GDP (K') under the conditions of rapid exchange (20 mM EDTA and 200 mM $(NH_4)_2SO_4$) was determined by a competitive binding experiment with [^{3}H]GDP essentially as described by Neal et al (1990). In these experiments, the incubation was for 5 min at room temperature. The data were analysed by a non-linear least squares procedure (Edsall and Gutfreund, 1983).

2.8 Fluorescence Measurements

2.8.1 *Steady State Fluorescence Measurements*

Fluorescence spectra and slow time course (down to $\approx$ 60 sec) measurements were made with a thermostated SLM 8000 photon counting spectrofluorimeter using 4 or 10 mm path length quartz cuvettes (Hellma). Data collection was made on HP 86 series or IBM computers for fast reactions or manually for slower time courses. The sample was protected from the excited light when readings were not being taken. Mant fluorescence was monitored with excitation at 366 nm (excitation slits 0.5 - 4 nm) and emission either through a monochromator at 442 nm (emission slits 4 nm) or through a Schott KV399 cut off filter. The fluorescence intensity of the sample cuvette was corrected for fluctuations in lamp intensity and/or photomultiplier tube efficiency by the use of a second, control cuvette of mantGDP. Using this system, the noise level was ca. 0.1% between points for rapid time courses ($t < 30$ min) and $< 1\%$ over 6 hours. Before readings were taken, the temperature of the solution had reached to within 0.1^{o}C of the final temperature. When a rapid thermal equilibration of the sample was required, this was achieved by dilution of a small volume of a concentrated solution of the stock sample (at 4^{o}C) into a much larger volume of buffer either at, or slightly above, the final working temperature (30^{o}C). The time taken for the equilibration using this procedure was typically 1 - 2 min, whilst $\approx$ 10 min were required when the complete sample (especially in the 10 mm path length cuvettes) was warmed from 4^{o}C. The use of the dilution procedure has lead to the identification of an additional process occurring rapidly after $p21^{ras}$ was warmed to 30^{o}C.

2.8.2 *Stopped Flow Spectrofluorimetric Measurements.*

2.8.2.1 Instrumental Design.

For faster time courses, a thermostatically controlled miniature stopped flow apparatus was used based on the design described by Eccleston (1987). Polychromatic light was produced by a Gates power supply (New York, USA) and an Oriel lamp housing (Connecticut, USA) containing a 100 W mercury arc lamp run at 5 A current. Monochromatic light was obtained using appropriate interference, bandpass or cut off filters (see below). The two reactant syringes (0.25 mL, 1725 C series, Hamilton) were pushed using a pneumatic pressure system (6 bar) and turbulent flow was achieved using a simple T-shape mixing chamber. Fluorescence from a quartz 10 x 1 x 1 mm flow through observation cell was monitored at 90^{o}C to the exciting light through suitable optical filters. The flow stopped when the back syringe (0.5 mL, 1750 C series, Hamilton) hit a metal block containing a trigger switch to initiate recording a short period before flow was arrested. Fluorescence emission was detected using a photomultiplier tube (high voltage range 300 - 400 V), the output of which was passed through a current - voltage converter, amplified (University of Pennsylvania, Biomedical Workshop) and the final signal collected on an oscilloscope (Nicolet 3091). Reaction traces were obtained with an instrumental time constant which was always less than 10% of the half time of the reaction of interest. The data were transferred to a HP86 computer and analysed using non-linear least squares fitting procedures (Edsall and Gutfreund, 1983).

2.8.2.2 Characterisation of the Stopped Flow Apparatus.

The stopped flow instrument was initially characterised using test reactions to determine the mixing efficiency of the T-chamber and the effective dead time of the apparatus. The latter parameter is the time taken for the solution in the mixing chamber to reach the observation cell. Since this is often of a similar magnitude to the half time of the reaction of interest, this delay reduces the observed amplitude of the reaction since a proportion of the reaction will have already occurred before observation starts. A suitable test reaction for fluorescence linked stopped flow is the quenching of the indole fluorescence of N-acetyl-tryptophanamide

(NATA) by reaction with N-bromo-succinamide (NBS). Indole fluorescence is monitored through UG-11 and WG-320 (Wratten and Kodak Eastman respectively) filters whilst exciting light is passed through a Corion G25-280 interference filter. 54 μM NATA in 50 mM NaH_2PO_4, pH 7.3 is mixed with 600 μM NBS in the same buffer at 23^{o}C and the exponential decay in fluorescence intensity monitored with time. The rate constant for this process was 93.4 s^{-1}. Extrapolation of the best fit line through the data to the starting fluorescence intensity of 27 μM NATA, yields the effective dead time of the instrument (at a negative value, Eccleston, 1987) which was determined to be 1.8 ($\pm$ 0.3) ms.

The second parameter to be determined is the mixing efficiency of the T-chamber which can be measured readily using fluorescent pH indicators. Since protonation reactions are instantaneous on the stopped flow time scale, the reaction of such indicators with either H^+ or OH^- should show no evidence of time dependence - the reactants should be uniformly mixed before reaching the observation cell. In these experiments, 4-methyl-umbelliferone (4-MeU) fluorescence was monitored through an S-10-440-S (Corion) filter whilst polychromatic exciting light was passed through a P10-365 filter (Corion). 10 μM 4-MeU in 100 mM NaH_2PO_4, pH 9.0 was mixed with 100 mM NaH_2PO_4, pH 6.0 at 23^{o}C and the fluorescence intensity of the indicator monitored with time. Such experiments indicated no change in fluorescence intensity over a period of 20 ms after mixing.

The instrument was also characterised with respect to the conditions required to change the composition of reactants in the observation cell. This is a significant problem because at the end of the sequence of reaction pushes (at a given reactant concentration) there is a finite volume of the reactants left in the syringes. Consequently, when the reactant concentration in the loading vial is changed, this will not lead quantitatively to a corresponding change in the syringe concentrations. To investigate this problem, the reaction of NATA with NBS was used (see above). 54 μM NATA was initially pushed against phosphate buffer to ensure that the reactant syringes were completely equilibrated with these reactants. The time dependence of the fluorescence intensity after mixing was recorded. At the end of the reaction, the reactant vial containing buffer was replaced with 400 μM NBS, and this solution introduced into the reaction syringe. The indole fluorescence of NATA was then quenched by reaction

with NBS and the dependence of the rate and amplitude of the fluorescence decay on the number of reaction pushes performed since changing one solution to NBS was determined. It was observed that after three reactions, the rate of the fluorescence change remained constant. Therefore, for all of the stopped flow experiments described in this thesis, the data are from the 4^{th} and subsequent reaction traces.

2.9 Measurement of the Elementary Rate Constants of the $p21^{ras}$.GTPase.

The rate of mantGTP cleavage (k_{+2}), mantGTP dissociation (k_{-1}) and mantGDP dissociation (k_{+4} in scheme 1) at $30^{o}C$ were measured essentially as described by Neal et al., (1990). Protein concentrations were based on the mant-assay (section 2.4.3.2) rather than using the [^{3}H]GDP binding assay (section 2.4.3.1). Additional modifications to these procedures included the preparation of the protein : nucleotide complexes by direct exchange (section 2.6) and the elution of mant-nucleotides from the ion exchange H.P.L.C column was monitored in real time with a Hitachi F-1050 flow through spectrofluorimeter linked to a Hewlett Packard 3390 A peak integrator. Between 0.1 - 0.3 nmoles of mant-nucleotides were loaded onto the column and elution was monitored with an instrumental sensitivity of 1-2 on the fluorimeter (excitation = 366 nm, emission = 442 nm).

The rate of GTP cleavage was determined by two methods. For slow time courses (generally > 20 min), the release of isotopically labelled $^{32}P_i$ (400 cpm $pmol^{-1}$, Amersham) from the $p21^{ras}$.[gamma-$^{32}P_i$]GTP complex (15 μM) was determined by nitrocellulose filtration. For faster time courses, the rate of P_i release was determined using the continuous phosphate release assay described by Webb, (1992) and Webb and Hunter (1992).

CHAPTER THREE:

PROTEIN PURIFICATION AND CHARACTERISATION

"However, it is not enough to know only that there is protein in our test tube - we need to know how much is present. Surprisingly, developing a quantitative assay for such enzymes is not as simple as might be expected."

(Manchester, (1951)) in "Biochemistry Today"

3.1 - Introduction.

The biophysical and biochemical study of $p21^{ras}$ described in this thesis requires relatively large quantities of protein material. Since the expression levels of $p21^{ras}$ *in vivo* are extremely low (yielding microgram amounts of $p21^{ras}$ from one purification procedure), the gene for the three $p21^{ras}$ proteins has been cloned and inserted into and purified from, E.coli (Gross et al., 1985 ; Hall and Self, 1986 ; Hall and Brown, 1985 ; Tucker et al., 1986, Lowe et al., 1991). From these expression systems, tens of milligrams of protein were obtained, predominantly as the Mg^{2+}.GDP complex. Whilst E.coli expressed $p21^{ras}$ proteins lack the lipid covalently attached to the COOH-terminus, they do appear to be biologically active when injected into mammalian cells (Bar-Sagi and Feramisco, 1986 ; Feramisco et al., 1984 ; Stacey and Kung, 1984). The explanation of this effect is the observation that the E.coli expressed proteins are substrates for the mammalian lipid modification system (Magee et al., 1987).

In this chapter, the procedures developed for the purification of $p21^{ras}$ and its subsequent biochemical characterisation are described. The E.coli expression system (donated by Dr A.

Hall, Institute for Cancer Research) contains both the gene for $p21^{N\text{-}ras}$ and also that which yields an ampicillin resistant phenotype of the transformed E.coli strain (strain GC42). The $p21^{ras}$ gene is under the control of the *trp* promoter and can therefore be induced to express $p21^{ras}$ after the addition of the tryptophan analogue, 3ß-indole acrylic acid (IAA, Hall and Self, 1986). The same purification and characterisation procedures are used for all of the three $p21^{ras}$ gene products and also for several single point mutants of these proteins. The procedures for the preparation and growth of the E.coli cultures (typically on a 40 litre scale) were usually identical to those described by Hall and Self (1986), although throughout the course of these studies, the subsequent purification procedure was extensively modified as described below.

3.2 Purification of $p21^{ras}$.GDP from *E.coli.*

Previous procedures for the purification of $p21^{ras}$ from E.coli (Hall and Self, 1986 ; Neal et al., 1988) yielded protein which was only 80 - 85 % pure (Neal, 1989). Protein impurities in these preparations included the bacterial GTP-binding protein (elongation factor Tu (EF-Tu)) and adenylate kinase (Neal, 1989). The presence of these impurities would complicate the interpretation and analysis of both equilibrium binding and kinetic experiments.

In the experiments described by Neal et al., (1988, 1990), these impurities were removed since the hydrophobic interaction HPLC procedure used to prepare the desired $p21^{ras}$.nucleotide complex (Feuerstein et al., 1987b) also afforded an additional purification step. However, the yields of $p21^{ras}$ after elution are typically only 10 - 15 % even when $\approx$ 10 mg of protein is used. In addition, the procedure is time consuming, requiring a minimum of 3 - 4 hours before the kinetic experiment can be started. However, an alternative procedure for the preparation of different protein : nucleotide complexes which offers no additional purification step has been developed (section 2.6). Thus, the methodology for the initial purification of $p21^{ras}$ from E.coli has been modified to remove both adenylate kinase and EF-Tu impurities. The $p21^{ras}$ obtained by this procedure is typically 95 % pure, and the yields are $\approx$ 50% higher than obtained compared with the procedure of Neal et al., (1988).

3.2.1 *The Purification Procedure.*

The growth of the E.coli strain, GC42, on a 40 litre scale and the expression of $p21^{ras}$ by these cultures was essentially that described previously (Hall and Self, 1986 ; Neal et al., 1988 ; Neal, 1989). A typical growth yielded ≈ 200 g wet weight of cells. On one occasion, the cells were grown overnight with a glucose feed system which produced ≈ 8 times the cell mass. In this case, the cells were divided into 200 g aliquots and frozen at -70°C until broken for purification of $p21^{ras}$. A 200 g aliquot of cells was resuspended and broken in 200 mL of 50 mM TrisHCl, pH 8.0, 1 mM $MgCl_2$, 10 mM DTT, 1 mM PMSF using a French press apparatus. The cell debris was pelleted in a Sorvall RC-3B centrifuge at 10,000 rpm for 20 min at 4°C. The supernatant was removed (conductivity ≈ 3 mmho, pH 6.8) and loaded directly onto a Q-Sepharose fast flow ion exchange column (400 mL, 4.5 cm x 25 cm) pre-equilibrated in 20 mM TrisHCl, pH 7.5, 20 mM NaCl, 1 mM $MgCl_2$, 10 mM DTT, 1 mM PMSF (conductivity = 2.5 mmho) at 3.5 mL min^{-1}. The column was washed with ≈ 700 mL of the same buffer until the A_{280} of the eluent returned to baseline absorbance (typically < 0.2). Protein was eluted with a linear NaCl gradient in the above buffer from 20 mM to 250 mM NaCl (Figure 3.1). Fractions were assayed for $p21^{ras}$ activity using the rapid exchange [^{3}H]GDP binding assay and the appropriate fractions pooled (peak activity at ≈ 130 mM NaCl). Under these conditions of ionic strength, elongation factor Tu does not elute during the gradient 20 - 250 mM NaCl, although it can be eluted with higher ionic strength buffer. Pooled fractions were made to 65 % saturation with ammonium sulphate, the pH of the sample adjusted to 7.5 with M TrisHCl, pH 8.5, and GDP added to a final concentration of 100 μM. The proteins were left to precipitate for 90 min at 4°C and then pelleted for 30 min at 4,400 rpm in a Sorvall RC5B rotor at 4°C. The solid pellet was resuspended in the low salt equilibration buffer used for the Q-Sepharose column (total volume 44 mL) and loaded onto an ACA44 gel filtration column (980 mL, 2.5 cm x 200 cm) at 0.35 ml min^{-1}. $p21^{ras}$ was eluted in the same buffer at 0.35 mL min^{-1} (Figure 3.2). Fractions 50 - 85 were assayed for [^{3}H]GDP binding activity and by SDS-PAGE. Fractions 70 - 83 were pooled (volume ≈ 120 mL), made to 10 mM DTT, and concentrated in an Amicon YM10 ultrafiltration apparatus to 12 mL. Aliquots (100 μL and 200 μL) were rapidly frozen and stored at -70°C until use. The DTT concentration was assayed using the DTNB colour test (Ellman, 1959) throughout

Figure 3.1 Elution of $p21^{ras}$.GDP from the Q-Sepharose Ion Exchange Column.

The supernatant from the crude E.coli cell extract ($\approx$ 600 mL in 50 mM TrisHCl, pH 8.0, 1 mM $MgCl_2$, 10 mM DTT, 1 mM PMSF; final pH = 6.8, conductivity = 3 mmho) was loaded onto a 400 mL (25 cm x 4.5 cm) Q-Sepharose fast flow ion exchange column pre-equilibrated in 20 mM TrisHCl, pH 7.5, 20 mM NaCl, 1 mM $MgCl_2$, 10 mM DTT, 1 mM PMSF (conductivity = 2.5 mmho) at 3.5 mL min^{-1}. The column was washed with $\approx$ 700 mL of the same buffer. At fraction # 75, a linear gradient of NaCl from 20 mM to 250 mM NaCl was applied (total volume = 3000 mL in 20 mM TrisHCl, pH 7.5, 1 mM $MgCl_2$, 10 mM DTT, 1 mM PMSF). Protein was eluted at 2.8 mL min^{-1} collecting 6 min fractions and the absorbance of the eluent determined at 280 nm. At the end of the gradient, the concentration of NaCl was stepped to 1 molar final concentration in the same buffer. SDS-PAGE and [^{3}H]GDP binding assays were used to detected the elution of $p21^{ras}$. The pool of $p21^{ras}$ was from fractions 130 - 175, corresponding to a [NaCl] of 100 - 160 mM NaCl.

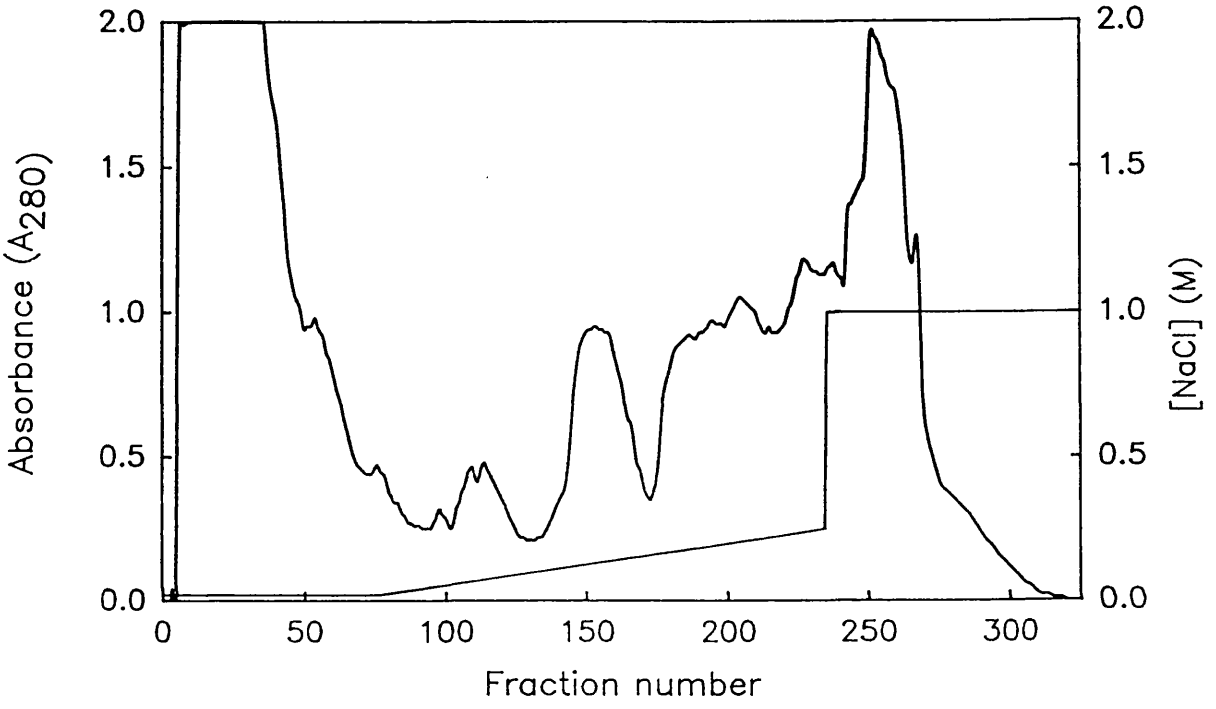
2.0
1.5
1.0
0.5
0.0
Absorbance (A_{280})
0
50
100
150
200
250
300
Fraction number
[NaCl] (M)

Figure 3.2 Elution of $p21^{ras}$.GDP from the ACA44 Gel Filtration Column

(A) The pellet from the ammonium sulphate precipitation of $p21^{ras}$ was resuspended in 44 mL of 20 mM TrisHCl, pH 7.5, 20 mM NaCl, 1 mM $MgCl_2$, 10 mM DTT, 1 mM PMSF and loaded onto a 980 mL ACA44 gel filtration column (200 cm x 2.5 cm) at 0.35 mL min^{-1}. The sample was washed onto the column with 3 x 15 mL of the same buffer and protein eluted at the same flow rate. Protein elution was monitored by absorbance at 280 nm, and $p21^{ras}$.GDP identified by SDS-PAGE (Figure 3.2.b) and [^{3}H]GDP binding assays. Fractions containing $p21^{ras}$ (70 - 83 inclusive, elution volume between 615 & 720 mL) were pooled, made to 10 mM DTT, concentrated by ultrafiltration, and stored at -70^{o}C.

(B) Elution of $p21^{ras}$.GDP was monitored by SDS-PAGE (section 2.2). 10 μL of the appropriate fractions (from 50 - 84) were prepared for electrophoresis as described (section 2.2). $p21^{ras}$.GDP was identified using an authentic $p21^{ras}$.GDP marker. The elution of $p21^{ras}$.GDP monitored by SDS-PAGE corresponded with the peak in absorbance at 280 nm and with the peak in [^{3}H]GDP binding activity.

(C) SDS-PAGE analysis of the final sample of $p21^{ras}$.GDP (5 μg) purified using this procedure. Densitometric scanning of the Coomassie stained gel suggested < 5 % protein impurity. No proteins with a mobility expected for EF-Tu could be detected by this technique, even when the gel was overloaded 10-fold (50 μg).

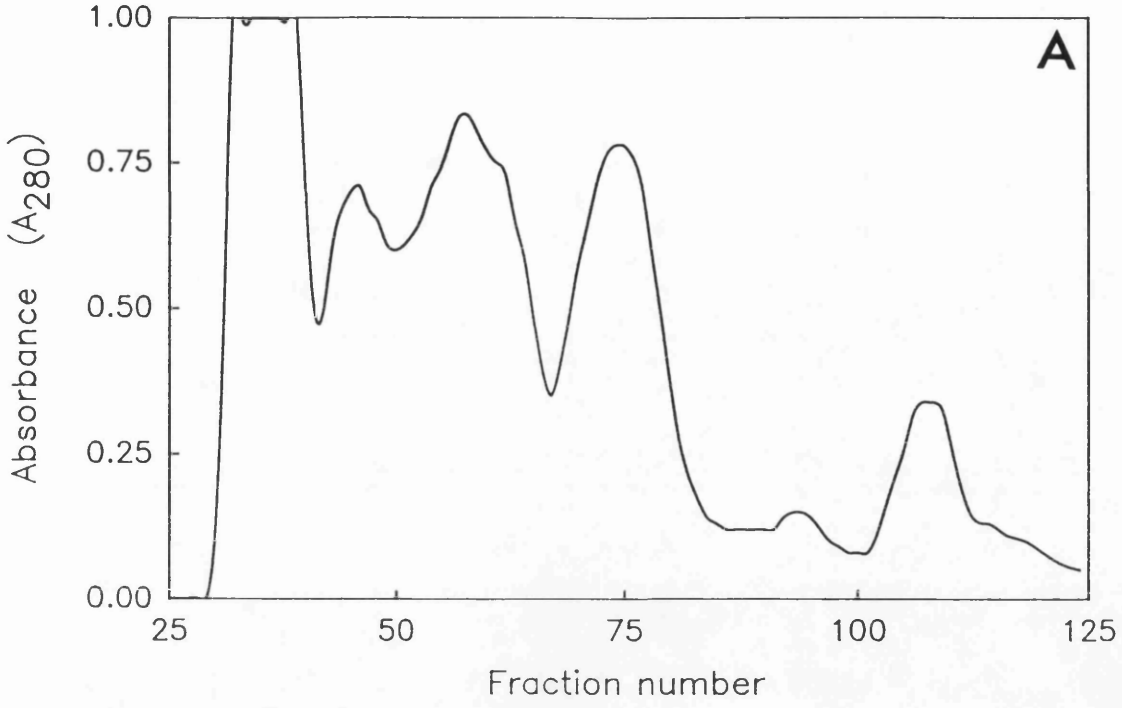
A
1.00
0.75
0.50
0.25
0.00
Absorbance (A280)
25
50
75
100
125
Fraction number

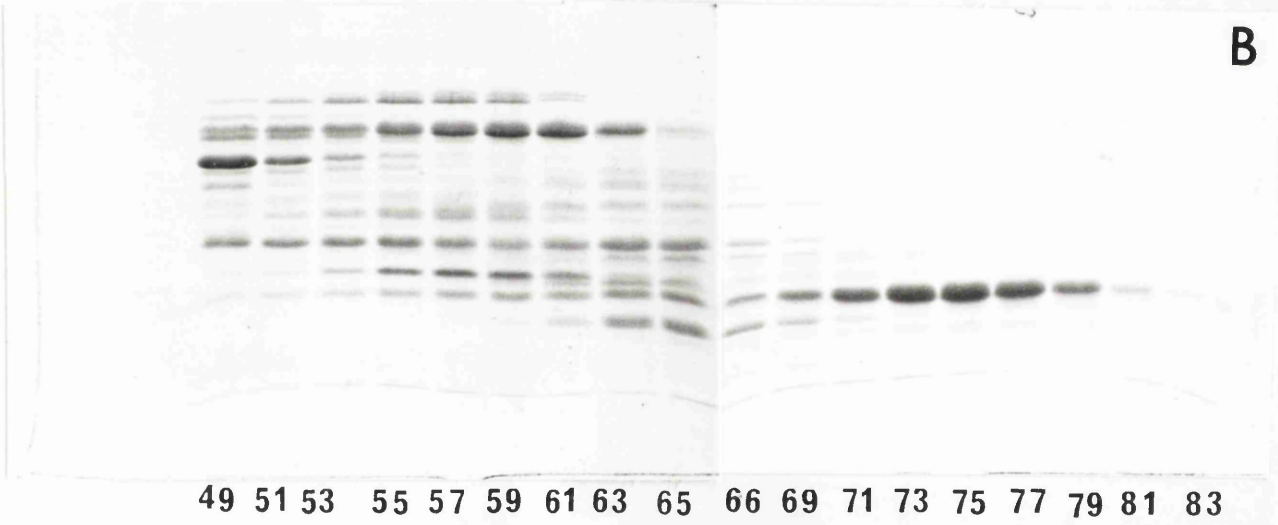
B
49 51 53 55 57 59 61 63 65 66 69 71 73 75 77 79 81 83


C

the purification procedure, and maintained at > 1 mM final concentration. The total yield from 200 g of cells using this procedure was typically 100 (± 20) mg of $p21^{ras}$ which is > 95 % pure. This yield (based on the Bradford technique (Bradford, 1976)) is ≈ 50 % greater than that obtained with the original methodology. The results of other assays for $p21^{ras}$ are discussed below.

2.3.2 *Modifications to the Original Procedure*

The capacity of the Q-Sepharose column was sufficient to allow total protein *and* nucleic acid to bind to the column and therefore the crude cell extract was loaded directly without the use of the overnight nucleic acid precipitation step. A considerable initial purification of the $p21^{ras}$ can be obtained because a large proportion of the protein in the cell extract elutes in the void volume of the column under the initial equilibration conditions.

The pool of $p21^{ras}$ eluting from the Q-Sepharose column was concentrated by ammonium sulphate precipitation, rather than by pressure ultrafiltration partly due to the long time required using this technique. However, it also affords an additional purification step. The precipitation of $p21^{ras}$ as monitored by the loss of [^{3}H]GDP binding activity from samples of cell extract and from a sample of purified $p21^{ras}$.GDP is essentially complete by 65 % saturation (Figure 3.3). However, it was noted that a considerable proportion of the protein in the crude cell extract remained in the supernatant at this concentration of ammonium sulphate, but which could be precipitated at 80 % saturation. At 40 % saturation, no protein could be detected to precipitate under these conditions. Consequently a 40% - 65 % ammonium sulphate cut would offer no additional purification over a one step 65 % precipitation and was therefore not used.

The column body chosen had an axial (length : diameter) ratio of 80 and protein was eluted at the optimal flow rate for this column (20 mL hr^{-1}). The ACA44 matrix was chosen since it has a fractionation range where $p21^{ras}$ (Mr ≈ 21,000) would elute just before the included volume of the column and thus allow purification away from other higher molecular weight impurities. $p21^{ras}$ was found to elute at ≈ 650 mL and was the last major protein to elute

Figure 3.3 Ammonium Sulphate Precipitation of $p21^{ras}$.GDP.

The pool of $p21^{ras}$.GDP from the Q-sepharose chromatography procedure was assayed for [^{3}H]GDP binding activity using the filter methods described in section 2.4.2.1. Using this assay, $\approx$ 10,000 cpm of radioactivity was bound to the filter when 5 μL of protein sample was assayed. Increasing amounts of solid ammonium sulphate were added to 3 mL of protein solution at 4^{o}C and the samples left for 1 hour. The samples were centrifuged on a bench centrifuge for 10 min at high speed and the supernatants removed. All of the supernatants were made up to the same volume with assay buffer. 5 μL of this solution was assayed for $p21^{ras}$.GDP activity by its ability to bind [^{3}H]GDP. Alternatively, purified $p21^{ras}$.GDP (1 μM) was treated as above and 10 μL of the supernatant assayed for [^{3}H]GDP binding activity. Binding activity values are quoted as a percentage of the value obtained in the absence of ammonium sulphate (crude extract = 8860 cpm, purified $p21^{ras}$ = 12500 cpm). Blank reactions containing [^{3}H]GDP but no protein sample when treated as above gave $<$0.5 % background radioactivity.

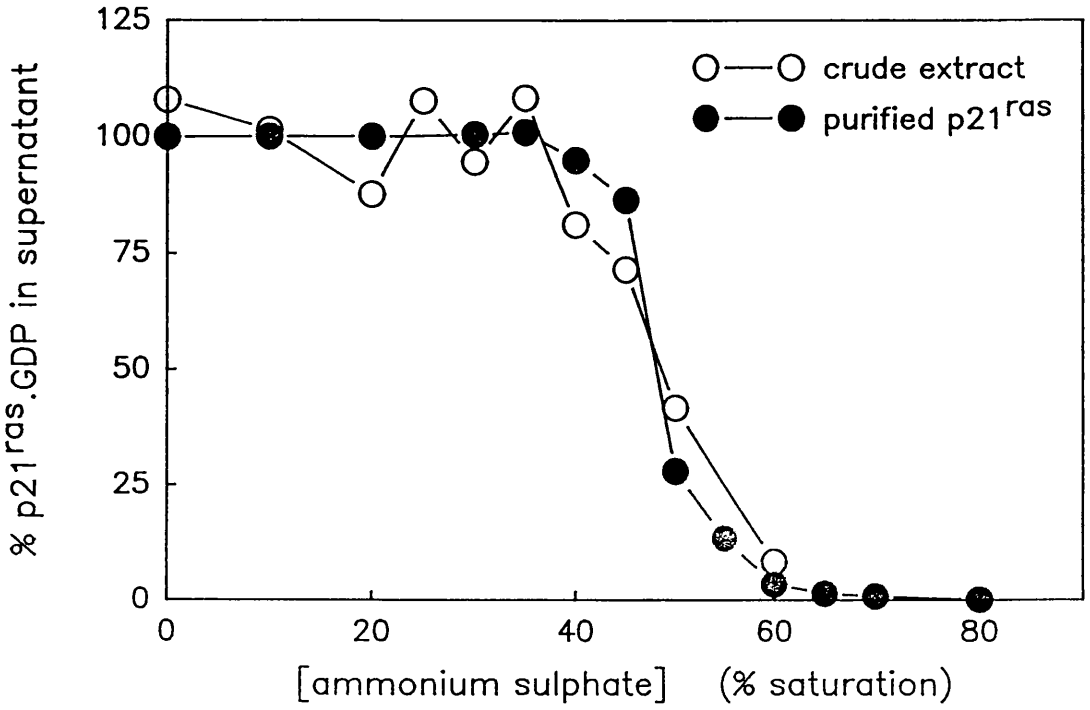
125
100
75
50
25
0
0
20
40
60
80
% p21ras.GDP in supernatant
[ammonium sulphate] (% saturation)
crude extract
purified p21ras

from this column. Whilst the G75 Sephadex column used previously shows $p21^{ras}$ as a shoulder from the one main protein elution peak, an individual peak of absorbance at 280 nm, which corresponds with the [^{3}H]GDP binding assays and with SDS-PAGE analysis, is observed using the ACA44 column. The presence of a discrete peak of $p21^{ras}$ is reflected in the high purity of the final pool (Figure 3.2.c). The purification procedure required 3 days.

Having purified the $p21^{ras}$ protein, it was characterised with respect to the total protein in the sample and the amount of "active" $p21^{ras}$ based on standard [^{3}H]GDP binding assays (Hall and Self, 1986 ; Neal et al., 1988). The discrepancy between the protein concentrations obtained by these two methods led to a detailed investigation of the active $p21^{ras}$ concentration discussed below, as determined by several different assays for $p21^{ras}$.

3.3 Characterisation of the $p21^{N\text{-}ras}$.GDP Preparation.

3.3.1 *Introduction.*

A kinetic investigation of the intrinsic GTPase mechanism of $p21^{ras}$ (Neal et al., 1988) involved the use of experiments which were first order or pseudo-first order with respect to $p21^{ras}$ concentration. Thus, the observed rates of the elementary processes were independent of $p21^{ras}$ concentration. The kinetic mechanism of the GAP-activated GTPase is usually studied with multiple turnovers of GAP and under conditions where [GAP] $<<$ [$p21^{ras}$.GTP] $<< K_d$ for the ras : GAP interaction. Under these experimental conditions, the rate of GTP hydrolysis catalysed by GAP is dependent on the $p21^{ras}$.GTP concentration. Thus, an accurate knowledge of the active $p21^{ras}$ concentration is required in these experiments. The most common assay for $p21^{ras}$ utilises the stoichiometric (1 mole of nucleotide per mole of protein) and high affinity ($K_d \approx 0.1$ nM) binding of guanine nucleotides to $p21^{ras}$ (Manne et al., 1984 ; Hall and Self, 1986, Neal et al., 1988). In this assay, $p21^{ras}$.GDP is incubated with an excess of radiolabelled nucleotide (usually [^{3}H]GDP) and the reaction mixture left to equilibrate for 60 min during which time the $p21^{ras}$.[^{3}H]GDP complex is formed by nucleotide exchange. The excess nucleotide is separated from $p21^{ras}$ by nitrocellulose filtration and the radioactivity of the filter-bound $p21^{ras}$.[^{3}H]GDP complex determined by liquid scintillation

counting.

Several groups have reported that this assay yields binding activities of > 0.9 mole of GDP per mole of protein (Tucker et al., 1986) , the latter parameter typically based on a Coomassie dye binding assay (Bradford, 1976 ; Sedmarck and Grossberg, 1977). Previous studies (Neal et al., 1988 ; Neal, 1989) indicated that the concentration of "active" $p21^{N\text{-}ras}$ protein obtained by the [^{3}H]GDP binding assay is typically only ≈ 30% of that obtained by the Bradford dye binding assay. A similar result has been obtained when the same assay has been used with other GTP-binding proteins (Tamir et al, 1990). This results was interpreted to show ≈ 70% of the $p21^{ras}$ is inactive with respect to nucleotide exchange. An alternative explanation of the low binding activity is that the assay is under-estimating the true active $p21^{ras}$ concentration, by up to 70%. In order to distinguish between these two possible extreme explanations, a sample of $p21^{ras}$ was assayed using the techniques described in section 2.4.

3.3.2 *Results of $p21^{ras}$ Assays.*

The results of the series of assays described in previous sections on one preparation of $p21^{N\text{-}ras}$.GDP are summarised in Figure 3.4. The protein concentrations are normalised to the value obtained by amino acid analysis (100 %). All three assays for total protein concentration yield essentially the same results within experimental error. It should be noted that for $p21^{ras}$, the Coomassie dye binding assays, such as those described by Bradford (1976) or BIORAD, should be used with BSA as standard. For $p21^{ras}$, the use gamma-globulin leads to a 1.8-fold over-estimation of the true $p21^{ras}$ concentration. The total $p21^{ras}$ concentration was determined by measuring the stoichiometric release of guanine nucleotide from the $p21^{ras}$.nucleotide complex by quantitative ion exchange HPLC. The results of this assay indicate total $p21^{ras}$ concentrations similar to total protein concentrations.

The [^{3}H]GDP binding assay described by Hall and Self (1986) involves the slow exchange of $p21^{ras}$-bound nucleotides for [^{3}H]GDP in 10 mM $MgCl_2$ for 60 min at 37^{o}C. Since the half time for the rate limiting GDP dissociation process is 30 min under these conditions, only 75% equilibration will have taken place during the course of the assay. In the experiments

Figure 3.4 Characterisation of the $p21^{ras}$.GDP Preparation by Multiple Assays.

The sample of $p21^{N\text{-}ras}$.GDP purified as described in section 3.2.2 was assayed by several methods described in section 2.4. All protein concentrations are normalised to the value obtained by amino acid analysis. [^{3}H]GDP binding assays were either performed in buffer B containing 10 mM $MgCl_2$ or in the presence of 20 mM EDTA and 200 mM $(NH_4)_2SO_4$ as indicated. Removal of excess nucleotide was performed either by nitrocellulose or gel filtration.

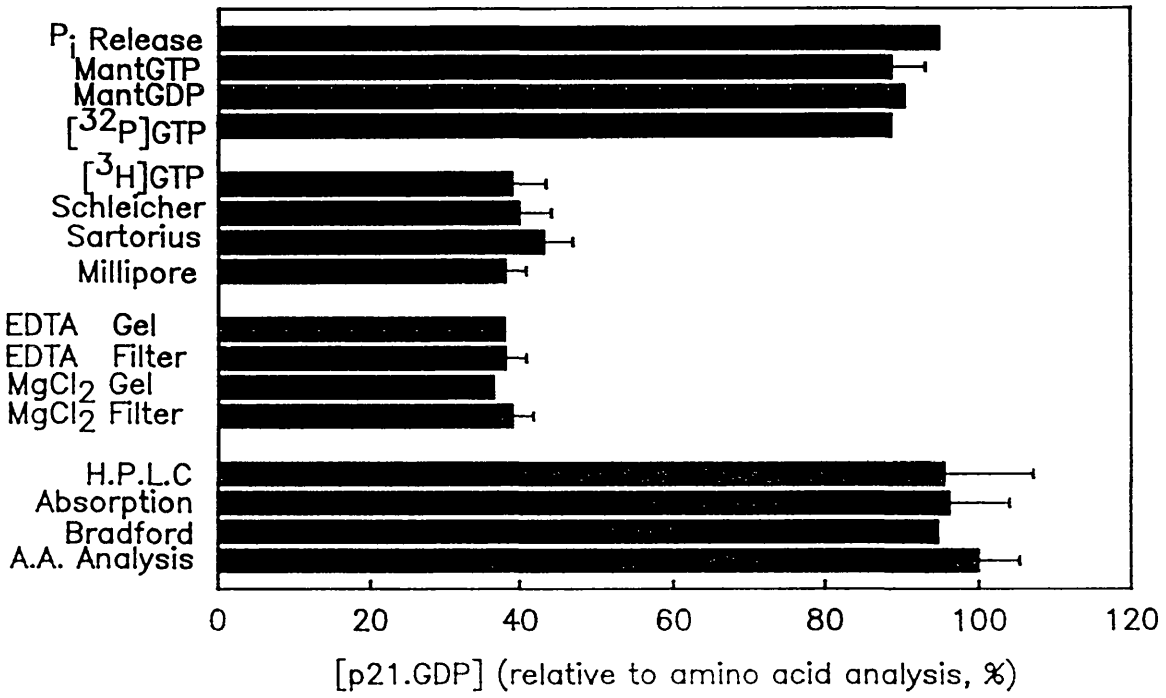
P_i Release
MantGTP
MantGDP
[^{32}P]GTP
[^{3}H]GTP
Schleicher
Sartorius
Millipore
EDTA Gel
EDTA Filter
$MgCl_2$ Gel
$MgCl_2$ Filter
H.P.L.C
Absorption
Bradford
A.A. Analysis
0
20
40
60
80
100
120
[p21.GDP] (relative to amino acid analysis, %)

described here, the incubations were performed for 180 min (≈ 98% equilibration), although the resultant binding activities were still only 35 - 40 % (Figure 3.4).

One explanation of this result is that the $p21^{ras}$.[^{3}H]GDP complex binds to the nitrocellulose filters with only 35 - 40 % efficiency. However, this appears unlikely since removal of the excess nucleotide by gel filtration yields similar binding activities to those obtained with nitrocellulose filtration (Figure 3.4). Strictly, this result indicates that the protein losses on the nitrocellulose filters are equal to those on the gel filtration column (60 - 65 %). However, control experiments indicated > 95% recovery of $p21^{ras}$.[^{3}H]GDP from the gel filtration column. HPLC analysis of the sample of [^{3}H]GDP indicated that ≈ 90 % of the radioactivity eluted at the position expected for GDP. Other peaks of radioactivity were detected in [^{3}H]GMP (≈ 5%) and at the solvent front (either [^{3}H]H_2O or [^{3}H]guanosine, ≈ 5%).

All of filter binding assays described in this chapter used one batch of nitrocellulose filters from Millipore. There are reports that some $p21^{ras}$ proteins bind with high efficiency only to specific filters from certain manufacturers (John et al., 1989). However, similar binding activities were obtained with three different types of nitrocellulose filter, either of 0.45 μm or 0.22 μm pore diameter. Significantly, different binding activities are obtained when the same sample of $p21^{ras}$ is assayed using different batches of the same type of nitrocellulose filter. This latter problem greatly hinders the use of the [^{3}H]GDP binding assay to measure the active $p21^{ras}$ concentration since the % binding activity obtained on a given preparation of $p21^{ras}$ and filters is variable.

Both EDTA (as a Mg^{2+} chelator) and $(NH_4)_2SO_4$ dramatically increase the rate of nucleotide release from $p21^{ras}$ (Hall and Self, 1986 ; Hoshino et al., 1987). By using a fluorescent GDP analogue (mantGDP), the rate of GDP dissociation from $p21^{ras}$ in 20 mM EDTA and 200 mM $(NH_4)_2SO_4$ at 20°C has been estimated to be ≈ 0.5 s^{-1} under these conditions, although the rate of mantGTP dissociation is ≈ 10-fold slower (≈ 0.06 s^{-1}). Addition of 20 mM EDTA and 200 mM $(NH_4)_2SO_4$ to the exchange buffer used in the [^{3}H]GDP binding assay reduces the equilibration time to 5 min at room temperature. This is particularly important for the products of the H-ras and K-ras genes, where the half time for the dissocia-

tion of GDP is ≈ 200 min (Mistou et al., 1992 ; chapter 8). The rapid exchange [^{3}H]GDP binding assay in EDTA and $(NH_4)_2SO_4$, with separation by either nitrocellulose or gel filtration, yields p21^{ras} binding activities similar to those obtained with the 180 min reaction in 10 mM $MgCl_2$ (Figure 3.4). When gamma-labelled [^{32}P]GTP is used in the rapid exchange gel filtration assay, much higher binding activities of ≈ 90 % are observed. The cause of this difference is not the different phosphorylation state of the nucleotide, since low (35%) binding activities are observed with [^{3}H]GTP.

The modulation of the exchange rate by EDTA and $(NH)_2SO_4$ can be utilised for the rapid preparation of nucleotide (GTP and GDP) complexes of p21^{ras} since the exchange rate is ≈ 1000-fold faster than the cleavage rate of GTP. Excess nucleotide, EDTA and $(NH_4)_2SO_4$ are rapidly removed by gel filtration performed at 4^{o}C. In contrast to the hydrophobic interaction HPLC method used by Neal et al., (1988, 1990), this direct exchange procedure allows the preparation of protein complexes with high yield (95 % recovery compared to 10 - 15 % by HPLC) and the complete procedure requires only 15 min (compared to 3 - 4 hours).

An assay for p21^{ras}, based on the binding of the fluorescent and chromophoric (2') 3'-(O-[N-methylanthraniloyl]) derivatives (Hiratsuka, 1983), has been developed. This assay, usually referred to as the "mant-assay", is now routinely used to determine active p21^{ras} concentrations. The assay is essentially the same as the rapid exchange [^{3}H]GDP gel filtration assay except that mantGDP or mantGTP are used, and the concentration of the p21^{ras}.mant-nucleotide complex determined from the absorbance of the mant-chromophore at 350 nm. Control experiments, following the absorbance of a solution of p21^{ras}.mantGDP with time after the addition of a large excess of GDP, demonstrated that there was no change in absorbance of mantGDP at 350 nm on dissociation from p21^{ras}. Consequently, the extinction coefficient of mantGDP and mantGTP free in solution (ϵ_{350} = 5.7 mM^{-1} cm^{-1}) was also used for the p21^{ras}.mant-nucleotide complexes. The binding activities obtained with this assay are ≈ 90 % using either mantGDP or mantGTP.

An assay for p21^{ras} has been developed based on the release of P_i after a single turnover of GAP-catalysed GTP hydrolysis by p21^{ras} (section 2.4.3.2, Webb, 1992 ; Webb and Hunter,

1992). $p21^{ras}$.GDP is stochiometrically converted to the GTP complex by direct exchange in EDTA and $(NH_4)_2SO_4$. Inorganic phosphate release is monitored using a coupled enzyme assay based on the phosphorolysis of a chromophoric guanosine analogue, methylthioguanosine (MESG) catalysed by purine nucleoside phosphorylase (PNPase). The differential absorbance of the nucleoside substrate and base product at 360 nm (11 mM^{-1} cm^{-1}) is used to follow the kinetics of production of P_i and calculate the [$p21^{ras}$.GTP]. The results of this assay for $p21^{ras}$ indicate binding activities of $\approx$ 95 %, similar to that obtained with the Mant-assay.

One significant difference between the [^{3}H]GDP binding assay and the Mant- or P_i release assays is that the radioactive assays are performed using [$p21^{ras}$.GDP] $\leq$ 1 μM whilst in the other assays, the final protein concentration is typically 10 - 20 μM (to obtain an A_{350} or a δA_{360} of $\geq$ 0.1). The [^{3}H]GDP binding assays were performed using 20 μM $p21^{ras}$.GDP, and the mant-assay was performed using 2 μM $p21^{ras}$.GDP ([$p21^{ras}$.mantGDP] determined spectrofluorimetrically using a standard curve of [mantGDP] against fluorescence intensity). However, the binding activities obtained under these conditions were not significantly altered by the change in protein concentration (30 % and 85 % for [^{3}H]GDP and mantGDP binding respectively. A series of experiments where [^{3}H]GDP was used to displace mantGDP from its complex with $p21^{ras}$ (c.f above) also gave low binding activities (in either EDTA or $MgCl_2$) of $\approx$ 30 %. The results obtained with either the [^{3}H]GDP binding assay or by quantitative HPLC are unaffected by prior treatment with GDP under direct exchange conditions.

Finally, a sample of $p21^{ras}$.GDP was further purified to > 99% homogeneity by SDS-PAGE using hydrophobic interaction HPLC (section 2.1.2). This sample of $p21^{ras}$ is therefore essentially free of protein contaminants which may interfere with the activity assays. In these experiments, the results obtained by amino acid analysis (100%) , absorption spectroscopy (98%), and the mant-assay (96%) all gave similar values of binding activity whilst the [^{3}H]GDP binding assays a gave $\approx$ 38 % activity.

3.3.3 *Discussion.*

The accurate determination of the active $p21^{ras}$ concentration is required for a kinetic analysis of the GAP-activated GTPase mechanism. Using the [^{3}H]GDP binding assay (Manne et al., 1985 ; Hall and Self, 1986) only 35 % apparent binding activity was observed. It was the aim of this set of experiments to determine if this was a true reflection of the $p21^{ras}$ concentration. The results presented here suggest that this assay under-estimates the true $p21^{ras}$ concentration by $\approx$ 3-fold.

The cause of the low [^{3}H]GDP binding activity remains unclear. It is not, as has been suggested (Neal et al., 1988 ; Neal, 1989), due to the presence of $\approx$ 65% inactive protein. From the results shown in Figure 3.4, this may account for $\approx$ 5 % of the protein sample. The suggestion by Neal and co-workers is based on the observation that nucleotide-free $p21^{ras}$ after elution from a hydrophobic interaction HPLC column yields > 90 % binding activity. Their interpretation of this result is that the inactive protein has been removed by the chromatography procedure. Indeed, when nucleotide-free $p21^{ras}$ was assayed by both the mant- and [^{3}H[GDP binding assays, similar binding activities of 90 % were observed. The explanation for this effect is still unknown, although it is likely to reflect the differing conformations of the 2 protein states.

In all of the experiments described in subsequent sections, the concentration of protein was calculated using the mant-binding or P_i release assays since these procedures appear to most estimate reliably the active $p21^{ras}$ concentration. The [^{3}H]GDP binding assay was used primarily to detect the presence of $p21^{ras}$ during column chromatography and for measuring the first order rate of [^{3}H]GDP dissociation from $p21^{ras}$.[^{3}H]GDP complex. The development of the rapid [^{3}H]GDP binding assay, therefore, greatly facilitates the purification of $p21^{ras}$. As Manchester (1951) pointed out, "developing a quantitative assay for such enzymes is not as simple as might be expected". This remark (in "Biochemistry Today") applies equally well to 1991 as to 1951 !

CHAPTER FOUR

THE KINETIC MECHANISM OF THE GAP_{365} - CATALYSED HYDROLYSIS OF GTP BY WILD TYPE $p21^{N\text{-}ras}$

"I am reminded of a quote, attributed to Dean Inge, that the word *bloody* had simply "become a notice that a noun is about to follow". The word *conformational* has simply become a sort of notice that "change" is about to follow".

Huxley., (1974)

4.1 Introduction

The kinetic mechanism for the $p21^{ras}$ GTPase shown in scheme 1 only includes intermediates with different chemical states. However, it is likely that conformational changes in $p21^{ras}$ occur during the GTP / GDP cycle to distinguish the biologically active and inactive states of the protein, and the presence of such conformational changes in $p21^{ras}$ is suggested from crystallographic data (Schlichting et al., 1990). Such isomerisation reactions are known to occur in the kinetic mechanisms of other nucleoside triphosphatases (Trentham et al., 1972, 1976 ; Woodward et al., 1991 ; Eccleston., 1981, 1984 ; Eccleston et al., 1985, 1988 ; Jameson et al., 1987, see Phil. Trans. R Soc. Lond. B , vol 336 for a detailed discussion of these mechanisms).

The inherent sensitivity of fluorophores to the nature of their environment suggested that fluorescence spectroscopy could be used to probe for postulated conformational changes. This technique has the advantage over crystallography that reactions are performed in solution and can be monitored over a wide range of time scales (from hours down to milliseconds).

Thus far, there have been three reports describing the use of fluorescence spectroscopy to study protein conformational changes in $p21^{ras}$ associated with the GTP cleavage reaction (Neal et al., 1990 ; Antonny et al., 1991 ; Rensland et al., 1991). The work described in this chapter is based largely on the results of Neal et al., (1990) which is discussed here briefly. The results reported in the other two papers bear directly on the conclusions of the work described in this thesis, and therefore will be discussed in chapter 10.

The experiments of Neal et al., (1990) were based on the use of the environmentally sensitive ribose-modified (2')3'-[O-(N-methylanthraniloyl)]- (mant) derivatives of guanine nucleotides (Hiratsuka., 1983). mantGTP and mantGDP were shown to be good analogues of the parent nucleotides both in terms of their equilibrium binding affinities and the rate constants for several steps in the intrinsic GTPase mechanism (k_{-1}, k_{+2}, k_{+4} in scheme 1). In all cases, the value for the mant-nucleotides were within a factor of 2 those of the parent nucleotide. These results provided the basis for the subsequent use of mant-nucleotides by several workers (John et al., 1990 ; Eccleston et al., 1991 ; Rensland et al., 1991 ; Reinstein et al., 1991 ; Mistou et al., 1992). Thus, modification of the ribose moiety has little effect on the interaction of guanine nucleotides with $p21^{ras}$ in contrast to modifications of the purine base which lead to drastic reductions in binding affinity to $p21^{ras}$ (and also to EF-Tu, Eccleston et al., 1989).

On binding to wild type $p21^{N\text{-}ras}$, mantGDP and mantGTP show a 2.8-fold and 3.0-fold enhancement in fluorescence intensity respectively. The difference in intensity between the diphosphate- and triphosphate-bound states of $p21^{ras}$ can be followed by incubating a stoichiometric 1:1 complex of $p21^{ras}$.mantGTP at $30^{o}C$ and monitoring the change in fluorescence intensity with time over the course of mantGTP hydrolysis. As predicted from the steady state spectra, an exponential decrease in fluorescence intensity of 8 - 10 % was observed, and this process occurred with the same rate constant as that of the chemical cleavage of mantGTP (determined by ion exchange H.P.L.C). There are three likely explanations of this result. The fluorescence change could arise from (a) a change in protein conformation during the cleavage step or (b) during the release of P_i from the $p21^{ras}$.mantGDP.P_i complex or (c) as a result of a protein conformational change which precedes the cleavage of the

terminal phosphate.

To distinguish between these three possibilities, the mant-derivative of a non-hydrolysable analogue of GTP, guanylylimidodiphosphate (GppNHp), was used since this compound cannot undergo either cleavage (a) or P_i release (b) steps. With mantGppNHp, a similar exponential decrease in fluorescence intensity occurred, although the amplitude of this process was $\approx$ 4 - 5 %. This result argues in favour of the third explanation (c), that of a protein conformational change occurring prior to the cleavage step (step 2a). In addition, since the *rate* of the fluorescence change with mantGppNHp is similar to that obtained with mantGTP, this suggests that the isomerisation process is rate limiting for the overall cleavage of GTP (scheme 4.1).

$$R + GTP \overset{1}{\rightleftharpoons} R{\cdot}GTP \overset{2a}{\rightleftharpoons} R^{*}{\cdot}GTP \overset{2b}{\rightleftharpoons} R{\cdot}GDP{\cdot}P_i \overset{3\ P_i}{\rightleftharpoons} R{\cdot}GDP \overset{4}{\rightleftharpoons} R + GDP$$

Scheme 4.1

It was the aim of the experiments described in this chapter to investigate the effect of GAP_{365} on the kinetic mechanism of GTP hydrolysis by $p21^{ras}$. In particular, the results are discussed in terms of the two-step model for the hydrolysis reaction proposed by Neal et al., (1990). All experiments described in this chapter were performed with wild type $p21^{N\text{-}ras}$. nucleotide complexes (15 μM) at 30^{0}C in buffer B (50 mM TrisHCl, pH 7.5, 100 mM NaCl, 10 mM $MgCl_2$, 10 mM DTT). In all cases, substoichiometric (i.e catalytic) concentrations of GAP_{365} were used, where the [GAP_{365}] is based on the value obtained with the BCA assay (Pierce, Smith et al., 1985 , section 2.3.2).

4.2 Effect of GAP_{365} on the Hydrolysis of $p21^{ras}$-Bound MantGTP and GTP.

The rate of mantGTP and GTP hydrolysis when bound to $p21^{N\text{-}ras}$ was measured by fluorescence linked ion exchange H.P.L.C and by the release of [gamma-^{32}P]P_i from [gamma-

^{32}P]GTP respectively (section 2.9). Reactions were performed in the absence (Figure 4.1.a) or presence (Figure 4.1.b) of 3 μM GAP_{365} respectively. Whilst the hydrolysis of mantGTP is slower than that of GTP in the absence of GAP_{365}, the GAP_{365}-catalysed hydrolysis of mantGTP is $\approx$ 3-fold faster than that of GTP over the range of GAP_{365} concentrations used. (Figure 4.1.c). Under the conditions used here (15 μM $p21^{ras}$.mantGTP in buffer B), the rate constants vary linearly with GAP_{365} concentration. It should be noted that under these conditions of ionic strength, the activation of the rate of GTP and mantGTP cleavage by GAP_{365} is relatively low (chapter 7).

4.3 Effect of GAP_{365} on the Rate of mantGTP Dissociation from Wild Type $p21^{ras}$.

The rate constants of mantGTP dissociation in the absence and presence of catalytic concentrations (0.3 μM) of GAP_{365} were measured using the cold chase technique described by Neal et al., (1988, 1990) (Figure 4.2.a). In this experiment, $p21^{ras}$.mantGTP (15 μM) is incubated with an excess of unlabelled GDP (1 mM) either in the presence or absence of 0.3 μM GAP_{365}. The relative rates of the dissociation (k_{-1}) and cleavage (k_{+2}) reactions determines the amount of hydrolysis which occurs during the time course of the dissociation reaction (Neal et al., 1988). The observed rate of mantGTP hydrolysis, $k_{obs} = k_{-1} + k_{+2}$, whilst the ratio of mantGDP to mantGTP at the end point equilibrium is given by the ratio of k_{+2} to $_{-1}$.

These results demonstrate that whilst the cleavage rate is significantly accelerated under these conditions (6 - 7 -fold), there is little effect on the rate of mantGTP dissociation. Higher concentrations of GAP_{365} ($>$ 0.3 μM) could not be used in these experiments since the cleavage rate would predominate and only an upper limit of k_{-1} would be obtained. The rate constant for the cleavage reaction determined from these experiments are comparable to those obtained directly from experiments described in Figure 4.1. Within experimental error, there is unlikely to be a significant difference between the two value of k_{-1} under these conditions. Subsequent experiments (chapter 8) have demonstrated that under saturating concentrations of GAP_{344}, the rate of mantGTP dissociation is reduced by a factor of $\approx$ 4.

Figure 4.1.Time course for the cleavage of GTP and mantGTP bound to $p21^{N\text{-}ras}$.

All experiments were performed at 30^0 in 50 mM TrisHCl, pH 7.5, 100 mM NaCl, 10 mM $MgCl_2$, 10 mM DTT (buffer B).

(A) Solutions of $p21^{N\text{-}ras}$.GTP [gamma-^{32}P] and $p21^{N\text{-}ras}$.mantGTP (15 μM) were incubated at 30^0C. At timed intervals, aliquots were removed from each sample and the extent of [gamma-^{32}P]GTP and mantGTP hydrolysis measured by nitrocellulose filtration and HPLC respectively. Solid lines represent the best fit to single exponentials. k_{obs}(GTP) = 2.7 x 10^{-4} s^{-1}, k_{obs} (mantGTP) = 1.8 x 10^{-4} s^{-1}.

(B) As for (A) except 3 μM GAP_{365} was added at t = 0 min. k_{obs} (GTP) = 3.3 x 10^{-3} s^{-1}, k_{obs} (mantGTP) = 9.8 x 10^{-3} s^{-1}. End points were <1% GTP or mantGTP in all cases.

(C) Dependance of the observed rate constants from experiments as above (A and B) on the concentration of GAP_{365}. Solid lines are the best fit to straight lines with gradients of 1.22 x $10^{-3}s^{-1}$ μM^{-1} GAP_{365} (GTP) and 3.21 x 10^{-3} s^{-1} μM^{-1} GAP_{365} (mantGTP)

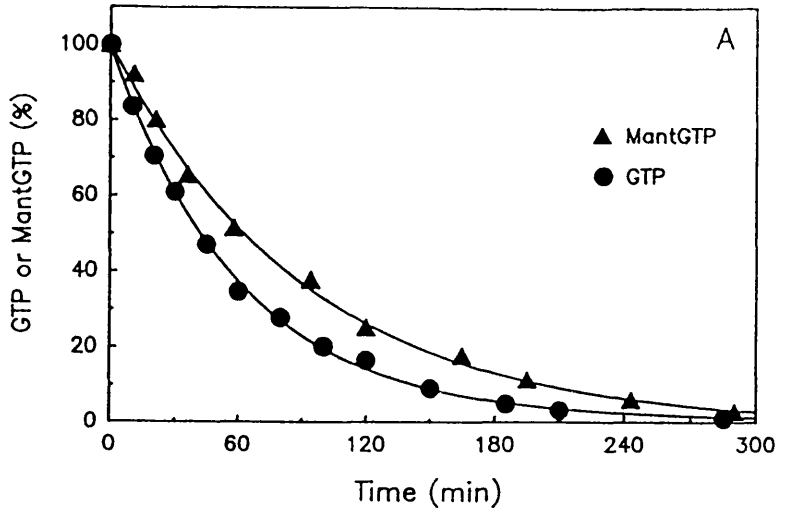
A
GTP or MantGTP (%)
100
80
60
40
20
0
0
60
120
180
240
300
Time (min)
MantGTP
GTP

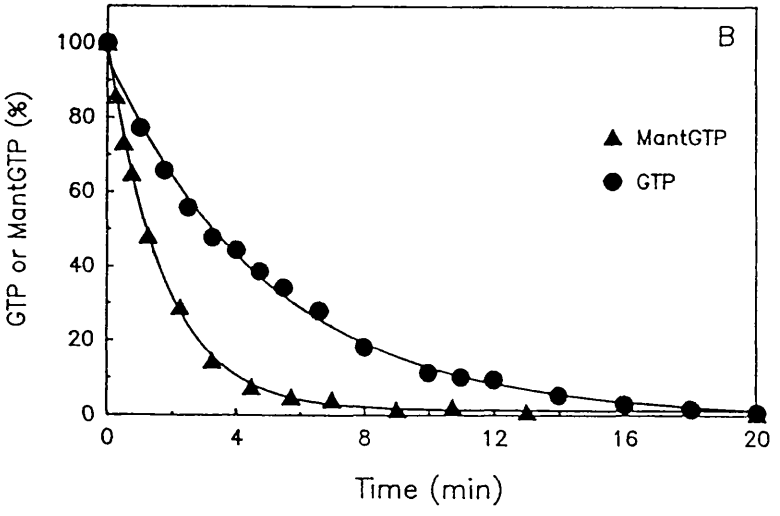
B
GTP or MantGTP (%)
100
80
60
40
20
0
0
4
8
12
16
20
Time (min)
MantGTP
GTP

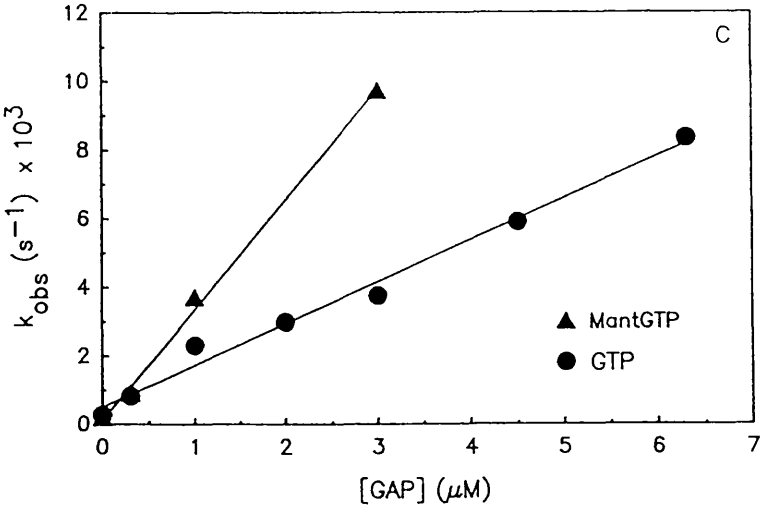
C
k_{obs} (s^{-1}) x 10^3
12
10
8
6
4
2
0
0
1
2
3
4
5
6
7
[GAP] (μM)
MantGTP
GTP

Figure 4.2. Effect of GAP_{365} on the rate of mantGTP and mantGDP dissociation from $p21^{N\text{-}ras}$.

(A) 15 μM $p21^{N\text{-}ras}$.mantGTP was incubated at 30°C in buffer B with 1 mM GDP in the presence or absence of 0.3 μM GAP_{365}. Aliquots were removed at timed intervals and analysed for the extent of mantGTP hydrolysis by HPLC. Solid lines are the best fits to single exponentials. (i) No GAP_{365} : $k_{obs} = 2.8 \times 10^{-4}\ s^{-1}$, end point = 27.2 % mantGTP, (ii) 0.3 μM GAP_{365} : $k_{obs} = 1.4 \times 10^{-3}\ s^{-1}$, end point = 4.3 % mantGTP. The calculated values of k_{-1} and k_{+2} are:-

no GAP_{365} :	$k_{-1} = 0.75 \times 10^{-4}\ s^{-1}$	$k_{+2} = 2.0 \times 10^{-4}\ s^{-1}$.
0.3 μM GAP_{365}:	$k_{-1} = 0.66 \times 10^{-4}\ s^{-1}$	$k_{+2} = 1.3 \times 10^{-3}\ s^{-1}$.

(B) 15 μM $p21^{N\text{-}ras}$.mantGDP in buffer B was incubated at 30°C in a fluorimeter, either in the presence (circles) or absence (squares) of 3 μM GAP_{365}. At t = 0 min, GDP was added to 1 mM final concentration and the fluorescence intensity (excitation = 366 nm, emission = 442 nm) monitored at timed intervals. The solid line is the best fit to a single exponential. In both experiments, $k_{obs} = 1.6 \times 10^{-4}\ s^{-1}$ and the end point was at 36% relative fluorescence.

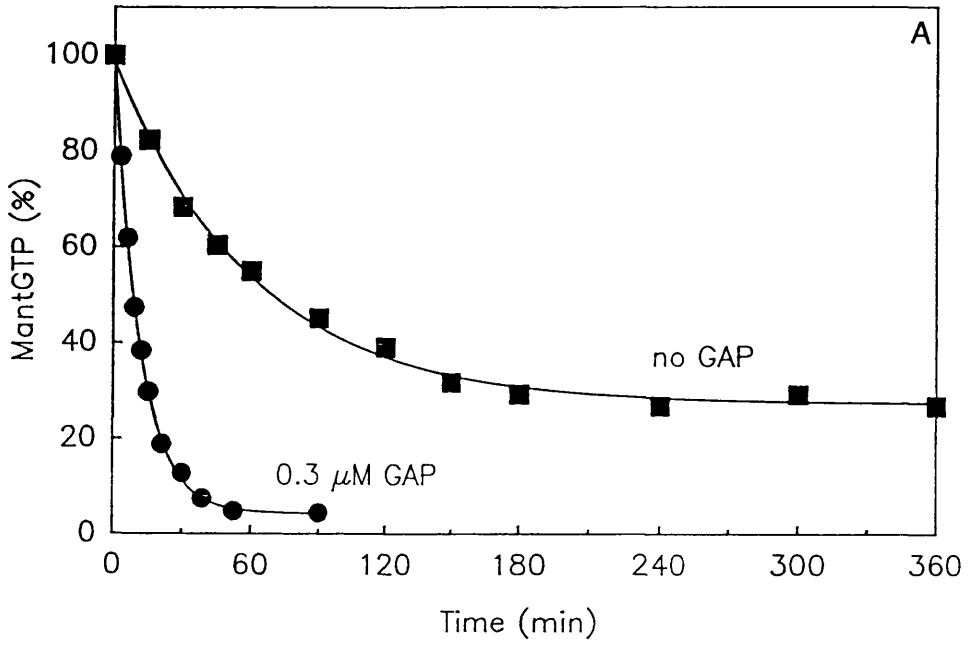
A
100
80
60
40
20
0
MantGTP (%)
no GAP
0.3 μM GAP
0
60
120
180
240
300
360
Time (min)

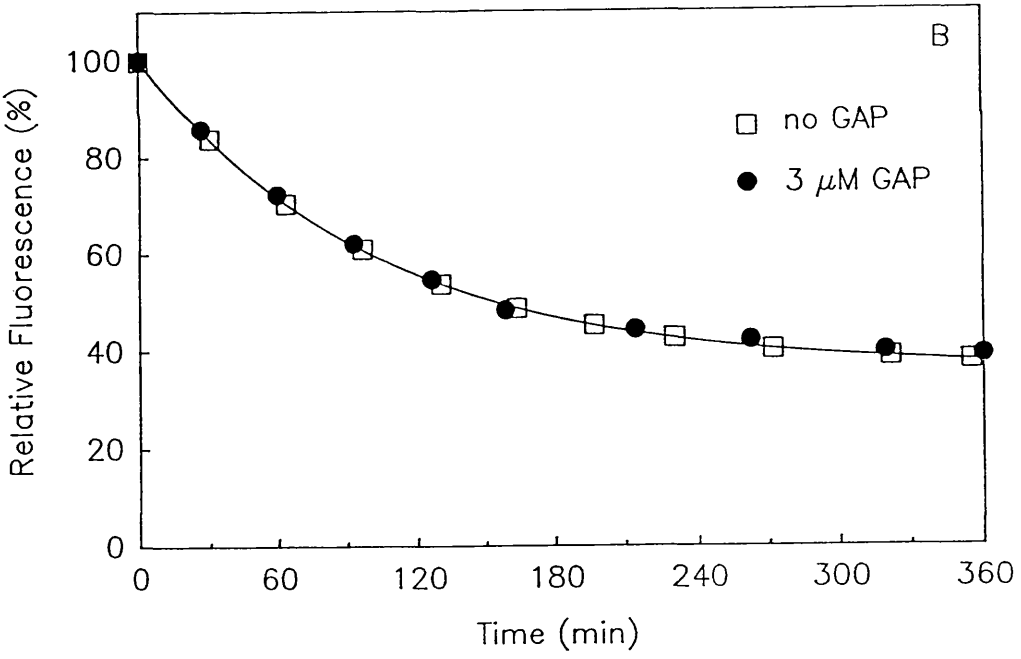
B
100
80
60
40
20
0
Relative Fluorescence (%)
no GAP
3 μM GAP
0
60
120
180
240
300
360
Time (min)

4.4 Effect of GAP_{365} on the Rate of mantGDP Dissociation from $p21^{ras}$.

The rate of mantGDP dissociation from 15 μM $p21^{ras}$.mantGDP in the presence of 1 mM GDP (k_{+4}) was measured by following the $\approx$ 65 % decrease in fluorescence intensity of mantGDP during the dissociation reaction (Neal et al., 1990). The rate of the dissociation reaction was determined either in the absence or presence of 3 μM GAP_{365} (Figure 4.2.b). Both the rate and amplitude of the fluorescence change were essentially identical whether in the presence or absence of GAP_{365} indicating that under these conditions, the rate of mantGDP dissociation was unaffected by GAP_{365}.

4.5 Fluorescence Changes Associated with the Hydrolysis of mantGTP by $p21^{N\text{-}ras}$.

4.5.1 *Fluorescence Changes of $p21^{ras}$.mantGTP in the Presence of GAP_{365}.*

The effect of GAP_{365} on the rate of the slow fluorescence change observed by Neal et al., (1990) and on the rate of mantGTP cleavage has been determined (Figure 4.3). Both the rate of the fluorescence change and the rate of mantGTP cleavage are accelerated by GAP_{365}. Over a 10-fold range of GAP_{365} concentrations (0.3 - 3 μM GAP_{365}), the fluorescence change and the chemical cleavage reaction occur with the same rate constant (Figure 4.4). The first order rate of the reaction was linearly dependent on GAP_{365} concentration over the range used. In contrast, there was no fluorescence change observed with $p21^{ras}$.mantGDP over the same time course in the presence of 0.3 μM and 3 μM GAP_{365}. Gel filtration analysis of the $p21^{ras}$.mantGDP samples at the end of the reactions showed that either in the presence or absence of GAP_{365}, there was no detectable free nucleotide present; greater than 99 % of the fluorescence eluted with the protein.

4.5.2 *Re-examination of the Fluorescence Changes of $p21^{ras}$.mantGTP In the Absence of GAP_{365}.*

The results shown in Figure 4.3 were obtained using protein : nucleotide complexes prepared via nucleotide-free apo-$p21^{ras}$ by hydrophobic interaction H.P.L.C (sections 2.1.2 and 2.6).

Figure 4.3 Effect of GAP_{365} on the fluorescence intensity of $p21^{N\text{-}ras}$.mantGTP and on the chemical cleavage rate of $p21^{N\text{-}ras}$.mantGTP.

15 μM $p21^{N\text{-}ras}$.mantGTP or $p21^{N\text{-}ras}$.mantGDP in buffer B at 4°C was warmed to 30°C in a fluorimeter cell (typically within 6-7 min). Recording was not initiated until the temperature of the solution had reached 30 (+/-0.05)°C. Fluorescence intensity was monitored at 442 nm (excitation 366 nm) with the excitation shutter closed between readings. Chemical cleavage of mantGTP was monitored by HPLC. Each data set is normalised to the zero time measurement.

(A) Effect of GAP_{365} on the fluorescence intensity of $p21^{N\text{-}ras}$.mantGTP. GAP_{365} was added to 0.3 μM and 3 μM final concentration at t = 0 min as indicated. Solid lines are the best fits to single exponentials (i) no GAP_{365}: $k_{obs} = 1.9 \times 10^{-4}$ s^{-1}, A = 7.6 %, (ii) 0.3 μM GAP_{365}: $k_{obs} = 0.90 \times 10^{-3}$ s^{-1}, A = 8.3 %, (iii) 3 μM GAP_{365}: $k_{obs} = 9.5 \times 10^{-3}$ s^{-1}, A = 6.3 %. No fluorescence change was observed with the corresponding mantGDP complexes after the addition of GAP_{365} to 0.3 μM or 3 μM.

(B) Time course for the chemical cleavage of mantGTP bound to $p21^{N\text{-}ras}$ measured by ion exchange HPLC under identical conditions to (A). Solid lines are best fits to single exponentials with end points at < 1% mantGTP in all cases. (i) no GAP_{365}: $k_{obs} = 1.8 \times 10^{-4}$ s^{-1}, (ii) 0.3 μM GAP_{365}: $k_{obs} = 0.95 \times 10^{-3}$ s^{-1} (iii) 3 μM GAP_{365}, $k_{obs} = 9.8 \times 10^{-3}$ s^{-1}.

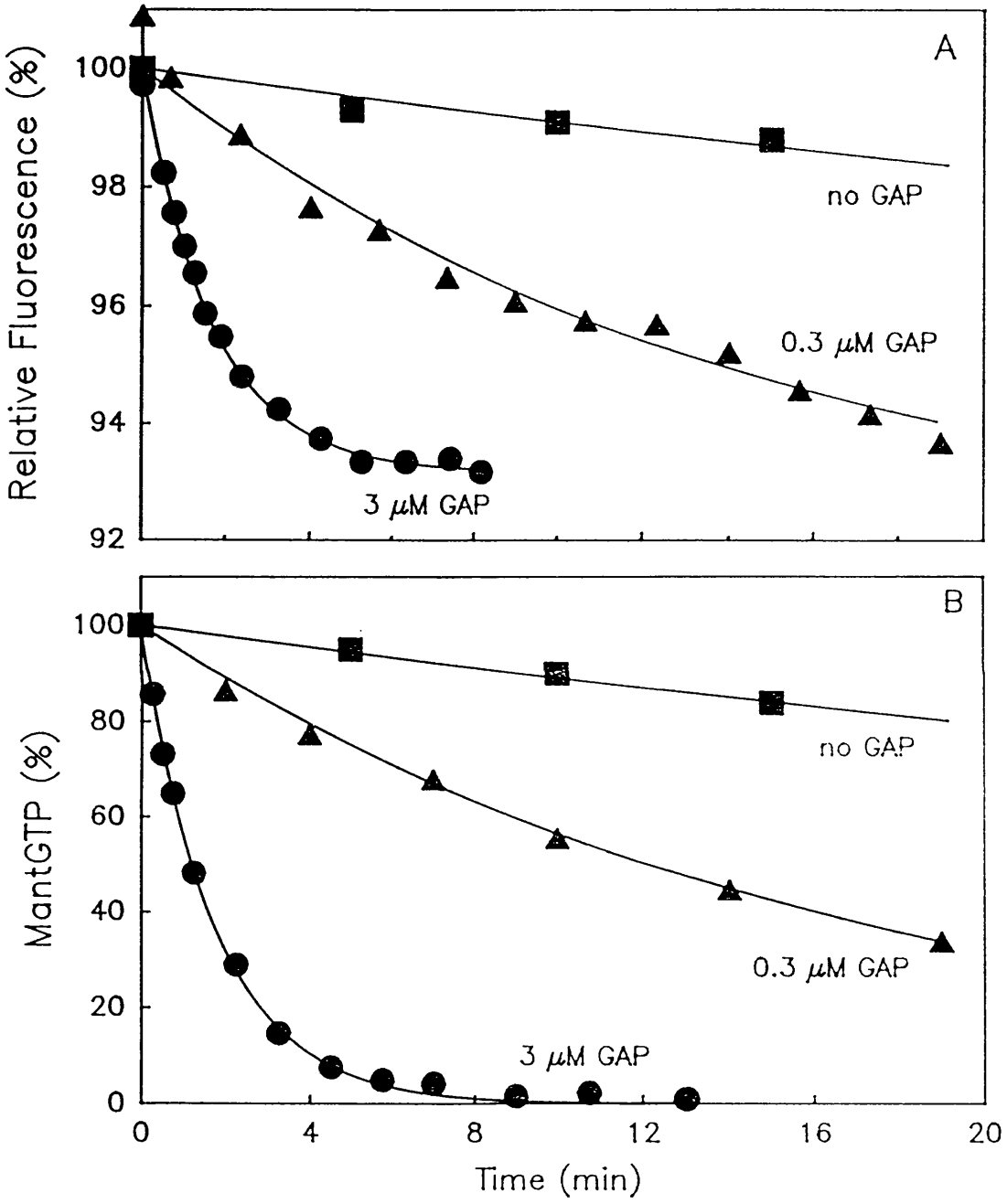
A
Relative Fluorescence (%)
100
98
96
94
92
no GAP
0.3 μM GAP
3 μM GAP
B
MantGTP (%)
100
80
60
40
20
0
no GAP
0.3 μM GAP
3 μM GAP
0
4
8
12
16
20
Time (min)

Figure 4.4 The dependence of the observed first order rate of the fluorescence change or the chemical cleavage of mantGTP on GAP_{365} concentration.

GAP_{365} was added to a solution of 15 μM $p21^{N\text{-}ras}$.mantGTP at 30°C in buffer B to a final concentration of 0 - 3 μM as described in Figure 4.3. The observed rate of the fluorescence change (A) and the chemical cleavage of mantGTP (B) is shown as a function of the final GAP_{365} concentration. The solid lines are best fits to straight lines with gradients of (A) 3.18×10^{-3} s^{-1} μM^{-1} GAP_{365} and (B) 3.21×10^{-3} s^{-1} μM^{-1} GAP_{365}.

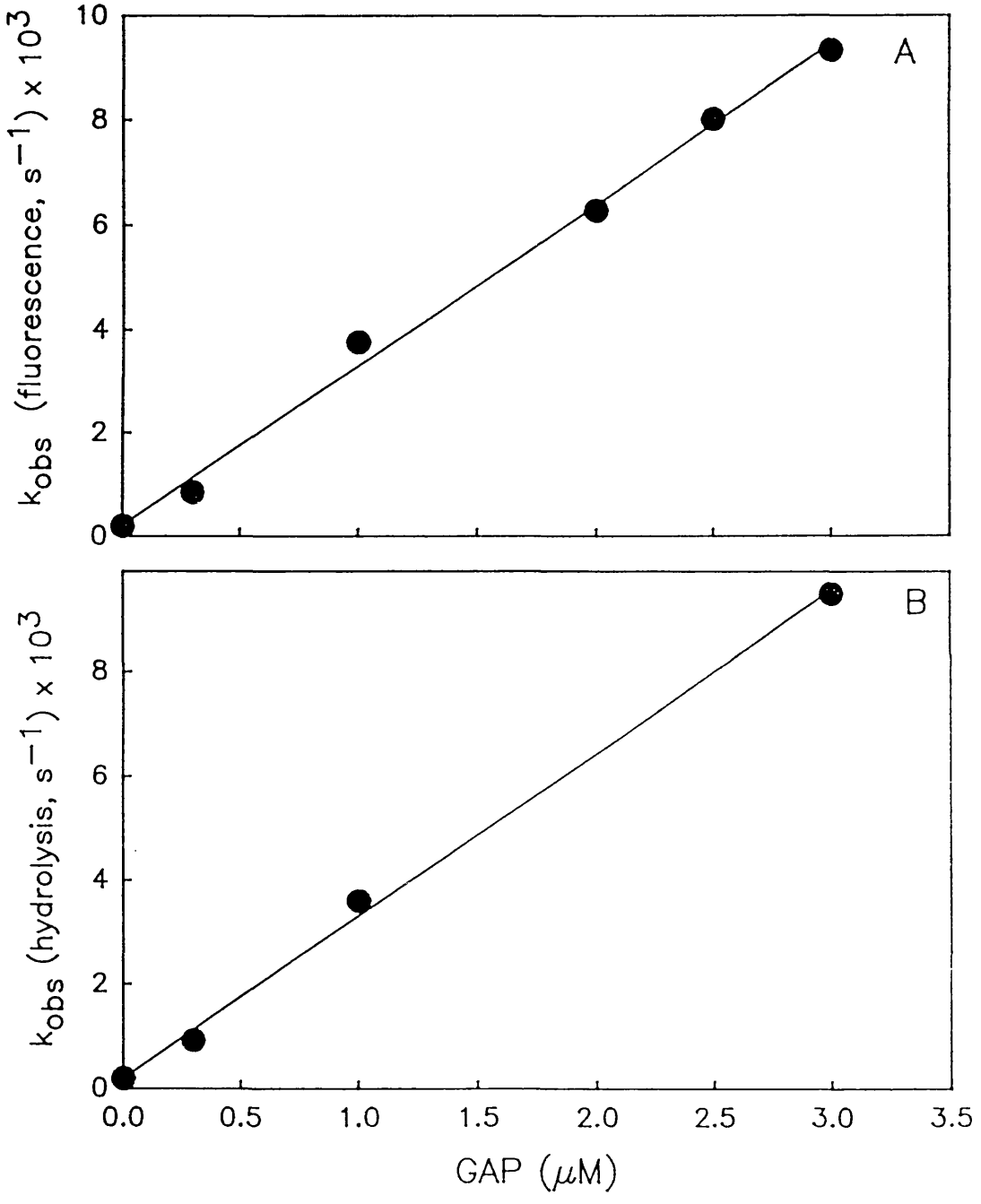
A
B
k_{obs} (fluorescence, s^{-1}) x 10^3
k_{obs} (hydrolysis, s^{-1}) x 10^3
0
2
4
6
8
10
0.0
0.5
1.0
1.5
2.0
2.5
3.0
3.5
GAP (μM)

Due to the low yield of $p21^{ras}$ from this procedure, the final concentration of $p21^{ras}$.mant-GTP was typically 15 - 20 μM and the sample (volume $\approx$ 1.5 mL) stored on ice at $\approx 2^{o}C$. Since the fluorescence intensity of the mant-fluorophore is sensitive to temperature (a $1^{o}C$ increase in temperature leads to $\approx$ 1 % decrease in fluorescence intensity), care was taken to ensure that the temperature of the sample in the thermostated fluorimeter cuvette holder had reached 30 ($\pm$ 0.05)^{o}C before recording was initiated. Using the large volume cuvette (1 cm x 1 cm), this time period was typically 10 min. Thus any processes occurring during this time would not have been observed in these experiments.

However, using the direct exchange procedure for the preparation of $p21^{ras}$.mantGTP (section 2.6), $p21^{ras}$.mantGTP complexes of up to 150 μM could be obtained. Therefore, by dilution of a small volume of stock $p21^{ras}$.mantGTP on ice into a much larger volume of buffer already at $30^{o}C$, the fluorescence experiments could be rapidly initiated in $\approx$ 1 min. When the fluorescence change *in the absence of* GAP_{365} was re-examined using this modified procedure, the decrease in intensity was observed to be biphasic in nature (Figure 4.5.a). An initial decrease in fluorescence intensity occurred with an amplitude of 4 - 5 % and a rate constant of 3.3×10^{-3} s^{-1}, and this was subsequently followed by a slower decrease in fluorescence intensity (amplitude $\approx$ 8% and rate = 2.1×10^{-4} s^{-1}). These two phases of the fluorescence changes seen with mantGTP will be referred to as the "fast" and "slow" phases respectively. The second, slow phase was that identified by Neal et al., (1990) which occurs with the same rate as that of mantGTP cleavage and is the same as that shown in Figure 4.4. Again, gel filtration analysis showed that no dissociation of nucleotide had occurred during the time course of the experiment.

To gain more information about the nature of the fluorescence changes, the anisotropy and the intensity were followed simultaneously during the time course of the fast and slow phases of the fluorescence changes in the absence of GAP_{365} (Figure 4.5.b). This was achieved by measuring the parallel (I_{Π}) and perpendicular ($I_{\perp}$) components of the fluorescence emission simultaneously using the fluorimeter in the T-format (section 2.7, see Jameson, 1984). The total fluorescence intensity (I_T) and total fluorescence anisotropy, r, are given by:

Figure 4.5 : Fluorescence Intensity and Anisotropy Changes Associated with the Intrinsic Hydrolysis of mantGTP by $p21^{N\text{-}ras}$.

(A) $p21^{N\text{-}ras}$.mantGTP (56.3 μM) at 4°C was diluted into buffer B at 30°C to a final concentration of 15 μM. The temperature of the solution reached 30°C in ca. 45 secs. The fluorescence intensity (excitation 366 nm, emission 442 nm) was followed with time (circles). The fluorescence intensity of a solution of $p21^{N\text{-}ras}$.mantGDP is also shown (triangles). The solid line through the circles is a double exponential best fit to the $p21^{N\text{-}ras}$.mantGTP data with $k_{obs,1} = 3.3 \times 10^{-3}\ s^{-1}$, $A_1 = 4.8$ %, $k_{obs,2} = 2.1 \times 10^{-4}\ s^{-1}$, $A_2 = 7.9$ %. The solid line through the triangles is a linear regression best fit to the $p21^{N\text{-}ras}$.mantGDP data.

(B) 15 μM $p21^{N\text{-}ras}$.mantGTP was incubated at 30°C in a fluorimeter and the anisotropy of the fluorophore was monitored with time (using $I_{\perp}$ and $I_{\parallel}$). Reactions were initiated as described in (A). The solid line is a best fit line to a single exponential, $k_{obs} = 2.8 \times 10^{-3}\ s^{-1}$, amplitude = 0.01. Inset: Same data but showing only the initial 30 min of the incubation. The fluorescence intensity data for this experiment were similar to those shown in (A) and could be fitted to a double exponential with $k_{obs,1} = 2.9 \times 10^{-3}\ s^{-1}$, $A_1 = 5.9$ %, $k_{obs,2} = 2.1 \times 10^{-4}\ s^{-1}$, $A_2 = 7.2$ %.

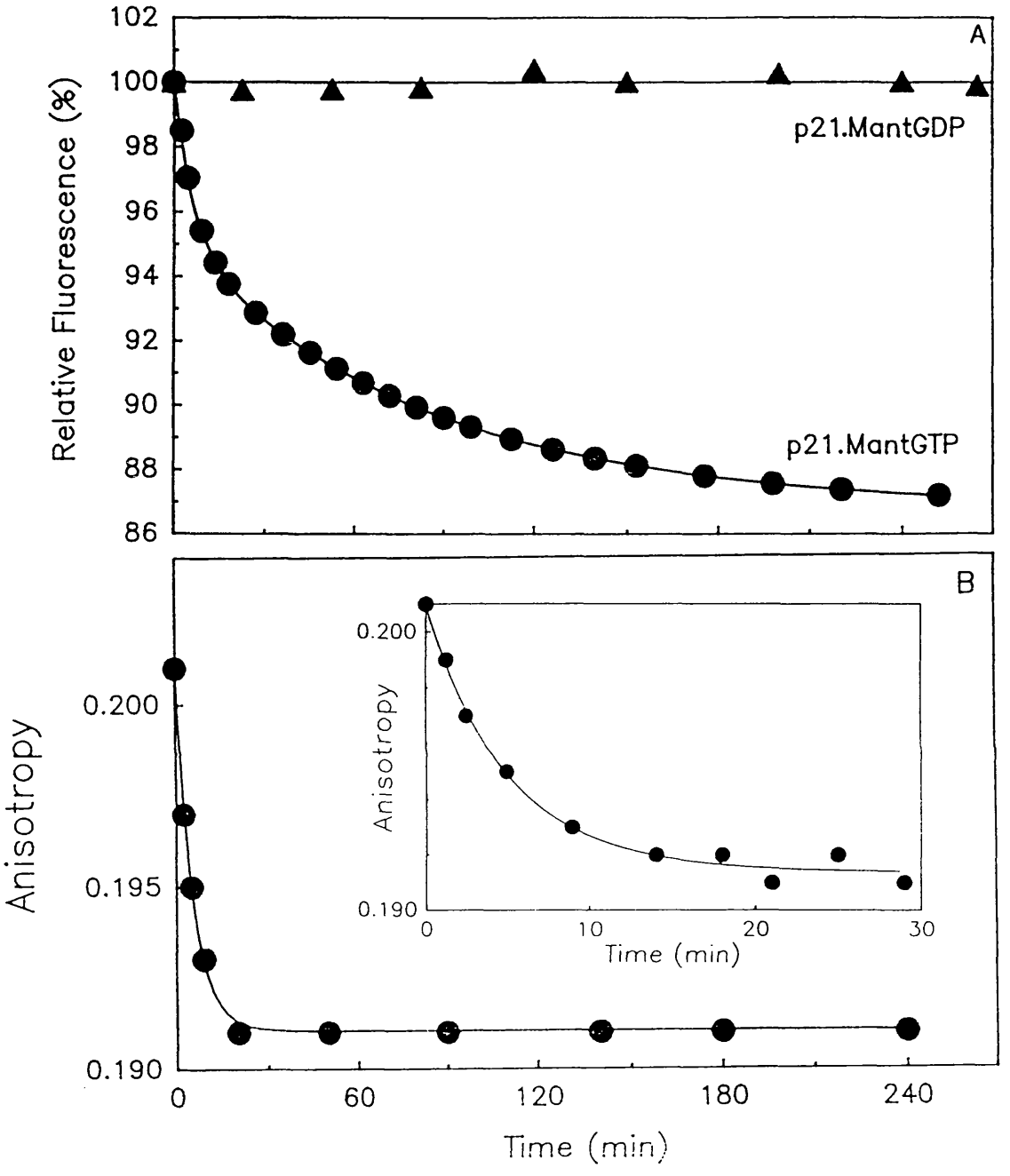
A
p21.MantGDP
p21.MantGTP
Relative Fluorescence (%)
102
100
98
96
94
92
90
88
86
B
Anisotropy
0.200
0.195
0.190
0
60
120
180
240
Time (min)
Anisotropy
0.200
0.190
0
10
20
30
Time (min)

$$I_T = I_{\Pi} + (2 \times I_{\perp})$$

$$r = (I_{\Pi} - I_{\perp}) \div I_T$$

The fluorescence intensity of the sample showed the same biphasic decrease described in Figure 4.5.a. The fast phase shows a decrease in anisotropy of $\approx$ 0.01 occurring with the same rate as that of the intensity change whilst the slow phase of the fluorescence change showed no change in anisotropy. This latter point provides additional evidence that there is no significant dissociation of nucleotides from $p21^{ras}$ during the time course of these experiments since there is a 10-fold decrease in anisotropy on dissociation of mant-nucleotides from $p21^{ras}$.

Mant-nucleotides exist as a mixture of the 2' and 3' isomers which can be separated by reverse phase H.P.L.C (section 2.5.1). When nucleotide elution is monitored by absorbance at 252 nm, the first of the two peaks comprises $\approx$ 60 % of the total absorbance at 252 nm. Several lines of evidence suggest that the first peak is the 3' isomer (Cremo et al., 1990 ; Rensland, et al., 1991 ; Neal et al., 1990). Results of experiments where (2'-mant)-3'5'cyclic GMP is rapidly hydrolysed to 2' mantGMP with 3'5' cyclic nucleotidase are consistent with previous assignments of these isomers. When the elution of the mant-nucleotide isomers is followed by fluorescence linked reverse phase H.P.L.C, the higher fluorescence intensity of the 3' isomer (see chapter 9) increases the apparent ratio of the 3' to 2' isomers to $\approx$ 70 : 30 (Figure 4.6.a).

Due to this difference, acyl migration of the 3' isomer to the 2' isomer when bound at the active site of $p21^{ras}$ could cause a reduction in fluorescence intensity during the mantGTP hydrolysis reaction. Quenching $p21^{ras}$.mantGTP complexes into perchloric acid stops acyl migration since the rate of migration is base catalysed and also denatures the protein. Reverse phase H.P.L.C of the supernatant demonstrated that at the start of the mantGTP hydrolysis reaction $\approx$ 97 % of the bound nucleotide was the 3' isomer. Furthermore, the percentage of the 3' isomer relative to the 2' isomer changed by $<$ 1 % during the time course of the hydrolysis (Figure 4.6.b - 4.6.d). Thus, acyl migration of the mant-fluorophore

Figure 4.6: Separation of the 2' and 3' Isomers of mant-Nucleotides Bound to $p21^{N\text{-}ras}$.

At timed intervals, aliquots were removed from a solution of 15 μM $p21^{N\text{-}ras}$.mantGTP in buffer B at 30^{o}C. The mant-nucleotides were displaced from the protein:nucleotide complex by acid treatment and analysed by reverse phase HPLC for the presence of the 2' and 3' isomers as described (section 2.5.1).

(A) Mixture of mantGDP and mantGTP (>98% pure by ion exchange HPLC).
The retention times for the 3' and 2' isomers of mantGTP and mantGDP under these conditions are: 3'mantGTP = 36 min, 2'mantGTP = 50 min, 3'mantGDP = 55 min, 2'mantGDP = 67 min.

(B) $p21^{N\text{-}ras}$.mantGTP after 2 min.

(C) $p21^{N\text{-}ras}$.mantGTP after 60 min.

(D) $p21^{N\text{-}ras}$.mantGTP after 240 min.

In all cases, the ratio of the 3' isomer of mantGTP and mantGDP bound to $p21^{N\text{-}ras}$ to the 2' isomer was > 25:1. The hydrolysis of mantGTP is consistent with the rate measured by ion exchange HPLC (Figure 4.1).

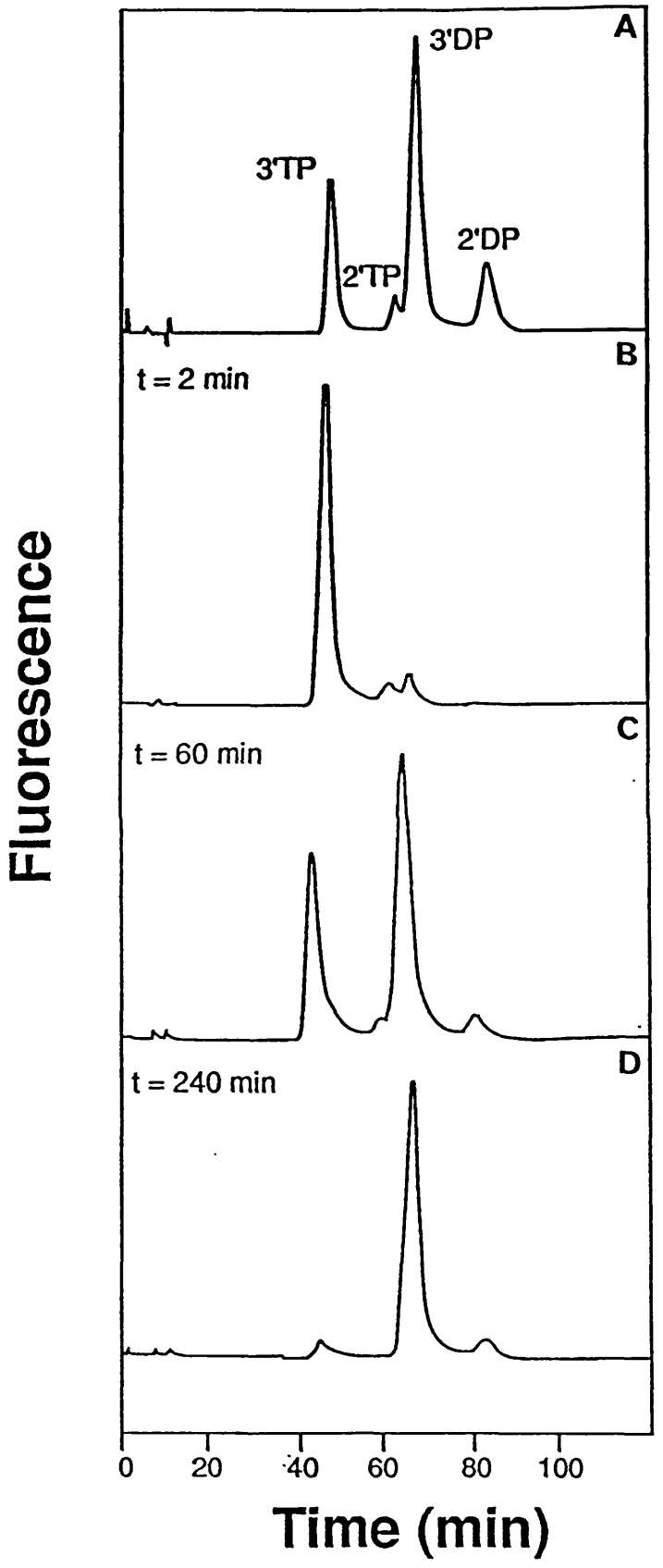
A
3'DP
3'TP
2'TP
2'DP
B
t = 2 min
C
t = 60 min
D
t = 240 min
Fluorescence
0
20
40
60
80
100
Time (min)

does not contribute to either the fast or slow phases of the fluorescence changes associated with mantGTP hydrolysis.

It is possible that the end of the fast phase may have been observed by Neal et al., (1990, J.F.E, pers. comm) although these workers assumed it was caused by incomplete thermal equilibration during the early time points in the reaction. The fast phase occurs independently of both the intrinsic and GAP_{344}-catalysed hydrolysis reactions (chapter 5) whilst GAP_{344} was found to have no effect on the rate of the fast phase (chapter 8). In subsequent experiments, to resolve the fluorescence changes associated with mantGTP hydrolysis from that of the fast phase, GAP_{365} was added after the fast phase was complete.

4.6 Fluorescence Changes of $p21^{ras}$.mantGppNHp in the Presence of GAP_{365}:

In light of the results obtained with the mantGTP complex, the fluorescence change with mantGppNHp was re-examined in the absence of GAP_{365},and taking measurements at earlier time points as described above. The fluorescence change associated with this reaction was also found to be biphasic in nature (Figure 4.7.a). The rates of the fast phase of the fluorescence change (2.9×10^{-3} s^{-1}) and the slow phase (1.9×10^{-4} s^{-1}) were essentially identical to that obtained with mantGTP. However, the amplitude of the slow phase was reduced with mantGppNHp. Again, it is the second slow phase of the fluorescence change that was identified by Neal et al., (1990).

When GAP_{365} was added to a solution of $p21^{ras}$.mantGppNHp, the slow phase was accelerated by GAP_{365} although the amplitude of the process ($\approx$ 4 %) remained unaltered (Figure 4.7.b). The rate constant of the process occurring after the addition of GAP_{365} varied linearly with GAP_{365} concentration up to 3 μM (Figure 4.7.c). The rate constants obtained with mantGppNHp are approximately 3-fold lower than those observed with mantGTP. HPLC analysis at intervals during the time course of the reactions indicated no significant hydrolysis of the nucleotide either in the presence or absence of GAP_{365} and gel filtration analysis demonstrated less than 1 % free nucleotide at the end of the reactions.

Figure 4.7: Change in Fluorescence Intensity on Incubation of the $p21^{N\text{-}ras}$.mant-GppNHp Complex at $30^{o}C$.

(A) 15 μM $p21^{N\text{-}ras}$.mantGppNHp in buffer B was warmed to $30^{o}C$ in a fluorimeter cell in ca. 1 min and the fluorescence intensity (excitation 366 nm, emission 442nm) monitored at timed intervals. The solid line is the best fit to a double exponential, $k_{obs,1} = 2.9 \times 10^{-3}\ s^{-1}$, $A_1 = 4.3\ \%$, $k_{obs,2} = 1.9 \times 10^{-4}\ s^{-1}$, $A_2 = 3.9\%$.

(B) 15 μM $p21^{N\text{-}ras}$.mantGppNHp in buffer B was warmed to $30^{o}C$ and the fluorescence intensity (excitation 366 nm, emission 442 nm) monitored at timed intervals over 40 min. (1) Open squares : the fluorescence intensity initially decreased exponentially ($k_{obs,1} = 3.5 \times 10^{-3}\ s^{-1}$, $A_1 = 3.2\ \%$), followed by a slow decrease in intensity. (2) Filled circles: as above except that GAP_{365} is added to 3 μM final concentration at 16 min. The data after the addition of GAP_{365} can be fitted to an additional single exponential ($k_{obs,2} = 3.6 \times 10^{-3}\ s^{-1}$, $A_2 = 4.2\ \%$). Ion exchange HPLC analysis indicated $< 1\%$ hydrolysis of the nucleotide at 3 μM GAP_{365} over a period of 240 min.

(C) Dependance of $k_{obs,2}$ on GAP_{365} concentration. The solid line is the best fit to a straight line with a gradient of $1.22 \times 10^{-3}\ s^{-1}\ \mu M^{-1}$ GAP_{365}.

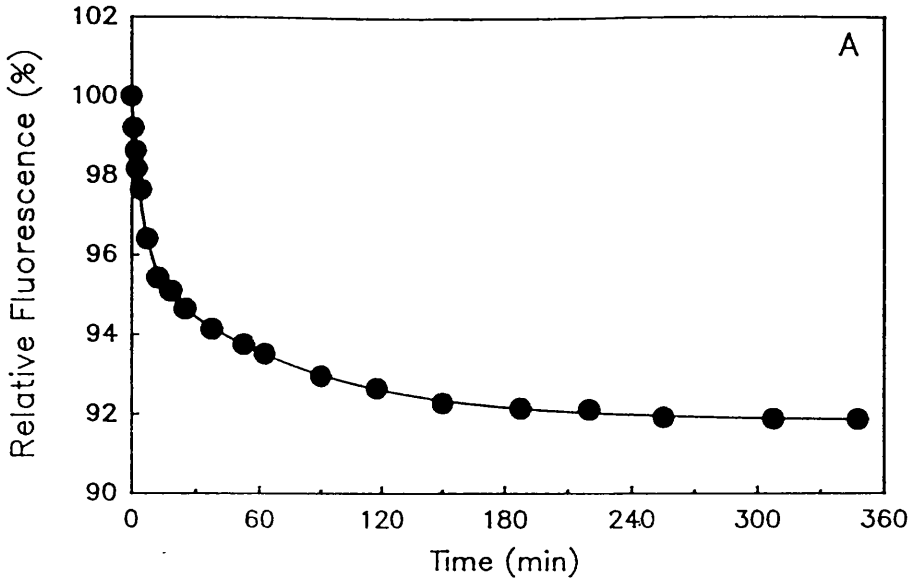
A
Relative Fluorescence (%)
102
100
98
96
94
92
90
0
60
120
180
240
300
360
Time (min)

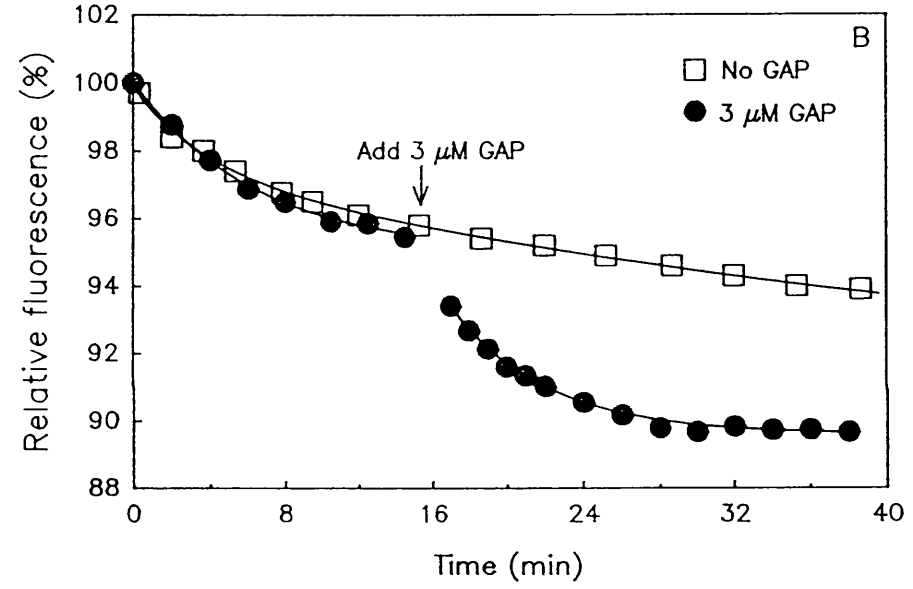
B
No GAP
3 μM GAP
Add 3 μM GAP
Relative fluorescence (%)
102
100
98
96
94
92
90
88
0
8
16
24
32
40
Time (min)

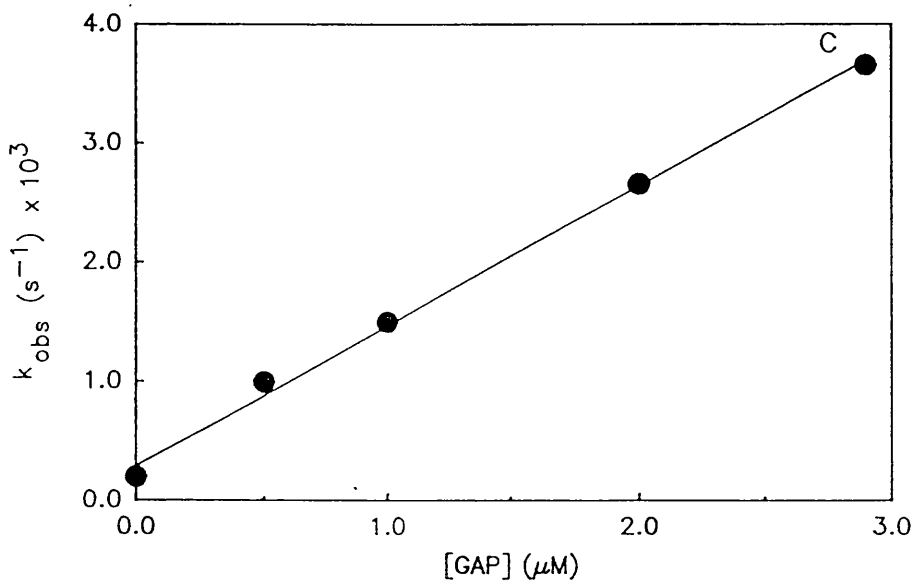
C
k_{obs} (s^{-1}) x 10^3
4.0
3.0
2.0
1.0
0.0
0.0
1.0
2.0
3.0
[GAP] (μM)

4.7 Discussion.

The work described in this chapter is concerned with the kinetic mechanism of the GAP_{365}-activated $p21^{ras}$.GTPase activity. Specifically, the exponential decreases in fluorescence intensity observed with the $p21^{ras}$.mantGTP and $p21^{ras}$.mantGppNHp complexes by Neal et al., (1990) have been re-examined and the effect of GAP_{365} on these changes determined.

Re-examination of these fluorescence changes but making measurements at a much shorter time after the initiation of the reaction showed them to be biphasic for both the mantGTP and mantGppNHp complexes. For mantGTP, the rate of the second phase occurred with the same rate as that of the cleavage reaction - with mantGppNHp, the second phase was the same as that identified by Neal et al., (1990).

One possible consequence of the Neal et al., (1990) model is that the conformational change associated with the slow fluorescence change observed with both mantGTP and mantGpp-NHp may be accelerated by GAP_{365} provided that the mant-nucleotides are good analogues in the GAP_{365}-activated mechanism. GAP_{365} accelerated the rate of mantGTP hydrolysis to a 3-fold greater extent than GTP which is likely to be due to the higher affinity of GAP_{365} for the $p21^{ras}$.mantGTP complex than for the $p21^{ras}$.GTP complex (chapter 5). The rate constant of the slow phase of the fluorescence change with mantGTP is accelerated linearly by GAP_{365} (15 μM $p21^{ras}$.mantGTP; 0 - 3 μM GAP_{365}) and occurs with the same rate constant as that of the chemical cleavage reaction. The use of mantGTP therefore provides a simple assay with which to follow the activation of the $p21^{ras}$ GTPase by GAP proteins.

The equivalent fluorescence change of the $p21^{ras}$.mantGppNHp complex is also accelerated by GAP_{365} over this range although to a lower extent; the activation at 3 μM GAP_{365} being 60-fold for mantGTP and 20-fold for mantGppNHp under these conditions of ionic strength where activation is low. These results provide strong support for the mechanism in which an isomerisation of the $p21^{ras}$.GTP complex (step 2a in scheme 4.1) controls the overall rate of the cleavage reaction and it is this isomerisation reaction which is promoted by GAP_{365}.

Despite extensive structural information about $p21^{ras}$ from X-ray crystallographic studies (section 1.4), it is difficult to correlate the fluorescence changes observed here with specific structures observed in the protein. Solution studies have suggested that $p21^{ras}$ can aggregate to form dimers or higher oligomers (John et al., 1988; Santos and Nebrada, 1989, Hazlett et al., 1990, see chapter 9). The observation that the fast phase of the fluorescence change is also associated with a decrease in fluorescence lifetime (τ_L, chapter 9) demonstrates that this process is associated with an increase in the rotational rate of the mant-fluorophore (Jameson, 1984). This increased in rotational rate could either reflect a change in the local environment of the mant-fluorophore (local rotation) or it could reflect an overall change in the rotational rate of the $p21^{ras}$.mantGTP complex as a whole (global rotation). The dissociation of higher oligomeric complexes may be the cause of the fast phase of the fluorescence change based on the decrease in fluorescence anisotropy. These possibilities will be further investigated and discussed in chapter 9, although other explanations cannot be excluded at this stage. Concentration and temperature dependence of the processes, combined with time resolved fluorescence measurements may help to investigate the nature of the fast phase. Neither of the two processes are the results of nucleotide dissociation (based on gel filtration and fluorescence anisotropy measurements) or acyl migration of the mant-fluorophore from the 3' to the 2' position. The preferential binding by $p21^{ras}$ of the 3' isomer over the 2' isomer may reflect the close proximity of the Val 29 main chain carbonyl group with the 2'-OH position (Pai et al., 1990) resulting in steric blocking of the mant-group at this position.

Based on the X-ray crystallographic structure of the $p21^{ras}$.GTP complex, Pai et al., (1990) have proposed a mechanism for the hydrolysis of GTP. They have suggested that the carbamoyl oxygen of the side chain of Gln 61 activates a water molecule at the active site of $p21^{ras}$ which acts as the nucleophile in the in-line GTP hydrolysis reaction (Feuerstein et al., 1989). The correct orientation of the Gln 61 side chain (with respect to activation of the water molecule) is proposed to be stabilised by conformational re-arrangement of neighbouring residues (residues 60 - 65). It is tempting to suggest that the conformational change associated with the second phase of the fluorescence decrease may represent a change in the structure of these residues from a catalytically inactive position to an active conformation. The large number of possible conformations that these residues can adopt ($> 2^6$ since their posi-

tion is poorly defined in the crystal structure of wild type $p21^{ras}$.GTP) would then explain the relatively slow rate of this isomerisation reaction ($\approx 10^{-4}$ s^{-1}). The model proposed by Pai et al., (1990) would suggest that once the active conformation had been achieved, the hydrolysis of the terminal phosphate would be rapid compared to the initial re-arrangement of these residues. This structural model is consistent with the two - step kinetic mechanism for the intrinsic GTP cleavage reaction proposed by Neal et al., (1990). ~~In terms of the model proposed by Pai et al., (1990)~~. From the results presented in this chapter, the primary effect of GAP_{365} would be to promote the re-arrangement of this constellation of residues into a catalytically active conformation.

The results described in this chapter are only partially consistent with those obtained by other groups investigating the kinetic mechanism of the GAP_{365}-activated $p21^{ras}$.GTPase of $p21^{H\text{-}ras}$ (Antonny et al., 1990; Rensland et al., 1991). These experiments will be discussed at the end of this thesis in chapter 10. Nevertheless, it is argued that the mant-fluorescence results shown here, combined with the characterisation of the protein : nucleotide complexes throughout the time course of the reactions over a range of GAP_{365} concentrations, provide strong evidence that GAP_{365} accelerates the rate of the isomerisation of the $p21^{ras}$.GTP complex and hence the overall rate of GTP hydrolysis.

CHAPTER FIVE

STOPPED FLOW STUDIES OF THE INTERACTION OF $p21^{ras}$ WITH THE CATALYTIC DOMAINS OF p120-GAP AND NEUROFIBROMIN.

"Our whole problem is to make the mistakes as fast as possible."

Wheeler (1956)

5.1 Introduction.

5.1.1 *Use of Single Turnover Enzyme Kinetics.*

The experiments described in chapter 4 have shown that it is probable that GAP accelerates the rate of the isomerisation of the $p21^{ras}$.mantGTP complex. However, they do not give any information about the elementary rate constants of the GAP_{365}-activated hydrolysis reaction which are required in order to define the important intermediates in this process. The experiments described in this chapter investigate the kinetic and equilibrium constants that govern the interaction of $p21^{ras}$.GTP with the catalytic domains of NF1 and p120-GAP. Like p120-GAP, the product of the neurofibromatosis type 1 gene, termed NF1-GAP, NF1 or neurofibromin, is thought to be a GTPase activating protein for $p21^{ras}$. The gene for neurofibromin has been cloned and sequenced (Viskochil et al., 1990; Cawthon et al., 1990; Wallace et al., 1990) and found to encode a protein containing a portion with considerable homology to the catalytic domain of p120-GAP (Xu et al., 1990; Buchberg et al., 1990). This region, the so-called GAP-related domain of neurofibromin (NF1-GRD), can be produced as a recombinant protein which indeed is a functional GAP for $p21^{ras}$ (Martin et al., 1990). Like p120-GAP, the GAP-related domain of NF1 has been reported ~~not~~ to fail to stimulate the GTPase of oncogenic mutants of $p21^{ras}$ and not to bind to effector mutants (Bollag and McCormick, 1991). These workers also proposed that whilst the affinity for NF1-GRD is 30-fold higher than for p120-GAP, the maximally activated $p21^{ras}$.GTPase rate (k_{cat}) is 30-fold lower.

The predominant kinetic approach used here is to perform single turnover experiments considering GAP or NF1 as enzymes catalysing the conversion of the substrate, $p21^{ras}$.GTP, to the products $p21^{ras}$.GDP and P_i. In these experiments, the GAP protein is mixed with $p21^{ras}$.GTP (or $p21^{ras}$.mantGTP) such that the GAP is in a large molar excess over $p21^{ras}$.GTP. The rate of hydrolysis then becomes very fast (on the sub-second time scale) which necessitates the use of rapid reaction approaches, specifically stopped flow techniques. Even though the stopped flow apparatus was designed for using small volumes of solution, it still required relatively large amounts of GAP (3- 4 mg of protein per experiment). Thus, recombinant catalytic domains of GAP (GAP_{344}, Skinner et al., 1991) and NF1 were used in these studies, since full-length proteins were not available in sufficient quantities. The portion of the NF1 gene that codes for residues 1195 - 1528 of human NF1 has been expressed in E.coli (section 2.1.3.2) to produce the catalytic domain of neurofibromin, will be abbreviated for simplicity to NF1. Expression systems for both GAP_{344} and NF1 were developed by Drs Skinner and Lowe at Wellcome Research Laboratories, Beckenham, Kent. Without these expression systems most of the experiments described in this chapter would not have been possible.

5.1.2 *Comparison Between Steady State and Single Turnover Kinetics.*

In contrast to single turnover kinetics, a steady state kinetic analysis (such as that described in chapter 4) is performed under conditions where [substrate] > > [enzyme] and each enzyme molecule undergoes multiple turnovers. The value of k_{cat} ($= V_{max} \div$ [enzyme]) defines the rate constant for the rate determining step but yields no information about which step it is. The other parameter obtained from steady state analyses, that of the Michaelis-Menten constant (K_m), is a function of several elementary rate constants, the precise form of which depends on the model proposed for the enzyme mechanism. In certain cases, the K_m approximates to the equilibrium dissociation constant, K_d, although in the absence of other independent confirmatory evidence, this should not be assumed.

The study of transient enzyme kinetics aims to provide information about the rate constants of the elementary steps in the mechanism. These values can only be determined when enzyme reactions are observed with a time resolution faster than the time taken for a single turnover to occur, so that the rate of formation and decomposition of intermediates (to their steady state concentrations) can be determined. The major approach to the study of transients of intermediates has been the use of spectroscopic signals (absorbance or fluorescence) arising from particular steps in the reaction pathway. This approach has been used in this chapter. Whilst such signals are often sensitive to small changes in the environment of the probe, they have the major disadvantage that in the absence of other evidence, it is often difficult to ascribe these changes to an individual molecular process in the reaction mechanism. For a complete analysis of the reaction mechanism of an enzyme, then the chemical state of the substrate throughout the time course of the reaction should also be determined (for example, by quenched flow techniques). The results presented here provide a preliminary characterisation of the kinetic mechanism of the GAP-activated $p21^{ras}$.GTPase.

5.2 Kinetic Studies of the Interaction of $p21^{ras}$ with GAP_{344}.

5.2.1 *Stopped Flow Recording of the Reaction of $p21^{N\text{-}ras}$.mantGTP with GAP_{344}.*

The reaction of 1 μM wild type $p21^{N\text{-}ras}$.mantGTP with excess GAP_{344} was performed at $30^{o}C$ in a fluorescence stopped flow apparatus. All concentrations reported here refer to those after mixing, i.e final observation cell concentrations. These reactions were performed under conditions of low ionic strength (20 mM TrisHCl, pH 7.5, 1 mM $MgCl_2$, 0.1 mM DTT, buffer C) for two reasons. Firstly, the experimental results obtained under these conditions could be directly compared to those reported by other groups (Reinstein et al., 1991; Rensland et al., 1991, Bollag and McCormick, 1991; Wiesmuller and Wittinghofer, 1992) using similarly low ionic strength buffer conditions. Secondly, only by using low ionic strength conditions, which produce the highest activation of the intrinsic GTPase of $p21^{ras}$, could the dependence of the rate of reaction on the GAP concentration be defined with confidence. Although the equilibrium and rate constants of the GAP activated mechanism are highly dependent on salt conditions (see chapter 6), the actual mechanism of the process is unlikely to vary.

Figure 5.1 shows the variation of the fluorescence intensity with time after mixing 1 μM $p21^{ras}$.mantGTP with 6 μM - 60 μM GAP_{344} in the stopped flow apparatus at 30°C. The decrease in fluorescence intensity could be fitted in all cases to a single exponential decay. The amplitudes of the fluorescence changes also increase with increasing concentrations of GAP, and the significance of this result will be discussed in section 5.3.4 and in more detail in chapter 6. The variation of the observed rate constant of the fluorescence change with [GAP_{344}] is shown in Figure 5.2 (open circles). Higher concentrations of GAP_{344} were not used partially due to the *amount* of material available and partially because of the practical difficulty in obtaining high *concentrations* of GAP_{344} (> 120 μM) in the syringe. The hyperbolic dependence of the observed rate constant can arise as a result of several mechanisms (Bagshaw et al., 1974) which are discussed in more detail in section 5.4.2. However, the simplest mechanism to explain the results is that there is a rapidly reversible formation of the $p21^{ras}$.mantGTP.GAP_{344} ternary complex (which has an enhanced fluorescence compared to that of $p21^{ras}$.mantGTP alone, chapter 6) and this step is followed by an essentially irreversible first order process. Based on the results presented in chapter 4, the most simple interpretation is that this process is the GAP-catalysed isomerisation reaction of $p21^{ras}$.mantGTP (scheme 5.1).

$$\text{p21.mantGTP + GAP} \underset{k_{-1}}{\overset{k_{+1}}{\rightleftharpoons}} \text{p21.mantGTP.GAP} \xrightarrow{k_{+2a'}} \text{p21}^{*}\text{.mantGTP.GAP}$$

(scheme 5.1)

The two parameters obtained from this hyperbolic dependence are the concentration of GAP_{344} required to obtain half-maximal k_{obs} (K_1' = 17.4 ± 3.0 μM) and the limiting value of the rate constant at saturating concentrations of GAP_{344} (k_{2a}' = 13.9 ± 0.9 s^{-1}). Assuming this mechanism, we can assign K_1' to the equilibrium dissociation constant (K_d) of the initial binding process (k_{-1} / k_{+1}) and k_{2a}' to the rate of the isomerisation reaction in the $p21^{ras}$.mantGTP.GAP_{344} complex (scheme 5.1).

Figure 5.1: Stopped Flow Recording of the Reaction of $p21^{ras}$.mantGTP With Excess GAP_{344}.

1 μM $p21^{N\text{-}ras}$.mantGTP in buffer C (20 mM TrisHCl, pH 7.5, 1 mM $MgCl_2$, 0.1 mM DTT) was rapidly mixed with 6 - 60 μM GAP_{344} in the same buffer at 30°C. GAP_{344} concentrations refer to final concentrations in the observation chamber (in μM) and are shown in the Figure. The voltage output from the photomultiplier tube was normalised to the first data point after the flow had stopped (as 100 % relative fluorescence intensity). Each of the individual traces could be fitted to a single exponential decay. Analysis of the residuals from these fits indicated that first order kinetics were sufficient to describe the change in intensity given the deviations of the experimental data from the predicted single exponential decay over the complete time course of the fluorescence change. Data was monitored over a sufficient time period for the reactions to go to completion (typically > 5 half times), and are plotted on this scale solely for clarity. Traces shown are averages of 4 individual traces. The rate constants obtained from these reactions are quoted in the text as the mean ($\pm \sigma_{n-1}$) for the 4 constituent traces.

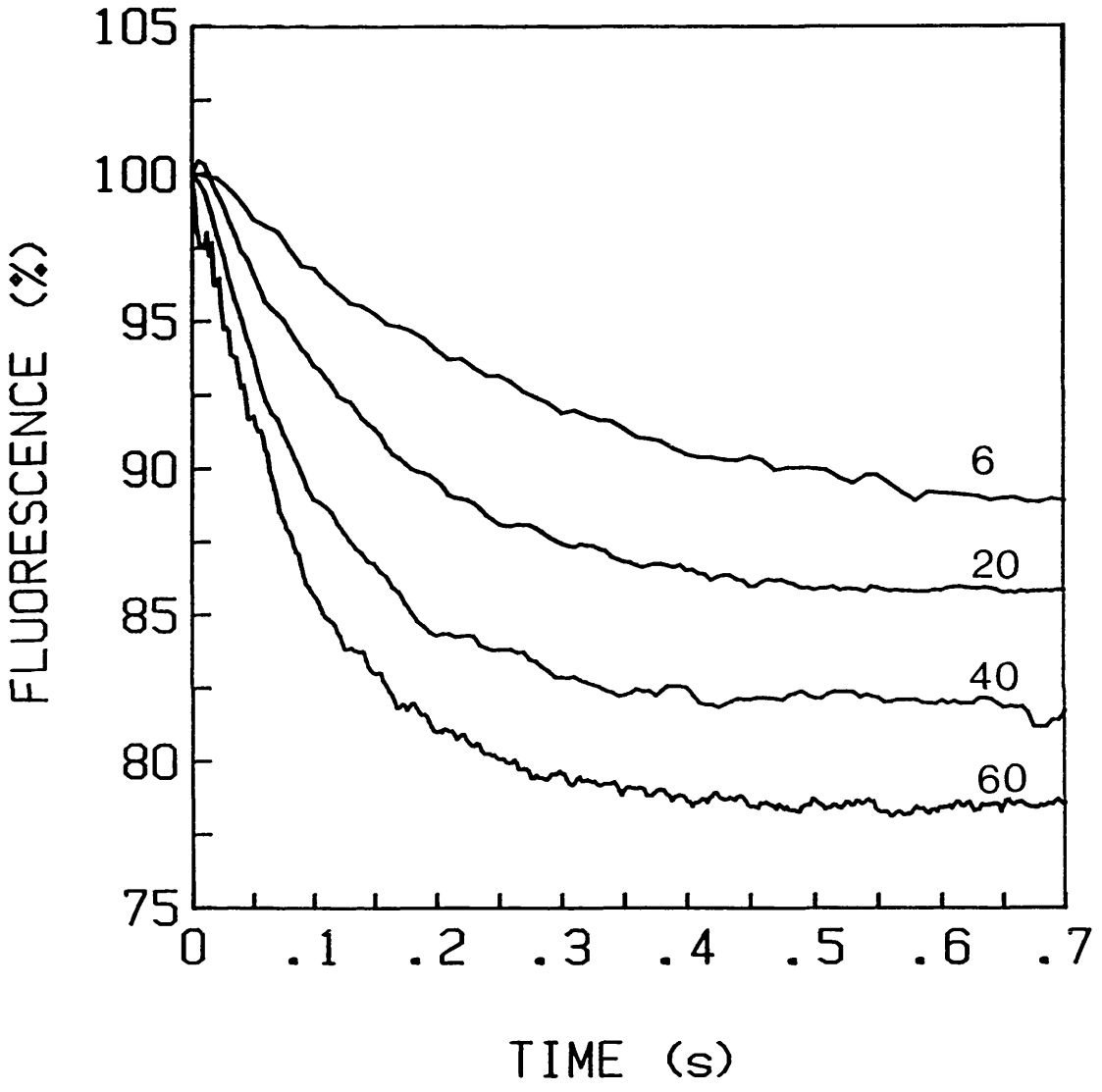
105
100
95
90
85
80
75
FLUORESCENCE (%)
0
.1
.2
.3
.4
.5
.6
.7
TIME (s)
6
20
40
60

Figure 5.2: Dependence of the Observed Rate Constant of the Fluorescence Change (k_{obs}) on GAP_{344} Concentration at 30°C.

The pseudo-first order rate constant, obtained by fitting the reaction traces from experiments such as those shown in Figure 5.1 to single exponential decays, was determined over a range of GAP_{344} concentrations.

(A) Open circles: Variation in the rate constant for the fluorescence changes shown in Figure 5.1 on GAP_{344} concentration where reactions were performed in buffer C. The solid line through the data is the best fit to a hyperbola where the [GAP_{344}] required to achieve 50 % of the maximal rate (K_1') = 17.4 ($\pm$ 3.0) μM, and the maximal rate as [GAP_{344}] $\rightarrow\infty$ (k_{2a}') of 13.9 ($\pm$ 0.9) s^{-1}.

(B) Filled circles: As for (A) except all buffers contained 20 mM NaCl in addition to buffer C. The solid line corresponds to values of K_1' = 32.6 ($\pm$ 8.6) μM and k_{2a}' = 12.8 ($\pm$ 1.6) s^{-1}.

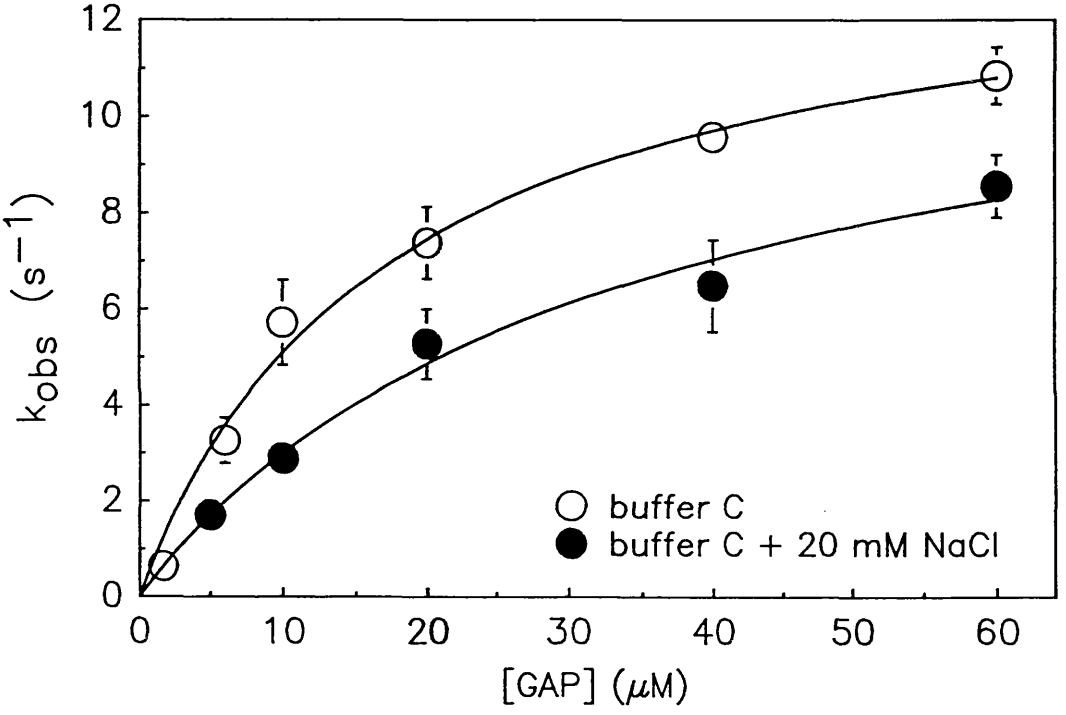
12
10
8
6
4
2
0
k_{obs} (s^{-1})
0
10
20
30
40
50
60
[GAP] (μM)
buffer C
buffer C + 20 mM NaCl

A biphasic decrease in the fluorescence intensity during the hydrolysis of mantGTP *in the absence of GAP* was observed (section 4.5.2). Stopped flow studies were performed to determine whether the rates of GAP_{344}-catalysed mantGTP hydrolysis were different at the beginning of the fast phase (t = 2 min) and at the end of the fast phase (t = 15 min). At a fixed GAP concentration (6 μM), identical rate constants for the GAP-activated rate of the fluorescence change were observed in both cases (Figure 5.3, k_{obs} = 1.85 ($\pm$ 0.12) s^{-1} after 2 min and 1.79 ($\pm$ 0.10) s^{-1} after 15 min). The smaller amplitude of the fluorescence change after incubation for 15 min can be attributed to the formation of $\approx$ 10 % $p21^{ras}$.mantGDP due to the intrinsic mantGTP cleavage rate at this temperature (half time $\approx$ 50 min). The large amount of noise that is seen in these traces during the first 200 ms of the reaction is due to mechanical vibration of the lamp, and can be reduced by physically isolating the lamp from the stopped flow benchtop (for example, see Figure 5.2). For all of the experiments described here, the sample of $p21^{ras}$.mantGTP was incubated at the final working temperature for 5 min before reaction with GAP_{344} or NF1.

5.2.2 *Effect of Ionic Strength on the Interaction of $p21^{ras}$ with GAP_{344} Studied By Stopped Flow Techniques.*

Stopped flow studies such as those described above were performed to determine whether increasing ionic strength affects the binding step (K_1') or the subsequent isomerisation (k_{2a}'), or both, and to determine the magnitude of the effect. The results of these experiments form the basis of the data analysis in chapter 6. In the stopped flow experiments, NaCl to a final concentration of 20 mM was added to all solutions, and the rate of the fluorescence change measured at different [GAP_{344}] (Figure 5.2). In the presence of 20 mM NaCl, the dependence of k_{obs} on [GAP_{344}] was markedly changed. The apparent equilibrium dissociation constant, K_1', = 33 ($\pm$ 9) μM was greater than that under the standard low salt conditions (17 ($\pm$ 3) μM), whereas the calculated value of k_{2a}' = 12.8 ($\pm$ 1.6) s^{-1} is not significantly different from that obtained previously. These data demonstrate that the primary effect of increasing NaCl concentrations is to reduce the affinity of GAP_{344} for $p21^{ras}$.mantGTP, whilst leaving the rate of the isomerisation largely unaffected.

Figure 5.3 : Reaction of $p21^{ras}$.mantGTP With GAP_{344} After Incubation of $p21^{ras}$.mantGTP for 2 or 15 min at 23°C.

Stopped flow recordings were performed using 6 μM GAP in buffer C exactly as described in Figure 5.2 except that the temperature of the reaction was 23°C. $p21^{ras}$.mantGTP samples were incubated for either 2 min or 15 min at 23°C (as indicated in the Figure) before reaction with GAP_{344}. The fluorescence changes could be fitted to single exponential decays with rate constants (mean ($\pm \sigma_{n-1}$), n= 4) of 1.85 ($\pm$ 0.12) s^{-1} after 2 min and 1.79 ($\pm$ 0.10) s^{-1} after 15 min.

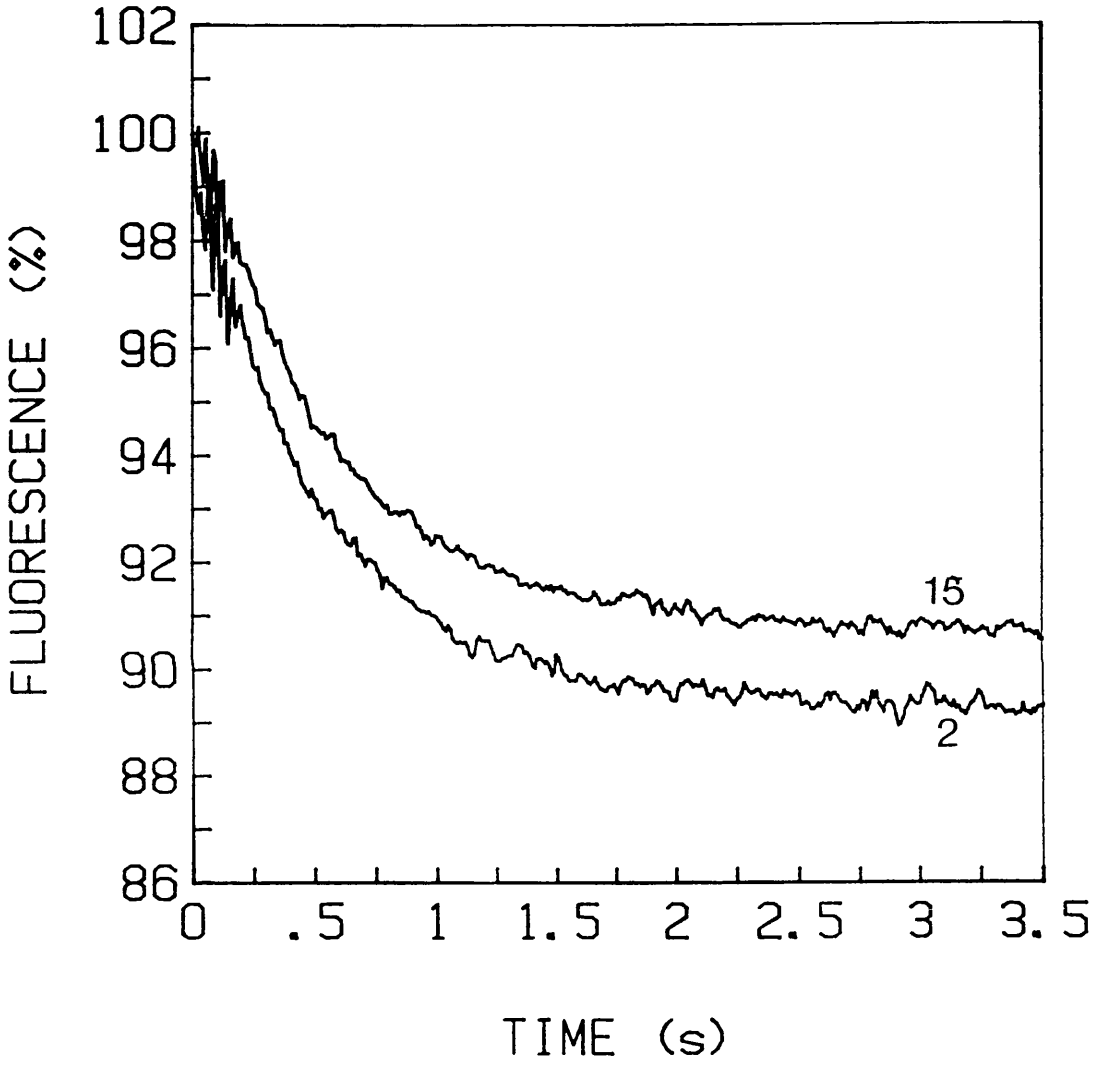
102
100
98
96
94
92
90
88
86
FLUORESCENCE (%)
15
2
0
.5
1
1.5
2
2.5
3
3.5
TIME (s)

The dependence of the observed rate of the fluorescence change on GAP_{344} concentration at 23°C is also hyperbolic (Figure 5.4). The values of K_1' and k_{2a}' obtained in buffer C at this temperature are 19 (± 5) μM and 7.8 (± 0.4) s^{-1} respectively. Thus, increasing the temperature of the reaction from 23°C to 30°C leads to a 1.8-fold increase in k_{2a}' whilst the equilibrium constant for the formation of the ternary complex is primarily unaffected. Reactions at 23°C have also been performed in the presence of 50 mM NaCl (Figure 5.4) although the resultant low binding affinity does not allow one to analyse the data with the same degree of confidence over the range of GAP_{344} concentrations used (up to 60 μM GAP_{344}). However, the results are consistent with the conclusion that the major effect of increasing ionic strength is a reduction in binding affinity (K_1'= 99 (± 10) μM and k_{2a}' = 12.1 (± 0.4) s^{-1}, curve A). Whilst these data show an apparent increase in the maximal rate of the fluorescence change, this value is critically dependent on the value of the rate constant at the highest concentration of GAP used (60 μM) which also has the largest standard deviations for this experiment. If the lower limit of the standard deviation is used (4.05 s^{-1}), then k_{2a}' = 8.1 (± 0.2) s^{-1} and K_1' = 59 (± 5) μM (curve B). Thus, these experiments show that within experimental error, the rate of the isomerisation reaction is unaffected by NaCl whilst the binding constant is increased by 3 - 5 -fold in the presence of 50 mM NaCl.

5.2.3 *Fluorescence Changes Associated with the Formation of the $p21^{ras}$.mantGTP.GAP Complex Studied by Stopped Flow Techniques.*

The results of the stopped flow experiments indicated that both the rate and amplitude of the fluorescence change observed after mixing $p21^{ras}$.mantGTP with excess GAP_{344} increased with increasing GAP_{344} concentration (Figure 5.1). Thus, at 6 μM GAP_{344} the amplitude of the exponential decay was 11% whilst at 60 μM GAP_{344}, this value increased to 22 %. The amplitude of the fluorescence change when $[GAP_{344}] \rightarrow 0$ is approximately 8 %, although this value is prone to high errors (± 2%) due to the limited amount of data when $[GAP_{344}] << K_1'$. The most simple interpretation of these observations is that there is a significant increase in fluorescence intensity upon formation of the $p21^{ras}$.mantGTP.GAP_{344} complex. This possibility is discussed in chapter 6.

Figure 5.4: Dependence of the Rate of the Fluorescence Change on GAP_{344} Concentration at $23^{o}C$.

Data were obtained exactly as described in Figure 5.2 except that all reactions were performed at $23^{o}C$ in buffer C (open circles) or in buffer C + 50 mM NaCl (filled circles). Data points are quoted as mean ($\pm \sigma_{n-1}$) of 4 separate determinations. The solid line through the open circles corresponds to a $K_1' = 18.8 (\pm 4.8)$ μM and $k_{2a}' = 7.8 (\pm 0.4)$ s^{-1}. Curve A represents the best fit of the raw data in the presence of 50 mM NaCl to a hyperbola where $K_1' = 99 (\pm 10)$ μM and $k_{2a}' = 12.1 (\pm 0.4)$ s^{-1}. Curve B is the best fit to the same data except that the rate constant at 60 μM GAP_{344} is taken to be the lower limit of the standard deviation of the mean (4.05 s^{-1} compared to 4.55 ($\pm$ 0.5) s^{-1}). Curve B corresponds to $K_1' = 59 (\pm 5)$ μM and $k_{2a}' = 8.1 (\pm 0.2)$ s^{-1}.

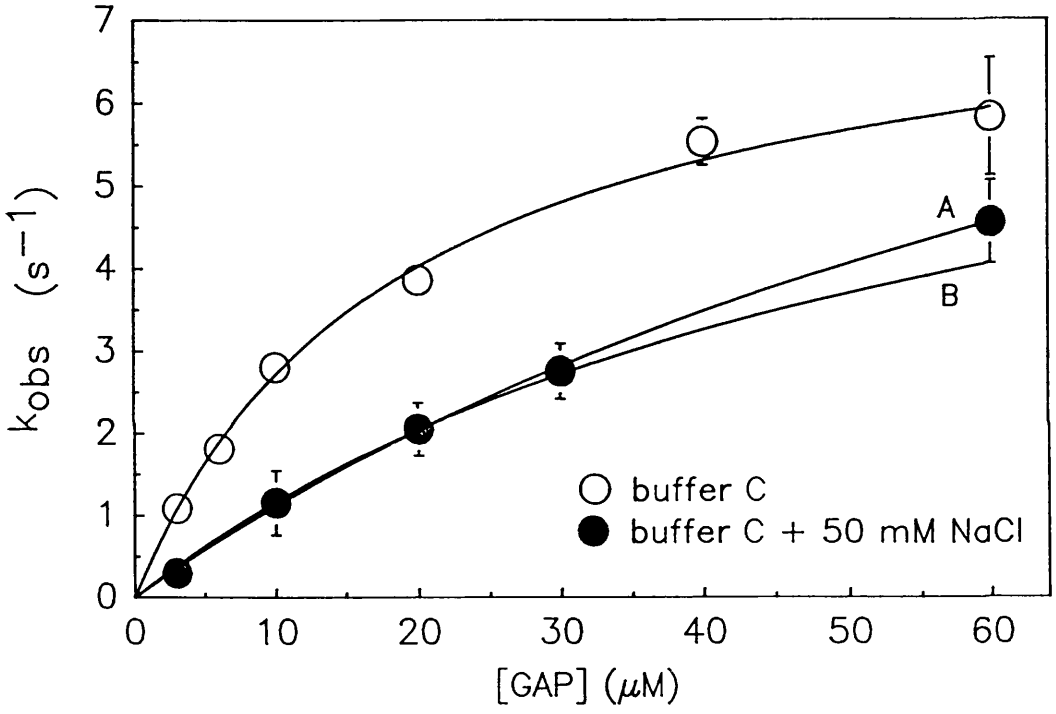
7
6
5
4
3
2
1
0
k_{obs} (s^{-1})
0
10
20
30
40
50
60
[GAP] (μM)
A
B
buffer C
buffer C + 50 mM NaCl

In many cases, the ability to perform transient kinetic studies is limited by the availability of a signal with which to monitor a specific process in the mechanism of interest. Consequently, alternative spectroscopic signals with which to monitor GAP_{344} binding to $p21^{ras}$.mantGTP were sought. With excitation at 280 nm, the reaction of 3 μM GAP_{344} with 1 μM $p21^{ras}$.mantGTP at 23°C leads to fluorescence amplitudes $\approx$ 2-fold higher than obtained by direct excitation of the mant-fluorophore at 366 nm, although the observed rates were independent of wavelength, Figure 5.5). This results suggests that there is likely to be fluorescence resonance energy transfer (FRET) between Trp 884 (the sole Trp residue in GAP_{344}) and the mant-fluorophore in the $p21^{ras}$.mantGTP.GAP_{344} complex (chapter 6). The larger amplitude of the signal when fluorescence emission is monitored via GAP_{344} is likely to be due to the fact that FRET only occurs when the donor and acceptor fluorophores are in close proximity (for example, in the ternary complex). Supporting evidence for the presence of FRET with GAP_{344} comes from steady state fluorescence intensity and fluorescence depolarisation experiments (chapter 6).

5.3 Kinetic Studies of the Interaction of $p21^{ras}$ With NF1.

5.3.1 *Stopped Flow Single Turnover Studies with $p21^{ras}$.mantGTP and NF1.*

The reaction of $p21^{ras}$.mantGTP with excess NF1 at 26°C is shown in Figure 5.6, where the majority of the data (from 0.1 - 1.5 sec, see below) could be fitted to a single exponential with a rate constant of 6.0 s^{-1}. The rate and amplitude of the fluorescence decay was essentially independent of the NF1 concentration over the range 2.1 - 7.4 μM. Lower concentrations of NF1 could not be used since they would not comply with pseudo-first order conditions. This is in contrast to the situation with GAP_{344} where the rate of the fluorescence change and its amplitude increase with increasing concentrations of GAP over the range 3 - 60 μM GAP (section 5.2.2 and 5.2.4). The amplitude of this slow fluorescence change (6 s^{-1}) was constant at 20 - 25% over the range of NF1 concentrations used. This value is similar to that observed with GAP_{344} at saturating concentrations (section 5.2.4). These results indicate that whilst the maximally activated rate of the fluorescence change (k_{2a}') is reduced by only a factor of $\approx$ 2 compared to GAP_{344}, the binding constant is significantly lower. Thus, under the condi-

Figure 5.5: Stopped Flow Recordings of the Reaction of $p21^{ras}$.mantGTP with GAP_{344} with Excitation at 280 nm or 366 nm.

Reactions were performed at 23°C with 3 μM GAP_{344} as described in Figure 5.5. Fluorescence emission was monitored through a Wratten 47 B filter whilst excitation was through interference filters at either 366 nm (Corion P10-365) or at 280 nm (Corion G25-280). Rates and amplitudes of the fluorescence changes were 1.04 ($\pm$ 0.11) s^{-1} and 6.2 ($\pm$ 0.9) % respectivly (excitation = 366 nm) and 1.17 ($\pm$ 0.16) s^{-1} and 11.6 ($\pm$ 1.4) % (excitation = 280 nm).

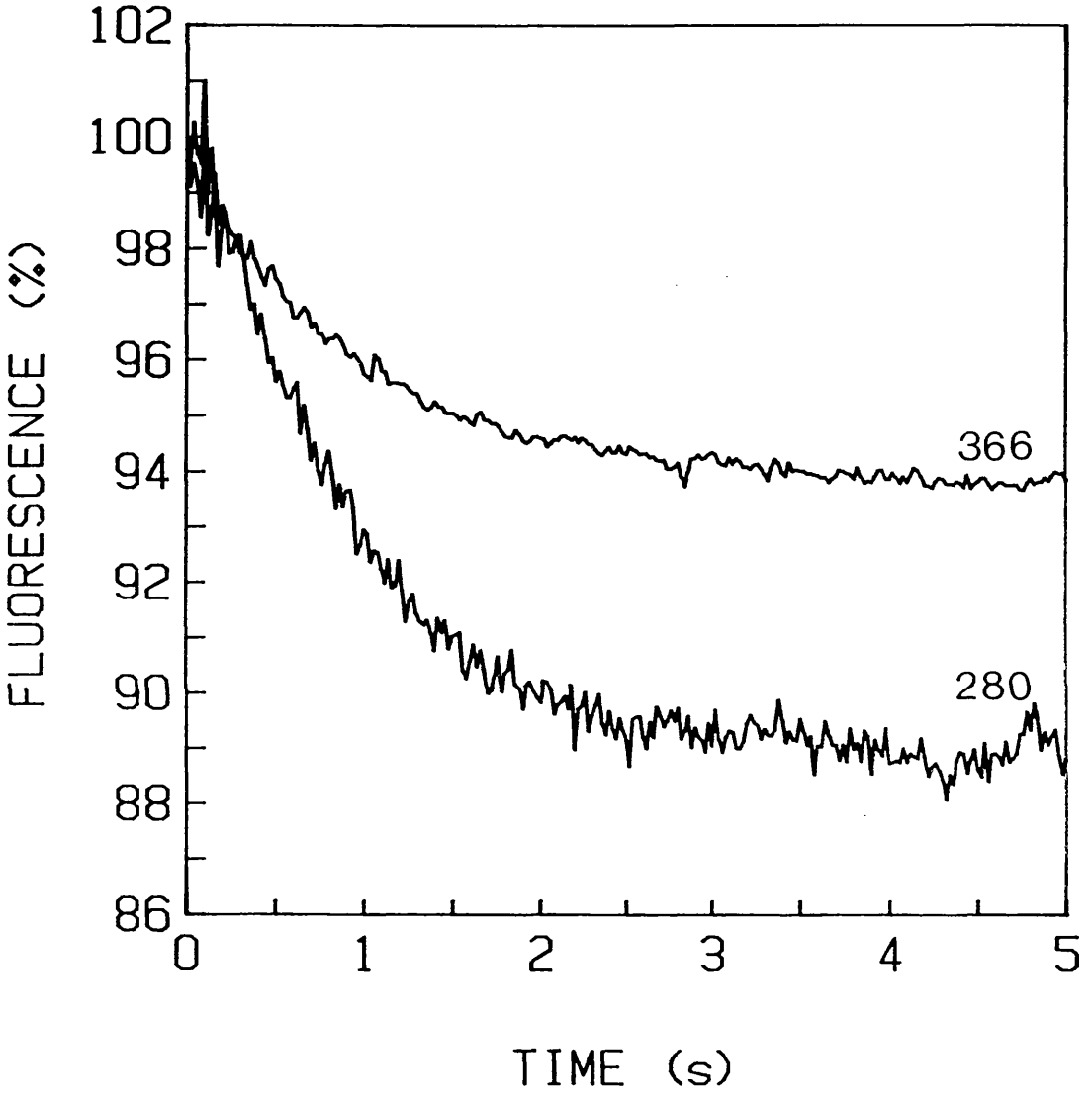
102
100
98
96
94
92
90
88
86
FLUORESCENCE (%)
366
280
0
1
2
3
4
5
TIME (s)

Figure 5.6 Stopped Flow Recording of the Slow Fluorescence Change Occurring During the Reaction of $p21^{ras}$.mantGTP with Excess NF1.

1 μM $p21^{ras}$.mantGTP in buffer C was rapidly mixed with 7.4 μM NF1 in the same buffer at 26^{o}C. Conditions were exactly as for Figure 5.1, where the flow stops at t = 0 sec. The data from 0.1 - 1.5 sec could be fitted to a single exponential decay with a rate constant of 6.0 s^{-1} and an amplitude of 20 %.

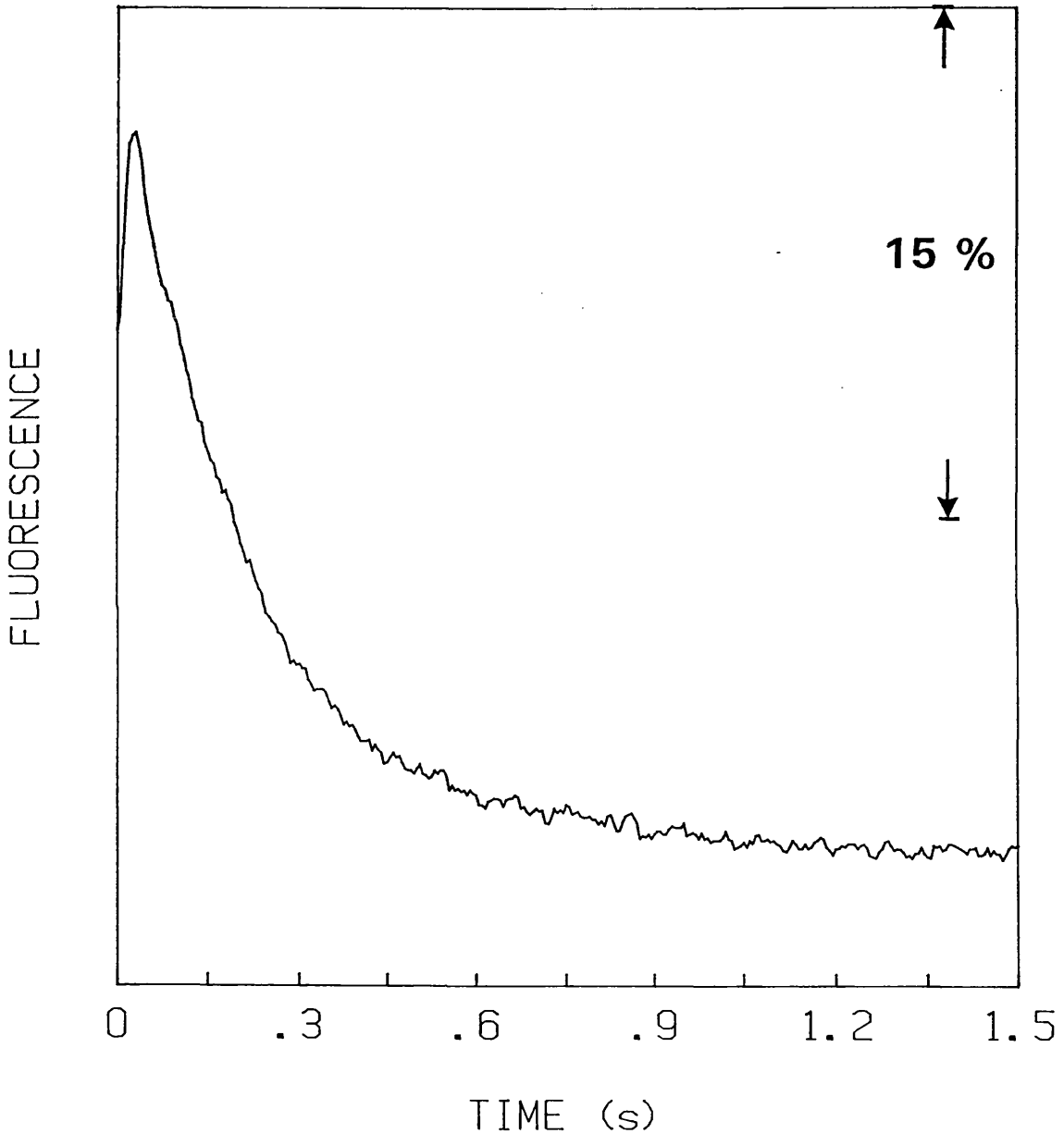
15 %
FLUORESCENCE
0
.3
.6
.9
1.2
1.5
TIME (s)

tions used in these experiments, saturation of $p21^{ras}$.mantGTP has been achieved even at the lowest concentration of NF1 used. It is not, however, possible to determine the exact value of the binding constant from these studies alone (see chapter 6), but suggest a K_d of $\leq$ 1 μM under these conditions of low ionic strength.

An interesting feature of the stopped flow experiments with NF1 was the consistent observation of an initial increase in fluorescence intensity occurring prior to the decrease in intensity (at 6 s^{-1}). The initial 150 ms of the reaction with 2.1 μM NF1 are shown in Figure 5.7.a (trace 1). No change in fluorescence intensity was observed when $p21^{ras}$.mantGTP was mixed with buffer under these conditions (Figure 5.7.a.2). The reaction with $p21^{ras}$.mantGTP could be described by 2 exponentials (where the rate of the second process = 6 s^{-1}) which gave an observed rate constant for the initial increase in intensity of 70 s^{-1}. At higher concentrations of NF1 (7.4 μM), the rate of this process increased to 170 s^{-1} (Figure 5.7.b.4) suggesting that this transient fluorescence change is monitoring a second order process. At the higher [NF1], the observed amplitude was reduced by $\approx$ 50 %, an observation which is consistent with the loss of a larger fraction of the total fluorescence change in the dead time of the instrument as the rate of the process is increased. Similar experiments with GAP_{344} and wild type $p21^{N\text{-}ras}$.mantGTP showed no evidence of a fluorescence intensity increase during the early time period of the reaction.

5.3.2 *Multiple Turnover Kinetic Studies of $p21^{ras}$.GTP with NF1..*

The rate of GTP hydrolysis with catalytic [NF1] was determined under conditions of low (buffer C) and high (buffer B) ionic strength. The results of these experiments are used in order to allow a direct comparison to be made with the multiple turnover k_{cat} results reported by other groups using this (Bollag and McCormick, 1991; Wittinghofer et al., 1992) and with the single turnover stopped flow studies reported previously.

Following the addition of NF1 (5 - 40 nM final concentration), the initial rate of hydrolysis of GTP bound to $p21^{N\text{-}ras}$ at 30°C in buffer B (50 mM TrisHCl, pH 7.5, 100 mM NaCl, 10 mM $MgCl_2$, 10 mM DTT) was determined from the rate of inorganic phosphate release (Webb,

Figure 5.7. Stopped Flow Recording of the Transient Increase In Intensity Occurring Immediately After Mixing $p21^{ras}$.mantGTP with NF1.

Reactions were performed as in Figure 5.6. The flow stops at time t = 0 sec.

Panel A: 1 μM $p21^{ras}$.mantGTP was rapidly mixed with either 2.1 μM NF1 (trace 1) or with buffer (trace 2). The reaction with NF1 leads to a transient increase in fluorescence intensity of 10 % ($k_{obs,1}$ = 70 s^{-1}) followed by a decrease in intensity ($k_{obs,2}$ = 6 s^{-1}) which appears linear when plotted on this time scale.

Panel B: As above except that the concentration of NF1 was either 2.1 μM (trace 3) or 7.4 μM (trace 4). The rate constant for the transient increase in intensity observed in (4) = 170 s^{-1}. The rate of the second slow phase was identical at both concentrations.

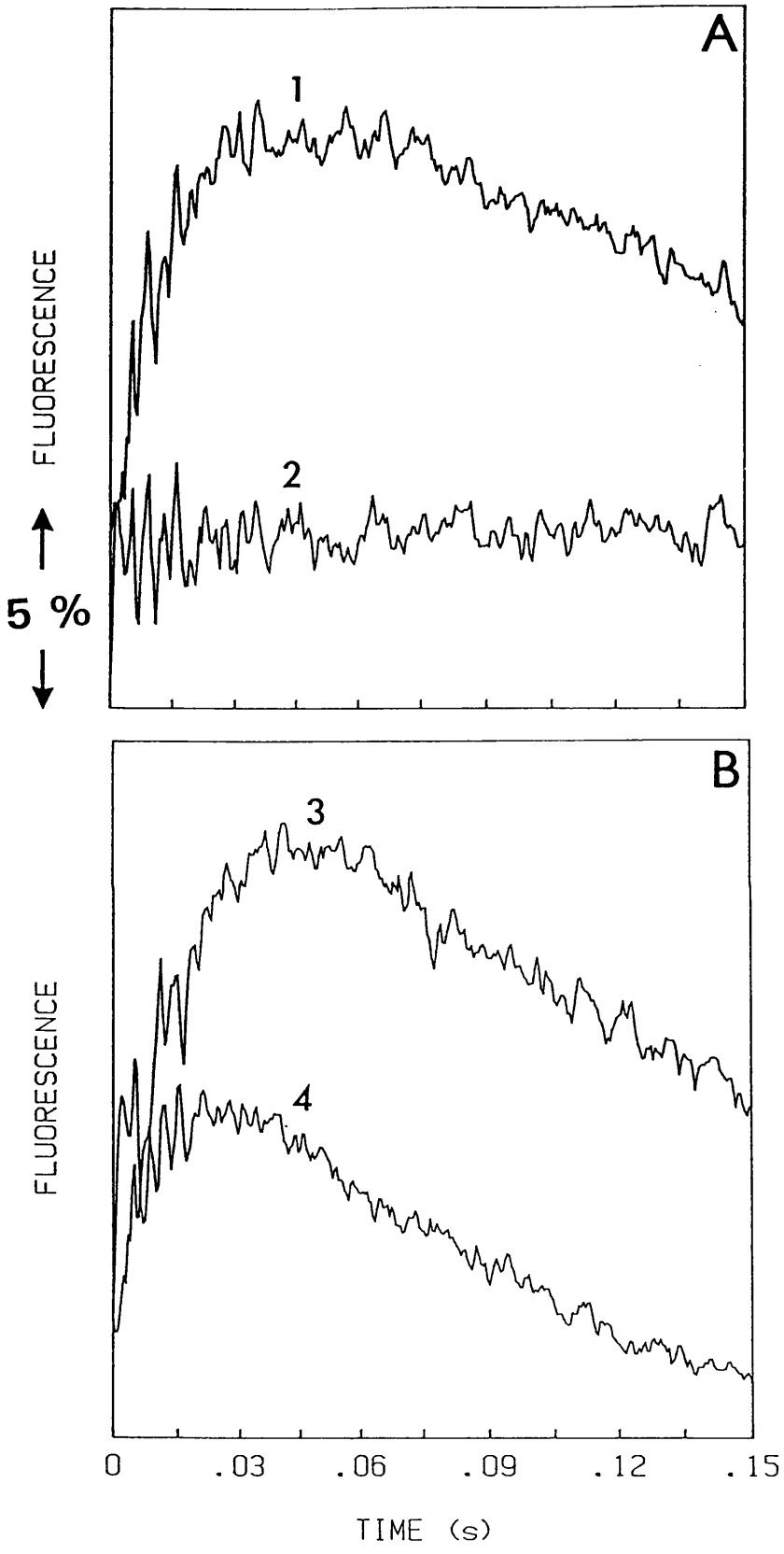
A
1
2
FLUORESCENCE
5 %
B
3
4
FLUORESCENCE
0
.03
.06
.09
.12
.15
TIME (s)

1992; Webb and Hunter, 1992, Figure 5.8.a). The initial rate varied linearly with NF1 concentration (gradient = 4.9 (± 0.26) s^{-1}) and was not significantly different for that obtained with the mantGTP complex (5.6 (± 1.0) s^{-1}). The k_{cat} value (at saturating $p21^{ras}$.GTP) obtained under multiple turnover conditions has been determined under identical conditions to those used in the stopped flow studies. The initial rate of P_i release at a fixed [NF1] (13 nM) was independent of the [$p21^{ras}$.GTP] over the range 5 - 20 μM (Figure 5.8.b) suggesting that near saturation of the NF1 had been achieved even at 5 μM $p21^{ras}$.GTP.

5.4. Discussion.

5.4.1 *Comparison of the Methods For Determining Equilibrium and Kinetic Constants for the GAP-Activated $p21^{ras}$.GTPase.*

The two basic parameters that define the activity of an enzyme are the affinity with which it binds to its substrate (the equilibrium dissociation constant, K_d), and the maximal rate of reaction at saturating concentrations of substrate (the turnover number or k_{cat}). Thus far, two procedures have been used to estimate the affinity with which $p21^{ras}$.GTP binds to fragments of p120-GAP and neurofibromin.

The most common method is to measure the initial rate of GTP hydrolysis ($v_{initial}$) as a function of [$p21^{ras}$.GTP] at a fixed catalytic concentration of the GAP (Gideon et al., 1992; Webb and Hunter, 1992; Wittinghofer et al., 1992; Reinstein et al., 1991). The dependence of $v_{initial}$ on [$p21^{ras}$.GTP] is analysed using Michaelis-Menten kinetics, although the K_m approximates to the equilibrium dissociation constant, K_d, only under certain circumstances. The value of the K_m is dependent only on a knowledge of the [$p21^{ras}$.GTP]. Alternatively, the affinity for GAP of a $p21^{ras}$ whose GTP cleavage rate is not activated by the GAP, (e.g oncogenic mutants or wild type $p21^{ras}$ complexed with non-hydrolysable GTP analogues), can be estimated by measuring the inhibitory effect of such $p21^{ras}$ proteins on the activity of catalytic amounts of the GAP acting on low concentrations of wild type $p21^{ras}$.GTP (Vogel et al., 1988; Webb and Hunter, 1992, Gideon et al., 1992). However, the calculation of the K_d by this procedure makes assumptions about the competitive nature of the inhibition.

Figure 5.8. Rate of NF1-Catalysed Hydrolysis of GTP and mantGTP by $p21^{ras}$.

Panel A : 15μM $p21^{ras}$.GTP or $p21^{ras}$.mantGTP in buffer B (50 mM TrisHCl, pH 7.5, 100 mM NaCl, 10 mM $MgCl_2$, 10 mM DTT) was incubated at 30^{0}C. Filled circles: The rate of GTP hydrolysis was determined by the continuous phosphate release assay described by Webb, (1992), and Webb and Hunter, (1992). NF1 was added to a final concentration of 5 - 40 nM and the change in absorbance of the solution at 360 nm monitored with time. The initial rate of the reaction, $v_{initial}$ was calculated from the rate of the absorbance change (extinction coefficient upon phosphorolysis = 11 mM^{-1} cm^{-1} at 360 nm) and is plotted as a function of [NF1] added. The solid line (B) is a best fit to a linear regression with a gradient of 4.9 ($\pm$ 0.3) s^{-1}. Open circles: The initial rate of mantGTP hydrolysis was determined by ion exchange H.P.L.C of th reaction mixtures containing 2 - 20.8 nM NF1. The solid line (A) is the best fit to a linear regression with a gradient of 5.6 ($\pm$ 1.0) s^{-1}.

Panel B: Reactions with $p21^{ras}$.GTP were performed exactly as described for (A) above except that the buffer contained 20 mM TrisHCl, pH 7.5, 1 mM $MgCl_2$, 0.1 mM DTT and the concentration of NF1 was maintained at 13.3 nM and the concentration of $p21^{ras}$.GTP was varied from 5 - 20 μM. The total amplitude of the absorbance changes varied with [$p21^{ras}$.GTP] as expected (Webb, 1992) whilst the initial rate of reaction was essentially independent of [$p21^{ras}$.GTP]. The initial rate of hydrolysis at saturating concentrations of $p21^{ras}$.GTP divided by the [NF1] (k_{cat}) was 6.1 ($\pm$ 0.1) s^{-1} (from the data points at 10, 15, and 20 μM $p21^{ras}$.GTP.

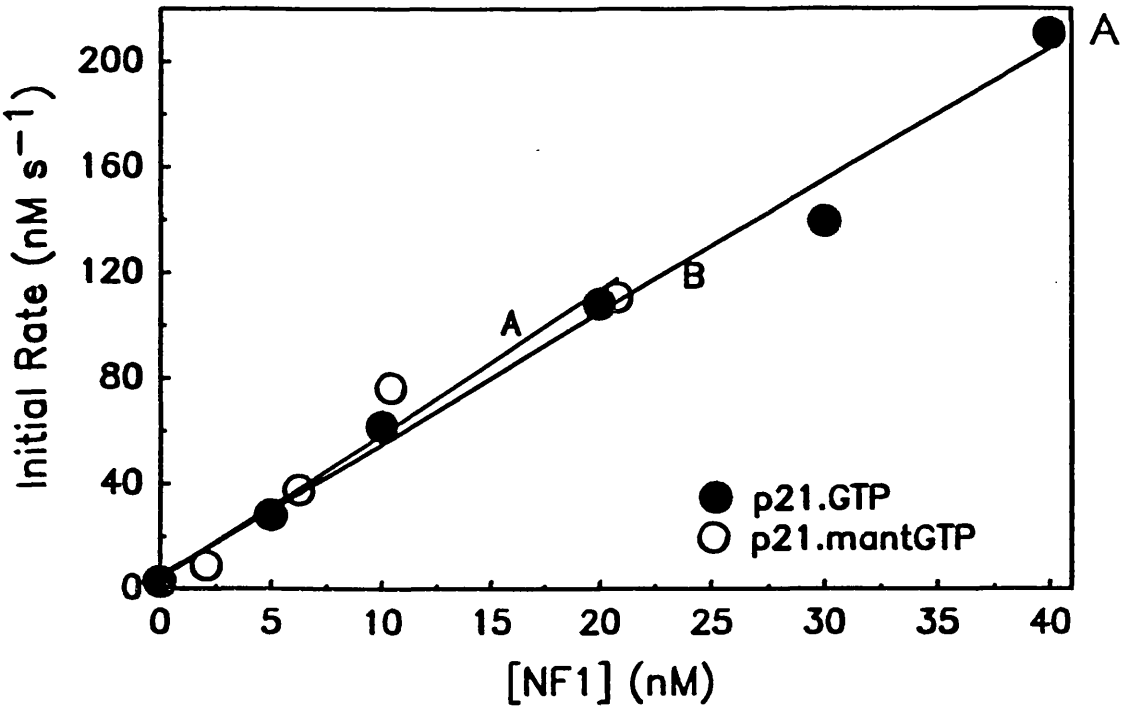
A
Initial Rate (nM s^{-1})
200
160
120
80
40
0
0
5
10
15
20
25
30
35
40
[NF1] (nM)
A
B
p21.GTP
p21.mantGTP

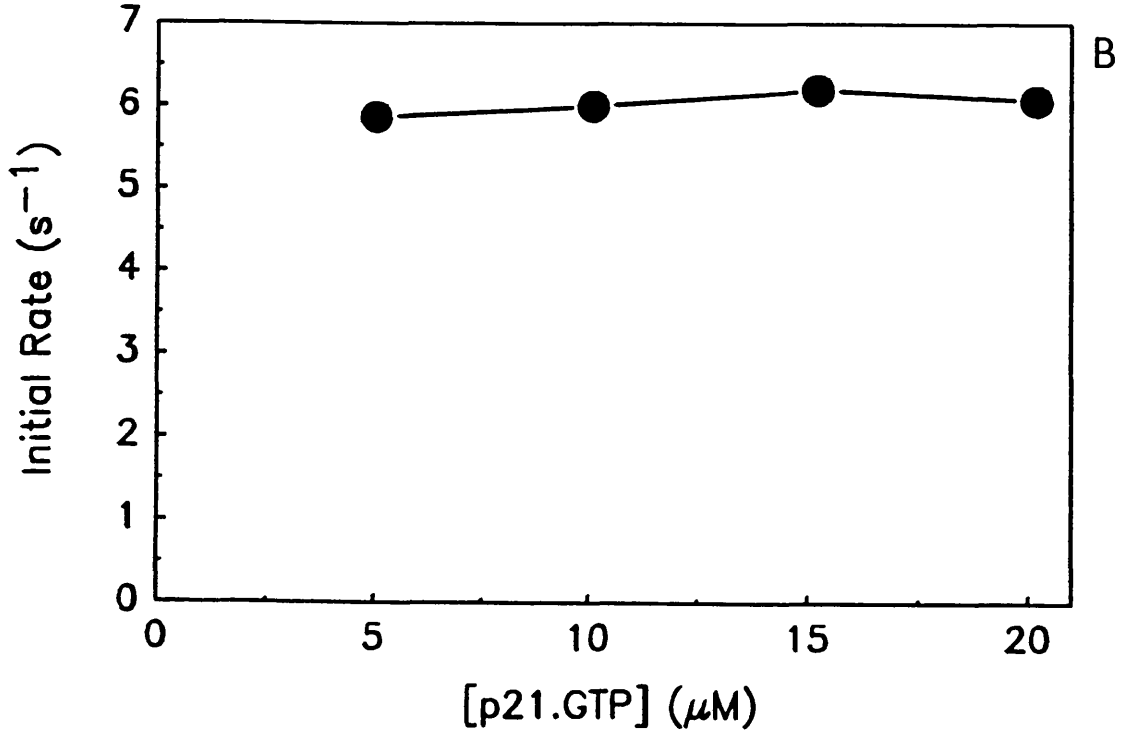
B
Initial Rate (s^{-1})
7
6
5
4
3
2
1
0
0
5
10
15
20
[p21.GTP] (μM)

The steady state turnover number of the enzyme, k_{cat}, defines the rate constant of the slowest step in the overall mechanism and is given by $V_{max} \div$ [enzyme]. Thus, converting the experimentally obtained value of V_{max} to the k_{cat} requires a knowledge of the molar concentration of active enzyme. In the literature, it has generally been assumed that $[GAP]_{active} = [GAP]_{total}$. If there were a significant proportion of inactive GAP, this would lead to erroneously low values for k_{cat}. Furthermore, these values are relative concentrations (compared to a protein standard in dye binding assays), rather than absolute concentrations (determined using a functional assay with which to measure the molar concentration of protein).

The stopped flow technique described in this chapter has been used to investigate the kinetic mechanism of the GAP_{344}- and NF1-activated $p21^{ras}$.mantGTPase. In addition to providing information about the mechanism, the results ~~have~~ also allow the determination of binding constants from the dependence of the rate of the fluorescence change on $[GAP_{344}]$. The major advantage of the stopped flow technique (where [GAP] >> $[p21^{ras}]$) for determining the maximal rate of GTP hydrolysis is that, in contrast to the steady state Michaelis-Menten analysis, it does not require a knowledge of the absolute concentration of the GAP. The lower limit of the K_d value that can be determined using stopped flow techniques is governed by the amplitude of the observed signal and the sensitivity of the fluorimeter. The determination of K_d values below $\approx$ 3 - 5 μM by stopped flow with mant-nucleotides is impractical, although modifications to the stopped flow procedure to extend this range to lower concentrations are discussed below.

(A) Stopped Flow Studies of the Interaction of $p21^{ras}$.mantGTP with GAP_{344} and NF1

The first - order rate of the fluorescence change observed after mixing $p21^{ras}$.mantGTP with excess GAP_{344} increases hyperbolically with GAP_{344} concentration. A similar dependence has been observed for many protein : ligand and protein : protein interactions (Hiromi, 1979). Two examples of such a dependence are the rate of ATP and GTP binding to myosin subfragment 1 (Bagshaw et al., 1974) and nucleotide-free $p21^{ras}$ (John et al., 1990). The possible reaction mechanisms that would lead to such a dependence have been described by Bagshaw et al., (1974), and are briefly discussed below. A good example of how the alternative mech-

anisms can be distinguished is afforded by the results obtained from studies of E.coli alkaline phosphatase (Halford et al., 1969; Halford, 1971, 1972).

5.4.2 *Two-step Binding Mechanisms for p21^{ras}.mantGTP with GAP.*

Consider the binding of p21^{ras}.mantGTP (R) to a GAP protein (G) followed by a unimolecular re-arrangement of the binary RG complex. The concentration of R and G at zero time after mixing are given by $[R]_0$ and $[G]_0$ respectively.

$$R + G \underset{k_{-1}}{\overset{k_{+1}}{\rightleftharpoons}} RG \underset{k_{-2}}{\overset{k_{+2}}{\rightleftharpoons}} RG^* \qquad (5.1)$$

A simplification of the kinetic analysis is to let the bimolecular process occur much more rapidly than the unimolecular isomerisation. Thus, when R and G are mixed, then RG is rapidly formed and if $[G]_0 >> [R]_0$, then the subsequent formation of RG^* is described by an exponential process where the observed rate, k_{RG*}, is given by equation 5.2:

$$k_{RG*} = \frac{k_{+2} \times [G]_0}{1 + K_d} + k_{-2} \qquad (5.2)$$

where the K_d is the equilibrium dissociation constant for the bimolecular step $= k_{-1} \div k_{+1}$. Thus, the observed first order rate of RG^* formation will vary hyperbolically with $[G]_0$. When $[G]_0 << K_d$, equation 5.2 simplifies to equation 5.3, whilst when $[G]_0 >> K_d$, then equation 5.4 is obtained.

$$k_{RG*} = [(k_{+2} / K_d) \times [G]_0] + k_{-2} \qquad (5.3).$$

$$k_{RG*} = k_{+2} + k_{-2} \qquad (5.4)$$

The equation for a simple one-step binding reaction approximates to that for a two step binding mechanism at low $[G]_0$. Under these conditions, k_{RG*} varies linearly with $[G]_0$

where the apparent second order association rate constant = (k_{+2} / K_d) and an intercept of k_{-2}. Although an expression for k_{RG*} has been obtained, this does not necessarily reflect the rate of the observed fluorescence change when R binds to G and isomerises to RG^* since the fluorescence intensity of R, RG, and RG^* may be different, as suggested in previous sections (see chapter 6). If this is the case, then at high $[G]_0$, the time dependence of the fluorescence change will be biphasic, the rapid phase representing the rate of RG formation and the slow phase RG^* formation.

A more detailed discussion of the nature of the fluorescence changes is given in chapter 6. However, at this stage, the data are interpreted assuming that (1) there is an increase in fluorescence intensity upon formation of the ternary RG complex (chapter 6) and (2) the isomerisation RG to RG^* is observed on the stopped flow time scale where the end product of the reactions has a lower fluorescence intensity than the ternary complex initially formed after mixing.

5.4.3 *Kinetic Mechanism of GAP_{344} Binding to $p21^{ras}$.mantGTP.*

Equation

Consider the reaction scheme shown in ~~Figure~~ 5.1. Such a mechanism can be used to explain the experimental data if it *assumed* that the rate of association and dissociation is rapid compared to the subsequent step in the mechanism. In these studies, however, experimental observations validate the use of this model (discussed in section 5.4.4). The subsequent decay of RG to RG^* at a rate of k_{RG*} is given by equation 5.2. From the data presented in Figure 5.2, then k_{RG*} plateaus at a rate of $\approx 14\ s^{-1} = k_{+2} + k_{-2}$. A lower limit can be placed on k_{-2} from the intercept of the hyperbola at low $[G]_0 = k_{-2}$. Whilst the errors inherent in this value are large due to the small number of points that can be obtained when $[G]_0 \approx [R]_0$, an upper limit of $0.2\ s^{-1}$ can be estimated. The second step is therefore quasi-irreversible (equilibrium constant > 70), and $k_{+2} + k_{-2} \approx k_{+2}$.

In the complex of $p21^{ras}$.mantGTP with GAP_{344}, the rate of the isomerisation reaction ($14\ s^{-1}$) is accelerated by a factor of $\approx 10^5$ over that in the absence of GAP_{344} ($2 \times 10^{-4}\ s^{-1}$). The results presented here do not yield any information as to the structural basis for, or the

chemical mechanism of, the very rapid hydrolysis of mantGTP in the presence of GAP. According to one model, GAP would stabilise the conformation of a series of residues which have been proposed to be involved in the catalytic reaction of water with GTP at the active site (Pai et al., 1990). In this case, the catalytically active conformation of these residues would then lead to hydrolysis of the nucleotide at a rate of 14 s^{-1}. In the other extreme model, then GAP itself would contribute residues to the active site and therefore the mechanism of GAP-catalysed hydrolysis would differ from that of the intrinsic GTPase reaction. A third possibility is a combination of both mechanisms - that the re-arrangement of the residues in $p21^{ras}$ occurs in addition to the contribution of residues in GAP to the active site. The results presented in chapter 4 would suggest either the first or third mechanisms.

Assuming the model shown in equation 5.2, then the apparent second order rate of mantGTP hydrolysis when $[G]_o << K_d$ is given by $k_{+2} / K_d = 8 \times 10^5\ M^{-1}s^{-1}$ from values of k_{+2} and K_d. The experimentally observed value under such conditions is $\approx 7 \times 10^5\ M^{-1}\ s^{-1}$ (Figure 5.2), similar to the calculated value assuming a 2 step binding mechanism. This value is also similar to the value of k_{cat} / K_m obtained by other groups ($4.2 \times 10^5\ M^{-1}\ s^{-1}$) using catalytic concentrations of GAP and varying the $p21^{ras}$.mantGTP concentration (Rensland et al., 1991). This latter observation suggests similar catalytic activities for the GAP preparations used in these two studies.

Alternative explanations for the hyperbolic dependence of the rate of the fluorescence change on $[GAP_{344}]$ cannot be unambiguously be rejected. These possibilities are discussed in Appendix 5.1, although for the reasons discussed therein, on balance, equation 5.1 is preferred to the alternative schemes, although unequivocal assignment of a precise two-step mechanism will be difficult (see Halford et al., 1969; Halford, 1971, 1972).

The biphasic fluorescence change associated with the hydrolysis of mantGTP by $p21^{ras}$ *in the absence of GAP* (section 4.5.2) suggests that two processes are occurring during this time period. The process giving rise to the fast phase of the fluorescence change could occur before the cleavage step or be independent of it. Stopped flow experiments indicated that the rate of the slow phase is accelerated at a fixed concentration of GAP_{344} to the same extent indepen-

dent of whether the reaction is initiated before or after the fast phase has occurred (Figure 5.4). This result suggests that latter interpretation, and would imply that the process associated with the fast phase of the fluorescence change is not a mandatory step in the ordered series of events involved in the GAP_{344}-activated $p21^{ras}$GTPase mechanism.

5.4.4 *Comparison of the Results Obtained with GAP_{344} Using Stopped Flow and Multiple Turnover Techniques.*

It is of interest to discuss these stopped flow results in light of other experiments performed concerning the kinetic mechanism of the GAP-activated $p21^{ras}$.GTPase mechanism. The multiple turnover rate of $p21^{ras}$.GTP hydrolysis (k_{cat}) with catalytic concentrations of GAP_{344} has been measured by following the rate of P_i release at different [$p21^{ras}$.GTP], yielding values of 4.9 ($\pm$ 0.3) s^{-1} and 5.0 ($\pm$ 0.2) s^{-1} for the GTP and mantGTP complexes respectively (A.E Nixon and M.R. Webb, unpublished results). The K_m values were 60 ($\pm$ 7) μM for $p21^{ras}$.GTP and 24 ($\pm$ 2) μM for $p21^{ras}$.mantGTP. The first consequence of the stopped flow results is that for GAP_{344}, the K_m values approximate to equilibrium dissociation constants since $k_{-1} >> k_{+2}$. As such, the K_d values obtained by this method agree well with those obtained from stopped flow experiments (and also from equilibrium binding studies where $K_d \approx 20$ μM for wild type $p21^{ras}$.mantGTP or $p21^{ras}$.mantGppNHp with GAP_{344}, Brownbridge et al., 1992). Secondly, they suggest that the ~~explanation of the~~ 3-fold higher rates of mantGTP cleavage compared to GTP cleavage observed in chapter 4 are due to a reduction in K_m for the mantGTP complex. The increased affinity of $p21^{ras}$.mantGTP for GAP_{344} suggests a direct interaction between the mant-fluorophore and GAP_{344}.

The k_{cat} value obtained from these multiple turnover studies (5 s^{-1}) is a measure of the slowest step in the cycle of GAP_{344}-activated GTP hydrolysis. By definition, the rate of the isomerisation reaction and GTP cleavage must be $\geq 5^{-1}$. This rate is 3-fold lower than that obtained from the stopped flow studies using excess GAP_{344}. A simple explanation for this discrepancy is that the method used to determine [GAP_{344}] (absorbance at 276 nm), and hence the concentration of GAP_{344} used in the k_{cat} calculations, is over-estimated by a factor of $\approx$ 3 . This appears unlikely based on the following argument. The K_d values ob-

tained from stopped flow are dependent on [GAP_{344}], whilst independent of [$p21^{ras}$.mant-GTP], whereas the K_d values obtained from multiple turnover experiments are dependent on [$p21^{ras}$.mantGTP] but independent of [GAP_{344}]. Thus, since the apparent K_d values obtained by both methods are similar ($\approx$ 20 μM), then either (a) both [$p21^{ras}$.mantGTP] and [GAP_{344}] are over-estimated by 3-fold or (b) both [$p21^{ras}$.mantGTP] and [GAP_{344}] reflect active protein concentrations within experimental error. As discussed in chapter 3, several reliable assays have been obtained with which to determine $p21^{ras}$.mantGTP concentrations, and therefore I would suggest that we can now treat these values with confidence. This argues against explanation (a) and suggests that the concentration of GAP_{344} (based on the absorbance at 276 nm) is similar to the total active concentration of GAP_{344}.

From the stopped flow results, the rate of the isomerisation reaction after the initial formation of the ternary complex is 14 s^{-1}. However, based on the amplitude dependence of the stopped flow reaction traces (see chapter 6), it seems probable that steps in the mechanism subsequent to the isomerisation, up to and including the dissociation of GAP_{344}, occur at $\geq$ 14 s^{-1} (chapter 6, Appendix 6.2). Thus an interpretation of these observations that is consistent with both stopped flow and multiple turnover results is that GAP_{344} dissociates rapidly ($\geq$ 14 s^{-1}) after the initial isomerisation reaction (14 s^{-1}), and then the slowest of the two subsequent steps (mantGTP cleavage and P_i release) occurs at 5 s^{-1} (from the k_{cat}). However, other explanations cannot be ruled out. For example, the rate limiting step for the multiple turnover of substrate could be an isomerisation of *GAP* (at 5 s^{-1}) after its interaction with $p21^{ras}$. Single turnover stopped flow experiments to measure the rate of P_i release under pseudofirst order conditions with respect to GAP_{344} are currently being performed in the laboratory to investigate these possibilities.

Gideon et al., (1992) have used multiple turnover conditions to compare the apparent k_{cat} for GAP_{334} (residues 714 - 1047) and full length GAP (residues 1 - 1047, p120-GAP). In these experiments, the initial rate of GTP hydrolysis was determined as a function of [$p21^{H\text{-}ras}$.GTP] by following the loss of [gamma]-labelled $^{32}P_i$ from the $p21^{H\text{-}ras}$.[^{32}]GTP complex yielding k_{cat} values of 4.2 s^{-1} for GAP_{334} and 19 s^{-1} for p120-GAP (all data at 25°C, see below). It is difficult to consider the significance of these results since no information was

given as to the assay used to determine GAP_{334} or p120-GAP concentrations. In a previous paper from the same group (Reinstein et al., 1991), protein concentrations were reported to be determined by the Bradford dye binding assay using BSA as standard, although it was not specified whether this assay was also used for p120-GAP. However, one cannot assume that BSA, GAP_{334}, and p120-GAP give the same colour yield in this assay. Indeed, standardising all protein concentrations on the calculated extinction coefficient at 276 nm (Gill and von Hippel, 1989 ; Mach et al., 1992), significant differences have been observed between the colour yields obtained with GAP_{344}, GAP_{365} and the NF1 fragments used in this thesis (by up to 3-fold). In the multiple turnover technique, the limitation of which is governed by an accurate knowledge of [GAP], it is perhaps surprising that so little emphasis has been placed on determining this value with confidence. The two-fold reduction in the K_m for p120-GAP over GAP_{334} may be more significant given that the determination of this value is independent of a knowledge of the molar concentration of active GAP protein. Thus, one can only consider these results with confidence when the proteins have been more thoroughly characterised with respect to the true active concentration.

Repeating the experiments of Gideon et al., (1992) with p120-GAP but performing the reactions at 37°C, Reinstein et al., (1991) quote a k_{cat} of 21 s^{-1}. This would suggest a very low temperature dependence of the k_{cat} with p120-GAP, in contrast to the observation that the rate of the fluorescence change observed in the stopped flow experiments is significantly temperature dependent. However, the results presented by Reinstein et al., (1991) are confused by the apparent contradiction between the k_{cat} values quoted for wild type $p21^{H\text{-}ras}$.GTP (21 s^{-1}) and the value that one can calculate from Figure 6B of that paper (12.6 s^{-1}, see footnote). Thus, the two values for the k_{cat} from Gideon et al., (1992) and Reinstein et al., (1991) differ by a factor of 2 using the same preparation of p120-GAP, $p21^{H\text{-}ras}$.GTP, and the same assay. This may be a reflection of the different percentage of active p120-GAP used in the two experiments, although it is entirely possible that there is a systematic difference between the two experiments which has not been discussed.

Footnote: From the value of the K_m then one can calculate that under these conditions (37°C) V_{max} = 3.8 μM min^{-1}, and since [p120-GAP] = 5 nM, then k_{cat} = 12.6 s^{-1}.

From the presently available data, it will be difficult to determine whether these relatively small changes in the kinetic constants obtained for p120-GAP and GAP_{334} are significant. The expression of large quantities of p120-GAP so as to allow stopped flow experiments to be performed would be required in order to directly determine the maximally activated rate of GTP hydrolysis and the K_d values for the two proteins. These studies will also allow one to estimate the concentration of active protein in the two preparations (as above). Thus, I would consider that only a complete analysis of the multiple turnover and single turnover experiments such as those described in this chapter will provide one with the available information with which to consider the results reported by Gideon et al., (1992) and Reinstein et al., (1991).

(B) Comparison of the Stopped Flow Results with GAP_{344} and NF1.

5.4.5 *Rate and Mechanism of the GAP_{344}- and NF1-Catalysed Isomerisation Reaction.*

The single most important feature of the catalytic domain of NF1 that distinguishes it kinetically from GAP_{344} or p120-GAP is the significantly higher affinity with which it binds to $p21^{ras}$.GTP (Martin et al., 1990; Bollag and McCormick, 1992). This difference forms the basis for the discussion of kinetic data presented in this section. Stopped flow studies have been performed using NF1 in excess over $p21^{ras}$.mantGTP, although the rate of the slow phase of the fluorescence changes observed in these experiments (6 s^{-1}) was essentially independent of the [NF1] between 2.1 - 7.4 μM NF1. Clearly, there is insufficient data to determine if a hyperbolic dependence of the observed rate on [NF1] is valid, as was the case for GAP_{344}. However, if one assumes such a model, then these results would suggest a significantly lower K_d for the binding reaction than observed with GAP_{344}. The absolute value of this equilibrium constant could not be determined with accuracy (see below) and one is unable to determine the intercept of the derivative plot, which corresponds to k_{-2} in equation 5.1 (see below).

One possibility to overcome these problems would be to use the highly fluorescent $p21^{ras}$.fluorescein-edGTP complex (section 2.5.3) at a final concentration of $\approx$ 50 nM, where

NF1 concentrations could be used which are both significantly greater than [$p21^{ras}$.fluorescein-edGTP] and also below the equilibrium constant for the formation of the ternary complex (estimated to be $\approx$ 0.5 - 1 μM, see below). Preliminary experiments have indicated that both the intrinsic- and GAP_{344}-catalysed cleavage reactions are associated with an increase in fluorescence intensity of 50 % (K.M ; J.F.E; J.P.Browne, unpublished results). An alternative approach would be to increase the ionic strength of the buffer used since the K_d for the binding reaction increases with increasing ionic strength (chapter 7). Thus, by choosing a set of conditions where the K_d is significantly greater than the [$p21^{ras}$.mantGTP], one would be able to use the $p21^{ras}$.mantGTP complexes whilst still obtaining kinetic information as to the nature of the binding reaction. This experiment would also indicate directly whether the maximal rate of the fluorescence change is salt dependent. The assumption inherent in this analysis is that the mechanism of the reaction is independent of ionic strength.

These results with mant-nucleotide complexes under these conditions of low ionic strength indicate that the rate of the fluorescence change with NF1 under these conditions (6 s^{-1} at 26 ^{o}C) is only 2-fold lower than that of GAP_{344} (14 s^{-1} at 30^{o}C). If the temperature dependence of the NF1-activated mechanism is similar to that of the GAP_{344}-activated mechanism, then these two rate constants will be even more similar. For GAP_{344}, k_{obs} = 14 s^{-1} $\approx$ k_{+2}, whilst with NF1, $k_{+2} \leq 6\ s^{-1}$ and $k_{+2} + k_{-2}$ (= 6 s^{-1}). This result nevertheless demonstrates that the equivalent domains in p120-GAP and neurofibromin are kinetically similar with respect to their maximally-activated $p21^{ras}$.GTPase activities. The original conclusion (Martin et al., 1990, Bollag and McCormick, 1991) that NF1-GRD was some 30-fold less active than p120-GAP at saturating concentrations of $p21^{ras}$.GTP may well be valid. If this is the case, then it would imply that the k_{cat} for p120-GAP should be some 15-fold greater than for GAP_{344}, and Gideon et al., (1992) have recently proposed a 4-fold difference between p120-GAP and GAP_{334}. However, the significance of these multiple turnover results is at present unclear (see above), and similar considerations apply to the limited amount of kinetic information available on NF1. It seems surprising given the widespread availability of GAP_{344} (or variants thereof) that a direct comparison between NF1-GRD and GAP_{344} was not made in the original paper of Bollag and McCormick (1991).

5.4.6 *Binding Kinetics for NF1 to $p21^{ras}$.mantGTP.*

In each of the stopped flow reactions described above, a consistent increase in fluorescence intensity of 10 - 15 % was observed during the first 100 ms after mixing. It should be stressed that whilst transient increases in fluorescence (of $\leq$ 1 %) were sometimes observed with GAP_{344}, this was only a rare occurrence. In contrast, much larger fluorescence enhancements was observed with NF1 in all of the stopped flow reactions. The most simple interpretation of this observation with NF1 is that it reflects the kinetics of the association reaction between $p21^{ras}$.mantGTP and NF1 which is sufficiently slow under these conditions for it to be observed using stopped flow techniques. Direct evidence in support of this model comes from the observation that, like GAP_{344}, the formation of the complex of NF1 with $p21^{ras}$.mantGTP is also associated with an increase in fluorescence intensity (see chapter 6). At present, one is unable to extract quantitative information from the kinetics of the fast fluorescence change (which may represent the binding reaction). However, preliminary data indicated that the rate of the fluorescence change increased with increasing concentrations of NF1 as predicted for a bimolecular reaction. A complete analysis of the concentration dependence of the rate and amplitude of this process is required before the kinetic mechanism of the binding reaction can be determined mechanistically.

A further consequence of the higher affinity of NF1 for $p21^{ras}$ than GAP_{344} is that one may be able to determine the rate of NF1 dissociation from a complex with $p21^{ras}$.mantGppNHp directly from displacement experiments with excess Leu 61 $p21^{ras}$.GTP in the stopped flow apparatus. For example, 1 μM $p21^{ras}$.mantGppNHp and 1 μM NF1 would be rapidly mixed with an excess of Leu 61 $p21^{H\text{-}ras}$.GTP (to prevent the rebinding of NF1 to the fluorescent nucleotide complex). NF1 dissociation would be monitored from the decrease in intensity upon dissociation. The dissociation of NF1 from the Leu 61 $^{H\text{-}ras}$.mantGTP complex is likely to be significantly slower than from wild type $p21^{ras}$. Alternatively, ionic strength jumps can be used to monitor the dissociation kinetics for a system where the equilibrium constant is sensitive to changes in the ionic strength of the medium (Lohman, 1984 a,b).

5.4.7 *Rates of NF1-Activated $p21^{ras}$.mantGTP and $p21^{ras}$.GTP Hydrolysis.*

With catalytic concentrations of NF1, the time dependence of P_i release following the NF1-activated GTP hydrolysis reaction could not be fitted to a single exponential since the initial rate of P_i release remained constant over a much longer period of time than would have been predicted from single exponential kinetics. This behaviour is expected if the substrate concentration used ([$p21^{ras}$.GTP] = 15 μM) is well above the K_m for NF1 (estimated to be $\leq$ 5 μM under these conditions of ionic strength). Simulations of the time course of the reaction using these values leads to the observed time dependence of the absorbance change.

The initial rate of mantGTP cleavage measured by H.P.L.C (5.6 s^{-1}) is similar to the k_{cat} with $p21^{ras}$.GTP (6 s^{-1}) and to the maximal rate of the fluorescence change (6 s^{-1}). Thus, for NF1, the multiple turnover k_{cat} is similar to that of the rate of the fluorescence change, k_{+2}, observed in the stopped flow. In contrast, with GAP_{344}, the rate of the fluorescence change (14 s^{-1}) is faster than the k_{cat} (5 s^{-1}). Further kinetic studies with both GAP_{344} and NF1 will allow one to determine the exact cause of this apparent difference. The rate constants obtained for the single turnover and multiple turnover experiments with GAP_{344} and NF1 are summarised in Table 5.1

One consequence of the observation that similar values are obtained for the multiple turnover k_{cat} and for the single turnover k_{+2} is that there is unlikely to be a significant proportion of inactive NF1 (or that the A_{276} assay over-estimates the true [NF1]). If one assumes, for example, 50 % inactive protein, then the "true" k_{cat} would be twice the apparent value obtained here, i.e 12 s^{-1}. Since this value must reflect the slowest step in the mechanism, it cannot be greater than k_{+2}, which has been estimated ($\approx$ 7 s^{-1} at 30°C) under conditions which are independent of the active NF1 concentration (stopped flow experiments). Equilibrium binding assays with NF1, which in one particular case provide a test of this possibility and allow one to estimate the active concentration of NF1, are the subject of the next chapter. The literature is at present confused due to the use of multiple turnover kinetics despite the lack of information concerning the extent of inactive GAP and NF1. Results presented in this, and the subsequent, chapter suggest that for our preparations of NF1 and

Table 5.1 Comparison Between Single and Multiple Turnover Data for GAP_{344} and NF1.

Protein	Rate of Reaction (s^{-1})			
	Single Turnover		Multiple Turnover	
	mantGTP	GTP	mantGTP	GTP
GAP_{344}	13.9[a]	N.D	5.0[b]	4.9[c]
NF1	6.0[d]	N.D	5.6[e]	4.9[f]
				6.1[g]

Notes:

(a): Stopped flow studies at 30°C in buffer C.

(b) and (c): Multiple turnover results monitoring inorganic phosphate release in buffer C at 30°C (A.E. Nixon, M.R. Webb, unpublished results).

(d): Stopped flow studies at 26°C in buffer C.

(e): Multiple turnover hydrolysis of mantGTP measured by ion exchange H.P.L.C at 30°C in buffer B.

(f): Multiple turnover hydrolysis of GTP measured by inorganic phosphate release at 30°C in buffer B.

(g): Multiple turnover hydrolysis of GTP measured by inorganic phosphate release at 30°C in buffer C.

N.D: not determined.

GAP_{344}, the total concentration of these proteins approximates (± 10%) to their active concentrations. Only when similar calculations with other preparations have been performed will one be able to compare the multiple turnover and single turnover kinetic results with those reported by other groups.

All of the possible intermediates identified thus far between the initial formation of the ternary complex ($p21^{ras}$.GTP.GAP) and the end product of the GAP-activated $p21^{ras}$.GTPase (p21.GDP + P_i + GAP) are shown in scheme 5.2.

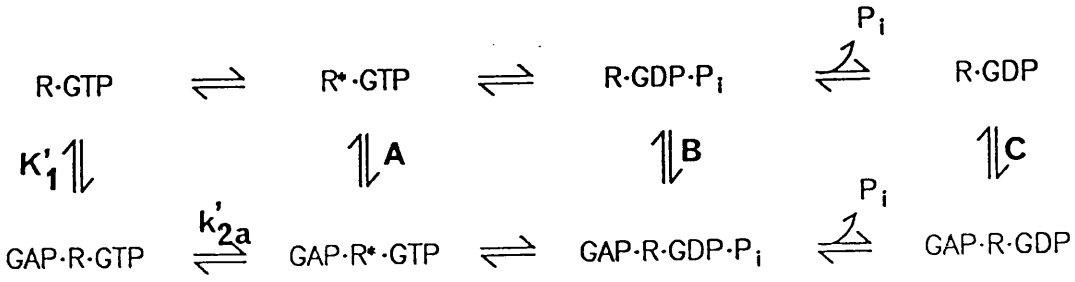

Scheme 5.2

It is not known from which intermediate in the mechanism GAP_{344} dissociates, although three possibilities are apparent. (a) After the isomerisation of $p21^{ras}$.mantGTP, (b) after cleavage of the terminal phosphate, or (c) after the release of inorganic phosphate, P_i. Future experiments aim to extend these preliminary studies and address these problems by using a combination of rapid reaction techniques combined with a variety of spectroscopic signals. In addition the possibility of conformational changes in GAP_{344}, p120-GAP, and NF1 occurring after a single turnover of $p21^{ras}$.GTP should be considered. If the three reactions labelled (a), (b), and (c) in Scheme 5.2, are found to be faster than the k_{cat} for GAP_{344}, then protein isomerisations of the free enzyme may be considered as the rate limiting step for the overall mechanism. Such isomerisation reactions may be important in relation to an effector function for either or both of these GAP proteins.

CHAPTER SIX

FLUORESCENCE CHANGES ASSOCIATED WITH THE FORMATION OF COMPLEXES OF $p21^{ras}$.mantGTP WITH GAP_{344} OR NF1

"Fluorescent probes are most useful for estimation of the local physical and structural characteristics of an unknown environment. However, one should not attempt to obtain absolute values for these parameters."

Valeur. (1991)

"The application of these methods, whilst appearing simple and straightforward, can be fraught with experimental artefacts."

Jameson and Hazlett, (1991)

6.1 Introduction.

The main impetus for this work came from the observation that the fluorescence changes observed in the stopped flow experiments increased significantly in amplitude over the range of [GAP_{344}] where a significant proportion of the $p21^{ras}$.mantGTP is complexed with GAP_{344}. In order to interpret the kinetic data obtained in these experiments, it became necessary to investigate whether the different intermediates in the mechanism had different fluorescence intensities. In addition, the differing amplitudes of the fluorescence transients

observed with excitation at 280 nm or 366 nm suggested that fluorescence resonance energy transfer may occur between Trp residues in GAP_{344} and the mant-fluorophore on $p21^{ras}$. The equilibrium titration experiments described in this chapter provide a test of these points.

6.2 Fluorescence Intensity Changes On Formation of the Ternary Complex Between $p21^{ras}$.mantGTP and GAP_{344}.

Equilibrium titration experiments were performed initially using the Gln → Leu 61 mutant of $p21^{H\text{-}ras}$ since this has (a) very slow intrinsic and GAP_{344}-activated GTP cleavage rates, and (b) binds to GAP_{344} with substantially higher affinity than the wild type protein (Vogel et al., 1988; Krengel et al., 1990, Brownbridge et al., 1992). Therefore the mantGTP complex of this mutant forms a relatively stable ternary complex with GAP_{344} at lower concentrations of GAP_{344} than the wild type protein. The fluorescence emission maximum of the Leu 61 $p21^{H\text{-}ras}$.mantGTP complex (435 nm, Figure 6.1.a) is similar to that of wild type $p21^{H\text{-}ras}$.mantGTP (Rensland et al., 1991). Sequential titration of GAP_{344} to this solution lead to a corresponding increase in the fluorescence intensity and a blue shift in the emission maximum to 430 nm (Figure 6.1.a). The largest fractional enhancement in fluorescence intensity was at 415 nm (60 % increase upon ternary complex formation) whilst at 442 nm or when monitoring through a KV399 cut off filter, then only a 25 % increase in intensity was observed. The different fluorescence enhancements observed at different emission wavelengths is due to the shift in the emission maximum in the ternary complex to lower wavelengths. These results therefore provide direct evidence for an increase in fluorescence intensity upon formation of the ternary complex.

The change in fluorescence intensity occurring upon complex formation was used to determine the equilibrium binding constant, K_d, for the interaction of GAP_{344} with the mantGTP complex of this mutant of $p21^{H\text{-}ras}$ (Figure 6.1.b), yielding a K_d of 2.5 μM - similar to the same value obtained from anisotropy measurements (3 μM, Brownbridge et al., 1992). In agreement with earlier reports using kinetic competition assays (Bollag and McCormick, 1991; Krengel et al., 1990; Vogel et al., 1988), this mutant binds to GAP_{344} with $\approx$ 10-fold higher affinity than does the wild type $p21^{ras}$ protein.

Figure 6.1 Fluorescence Emission Spectra of Leu 61 $p21^{H\text{-}ras}$.mantGTP In the Presence and Absence of GAP_{344}.

Panel A: 1 μM Leu 61 $p21^{H\text{-}ras}$.mantGTP in buffer C at 30°C was excited with light at 358 nm (excitation slit widths = 2 nm). Uncorrected fluorescence emission intensity was monitored from 380 nm - 520 nm as shown where the fluorescence intensity at 435 nm = 100 % relative fluorescence (curve A). GAP_{344} (containing 1 μM Leu 61 $p21^{H\text{-}ras}$.mantGTP) was added to a final concentration of 24 μM and the fluorescence emission spectrum re-determined (curve B).

Panel B: The fluorescence intensity (excitation = 358 nm, emission = 430 nm, slit width = 2 nm and 4 nm respectively) of a solution of 1 μM Leu 61 $p21^{H\text{-}ras}$.mantGTP in buffer C is shown as a function of the concentration of added GAP_{344}. The concentration of $p21^{ras}$.mantGTP was maintained at 1 μM throughout the titration. The fluorescence intensity in the absence of GAP_{344} is defined as 100 % relative fluorescence at 430 nm. The solid line is the best fit line of the data to a modified hyperbola (see Appendix 6.1 and Brownbridge et al., 1992) yielding a K_d of 2.5 μM and a maximal fluorescence enhancement at this wavelength of 41 %.

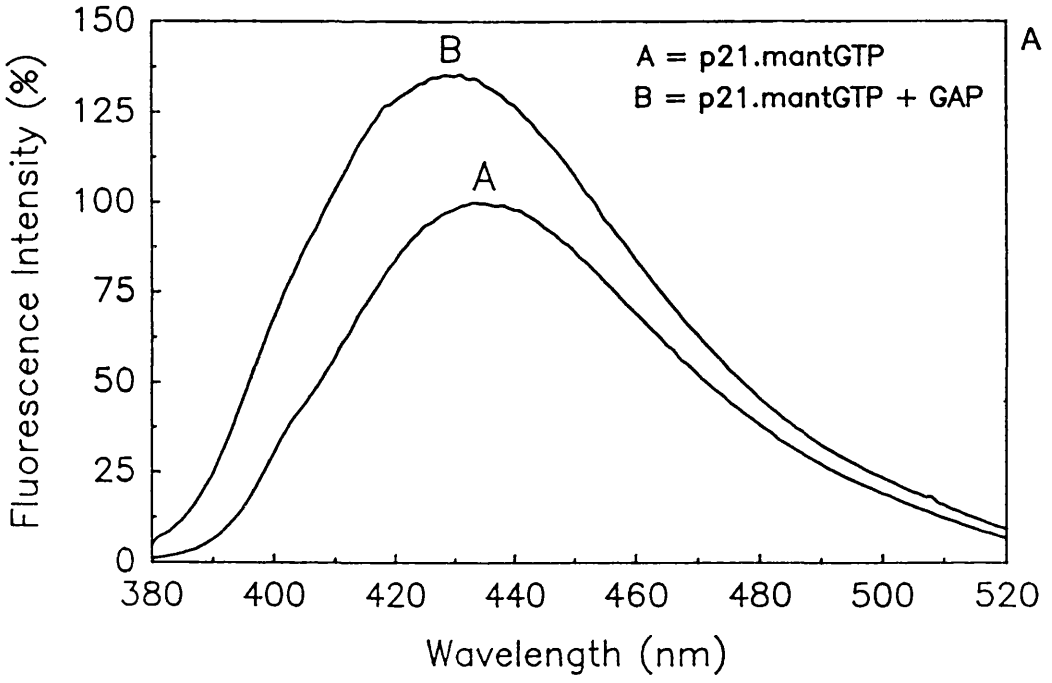
A
A = p21.mantGTP
B = p21.mantGTP + GAP
B
A
Fluorescence Intensity (%)
150
125
100
75
50
25
0
380
400
420
440
460
480
500
520
Wavelength (nm)

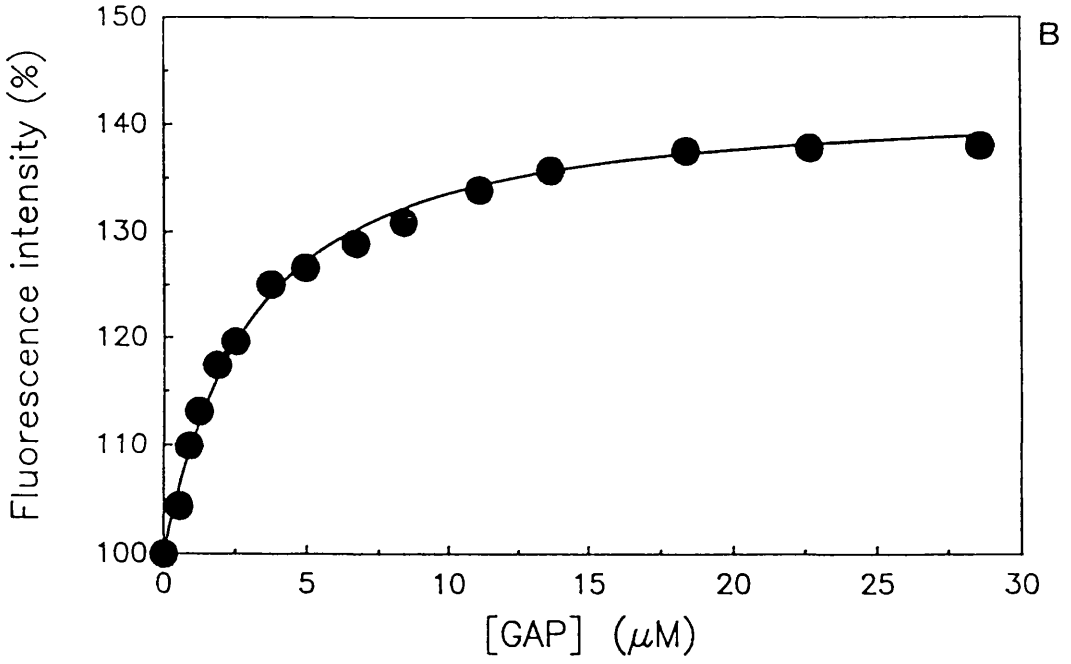
B
Fluorescence intensity (%)
150
140
130
120
110
100
0
5
10
15
20
25
30
[GAP] (μM)

During the time course of the fluorescence intensity titration experiments, the fluorescence intensity of Leu 61 $p21^{H\text{-}ras}$.mantGTP, when saturated with GAP_{344}, decreased exponentially with a rate constant of 2.2×10^{-4} s^{-1} (Figure 6.2.a). Ion exchange H.P.L.C analysis of the reaction mixture during the time course of this fluorescence change (Figure 6.2.b) indicated that the hydrolysis of mantGTP occurred with a similar rate constant ($2.4 (\pm 0.1) \times 10^{-4}$ s^{-1}). These results suggest that the decrease in fluorescence intensity reflects the rate of hydrolysis to $p21^{ras}$.mantGDP, to which GAP_{344} binds only weakly ($K_d \geq 300$ μM). The fluorescence intensity at the end of the reaction was however ≈ 5 % above that of $p21.^{ras}$.mantGTP alone. The slightly higher fluorescence intensity at the end of the reaction compared to that of $p21^{ras}$.mantGTP may be due to the small, but finite, amount of complex that is formed between $p21^{ras}$.mantGDP and GAP_{344} under these conditions. The corresponding rate of the fluorescence anisotropy change when measured on the same solution was 2.0×10^{-4} s^{-1} (Brownbridge et al., 1992). Since the intrinsic rate of mantGTP hydrolysis by this mutant in the absence of GAP_{344} is 0.12×10^{-4} s^{-1} (Figure 6.2.b), then GAP_{344} causes a maximal 20-fold acceleration of the GTPase of this mutant compared to 70,000 for wild type $p21^{N\text{-}ras}$.mantGTP.

6.3 Fluorescence Intensity Changes on Formation of the Ternary Complex of $p21^{ras}$.mantGTP with NF1.

Similar experiments to those described above were performed with the GAP-related domain of NF1. The higher affinity with which NF1 binds to $p21^{ras}$ compared to GAP_{344} allowed these experiments to be performed with the wild type $p21^{N\text{-}ras}$ protein. Unlike the Leu 61 $p21^{ras}$ mutant, the intrinsic mantGTP cleavage rate of the wild type $p21^{N\text{-}ras}$ is strongly stimulated by NF1, and therefore the non-hydrolysable mantGppNHp complexes were used for these titration experiments.

The fluorescence emission spectrum of 1 μM $p21^{N\text{-}ras}$.mantGppNHp in the absence and presence of a saturating concentration of NF1 (6.6 μM) is shown in Figure 6.3.a. The fluorescence emission maximum is blue shifted from 440 nm in the absence of NF1 to 435 nm in the ternary complex, and there is a corresponding increase in fluorescence intensity. The abso-

Figure 6.2 Maximal Rate of GAP_{344} Activated Leu 61 $p21^{H\text{-}ras}$.mantGTP Hydrolysis.

15 μM Leu 61 $p21^{H\text{-}ras}$.mantGTP in buffer C was incubated with 60 μM GAP_{344} at 30°C. Panel A: The fluorescence intensity (excitation = 358 nm, emission = 430 nm) was followed with time. The fluorescence intensity of 15 μM Leu 61 $p21^{H\text{-}ras}$.mantGTP in the absence of GAP_{344} is defined as 100 % relative fluorescence. The decrease in fluorescence intensity could be fitted to a single exponential with a rate constant of 2.2×10^{-4} s^{-1} and an amplitude of 36 %. The end point of the fluorescence change is $\approx$ 5 % above that of Leu 61 $p21^{H\text{-}ras}$.mantGTP alone.

Panel B: The rate of mantGTP hydrolysis under these conditions was determined by ion exchange h.p.l.c of the reaction mixture as described in section 2.8. Curve A is the best fit to a single exponential with a rate constant of 2.4×10^{-4} s^{-1}. Curve B shows the initial portion of the hydrolysis rate of mantGTP in the absence of GAP_{344}. This reaction was monitored for 12 hours ($\approx$ 50 % hydrolysis) in order to define the rate constant more accurately. The solid line is the best fit of the data (up to 12 hours) to a single exponential assuming an end point of 100 % $p21^{ras}$.mantGDP where $k_{obs} = 0.12 \times 10^{-4}$ s^{-1}. All of the $p21^{ras}$ proteins studied in this thesis reach end points of < 5 % $p21^{ras}$.mantGTP.

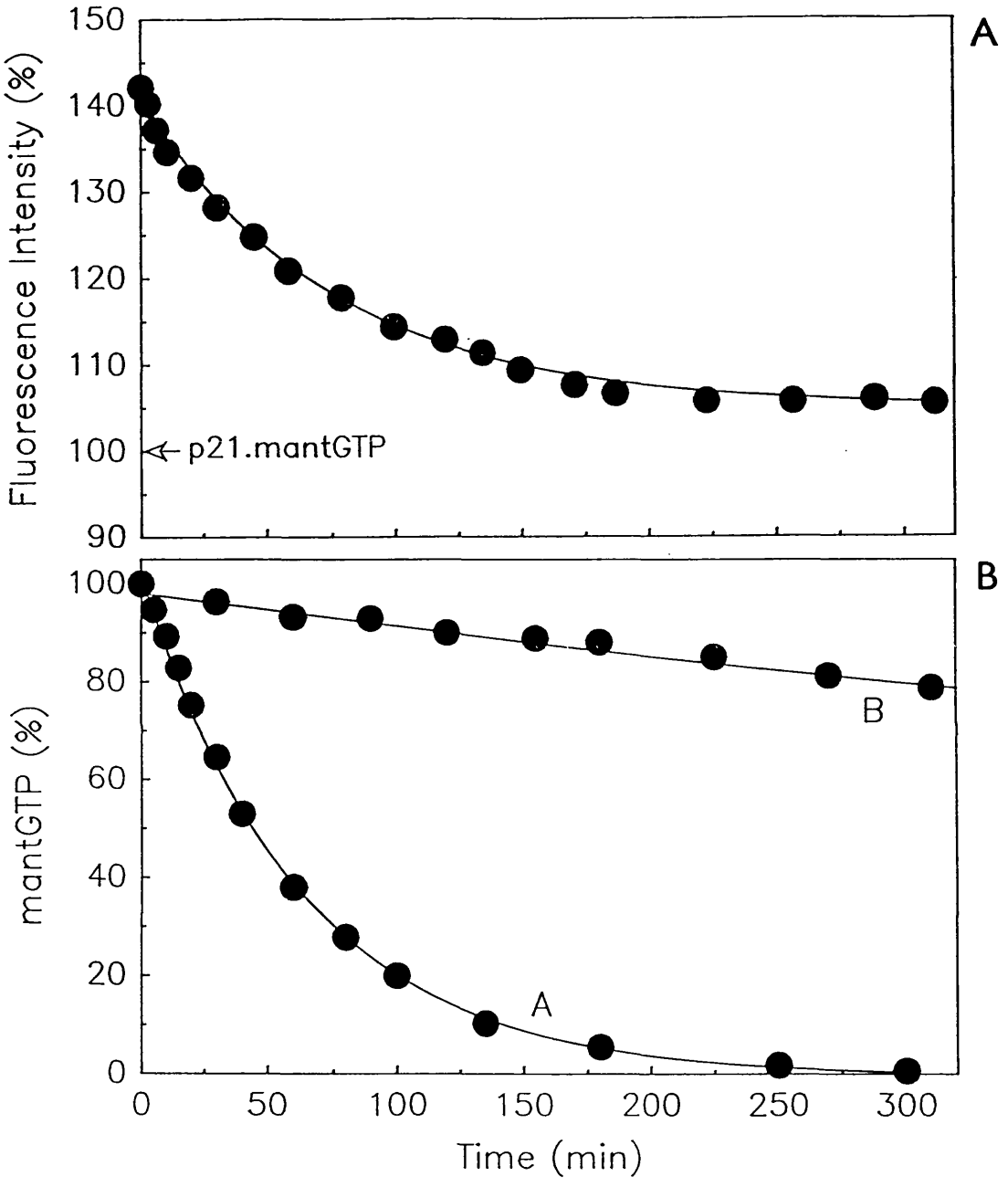
A
B
Fluorescence Intensity (%)
150
140
130
120
110
100
90
← p21.mantGTP
mantGTP (%)
100
80
60
40
20
0
B
A
0
50
100
150
200
250
300
Time (min)

Figure 6.3 Fluorescence Emission Spectra of $p21^{N\text{-}ras}$.mantGppNHp in the Presence and Absence of NF1.

Panel A: 1 μM $p21^{N\text{-}ras}$.mantGppNHp in buffer C at 30°C was excited with light at 364 nm (slit widths = 2 nm). The uncorrected fluorescence emission spectrum was determined from 400 - 550 nm (curve A) where the fluorescence intensity at 440 nm = 100 % relative fluorescence. NF1 (containing 1 μM $p21^{N\text{-}ras}$.mantGppNHp) was then added to a final concentration of 6.6 μM and the spectrum de-determined (curve B).

Panel B: The fluorescence intensity (excitation = 364 nm, emission = 410 nm, slit widths = 2 nm and 4 nm respectively) of 1 μM $p21^{N\text{-}ras}$.mantGppNHp in buffer C is plotted as a function of the concentration of added NF1. 100 % relative fluorescence is defined as the intensity at this emission wavelength in the absence of NF1. The solid line is the best fit to the data (Appendix 6.1) where K_d = 1.0 ($\pm$ 0.1) μM and the maximal fluorescence enhancement is 42%.

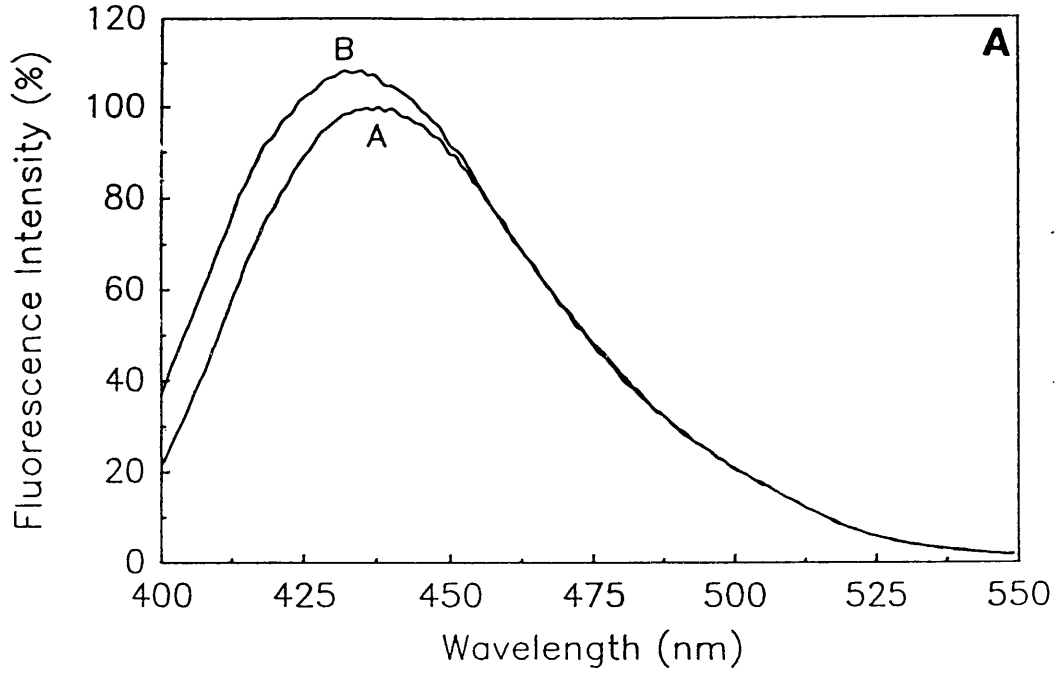
A
B
A
Fluorescence Intensity (%)
120
100
80
60
40
20
0
400
425
450
475
500
525
550
Wavelength (nm)

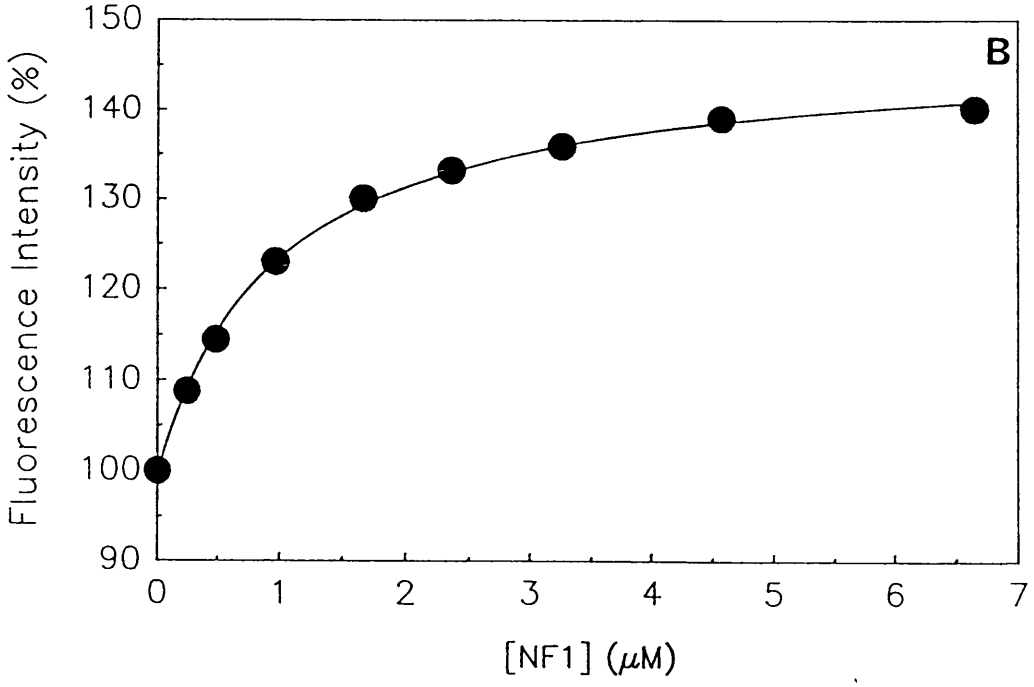
B
Fluorescence Intensity (%)
150
140
130
120
110
100
90
0
1
2
3
4
5
6
7
[NF1] (μM)

lute value of this fluorescence enhancement depends critically on the wavelength, such that the maximum difference between the two spectra occurs at 410 nm (40 % increase). Monitoring the fluorescence emission through a KV399 cut off filter resulted in only a 15 % increase in fluorescence intensity upon complex formation. The change in fluorescence intensity upon addition of NF1 was used to calculate the equilibrium constant for complex formation (K_d = 1.0 ($\pm$ 0.1) μM, Figure 6.3.b)

6.4 Changes In Fluorescence Resonance Energy Transfer and Anisotropy Between $p21^{ras}$.mantGTP and Tryptophan Residues in GAP_{344} and NF1.

Excitation of the $p21^{ras}$.mantGTP complex at 280 nm in the stopped flow experiments lead to 2-fold increase in the amplitudes of the fluorescence transients observed. The possibility of fluorescence resonance energy transfer (FRET) was therefore investigated since this would provide one explanation for the amplitude difference. The fluorescence intensity excitation spectra of Leu 61 $p21^{ras}$.mantGTP in the absence and presence of 16 μM GAP_{344} (emission through a KV399 filter) show an increase in intensity both at 364 nm (see above) but also at 284 nm (Figure 6.4.a). The fluorescence intensity at both 284 nm and 364 nm decreased exponentially with a rate comparable to that determined for the rate of mantGTP hydrolysis (2.3×10^{-4} s^{-1} at 284 nm and $2.6 \times 10^{-4} s^{-1}$ at 360 nm). These spectra suggests that in the ternary complex, FRET occurs from Trp 885 in GAP_{344} (the sole Trp residue in this fragment of GAP) to mantGTP on $p21^{ras}$ (see section 6.5). The fluorescence enhancement of the secondary excitation peak between 270 - 300 nm is characteristic of energy transfer with a Trp residue as the donor, and is due to the absorption of light in this region of the spectrum by Trp 885 in GAP_{344}. Since the fluorescence emission spectrum of GAP_{344} overlaps the absorption spectrum of mantGTP, then some of the excitation energy absorbed by Trp 885 is transferred to the mant-fluorophore, which then emits at 440 nm. The efficiency of FRET, Φ_T, that is observed depends on several factors, one of which is the donor : acceptor distance, R, where $\Phi_T \propto R^{-6}$. The proportionality constant in this relationship is dependent on the particular properties of the system. Thus, FRET only occurs to any significant extent when R is small, i.e in the ternary complex. It is not known why the $p21^{ras}$.mantGTP complex in the absence of GAP or NF1 shows a minor excitation peak since wild type $p21^{ras}$ contains no Trp

Figure 6.4 Changes in Fluorescence Resonance Energy Transfer and Anisotropy On Formation of the Ternary Complex With GAP_{344}.

Panel A: The uncorrected fluorescence excitation spectrum of 1 μM Leu 61 $p21^{H\text{-}ras}$.mantGTP in buffer C at 30°C (emission through a KV399 filter) was determined from 240 - 380 nm (curve A) where the fluorescence intensity at 364 nm = 100 % relative fluorescence. GAP_{344} (containing 1 μM Leu 61 $p21^{H\text{-}ras}$.mantGTP) was added to a final concentration of 16 μM and the excitation spectrum re-determined (curve B).

Panel B: As for (A) above except that the fluorescence anisotropy of the sample was determined as a function of excitation wavelength. Curves A and B refer to the spectra obtained in the absence and presence of GAP_{344} respectively. An increase in anisotropy is observed at high wavelengths (e.g 360 nm) after the addition of GAP_{344} whilst between 270 - 305 nm, the anisotropy decreases.

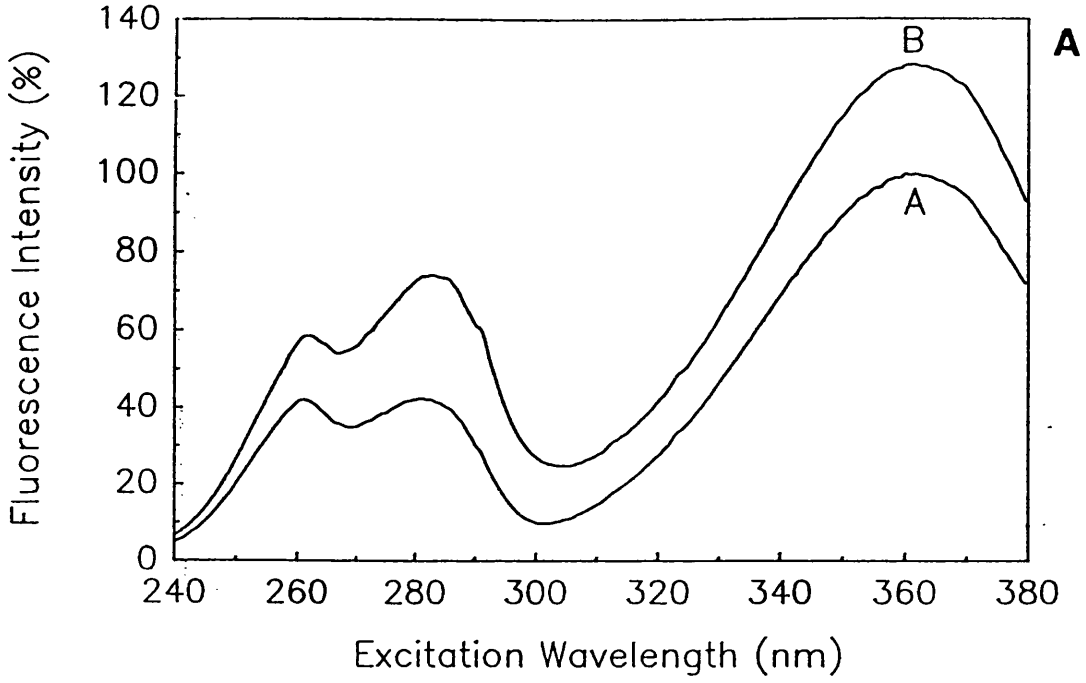
A
Fluorescence Intensity (%)
140
120
100
80
60
40
20
0
240
260
280
300
320
340
360
380
Excitation Wavelength (nm)
B
A

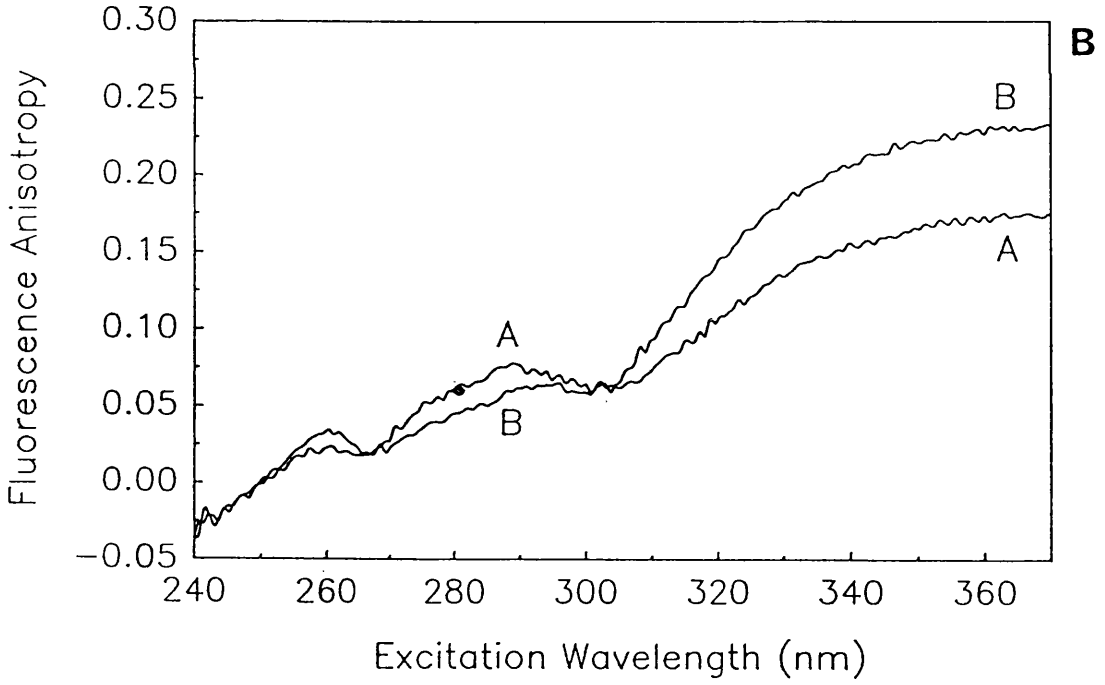
B
Fluorescence Anisotropy
0.30
0.25
0.20
0.15
0.10
0.05
0.00
−0.05
240
260
280
300
320
340
360
Excitation Wavelength (nm)
B
A
A
B

residues. However, the size of this peak is known to be dependent on the particular ras gene products used (c.f Figure 6.4.a with H-ras and Figure 6.5.a with N-ras).

Direct evidence for the presence of energy transfer in the ternary complex comes from measurements of the excitation wavelength dependence of the anisotropy of Leu 61 $p21^{ras}$.mantGTP in the presence and absence of GAP_{344} (Figure 6.4.b). The effect of GAP_{344} on the observed wavelength dependence can be readily explained in terms of FRET from Trp 885 to $p21^{ras}$.mantGTP. The cause of this effect is discussed in more detail in section 6.5. Under certain conditions (related to the relative orientations of the Trp and mant-fluorophores in the ternary complex), then FRET to the acceptor is equivalent to a rotation of the plane of the polarised light, which thus leads to a reduction in anisotropy of the mant-fluorophore in the region of the U.V spectrum where Trp 885 is excited (270 - 300 nm). In contrast, at high wavelengths away from the excitation wavelengths for Trp 885 (such as 366 nm), there is no depolarisation due to energy transfer and an increase in anisotropy is observed. To a first approximation, this reflects the slower overall rotational rate of the ternary complex compared to that of $p21^{ras}$.mantGTP alone. The fluorescence anisotropy at 366 nm decreased upon incubation at 30°C to 0.182, occurring with a rate constant of 2.1×10^{-4} s^{-1}. The anisotropy at 290 nm increased during this time period with a rate comparable to that obtained monitoring fluorescence at 366 nm (half time $\approx$ 55 min) , although the relatively small amplitude of the signal change (0.02) makes the exact determination of a rate constant difficult.

The equivalent fluorescence studies with wild type $p21^{N\text{-}ras}$.mantGppNHp and NF1 show a similar wavelength dependence of the excitation intensity and anisotropy spectrum to that observed with GAP_{344} (Figures 6.5.a and b). For this fragment of NF1 there are 4 Trp residues, although there is no Trp residue at, or near to, the position equivalent to codon 885 in GAP_{344}. Whilst the enhancement of the peak at 284 nm is less pronounced than with GAP_{344}, the changes in anisotropy are similar for the two proteins, and the depolarisation is restricted to the part of the excitation spectrum between 275 - 305 nm.

Figure 6.5 Changes in Fluorescence Resonance Energy Transfer and Anisotropy on Formation of the Ternary Complex with NF1.

Panel A: The uncorrected fluorescence excitation spectrum of a solution of 1 μM $p21^{N\text{-}ras}$.mantGppNHp at 30^{o}C in buffer C (emission at 440 nm) was determined from 250 - 400 nm where the fluorescence intensity at 364 nm = 100 % relative fluorescence (curve A). NF1 (containing 1 μM $p21^{N\text{-}ras}$.mantGppNHp) was added to a final concentration of 6.6 μM , and the spectrum re-determined (curve B).

Panel B: As for (A) above except that the fluorescence anisotropy of the solution was determined as a function of excitation wavelength. Curves A and B refer to the spectra obtained before and after the addition of NF1 respectively.

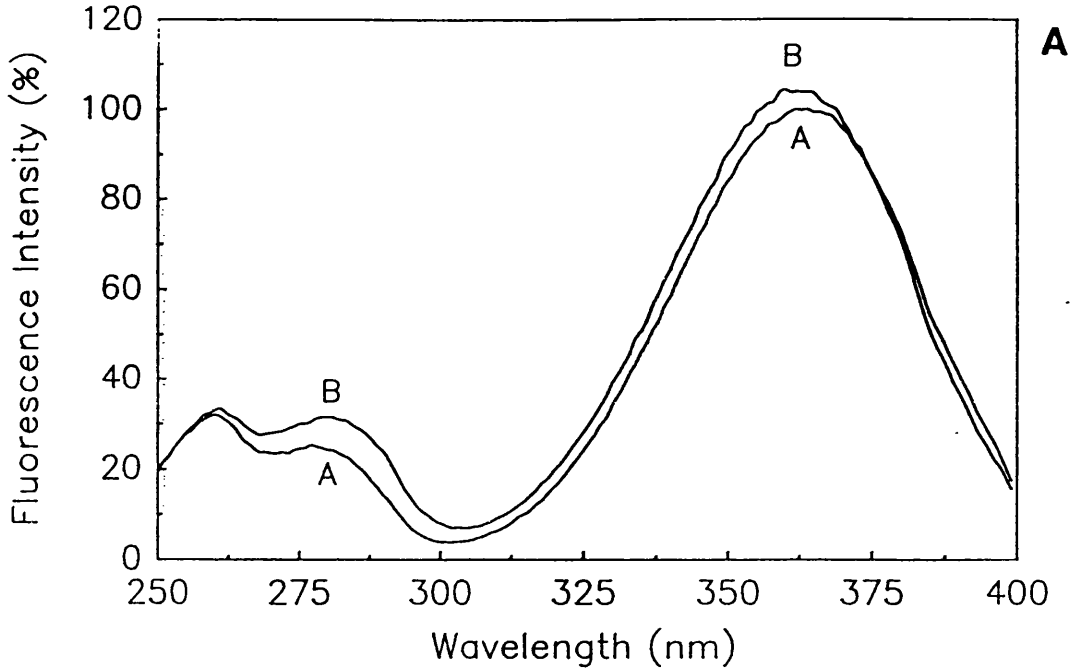
A
Fluorescence Intensity (%)
120
100
80
60
40
20
0
B
A
B
A
250
275
300
325
350
375
400
Wavelength (nm)

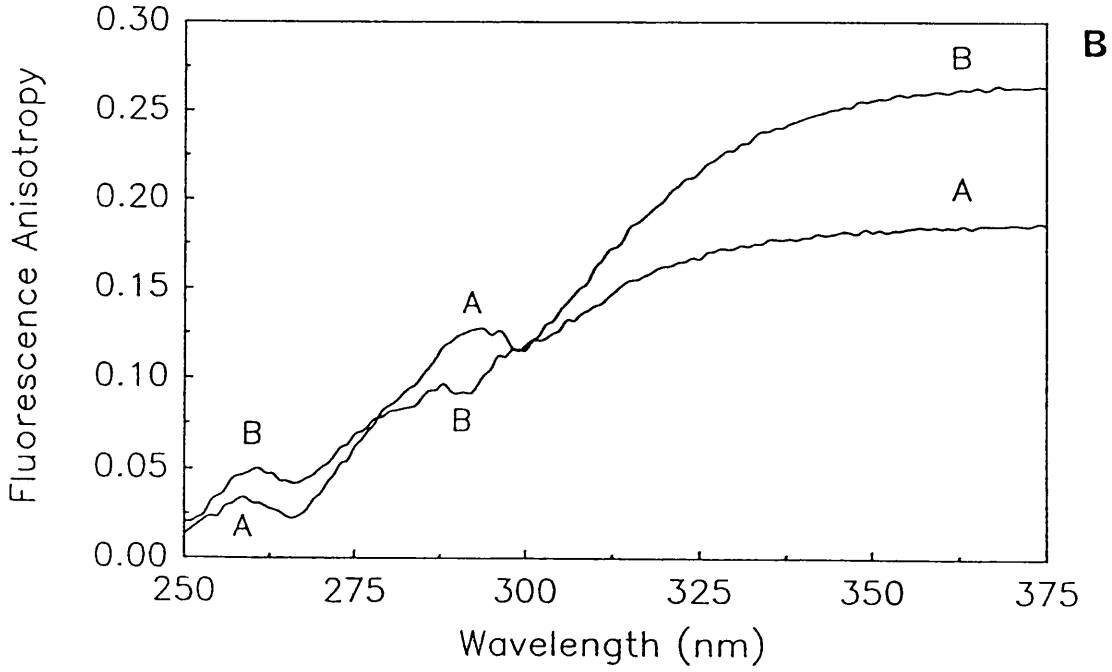
B
Fluorescence Anisotropy
0.30
0.25
0.20
0.15
0.10
0.05
0.00
B
A
A
B
B
A
250
275
300
325
350
375
Wavelength (nm)

The difference in anisotropy at high wavelengths can be used to monitor complex formation. Titration of NF1 into 1 μM $p21^{ras}$.mantGppNHp was used to calculate an equilibrium constant of 0.8 ($\pm$ 0.1) μM (Figure 6.6.a). This value is similar to that obtained whilst monitoring the change in fluorescence intensity (1.0 $\pm$ 0.1 μM).

Titration experiments with the Leu 61 $p21^{H\text{-}ras}$.mantGTP complex also gave the expected increase in anisotropy (Figure 6.6.b) and intensity (Figure 6.6.c) although in this case, the affinity was too high to measure accurately using the standard methodology since the shape of the titration curve was too close to linear. The estimated value of the K_d under these conditions must be $<<$ 0.1 μM. Due to the high affinity of this mutant for NF1, when the active [NF1] in the cuvette reaches the total concentration of binding sites for NF1 (see section 6.5), then the change in the fluorescence signals plateaus rapidly. The concentration of final [NF1] at the breakpoint of the curves shown in Figures 6.6.b and 6.6.c is 0.83 μM for the anisotropy data and 1.12 μM for the intensity data.

The slow reduction in intensity and anisotropy which occurs following the addition of saturating concentrations of GAP_{344} to Leu 61 $p21^{ras}$.mantGTP was also observed with NF1 (5 μM Leu 61 p21.mantGTP + 6 μM NF1). Both fluorescence signals decreased exponentially with rate constants of 7.33 ($\pm$ 0.03) x 10^{-5} s^{-1} for the anisotropy change and 6.98 ($\pm$ 0.02) x 10^{-5} s^{-1} for the intensity change. The rate of mantGTP cleavage under these conditions (7.58 ($\pm$ 0.32) x 10^{-5} s^{-1}) is similar to that obtained from the rates of either of the fluorescence changes. Thus, the maximally activated rate of mantGTP hydrolysis by this mutant in the ternary complex with NF1 is 5.9-fold higher than that of the intrinsic rate of mantGTP cleavage compared to 30,000 fold for wild type $p21^{N\text{-}ras}$.mantGTP. It was observed that the anisotropy at the end of the cleavage reaction (0.195) was significantly higher than that of $p21^{ras}$.mantGTP alone (0.184), even though $p21^{ras}$.mantGTP and $p21^{ras}$.mantGDP have similar anisotropies. This difference may be due to the formation of a small fraction of the $p21^{ras}$.mantGDP.NF1 ternary complex under these conditions.

Figure 6.6 Binding of NF1 to Wild Type and Leu 61 $p21^{ras}$.mant-Nucleotide Complexes.

Panel A: NF1 was titrated into a solution of 1 μM $p21^{N\text{-}ras}$.mantGppNHp in buffer C at 30^{o}C. The fluorescence anisotropy (excitation = 364 nm, emission through a KV399 filter) was determined after each addition of NF1. The solid line is a best fit to the data (appendix 6.1) yielding a K_d = 0.8 ($\pm$ 0.1) μM and an amplitude of 0.082.

Panel B: As for (A) except that Leu 61 $p21^{H\text{-}ras}$.mantGTP was used rather than the wild type N-ras protein. The amplitude of the anisotropy increase was 0.086. The vertical line shows the "breakpoint" in the titration curve. The concentration of NF1 in the cuvette at this point was 0.83 μM.

Panel C: As for (B) except the fluorescence intensity was monitored as a function of [NF1]. The amplitude of the fluorescence intensity increase was 15 % and the [NF1] at the break-point in the titration curve was at 1.12 μM.

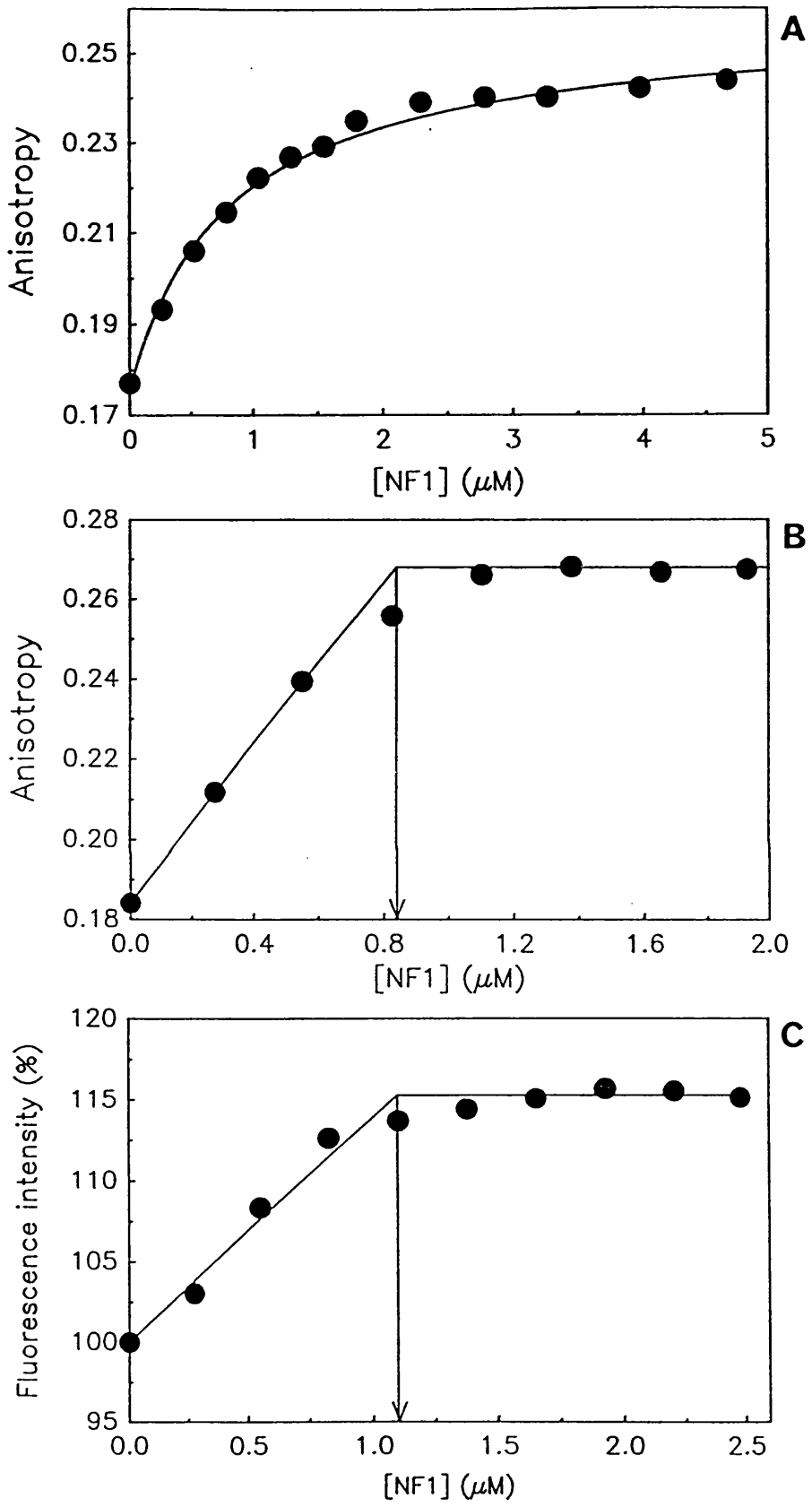
A
Anisotropy
0.25
0.23
0.21
0.19
0.17
0
1
2
3
4
5
[NF1] (μM)
B
Anisotropy
0.28
0.26
0.24
0.22
0.20
0.18
0.0
0.4
0.8
1.2
1.6
2.0
[NF1] (μM)
C
Fluorescence intensity (%)
120
115
110
105
100
95
0.0
0.5
1.0
1.5
2.0
2.5
[NF1] (μM)

6.5 Discussion.

6.5.1 *Changes In Fluorescence Emission Intensity with GAP_{344} and NF1.*

The results presented in this chapter indicate that the mant-nucleotides when bound to $p21^{ras}$ undergo an increase in fluorescence intensity upon formation of the ternary complex with GAP_{344}, an to a lesser extent, with NF1. The nature of the fluorescence enhancements with the two proteins are similar, but not identical, with significant differences in the magnitude of the effect and the wavelength dependence of the emission spectra. For both proteins, the emission maximum is blue shifted by $\approx$ 5 nm on complex formation.

It is of interest to consider the origin and cause of this fluorescence change. The crystal structure of $p21^{H\text{-}ras}$.mantGppNHp has been obtained (Goody et al., 1992) and shows that the fluorophore is stacked onto Tyr 32 of the effector loop. Since it has been proposed that GAP_{344} and NF1 bind to this region of $p21^{ras}$, one might consider that the increase in fluorescence is due to a change in the environment of the fluorophore in the ternary complex. The mant-nucleotides in aqueous solution show an increase in fluorescence intensity and a blue shift in the emission maximum as the polarity of the environment is reduced (Hiratsuka, 1983). This is similar to that observed here and might suggest that the binding of the GAP protein excludes water molecules from the environment of the fluorophore. However, fluorescence emission is highly dependent on several factors, and as such one should be cautious in drawing conclusions about the hydrophobicity of an environment based on the wavelength dependence of the emission intensity (Longworth, 1983). The interaction which gives rise to the change in fluorescence intensity may also be responsible for the higher affinity of GAP_{344} for the $p21^{ras}$.mantGTP complex (chapter 5).

6.5.2 *Interpretation of the Fluorescence Changes Observed in the Stopped Flow Experiments with GAP_{344} and NF1.*

The simplest explanation of the origin of the fluorescence change observed in the stopped flow experiments with GAP_{344} and NF1 is that it is monitoring the decrease in intensity

occurring during the $p21^{ras}$.mantGTP to $p21^{ras*}$.mantGTP isomerisation reaction (chapter 4). However, the observation that the amplitude of this process increases with increasing GAP_{344} concentration indicates that additional steps in the mechanism occur with a change in fluorescence intensity. The results of the stopped flow experiments that form the basis of the interpretation are:

(1) The slow change in fluorescence intensity (maximal rate = 14 s^{-1}) can be fitted to a single exponential decay over the complete range of [GAP_{344}].

(2) The amplitude of the fluorescence signal increases with [GAP_{344}].

(3) The starting amplitude of the signal when [GAP_{344}] $\rightarrow$ 0 is $\approx$ 8 %.

(4) The rate of the fluorescence change varies hyperbolically with [GAP_{344}].

(5) The amplitudes of the fluorescence changes with NF1 were constant at 20 - 25 % over the [NF1] used.

The primary assumption in this model is that GAP_{344} and NF1 bind only weakly to the end product of the catalytic reactions, such that over the concentration range used (3 - 60 μM GAP_{344} and 2 - 7 μM NF1), the majority of the GAP protein will be free in solution at the end of the reaction. It is not known from *which particular* intermediate GAP_{344} and NF1 dissociate (see scheme 5.2 in chapter 5). However, the equilibrium constant for interaction of wild type $p21^{ras}$.mantGDP with GAP_{344} and NF1 are $\geq$ 500 μM and 38 μM respectively (Brownbridge et al., 1992). The end product of the reaction of $p21^{ras}$.mantGTP with GAP_{344} and NF1 is $p21^{ras}$.mantGDP, P_i, and the free (i.e uncomplexed) GAP protein. Since the fluorescence intensity of this mixture will be defined solely by the fluorescence intensity of 1 μM $p21^{ras}$.mantGDP, the end point fluorescence must be constant irrespective of the GAP concentration. Consider the reactions with GAP_{344}. The rate of the reaction to attain that end point varies hyperbolically with [GAP_{344}] as described in chapter 5. Thus, the larger amplitudes of the fluorescence changes observed indicates that the fluorescence intensity immediately after the dead time of the instrument ($\approx$ 2 ms after mixing) increases correspondingly with [GAP_{344}]. This can be readily explained if it is assumed that the ternary complex has a higher fluorescence intensity than $p21^{ras}$.mantGTP alone and that the binding reaction is rapidly reversible such that the approach to equilibrium of the binding step is

complete within the dead time of the stopped flow. This model can therefore be used to qualitatively explain the amplitude dependence of the fluorescence transients. According to this model, then the amplitude of the transient rise in fluorescence intensity upon formation of the ternary complex should vary hyperbolically with [GAP_{344}] according to the equilibrium dissociation constant for the binding step. The amplitude of this process at saturating concentrations of GAP_{344} would be $\approx$ 25 % (from the steady state titrations). However, it is not possible to determine the amplitude of this process directly since the reaction is complete within the dead time of the stopped flow.

For the reaction with NF1, then a similar model can be proposed, although one is able to extract a limited amount of quantitative information about the amplitudes of the fluorescence changes associated with the interconversion of the different intermediates in the mechanism. In this case, the binding reaction may not be rapidly reversible since evidence was obtained that this process may occur during the initial 100 ms of the stopped flow reactions. The amplitude of this initial transient was similar to that observed in the steady state titrations (10 - 15 %) whilst the amplitude of the slow phase of the fluorescence change with NF1 was considerably larger than this (20 - 25 %). The amplitude of the second step was constant over the concentration range used, which would be consistent with the lower K_d for NF1 compared to GAP_{344}. Based on the proposed model, this would imply that there is a 5 - 10 % reduction in fluorescence intensity occurring during the slow phase of the fluorescence change which cannot be accounted for by the increase in intensity on formation of the initial ternary complex. It does not seem unreasonable to propose that this additional amplitude reflects the fluorescence change occurring during the isomerisation and mantGTP cleavage reactions described in chapter 4, and which has also been observed with NF1. For GAP_{344}, such calculations are not possible since we are unable to compare the amplitudes of the initial transient (which occurs too rapidly to follow) with the overall amplitude of the fluorescence change of the slow phase. However, as [GAP_{344}] $\rightarrow$ 0, the amplitude of the fluorescence change is $\approx$ 6 - 8 %, suggesting that there is an additional fluorescence change which cannot be accounted for solely in terms of the fluorescence intensity increase on binding.

Despite the above, one should be aware that the use of amplitude data from stopped flow experiments is not as reliable as that of the rates of reaction. The observed signal from a fluorescent solution is not as constant as observed in photon counting spectrofluorimeters, such as the SLM 8000 series used in this thesis. The degree of extraneous or scattered light cannot be controlled with confidence, and will affect the amplitudes of the fluorescence changes. Finally, the lamp used in stopped flow experiments is not as stable as that used in photon counting fluorimeters. Bearing these problems in mind, the fluorescence changes have been interpreted as described above. The model is offered as a plausible explanation of the kinetic and amplitude data presented, without placing too much significance on the exact values of the amplitudes of the individual fluorescence changes observed. This model is self consistent with the equilibrium binding studies described in this chapter.

A consequence of this model is that a fraction of the fluorescence change observed in the slow phase of the stopped flow experiments would be due to the decrease in fluorescence intensity upon dissociation of GAP_{344} and NF1 from an as yet undefined $p21^{ras}$.mant-nucleotide.GAP (see scheme 5.2 in chapter 5). As described in Appendix 6.2, simulations of the time dependence of the fluorescence changes predicted using the model presented above, are only compatible with the experimental data when the rate of GAP_{344} dissociation (k_{+3}) is rapid compared to the rate of the isomerisation reaction (k_{+2}) where $k_{+3} \geq 50 - 100\ s^{-1}$.

6.5.3 *Changes In Energy Transfer and Anisotropy in the Ternary Complex.*

(a) Principles of Polarisation Measurements.

The interpretation of both of these fluorescence changes relies on a discussion of the origins of fluorescence polarisation (see Jameson., 1984 and Valeur., 1991). This discussion can also be used to explain the FRET experiments described in chapter 8 using Trp mutants of $p21^{ras}$. Polarisation (P) and anisotropy (r) are related to each other according to the equation $r = (2 \times P) / (3 - P)$. Anisotropy has appeared more recently to replace polarisation since the former term enjoys the principle of *direct* additivity (Jablonski, 1965, see Appendix 6.1). In a mixture of fluorescent species, the observed anisotropy, r_{obs}, is related to the anisotropy of the i-

th component, r_i, and its fractional contribution to the observed intensity, f_i, (where $\Sigma^i . f_i = 1$) according to the equation:

$$r_{obs} = \Sigma^i . f_i r_i \qquad (6.1)$$

This property simplifies the mathematical treatment of equilibrium binding titrations with GAP_{344} and NF1 since the equivalent relationship for the additive functions of polarisation is more complex (Weber, 1952). Polarisation measurements are performed with polarising materials inserted in the excitation and emission light paths. The relative fluorescence intensities of the sample are determined as a function of the relative orientations of the polarisers. Anisotropy is defined by equation 6.2:

$$r = (I_{II} + I_{\perp}) / (I_{II} + 2 \times I_{\perp}) \qquad (6.2)$$

where I_{II} and $I_{\perp}$ are the emission intensities observed through polarisers orientated parallel and perpendicular to the vertical axis of the laboratory ; incident light is defined to have parallel polarisation. The denominator in equation 6.3 is equal to the total fluorescence emission intensity, I_{total}.

The absorption of light by aromatic compounds (such as Trp and mant-fluorophores) occurs with a well defined directionality such that the electric vector of incident light will be preferentially absorbed by those fluorophores with the appropriate orientation in solution. The absorption of light results in a re-distribution of the electron cloud of the fluorophore, and the formation of a dipole moment in the excited state that is usually quite different from that of the ground state dipole. If nothing happens to disturb the directionality of the excited dipoles during the lifetime of the excited state, an emission that preserves the polarisation direction of the exciting light is observed (the limiting anisotropy, $r_0 = 0.4$). At lower wavelengths (higher energies) we may excite into higher states which may have excited state dipoles that are at a large angle relative to that of the emission dipole. This phenomenon leads to a wavelength dependence of the anisotropy of the emission *even in the absence of any distorting influences.* This is the explanation for the wavelength dependence of the anisotropy of

$p21^{ras}$.mantGTP in solution.

(b) Processes Leading To Fluorescence Depolarisation.

In practice however, the orientation of the excitation and emission dipoles changes as a result of several effects. Firstly, a rapid (10^{12} s^{-1}) loss of energy through vibrational coupling modes brings the system back to the lowest vibrational level of the first electronic state and is usually associated with a change in the orientation of the excited state dipole. Secondly, rotation of the fluorophore due to Brownian motion, or the transfer of energy to a different fluorophore with a different orientation also leads to fluorescence depolarisation at a given wavelength. The primary interest in polarisation measurements stems from the fact that the extent of energy transfer and rotation of the fluorophore vary depending on the exact nature of the system.

(c) Principle of Fluorescence Resonance Energy Transfer.

Electronic excitation energy can be transferred from a donor to a suitable acceptor provided that the emission spectrum of the donor overlaps the absorption spectrum of the acceptor. In the specific case described here, the emission maximum for GAP_{344} tryptophan fluorescence $\approx$ 340 nm whilst the excitation maximum for mantGTP is $\approx$ 360 nm. According to Försters theory of non-radiative fluorescence resonance energy transfer (Förster, 1948, 1949), the extent (more precisely, the rate) of transfer depends on the inverse sixth power of the distance between donor and acceptor, R. In this method of transfer, deactivation of the donor and excitation of the acceptor is occur$\overset{s}{\lambda}$simultaneously *without emission of photons during this process.* When the spectral condition stated above is valid, then the energy of some of the emission transitions of the donor are equal to the energy of the absorption transitions of the acceptor. The fact that the extent of FRET shows a very strong dependence on R means that FRET will only occur to any significant extent when R is small. When R < 8 Å, then Försters theory breaks down (Dexter, 1964). The exact distance dependence is a complex function of many variables (see Valeur, 1991 for a discussion of these problems)

(d) Interpretation of the Fluorescence Excitation Intensity and Polarisation Spectra.

Since it is extremely unlikely that the transition moments of Trp 885 and the mant-fluorophore are parallel, the presence of FRET is equivalent formally to a rotation of the transition dipole before the emission process occurs. As such, there will be a reduction in fluorescence anisotropy for the reasons discussed above. At high wavelengths depolarisation from the limiting value of r_0 will only occur due to Brownian motion of the fluorophore (see below). However, as the wavelength is reduced such that the incident light excites Trp 885 to a particular transition dipole and where FRET now occurs according to Försters theory, depolarisation will occur. In addition, the fluorescence excitation spectrum of the acceptor will be modified to account for the wavelength dependence of the donor excitation. As such, a secondary peak in the excitation intensity spectrum will be observed. As the mantGTP is hydrolysed to mantGDP (at a rate of $\approx 2.4 \times 10^{-4}$ s^{-1} for the Leu 61 mutant and 14 s^{-1} for wild type $p21^{N\text{-}ras}$), the ternary complex dissociates and the donor : acceptor distance becomes sufficiently large that depolarisation due to FRET becomes negligible. The fluorescence intensity excitation spectrum changes correspondingly. The lower extent of FRET that is observed with NF1 compared to GAP_{344} is a complex function of several parameters and in the absence of a detailed fluorescence study, one should be cautious in concluding that a low extent of FRET is due to a change in donor : acceptor distance alone.

At higher wavelengths (such as 366 nm) the fluorescence anisotropy of the ternary complex is greater than that of $p21^{ras}$.mantGTP alone. The extent to which the emission dipoles are randomised prior to the radiative process depends on the lifetime of the excited state (τ_L) and the rate of rotation of the fluorophore. The latter parameter is described in terms of the rotational relaxation time, σ (the time for a fixed direction to rotate through an angle equal to arccos (e^{-1}) about the principal axis of rotation). Thus if $\sigma << \tau_L$, then $r_{obs} \rightarrow r_0$, whilst when $\sigma >> \tau_L$, then $r_{obs} \rightarrow 0$. The value of σ is related to the hydrodynamic properties of the complex to which the fluorophore is attached (including the solvent viscosity, the molar volume of the rotating unit (V), and the temperature.) V in this equation provides the hydrodynamic basis for the concept of "molecular size" when applied to anisotropy measurements.

Thus when the $p21^{ras}$.mantGTP complex interacts with GAP_{344} or NF1, there is an increase in the molar volume of the complex which leads to a corresponding increase in σ such that r_{obs} increases. However, since the intensity of the ternary complex is higher than that of $p21^{ras}$.mantGTP alone, an increase in lifetime is likely to occur. This will affect the amplitude of the change in anisotropy on complex formation since r_{obs} is dependent on both σ and τ_L. This treatment explains the observation of an increase in anisotropy during the titration experiments where the fluorophore is rigidly attached to the protein. However, in practice, the fluorophore itself can have some local motion independent of that of the ternary complex as a whole. This "local motion" is usually relatively rapid (low anisotropy) and will affect the observed anisotropy which is a weighted average of the global and local motions. Therefore, a change in local motion upon complex formation will also affect the observed amplitude of the anisotropy change. Only when time resolved measurements are made can one deconvolute the global and local motions of the fluorophore.

In many cases, however, one is relatively unconcerned with the molecular origins of a change in anisotropy associated with a binding reaction, and simply uses the signal to follow the extent of complex formation (e.g Brownbridge et al., 1992) by steady state methods. If this is the case, then the limitations of the steady state method in providing molecular information on the hydrodynamics of the system should be borne in mind. The problem associated with this technique then reduces to determining the relative fractions of bound and free ligand according to equation 6.1 (the additivity of fluorescence anisotropy). This equation shows that in order to describe the molar concentration of the ternary complex in a titration experiment as a function of the observed anisotropy, r_{obs}, one must account for the change in fluorescence intensity. Since the emission maxima of $p21^{ras}$.mantGTP and the ternary complex are different, an absolutely rigorous treatment of the change in anisotropy must also account for the sensitivity of the detector elements to the respective emission wavelengths.

6.5.4 *Use of the Fluorescence Signals for Kinetic and Equilibrium Binding Studies.*

The majority of the information that has been obtained concerning the transients of intermediates in enzyme kinetics has come from the use of spectroscopic probes within the system.

The information content of fluorescence data is typically greater than that of absorption spectroscopy, although circular dichroism measurements can offer additional information. In addition, a fluorophore can often be observed selectively in an environment containing many absorbing, but non-fluorescent components. Finally, emission properties are usually more sensitive to environmental effects than the corresponding absorption parameters. Whilst this latter feature is useful, it necessarily complicates the interpretation of a change in a fluorescence property in terms of a particular molecular process.

Fluorescence resonance energy transfer provides larger signals with which to monitor the GAP_{344}-activated mantGTPase reaction. This signal could be used in stopped flow studies to follow the hydrolysis of mantGTP by mutants of $p21^{ras}$ which show no fluorescence intensity change during the binding or cleavage reaction but which bind GAP_{344} with reasonable affinity. In addition, the larger amplitudes of the signals with FRET may allow one to work at lower $p21^{ras}$.mantGTP concentrations in the stopped flow.

It was hoped that the spectroscopic signals described here would allow the determination of the association and dissociation rate constants for the binding of GAP_{344} to $p21^{ras}$.mantGTP. Whilst preliminary experiments suggest that this may be possible with NF1, the rapidly reversible nature of the binding step with GAP_{344} do not allow one to estimate these rate constants by stopped flow techniques. Pressure relaxation studies have been performed (in collaboration with Dr M. Geeves, Dept. of Biochemistry, University of Bristol) since this technique has a much lower "dead time" compared to stopped flow ($\approx$ 200 μs). These studies used the Leu 61 $p21^{H\text{-}ras}$.mantGTP complex since it was hoped that this mutant may have a slower GAP_{344} dissociation rate than wild type $p21^{ras}$.mantGTP. In this technique, a mixture of $p21^{ras}$.mantGTP and GAP_{344} at equilibrium is subjected to hydrostatic pressure, such that the equilibrium may be partially shifted. When the pressure is released, the system returns to the original equilibrium mixture, the kinetics of which are monitored by an appropriate spectroscopic signal. However, no convincing evidence could be obtained for a change in intensity during time period of the re-equilibration which suggests that the system was not perturbed sufficiently by pressure to give a detectable fluorescence change.

As a consequence of these titration experiments, equilibrium binding assays have been developed (for example, see Brownbridge et al., 1992). These assays have significant advantages over kinetic methods for the determination of binding constants. In particular, these methods allow the determination of high affinity binding constants and as such are important for studies of the interaction of $p21^{ras}$.GTP with NF1. The Leu 61 mutant of $p21^{ras}$ has often been used as a competitor of wild type $p21^{ras}$ in GAP-binding studied. The finding that the rate of mantGTP hydrolysis by the Leu 61 when saturated with GAP_{344} is significant (half time $\approx$ 50 min) suggests that this factor should be considered in the design of experiments using this mutant and GAP_{344}. Similar problems would only be encountered with NF1 if the experiments were to be performed over a much longer period of time.

The one signal that is relatively independent of the nature of the GAP protein is the increase in steady state anisotropy at high excitation wavelengths (366 nm). All three fluorescence signals (intensity, anisotropy, and energy transfer) can be used to determine equilibrium binding constants. However, only the change in fluorescence intensity and anisotropy have been used here in titration experiments. The values of the K_d obtained are similar by both methods and are in the range of 1μM for the binding of NF1 to the mantGppNHp complex of wild type $p21^{N\text{-}ras}$. When these experiments were repeated for the equivalent complex with wild type $p21^{H\text{-}ras}$, then an equilibrium constant of 0.25 μM was obtained. In contrast, titration experiments with GAP_{344} indicated similar binding affinities for both $p21^{N\text{-}ras}$.mantGppNHp and $p21^{H\text{-}ras}$.mantGppNHp (18 μM). These results suggest that NF1 binds to $p21^{N\text{-}ras}$ some 20-fold more tightly, and to $p21^{H\text{-}ras}$ some 80-fold more tightly, than does GAP_{344}. Similar conclusions have been made using multiple turnover kinetic assays (Bollag and McCormick, 1991). Since the effector loop, which may be the site for NF1 and GAP_{344} binding, are identical between $p21^{N\text{-}ras}$ and $p21^{H\text{-}ras}$, it seems probable that other residues in $p21^{ras}$ also contribute to the binding site for these proteins. This notion is strongly supported by protein engineering studies with chimeric ras / rap proteins which demonstrate that sequences flanking residues 32 - 40 determine the differing biological activities of these two proteins (Zhang et al., 1990).

In all of the kinetic mechanisms described in this thesis, it has been assumed that $p21^{ras}$ binds to GAP and NF1 with a 1 : 1 stoichiometry. Based on this assumption, then for very high affinity interactions ($K_d << [p21^{ras}]$), such as NF1 binding to Leu 61 $p21^{H\text{-}ras}$.mantGTP, saturation of $p21^{ras}$ occurs rapidly when $[NF1]_{active} = [p21^{ras}]$, and a breakpoint in the titration curve was observed. Thus, if one can determine the [$p21^{ras}$.mantGTP] with accuracy, then under these conditions, one can determine the concentration of active NF1. The titration curves with NF1 yielded a breakpoint of $\approx$ 1 μM - similar to the concentration of $p21^{ras}$.mantGTP, suggesting that the molar concentration of active NF1 is similar to the value calculated from the absorbance of the preparation at 276 nm (Gill and von Hippel, 1989 ; Mach et al., 1992). In support of this conclusion, it has been proposed based on a kinetic argument (chapter 5), that it is unlikely for there to be a significant proportion of inactive NF1. Time resolved measurements of the complex between Leu 61 $p21^{H\text{-}ras}$.mantGTP and NF1 may indicate whether the rotational rate of the complex is consistent with a 1:1 stochiometry.

6.5.6 *Summary.*

The results of these experiments have been used to propose a model which allows one to qualitatively interpret the transient changes in fluorescence intensity observed during the GAP_{344}- and NF1-activated mantGTPase mechanism of $p21^{ras}$. Both the change in energy transfer and intensity can be used for stopped flow studies, whilst at present, anisotropy measurements on a millisecond time scale are not possible. This latter technique has however been used to calculate the equilibrium dissociation constants for combinations of proteins which are not readily determined by kinetic methods (for example, see Brownbridge et al., 1992). In many cases, the unambiguous characterisation of a change in fluorescence anisotropy or energy transfer at the hydrodynamic and molecular level requires information that can only be obtained from time resolved fluorescence methods. Finally, these studies have demonstrated that an accurate determination of binding constants by anisotropy titrations can only be obtained when the fluorescence intensity of the ternary complex relative to the $p21^{ras}$.mant-nucleotide binary complex has been determined.

CHAPTER SEVEN

EFFECT OF IONIC STRENGTH ON THE INTERACTION OF $p21^{ras}$ WITH GAP_{344} AND NF1

"I was curious about the emphasis the authors (Moore et al., 1992) put on the effect of ionic strength, as ras inside the cell, which is the only place it ever does its job, is in a medium of substantial ionic strength. Is it of any particular help to think about its action and how it works at zero ionic strength ?"

R.H. Michell (1992)

7.1 Introduction.

In comparison with the data presented by other groups (for example, Reinstein et al., 1991; Rensland et al., 1991; Antonny et al., 1991; Wiesmuller and Wittinghofer, 1992; Bollag and McCormick, 1991), the activation by GAP_{365} of the intrinsic GTP cleavage rate of $p21^{ras}$ observed in chapter 4 was relatively weak. Thus, concentrations of GAP $\approx$ 100-fold higher than used by other groups are required to obtain similar extents of activation. Whilst GAP_{365} is $\approx$ 10-fold less active on a mg / mg basis than GAP_{344} (see chapter 8), the activations are still an order of magnitude lower than those reported by other groups. As mentioned above, the ionic strength conditions of the two sets of experiments are significantly different - those described in chapter 4 were performed under high ionic strength (buffer B) whilst those reported by others were performed in low ionic strength buffer (similar to buffer C). To investigate whether this was the cause of the different extents of activation, and to investigate the reports that the activation by GAP is salt dependent (Vogel et al., 1988, Wiesmuller and Wittinghofer, 1992), a study of the effect of different NaCl concentrations on the interaction

of $p21^{ras}$.mantGTP with GAP_{344} and NF1 was undertaken. The results of these experiments are also important when one wishes to consider the *in vivo* activation of the intrinsic GTP cleavage rate by GAP_{344} and NF1, since these reactions occur in a medium of ionic strength estimated to be $\approx$ 150 mM.

The stopped flow studies described in chapter 5 indicated that the primary effect of increasing NaCl concentrations is to reduce the affinity of GAP_{344} for $p21^{ras}$.mantGTP, whilst leaving the rate of the isomerisation largely unaffected. Quantitatively, the equilibrium dissociation constant is increased by 100 % (over the value obtained under standard low salt conditions) in the presence of $\approx$ 20 - 25 mM NaCl, although this estimate is subject to relatively high errors due to the limited amount of data.

Several groups have estimated the ionic strength dependence of the GAP-activated $p21^{ras}$.GTPase mechanism (Vogel et al., 1988; Wiesmuller and Wittinghofer, 1992 and references therein) by a different approach. These experiments involve the measurement of the multiple turnover of rate of $p21^{ras}$.GTP hydrolysis in the presence of catalytic concentrations of GAP, under conditions where [$p21^{ras}$.GTP] $<<$ K_1' $>>$ [GAP]. The inhibition of the rate of GTP hydrolysis by NaCl has been reported in terms of an IC_{50} value, the concentration of NaCl required to reduce the apparent rate of hydrolysis to 50% of the starting value. These studies provide no information about which step in the mechanism is affected by NaCl, and as discussed in more detail in section 7.5, the absolute value of the IC_{50} only reflects the apparent ionic strength dependence of the mechanism under the specific experimental conditions used. Similar experiments have been reported with the catalytic domain of NF1 (Wiesmuller and Wittinghofer, 1992), and based on these results, it has been concluded that the GAP_{344}- and NF1-activated mechanisms shows different salt sensitivities.

7.2 Effect of NaCl on the Rate of $p21^{ras}$.mantGTP Hydrolysis in the Presence of Catalytic Concentrations of GAP_{344}.

Similar experiments to those described by Wittinghofer et al., (1992) were performed in 20 mM TrisHCl, pH 7.5, 1 mM $MgCl_2$, 0.1 mM DTT, at 30°C (buffer C) where [$p21^{ras}$.mant-

GTP] = 5 μM and [GAP_{344}] = 0.2 μM. The rate of mantGTP cleavage by $p21^{N\text{-}ras}$ was determined by following the rate of release of inorganic phosphate using the continuous absorbance assay described by Webb and Hunter (1992). In figure 7.1.a, the rate of reaction, as a percentage of the rate in the absence of added NaCl, is plotted as a function of the final [NaCl]. The change in absorbance at 360 nm after the addition of GAP_{344} could be fitted assuming single exponential kinetics. The reduction in rate observed upon addition of NaCl is identical when measured by either the rate of P_i release or the rate of the fluorescence change after the addition of GAP_{344} (exponential decrease in fluorescence of $\approx$ 7 %). It is not clear how the inhibition of the GAP-activated $p21^{ras}$.GTPase by NaCl should be interpreted quantitatively (see section 7.5). The reduction in hydrolysis rate with increasing [NaCl] gave an IC_{50} of $\approx$ 40 mM NaCl under these conditions from the data presented in Figure 7.1.a.

The rates of GAP_{344}-catalysed $p21^{ras}$.mantGTP hydrolysis obtained under the conditions of low ionic strength (11 x 10^{-3} s^{-1}) are comparable with those obtained by other groups under similar experimental conditions, suggesting that the different expression systems for GAP_{344} yield proteins with very similar catalytic activities. Specifically, Rensland et al., (1991) reported single exponential rate constants for the fluorescence change with 5 μM wild type $p21^{H\text{-}ras}$.mantGTP of $\approx$ 10^{-2} s^{-1} at 37°C with "ca. 50 nM GAP_{334}". Whilst no information was supplied as to the assay used for GAP_{334} or $p21^{H\text{-}ras}$.mantGTP, and given that the temperature of the reaction was 37°C, the activations are clearly comparable between the two laboratories.

7.3 Effect of NaCl on the Rate of $p21^{ras}$.mantGTP Hydrolysis in the Presence of Catalytic Concentrations of NF1.

The equivalent experiment described above for GAP_{344} has been performed with the catalytic domain of NF1. However, the data analysis is complicated in this case by the low equilibrium dissociation constant for the interaction of NF1 with $p21^{ras}$.mantGTP ($\approx$ 1 μM, chapter 6). For the simple case where $k_{obs} \propto 1/K_d$ then $p21^{ras}$.mantGTP concentrations of $\approx$ 0.1 μM would be required to ensure that [$p21^{ras}$.mantGTP] << K_d. This immediately precludes the use of the phosphate release assay due to its relatively low sensitivity. Further-

Figure 7.1: Effect of NaCl on the Rate of GAP_{344}-and NF1-Catalysed Hydrolysis of mant-GTP by $p21^{N\text{-}ras}$.

Panel A: 5 μM $p21^{N\text{-}ras}$.mantGTP in buffer C was incubated in the presence of 0.2 μM GAP_{344}. The rate of mantGTP cleavage was determined by monitoring the rate of inorganic phosphate release using the continuous absorbance assay (Webb, 1992; Webb and Hunter, 1992). As essentially identical dependence of the rate on NaCl concentration was observed by measuring the rate of the fluorescence change after the addition of GAP_{344}. The rate of reaction is expressed relative to the rate in the absence of added NaCl (1.1×10^{-2} s^{-1}). Data points are shown as mean ($\pm \sigma_{n-1}$, n = 2 - 4). The rate of GTP hydrolysis was reduced to 50 % of the value in the absence of added NaCl (IC_{50}) after the addition of $\approx$ 40 mM NaCl.

Panel B: 1 μM $p21^{ras}$.mantGTP in buffer C was incubated with 10 nM NF1 and varying concentrations of NaCl as shown. The rate of mantGTP hydrolysis was determined from the exponential rate of the fluorescence change occurring after the addition of NF1. Data are plotted as a percentage of the rate observed in the absence of added NaCl (6.78×10^{-2} s^{-1}). Under these conditions, the IC_{50} is $\approx$ 60 mM NaCl.

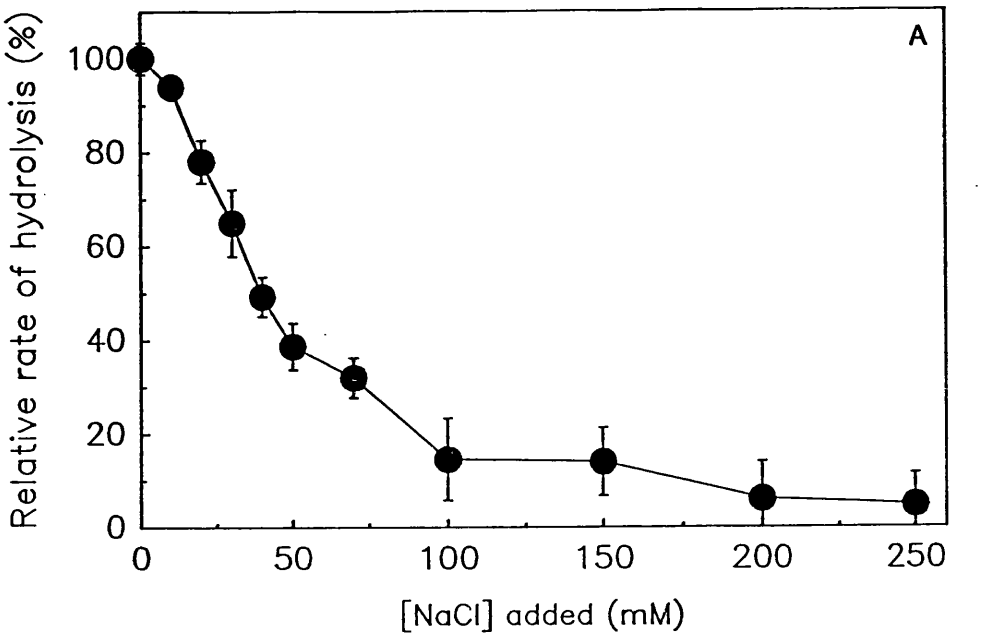
A
Relative rate of hydrolysis (%)
100
80
60
40
20
0
0
50
100
150
200
250
[NaCl] added (mM)

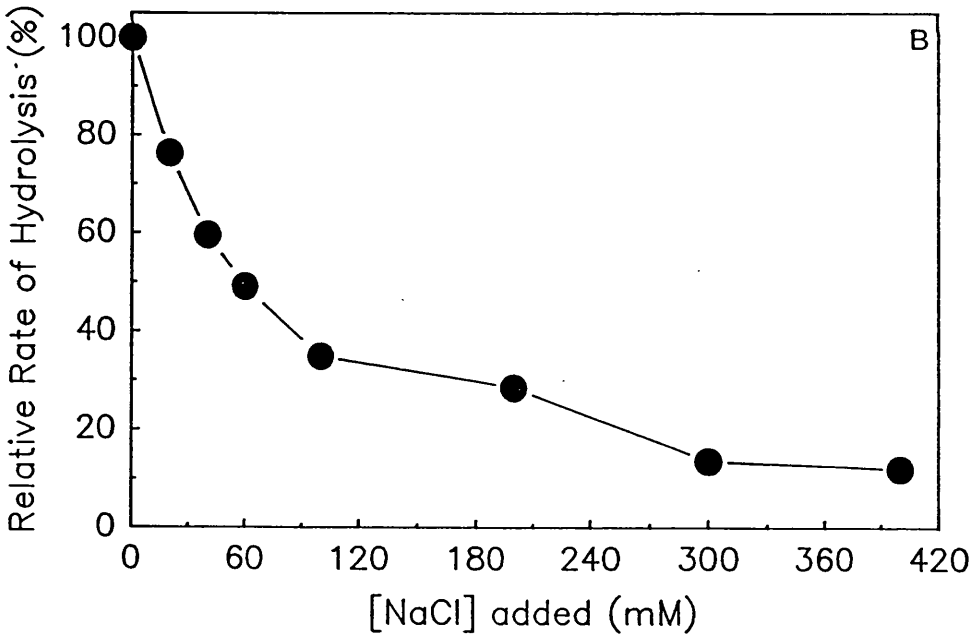
B
Relative Rate of Hydrolysis (%)
100
80
60
40
20
0
0
60
120
180
240
300
360
420
[NaCl] added (mM)

more, the low quantum yield and extinction coefficient of the mant-fluorophore, combined with the low amplitude of the fluorescence signal makes working at these concentrations impractical. These kinetic experiments have been performed at 1 μM $p21^{ras}$.mantGTP and 10 nM NF1 and the data analysis has been modified to account for the fact that $[p21^{ras}] \approx K_d$ (section 7.5). The rate of the fluorescence change with different concentrations of NaCl added to buffer C yielded an IC_{50} under these conditions of 60 mM NaCl (Figure 7.1.b).

7.4 Effect of Ionic Strength on the Interaction of $p21^{ras}$ with NF1 Using Equilibrium Binding Assays.

The analysis of the data obtained from the multiple turnover experiments described above requires several assumptions to be made concerning the mechanism of inhibition. Since the major effect of ionic strength is on the equilibrium constant for the initial binding reaction (chapter 5), then the ionic strength dependence of the mechanism should be similar to that of the K_d. The most direct, quantitative and conclusive method to determine the effect of NaCl on the equilibrium constant is to measure ternary complex formation directly at a given concentration of NaCl.

The titration curve for the binding of NF1 to wild type $p21^{N\text{-}ras}$.mantGppNHp in the absence and presence of 50 mM NaCl and 100 mM NaCl is shown in Figure 7.2.a. The dependence of the equilibrium dissociation constant on the [NaCl] added is shown in Figure 7.2.b. These data provide direct quantitation of the effect of NaCl on the K_d and demonstrate that the equilibrium constant is increased by a factor of 2 by addition of $\approx$ 20 mM NaCl. A similar dependence is obtained when the equilibrium constant is determined when using the change in fluorescence intensity upon complex formation. It is important to stress that this technique has the major advantage that it makes no assumptions about the nature of the inhibition by NaCl and is independent of the [$p21^{ras}$.mant-nucleotide] used relative to the K_d at any given salt concentration. As such, the results of these experiments are proposed to accurately reflect the dependence of the equilibrium dissociation constant on the [NaCl] added to the medium.

Figure 7.2: Effect of NaCl on the Equilibrium Constant for the Interaction of $p21^{ras}$.mant-GppNHp with NF1.

Panel A: 1 μM $p21^{N\text{-}ras}$.mantGppNHp in buffer C alone (curve A) was incubated with varying concentrations of NF1. The steady state anisotropy after each addition was determined using the fluorimeter in the T-format with excitation at 366 nm and emission monitored through a KV399 filter. Data were fitted to the derived equations for the anisotropy change on formation of the ternary complex (Brownbridge et al., 1992). These titration curve were repeated in the presence of 50 mM NaCl (curve B) and 100 mM NaCl (curve C) as shown. Solid lines correspond to K_d values of 0.85 ($\pm$ 0.09) μM for A, 3.01 ($\pm$ 0.11) μM for B, and 4.93 ($\pm$ 0.42) μM for C. The amplitudes of the changes were 0.082 (A), 0.082 (B) and 0.077 (C) whilst starting points were at 0.177 ($\pm$ 0.001) in all cases.

Panel B: The values of the equilibrium constant at different concentrations of NaCl obtained from experiments such as those shown in Figure 7.2.a are plotted as a function of the [NaCl] added to the medium. The data for K_d at 20 mM NaCl (1.4 ($\pm$ 0.21) μM) was not shown in Figure 7.2.a for clarity since the initial starting anisotropy was lower than for the data at 0 mM, 50 mM , and 100 mM NaCl. The solid line through the data in Panel B is the best fit to a linear regression with a gradient of 0.042 μM mM^{-1} NaCl. Thus, the equilibrium constant is increased by a factor of 100 % in the presence of $\approx$ 20 mM Nacl.

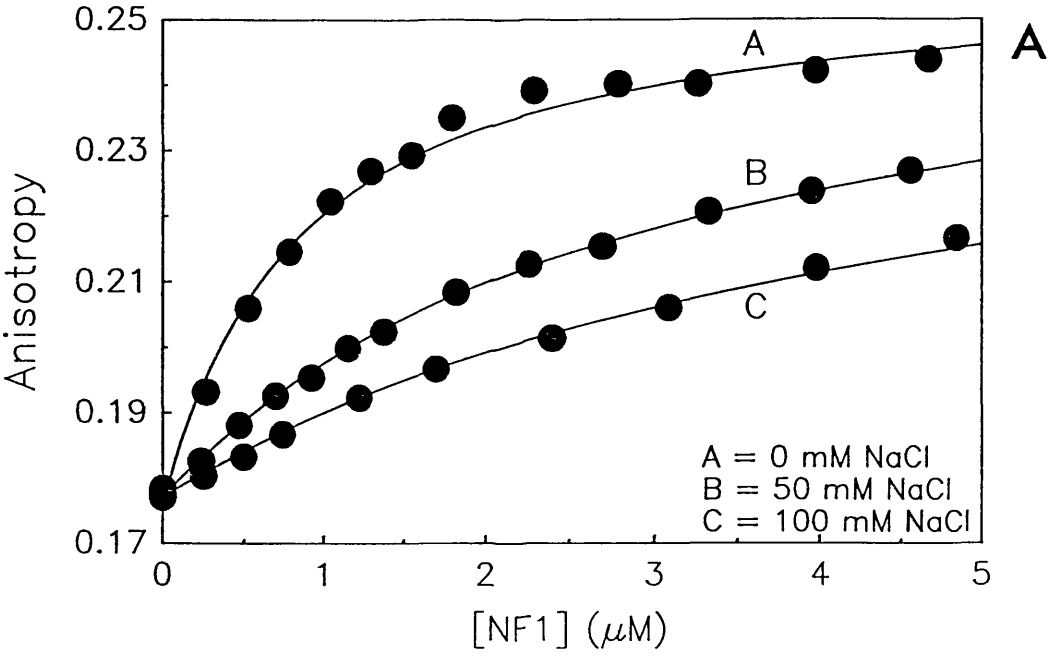
A
0.25
0.23
0.21
0.19
0.17
Anisotropy
A
B
C
A = 0 mM NaCl
B = 50 mM NaCl
C = 100 mM NaCl
0
1
2
3
4
5
[NF1] (μM)

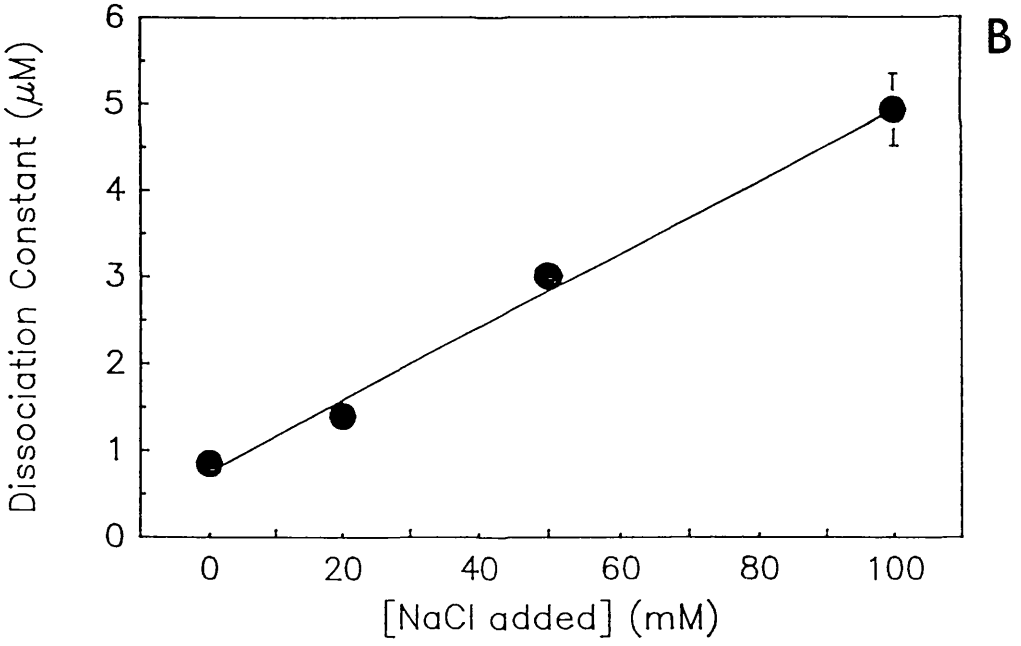
B
6
5
4
3
2
1
0
Dissociation Constant (μM)
0
20
40
60
80
100
[NaCl added] (mM)

Figure 7.3. Simulations of the Effect of NaCl on The Equilibrium Between $p21^{ras}$.mantGTP and GAP_{344}.

The model treats NaCl as a competitive inhibitor (I) of the interaction of $p21^{ras}$.mantGTP (R) with a GAP (G, either GAP_{344} or NF1). The binding of NaCl is defined by the equilibrium inhibitor constant, K_I, whilst the equilibrium dissociation constant for the binding of R to G is given by K_d. R_o and G_o refer to the concentrations of R and G respectively. The concentration of the RG complex formed as a function of inhibitor, I, is given by the following equation whose derivation is given in Appendix 7.X :

$$[RG] = [X - (\sqrt{\{X^2 - 4\,K_I^2.R_o.G_o\}})] \div 2\,K_I$$

$$\text{where } X = K_I.R_o + K_I.G_o + K_d\,(I + K_I)$$

(A) Variation of [RG] with I according to the above equation when R_o = 5 μM, G_o = 0.2 μM and K_d = 17.4 μM. Curves are shown for different values of K_I where (1) = 10 mM, (2) = 20 mM, (3) = 30 mM, (4) = 50 mM, (5) = 75 mM, (6) = 100 mM, and (7) = 200 mM. Under these conditions IC_{50} values roughly approximate to K_I values.

(B) As for (A) except $R_o = G_o = K_d$ = 1 μM. K_I values are numbered as follows; (1) = 10 mM, (2) = 20 mM, (3) = 40 mM, (4) = 60 mM, (5) = 100 mM. Under these conditions, IC_{50} values are 2.5-fold greater than K_I values and hence under-estimate the ionic strength sensitivity of the equilibrium between R and G.

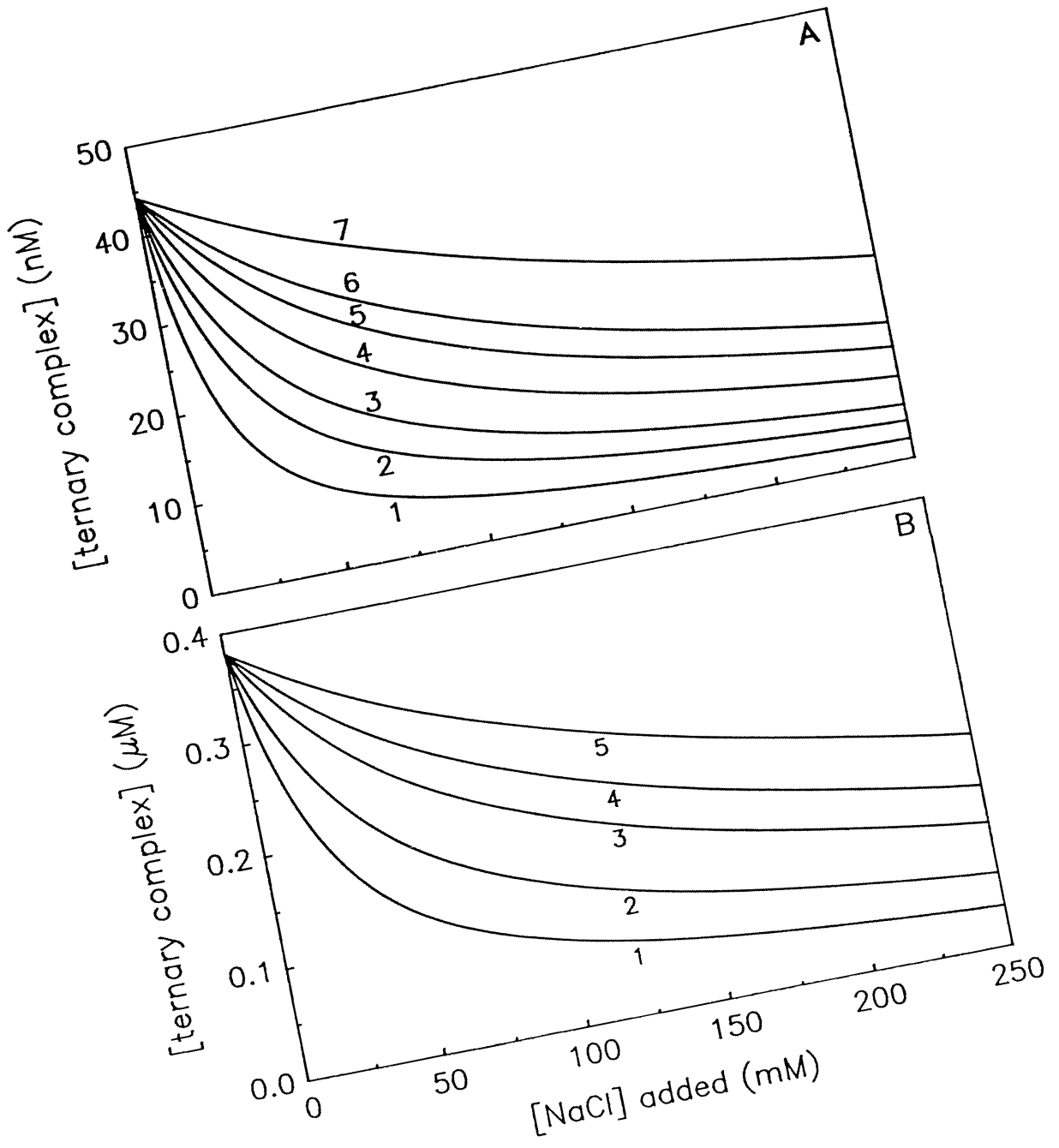
A
50
40
30
20
10
0
[ternary complex] (nM)
7
6
5
4
3
2
1
B
0.4
0.3
0.2
0.1
0.0
[ternary complex] (μM)
5
4
3
2
1
0
50
100
150
200
250
[NaCl] added (mM)

7.5 Discussion.

If one wishes to consider the *in vivo* activities of GAP_{344} and NF1 then it is necessary to determine how their activity is modulated by ionic strength. Most *in vitro* kinetic studies with purified GAP proteins have been performed under conditions where there is sufficient buffering capacity whilst keeping the ionic strength to a minimum (usually ionic strength (I) $\approx$ 20 mM). Thus far, there has been one report of experiments to compare the salt sensitivities of the GAP_{344}- and NF1-activated $p21^{ras}$.GTPase mechanisms (Wiesmuller and Wittinghofer, 1992). In these experiments, the ionic strength dependence has been estimated by measuring the rate of hydrolysis of GTP by $p21^{ras}$ in the presence of varying [NaCl] (Vogel et al., 1988; Wiesmuller and Wittinghofer, 1992). The results have been reported in terms of an IC_{50} value, although no data was presented concerning the shape of the inhibition curve. The IC_{50} values are in the range 30 - 40 mM NaCl for GAP_{344} under conditions where [$p21^{ras}$.GTP] << K_d. Replacing NF1 for GAP_{344} in this assay and under identical conditions, Wiesmuller and Wittinghofer, (1992) reported an IC_{50} value of 200 mM NaCl. When similar experiments were performed here with $p21^{N\text{-}ras}$.mantGTP, IC_{50} values of $\approx$ 40 mM NaCl were obtained for GAP_{344} and $\approx$ 60 mM NaCl for NF1 (for the exact experimental conditions, see legends to Figures 7.1).

The inhibitory effect of NaCl on the GAP-catalysed rate of GTP hydrolysis is referred to here as an ionic strength effect, although in theory it could be due to a specific effect of Na^+ or Cl^- ions. However, similar experiments using different salts (P.N. Lowe, pers. comm. and M.R. Webb, pers. comm.) suggest that the observed effect is indeed a non-specific effect of ionic strength.The major problem associated with the use of the multiple turnover procedure is the formulation of a model with which to quantitatively interpret the inhibition data. The extent of inhibition observed at a given [NaCl] will depend critically on the degree of saturation of the GAP protein, and hence on the concentrations of $p21^{ras}$.GTP and the GAP, and on the K_d. One model would be to treat NaCl as a competitive inhibitor since a compound which binds to the GAP and raises the K_m but does not alter the V_{max} can formally be treated using steady state kinetics in the same way as a competitive inhibitor. A compound which binds to the substrate ($p21^{ras}$.GTP) will display complex kinetics at high concentrations of

substrate. In terms of the elementary steps of the mechanism, a change in the ionic strength is likely to affect the observed rate of mantGTP hydrolysis in a complex manner. As such, the ionisation state of both proteins will be changed as will the rates of ternary complex formation and dissociation. The competitive inhibitor model described below is used so as to allow the discussion of the experimental data.

Using this model, the ionic strength dependence of ternary complex formation would be defined by the inhibitor constant, K_I, for NaCl. The concentration of the ternary complex can be calculated as a function of the [NaCl] for a range of values of K_I (Appendix 7.1). The results of such calculations where [$p21^{ras}$.mantGTP] = 5 μM and [GAP_{344}] = 0.2 μM (as used in Figure 7.1) is shown in Figure 7.3.a. One can see that the IC_{50} value of $\approx$ 40 mM NaCl would correspond to a K_I of $\approx$ 30 mM NaCl using this model. Thus, there is only a small difference between the IC_{50} and K_I values when [$p21^{ras}$.mantGTP] is 4-fold below the K_d. The discrepancy however becomes more significant when [$p21^{ras}$.mantGTP] $\approx$ K_d (Figure 7.3.b). The IC_{50} value obtained is therefore critically dependent on the relative concentrations of $p21^{ras}$.GTP and GAP_{344} (or NF1) used and on the equilibrium constant for the interaction. Thus, the value of the IC_{50} cannot be used as a constant with which to fully describe the salt dependence of the equilibrium. Only when the concentration of $p21^{ras}$.GTP is at least an order of magnitude below the K_d does the IC_{50} approximate to the K_I.

Thus, the K_d was measured directly over a range of ionic strength conditions. This has the advantage that it makes no assumptions concerning the nature of the inhibition and is associated with none of the problems inherent in the kinetic competition analysis described above. This then allows one to describe the variation in K_d with [NaCl] in absolute terms. If the competitive inhibitor model is valid for the interpretation of these effects, then one would expect similar K_I values by both techniques. The variation in the value of the K_d obtained from stopped flow experiments on the [NaCl] (chapter 5) is summarised graphically in Figure 7.4.a. Note that the value used for 50 mM NaCl is that obtained from curve B in Figure 5.4 since the calculated value of k_{2a}' from this curve is similar to that obtained in the absence of NaCl and experiments at lower concentrations of NaCl (20 mM) demonstrated that the value of k_{2a}' is independent of [NaCl]. These data suggest that the [NaCl] required to increase the

Figure 7.4 Effect of NaCl on the Equilibrium Constant for the Interaction of $p21^{N\text{-}ras}$.mant-GTP with GAP_{344} and NF1.

Panel A: The values of the K_d obtained from stopped flow studies is plotted as a function of the [NaCl] added to the medium. The K_d values used are those described in the text of chapter 5.

Panel B: Equilibrium dissociation constants for GAP_{344} and NF1 have been normalised to the value obtained in the absence of added NaCl (relative dissociation constant = 1). K_d values used are those obtained in chapter 5 from stopped flow experiments (GAP_{344}) and from anisotropy titrations with $p21^{ras}$.mantGppNHp (Figure 7.2.b for NF1). The relative dissociation constant is plotted as a function of the [NaCl] added to buffer C.

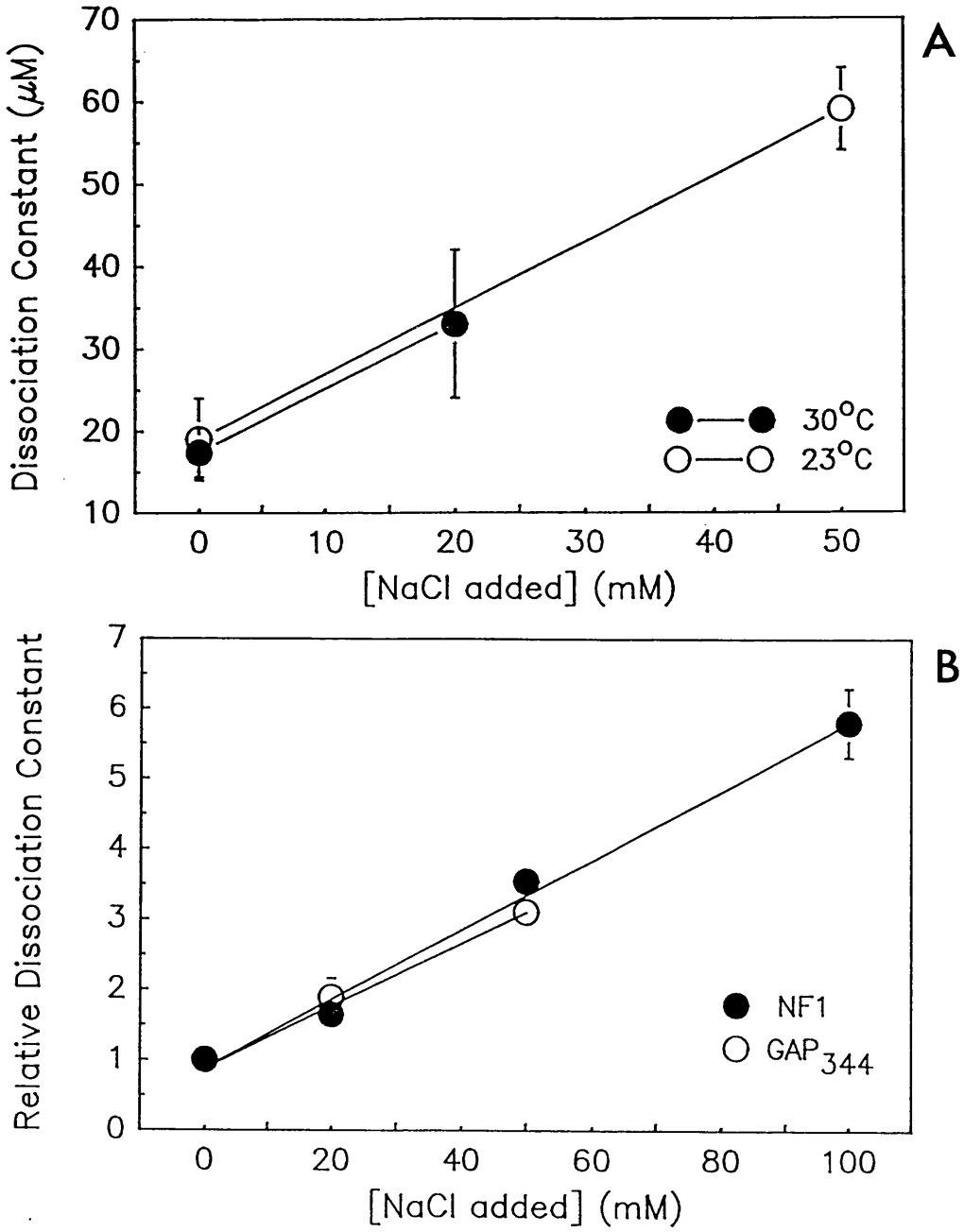
A
Dissociation Constant (μM)
70
60
50
40
30
20
10
0
10
20
30
40
50
[NaCl added] (mM)
30°C
23°C
B
Relative Dissociation Constant
7
6
5
4
3
2
1
0
0
20
40
60
80
100
[NaCl added] (mM)
NF1
GAP344

K_d for the interaction of $p21^{ras}$.mantGTP with GAP_{344} by 100 % is not dissimilar to that observed for NF1 (Figure 7.4.b).

The NaCl dependence data (IC_{50} and K_I) from all of the experiments with GAP_{344} and NF1, are summarised in Table 7.1. Also included are the data from Wiesmuller and Wittinghofer (1992) for comparison. Given the conditions used by these workers (where [$p21^{H\text{-}ras}$.GTP] = 1 μM and K_d for the binding reaction = 0.3 μM), their value for the IC_{50} = 200 mM NaCl corresponds to a K_I of 40 mM. Thus, the reported difference between the IC_{50} for the inhibition of GAP_{334} and NF1 is primarily due to the higher affinity of NF1 for $p21^{H\text{-}ras}$.GTP than GAP_{334}. It is likely therefore that the effect of NaCl on the two proteins is similar, and the results of the experiments described in this chapter are consistent with this view. Based on the experimentally determined values of the IC_{50}, Wiesmuller and Wittinghofer (1992) concluded that NF1 was less salt sensitive than GAP_{344}. In view of the flaw in the data analysis, this conclusion appears invalid.

It has been possible to demonstrate that for GAP_{344}, the effect of NaCl is to increase the equilibrium dissociation constant whilst leaving the value of k_{cat} unchanged. Similar stopped flow experiments have not been performed with NF1 over a range of salt concentrations, and thus one cannot unambiguously conclude that the same mechanism applies to NF1. However, the marginal reduction in the rate of $p21^{ras}$.GTP hydrolysis catalysed by NF1 which was observed in chapter 5 under conditions of low and high ionic strength can be primarily accounted for by an increase in the K_d. The reduction in the concentration of ternary complex (at a fixed [NF1] measured by fluorescence anisotropy) following the addition of varying concentrations of NaCl parallelled the decrease in catalytic activity. This result also suggests that the high sensitivity of NF1 to ionic strength is due mainly to an effect on the equilibrium constant.

The high ionic strength dependence of the binding equilibrium raises important questions as to the *in vivo* level of GAP_{344}- and NF1-activation since the intracellular ionic strength is $\approx$ 150 mM. This would suggest that under these conditions the K_d for GAP_{344} is in the order of 100 - 200 μM, and 10 - 20 μM for NF1. It is difficult to interpret this value in physiological

Table 7.1 : Effect of NaCl Concentration on the Interaction of $p21^{ras}$ with GAP_{344} and NF1.

$p21^{ras}$	GAP_{344}		NF1	
	IC_{50} (mM)	K_I (mM)	IC_{50} (mM)	K_I (mM)
$p21^{N\text{-}ras}$.mantGTP [a]	40 [c]	30 [c]	60 [e]	25 [e]
	20 - 25 [d]		20 - 25 [f]	
$p21^{H\text{-}ras}$.GTP [b]	40 [g]	30 - 35 [g]	200 [h]	40 [h]

Notes:

(a) From this work.

(b) From Wiesmuller and Wittinghofer (1992)

(c) From kinetic assays where [$p21^{N\text{-}ras}$.mantGTP] = 5 μM and K_d = 17.4 μM. IC_{50} values are converted to K_I values using the model described in the text and using the simulations shown in Figure 7.3.

(d) From stopped flow experiments described in chapter 5.

(e) From kinetic assays where [$p21^{N\text{-}ras}$.mantGTP] = 1 μM and K_d = 0.8 μM.

(f) From the anisotropy titration experiments with $p21^{N\text{-}ras}$.mantGppNHp.

(g) Calculated from the results of kinetic assays described by Wiesmuller and Wittinghofer (1992) where [$p21^{H\text{-}ras}$.GTP] = 1 μM and K_d = 8 μM.

(h) Calculated from the results of kinetic assays described by Wiesmuller and Wittinghofer (1992) where [$p21^{H\text{-}ras}$.GTP] = 1 μM and K_d = 0.3 μM.

(c) , (e), (g) and (h) assume a competitive inhibitor model.

terms since at present there is no recognised value for the intracellular concentrations of $p21^{ras}$, NF1 or p120-GAP. Furthermore, full length GAP (p120-GAP) may show a different ionic strength dependence from GAP_{344}, and in addition the association of $p21^{ras}$ and GAP with membranes *in vivo* may increase their local concentrations significantly. Such changes will however need to be dramatic if the *in vivo* activation of the intrinsic GTPase activity of $p21^{ras}$ is to be stimulated to an extent comparable with that observed in these *in vitro* studies.

The primary interest in determining the K_I for inhibition by NaCl of GAP_{344} is to compare it to that of NF1, since this may provide clues as to the *in vivo* level of GTPase activation and hence the relative importance of the two proteins as negative regulators of $p21^{ras}$ function. However, these data do not indicate any differential regulation of the activity of the two enzymes by NaCl. As such, *in vivo*, as *in vitro*, one might expect the K_d for NF1 to significantly lower than that for GAP_{344}. These studies illustrate the importance of controlling experimental conditions when comparing kinetic data from different laboratories.

CHAPTER EIGHT

THE INTERACTION OF SINGLE POINT MUTANTS OF $p21^{ras}$ WITH GAP PROTEINS.

"..... we must consider carefully whether the proposed change (in sequence) will lead to properly interpretable results and to a better understanding of the catalytic mechanism. .... In short, we need to look at enzyme systems which are well characterised in structural, mechanistic and energetic terms. Only then shall we be in a position to evaluate the consequences of amino-acid replacement"

Raines, Straus, Gilbert, and Knowles (1986).

8.1 Introduction.

The experiments described thus far have concentrated on the GAP- and NF1-activated mechanism of the wild type $p21^{ras}$ protein GTPase activity. However, the interest in these proteins has been fuelled to a large extent by the observation that single point mutants of $p21^{ras}$ are found in up to 30 % of human malignancies (see sections 1.1 and 1.5). These mutations are typically found in a small number of "hot spots" at residues 12, 13, 59, and 61. In addition, the use of molecular biology techniques has led to the expression and purification of a wide range of mutant $p21^{ras}$ proteins, although few of these have subsequently been identified *in vivo*. Nevertheless, a number of these mutants have altered biological activities, notably with respect to their ability to transform or differentiate cells when cultured *in vitro*. The effect of the mutations that lead to an oncogenic phenotype is to increase the steady state level of GTP-bound $p21^{ras}$ in the cell. As discussed by Neal et al., (1988), the ratio of the [$p21^{ras}$.GDP] to the [$p21^{ras}$.GTP] is defined by the ratio of the *in vivo* values of the GTP

cleavage (k_{+2}) and GDP (k_{+4}) rate constants. Thus, transforming mutations either increase k_{+4} (e.g at Phe 28, Asp 116, Lys 117, Asp 119 or Thr 144) or, more commonly, reduce the *in vivo* rate of GTP hydrolysis (e.g at Gly12, Gly 13 , and Gln 61).

The aim of the experiments described in this chapter is to characterise a number of these mutants kinetically with respect to their interaction with guanine nucleotides and with the catalytic domains of p120-GAP and NF1. Of the $p21^{ras}$ mutants that have been studied in this thesis, emphasis will be placed here on the results obtained with four of them. Where relevant, the other mutants (Gly 12 → Asp or Val ; Gln 61 → Leu) will be mentioned briefly. The rate constants for the intrinsic and GAP-activated GTPase mechanisms of these additional mutants are given in Appendix 8.1. These studies have been complemented by the structural information that has been obtained for several point mutants of $p21^{H\text{-}ras}$ (Krengel et al., 1990). The techniques applied to the study of these mutant proteins are based on those used previously with wild type $p21^{ras}$. The catalytic activities of GAP_{344} and GAP_{365} have been compared since both are used in this chapter.

One problem associated with the use of these mutant proteins is that they have been obtained from different laboratories (see section 2.1) and as such are in different $p21^{ras}$ "backgrounds" (N-, K-, or H-ras). While the three $p21^{ras}$ gene products behave in a kinetically similar fashion, their properties are not identical. Where possible, the results of kinetic measurements on a particular mutant protein have therefore been compared to the wild type protein of the same background.

8.2 Comparison Between the Catalytic Activity of GAP_{344}, GAP_{365}, and NF1

The initial rate of mantGTP hydrolysis by wild type $p21^{N\text{-}ras}$ was determined as described in Figure 5.8 with catalytic concentrations of GAP_{365}, GAP_{344}, and NF1. All protein concentrations were standardised using the predicted extinction coefficient at 276 nm (section 2.3.4) which gave initial rates of 0.42 s^{-1} for GAP_{344}, 0.032 s^{-1} for GAP_{365}, and 5.6 s^{-1} for NF1. Thus, under these conditions, GAP_{344} is 13-fold more active than GAP_{365}, whilst NF1 is some 13-fold more active compared to GAP_{344}. The differing activities of these proteins will

reflect not only changes in K_m and V_{max}, but also the molar concentration of active protein. In addition, whilst GAP_{344} and NF1 can be readily prepared ≈ 99 % pure, GAP_{365} preparations typically contain 10 - 20 % protein impurity.

8.3 Interaction of the Phe 28 → Trp Mutant of Truncated Ki-ras with Guanine Nucleotides and GAP.

The aromatic interaction of Phe 28 with the guanine base of GTP and GDP (Pai et al., 1990) may be at least partly responsible for the very high affinity ($K_d << 10^{-9}$ M) with which $p21^{ras}$ binds GTP and GDP. Indeed, a Phe 28 → Leu mutant, where this aromatic interaction is lost, has a 30 - 150 fold faster GDP dissociation rate than wild type $p21^{ras}$ (Schlichting et al., 1988 ; Reinstein et al., 1991 ; Mistou et al., 1992). The Phe 28 → Trp mutant was studied in order to determine the relative importance of the residue at this ~~codon~~ position for the binding affinity of guanine nucleotides.

The uncorrected fluorescence intensity and polarisation excitation spectra of wild type and Trp 28 $p21^{Ki\text{-}ras}$ mantGDP complexes clearly demonstrated that energy transfer occurs between Trp 28 and the mant-fluorophore (see chapter 6). The mutation is, however, unlikely to affect the local motion of the mant-fluorophore situated near to Tyr 32 since the anisotropy at > 340 nm is identical between wild type and mutant proteins. The hydrolysis of mantGTP by Trp 28 $p21^{Ki\text{-}ras}$ is associated with an 8 - 10 % reduction energy transfer compared to the mantGTP complex, although there is no change in intensity at 366 nm. The rate of the fluorescence change at 285 nm occurring after the addition of GAP_{365} to the Trp 28 $p21^{Ki\text{-}ras}$.mantGTP complex is identical to the rate of mantGTP cleavage determined by ion exchange H.P.L.C. The initial rate of GAP_{344}-activated mantGTP hydrolysis (under the conditions used in section 8.2) was estimated to be 0.47 (± 0.08) s^{-1} for wild type $p21^{Ki\text{-}ras}$ and 0.35 (± 0.07) s^{-1} for the Trp 28 mutant.

The rate constants for the intrinsic triphosphate hydrolysis and diphosphate dissociation reactions of the wild type and mutant proteins are summarised in Table 8.1. The Phe 28 → Trp mutation produces only a limited (< 4-fold) change in reduction in any of the rate con-

Table 8.1 Kinetic Constants for the Wild Type (Phe 28) and Trp 28 $p21^{Ki\text{-}ras}$.GTPase Activities.

Protein	Rate Constant (x 10^{-4} s^{-1})			
	GTP Cleavage		GDP Dissociation	
	GTP	MantGTP	GTP	mantGTP
Wild Type	1.8[a]	0.83	1.6[a]	0.53
Phe 28 → Trp	0.81	1.2	3.0	5.0

Note:

All reactions were performed in buffer B as described in section 2.9 except for (a) which were performed at 37°C.

stants measured for either GTP or mantGTP. Thus, unlike the Leu 28 mutant, the mantGDP and GDP dissociation is only marginally faster than that of the wild type protein. If the increase in GDP dissociation rate reflects a corresponding decrease in binding affinity, as proposed by Reinstein et al., (1991), this implies that the Trp 28 mutant binds GDP with an affinity similar to that of the wild type protein. Thus, the maintenance of the aromatic side chain at this position preserves the high affinity for guanine nucleotides.

A consequence of these results is that *in vivo*, the ratio of the GTP cleavage rate (k_{+2}) to the GDP dissociation rate (k_{+4}) where $k_{+2} / k_{+4} = [p21^{ras}.GDP] / [p21^{ras}.GTP]$, would be expected to be similar to that of wild type $p21^{ras}$. Confirmatory evidence for this suggestion comes from the results of DNA transfection assays with Trp 28 $p21^{ras}$ into NIH 3T3 cells (Guiterrez et al., 1989) which demonstrate that this mutant is normally active but non-transforming. Thus, a 3-4 fold increase in $[p21^{ras}.GTP]/[p21^{ras}.GDP]$ is insufficient to lead to an oncogenic phenotype. In contrast, the Leu 28 mutant induces neurite differentiation in PC 12 cells, (equivalent to transformation of NIH 3T3 cells) since the rate of GDP dissociation is sufficiently fast for this mutant to exist significantly in the GTP-bound form.

8.4 Interaction of the Gly 12 → Pro $p21^{Ki\text{-}ras}$ Mutant with GAP and NF1.

The Gly 12 → Pro mutation is unusual in that the resulting mutant protein is only weakly oncogenic compared to all other codon 12 mutants (Seeburg et al., 1984 ; Ricketts and Levinson, 1988). To investigate the possible kinetic explanations of this phenomenon, the interaction of Pro 12 $p21^{ras}$ with GAP_{344} and NF1 has been investigated.

8.4.1 *Intrinsic Pro 12 mantGTPase Mechanism.*

The intrinsic mantGTP hydrolysis reaction of truncated wild type $p21^{Ki\text{-}ras}$ (residues 1 - 166) is associated with a *single exponential* decrease in fluorescence intensity of 11.3 % occurring with a rate constant of 0.83×10^{-4} s^{-1} at 30°C (Figure 8.1.a). Thus, for this protein, no evidence of the fast phase of the fluorescence change was observed even though the experiments were initiated as rapidly as with $p21^{N\text{-}ras}$.mantGTP (within ≈ 1 min). With the Pro 12 mutant, a similar single exponential decrease in fluorescence intensity occurs (k_{obs} = 1.6 x

Figure 8.1 : Fluorescence Changes Associated with the Hydrolysis of mantGTP by Truncated (residues 1 - 166) Wild Type and Pro 12 $p21^{Ki\text{-}ras}$.

Panel A: 15 μM wild type $p21^{Ki\text{-}ras}$ was incubated at 30°C in buffer B. The sample was warmed from storage on ice to 30°C in 1 min. The fluorescence intensity (excitation = 366 nm ; emission through a KV399 filter) was monitored with time. The solid line is a best fit to an exponential with a rate constant of 0.83×10^{-4} s^{-1} and an amplitude of 11.5 %. The rate of mantGTP cleavage determined by ion exchange H.P.L.C (0.83×10^{-4} s^{-1}) was identical to the rate of the fluorescence change.

Panel B: As for (A) except that the Gly 12 → Pro mutant was used. The solid line is the best fit to a single exponential with a rate constant of 1.6×10^{-4} s^{-1} and an amplitude of 10.3 %. The rate of mantGTP cleavage determined by ion exchange H.P.L.C under the same conditions was 1.7×10^{-4} s^{-1}.

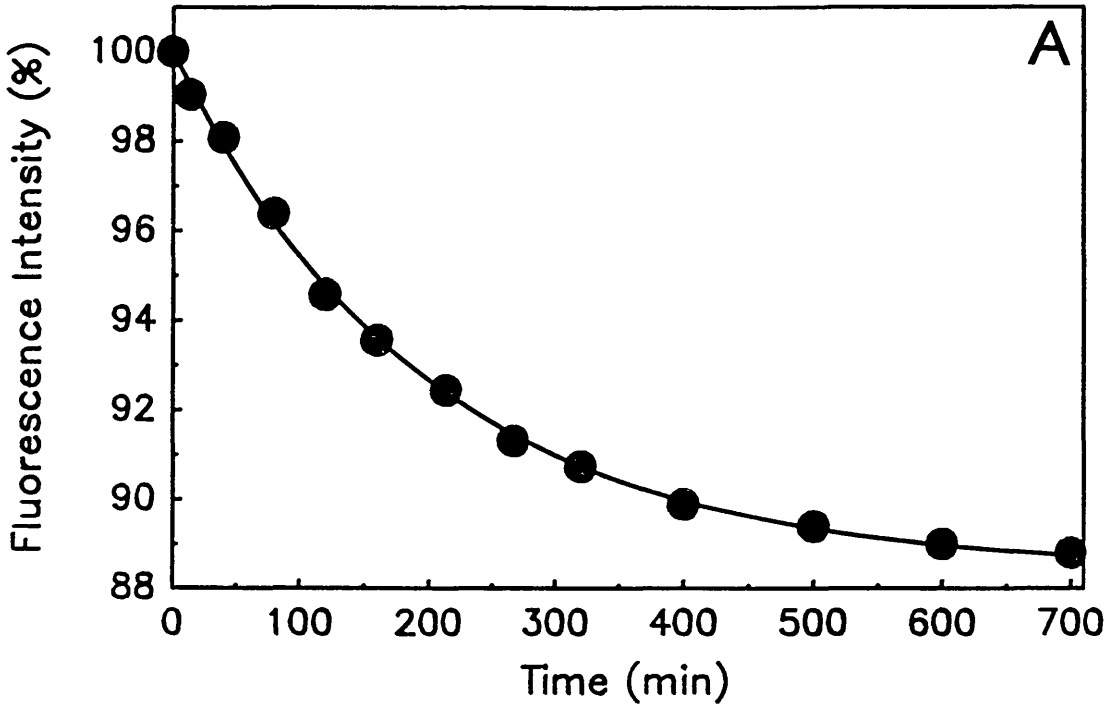
A
Fluorescence Intensity (%)
100
98
96
94
92
90
88
0
100
200
300
400
500
600
700
Time (min)

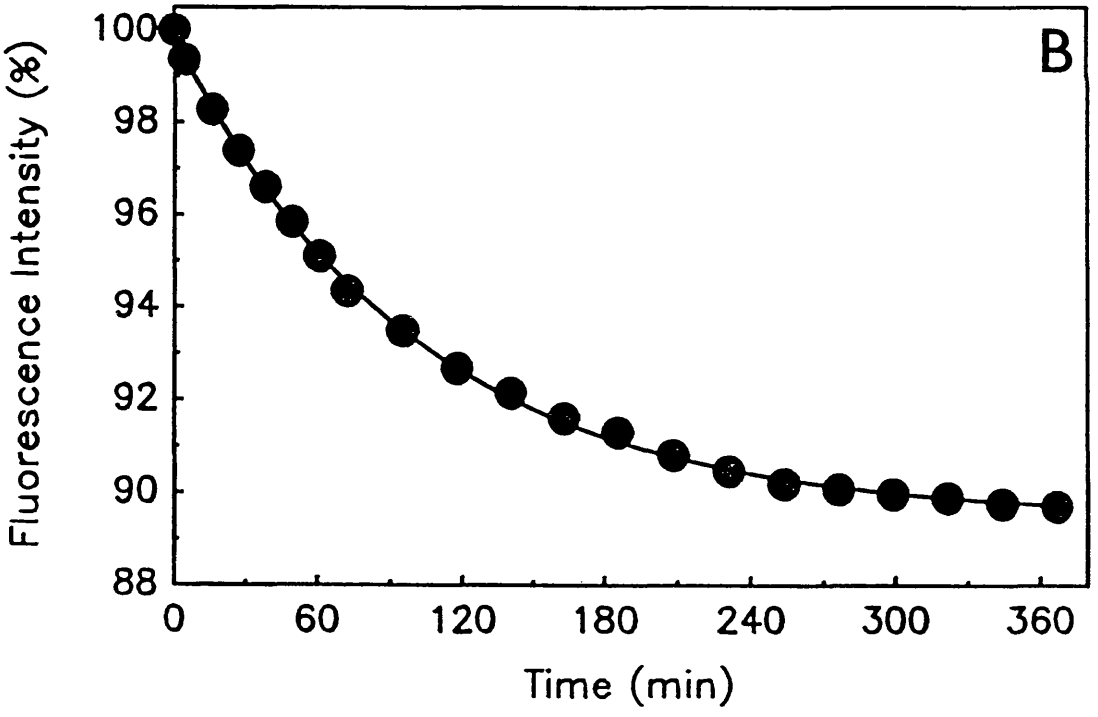
B
Fluorescence Intensity (%)
100
98
96
94
92
90
88
0
60
120
180
240
300
360
Time (min)

10^{-4} s^{-1}, amplitude = 10.3 %, Figure 8.1.b) with the same rate constant as that of the chemical cleavage of mantGTP (1.7 x 10^{-4} s^{-1}). Gel filtration controls indicated < 1 % free nucleotide at the end of the fluorescence change. Thus, the Pro 12 mutant undergoes the same conformational change identified in the wild type Ki-ras protein. The intrinsic rates of mantGTP (1.7 x $10^{-4}s^{-1}$) and GTP (2.2 x 10^{-4} s^{-1}) hydrolysis for the Pro 12 mutant are ≈ 2-fold faster than that of the wild type protein (0.83 x 10^{-4} s^{-1} for mantGTP and 1.2 x 10^{-4} s^{-1} for GTP).

The absence of the fast phase of the fluorescence change (which was observed previously with $p21^{N\text{-}ras}$.mantGTP, chapter 4) in these experiments may be related to the truncation of the $p21^{Ki\text{-}ras}$ proteins at the COOH-terminus (containing residues 1 - 166). To investigate this possibility, the nature of the fluorescence changes associated with the hydrolysis of mantGTP by full length (residues 1 - 186) and truncated (residues 1 - 166) $p21^{H\text{-}ras}$ were investigated. However, for both H-ras proteins, biphasic descreases in fluorescence were observed, although the amplitude of the fast phase (≈ 2.5 %) was smaller than observed with $p21^{N\text{-}ras}$.mantGTP (≈ 4- 5 %). The second slow phase with the H-ras proteins was accelerated by GAP_{365} to a similar extent as observed for the N-ras and Ki-ras $p21^{ras}$.mantGTP complexes under identical conditions. This result suggests that the absence of the fast phase of the fluorescence change with the truncated Ki-ras proteins was not due to the removal of the COOH-terminal 20 amino acids. Rather, the single exponential behaviour appears to be a property of the Ki-ras gene products. Either the fast phase of the fluorescence change is absent with $p21^{Ki\text{-}ras}$ or it occurs too rapidly to measure using these techniques.

8.4.2 *GAP-Activated Pro 12 mantGTPase Mechanism.*

An extension of these studies is to determine if the intrinsic mantGTP cleavage rate is stimulated by GAP since this may provide an explanation for the low oncogenicity of this mutant. The addition of 30 μM GAP_{344} to a solution of 15 μM Pro 12 $p21^{Ki\text{-}ras}$ in buffer B lead to an increase in the first order rate of the fluorescence change (8.69 $\pm$ 0.29 x 10^{-4} s^{-1}) and of the chemical cleavage rate of mantGTP (8.81 $\pm$ 0.14 x 10^{-4} s^{-1}). This concentration of GAP_{344} in buffer B therefore leads to a 5-fold stimulation of the intrinsic rate of mantGTP hydrolysis.

From the results presented above for wild type $p21^{Ki\text{-}ras}$ under these conditions, one can estimate that the observed stimulation with the Pro 12 mutant is some three orders of magnitude lower than for the wild type protein. This value was determined with more accuracy by performing the fluorescence experiments over a range of GAP_{344} concentrations, although in these experiments the ionic strength of the buffer was reduced (25 mM TrisHCl, pH 7.5, 50 mM NaCl, 5 mM $MgCl_2$, 5 mM DTT) since this increases the affinity of $p21^{ras}$ for GAP_{344} (chapter 7). The rate of the fluorescence change was found to vary linearly with GAP_{344} concentration where the initial rate of the fluorescence change (1.2×10^{-3} $\mu M\ s^{-1}$ μM^{-1} GAP_{344}) is 1100-fold lower than observed with wild type $p21^{ras}$ under these conditions of reduced ionic strength ($1.33\ \mu M\ s^{-1}\ \mu M^{-1}\ GAP_{344}$).

The lower activation of the Pro 12 mutant by GAP could be due to either a change in the binding affinity, or a change in the maximally activated rate of hydrolysis, or both. To investigate these possibilities, the rate of the fluorescence change with Pro 12 $p21^{ras}$.mantGTP was determined using conditions where $[GAP_{344}] >> [p21^{ras}.mantGTP]$. These experiments are therefore analogous to the stopped flow experiments described in chapter 5 with wild type $p21^{N\text{-}ras}$.mantGTP. In order to compare results directly, the ionic strength and temperature of these experiments were the same as described in chapter 5 (buffer C, 30°C). Even under these conditions of low ionic strength and high $[GAP_{344}]$, the reactions were sufficiently slow to be performed using manual mixing techniques. Three representative fluorescence changes are shown in Figure 8.2.a where 1 μM Pro 12 $p21^{Ki\text{-}ras}$.mantGTP was mixed with 6 - 60 μM GAP_{344} in buffer C at 30°C. The value of the fluorescence intensity immediately after the addition of GAP_{344} is defined as 100 % relative fluorescence. These reaction traces are qualitatively similar to those observed with wild type $p21^{N\text{-}ras}$.mantGTP in the stopped flow experiments (see Figure 5.1). Thus, both the rate and amplitude of the fluorescence change increased with increasing GAP_{344} concentration. The dependence of the first order rate of the fluorescence change on GAP_{344} concentration is shown in Figure 8.2.b. The data could be fitted well to a hyperbola with a maximal rate of $19.0 \times 10^{-3}\ s^{-1}$ at saturating $[GAP_{344}]$ and an equilibrium dissociation constant of 24 μM. The rate when $[GAP_{344}] \rightarrow 0$ is $\approx 1 \times 10^{-3}\ s^{-1}$, although this value is subject to large errors ($\pm\ 0.5 \times 10^{-3}\ s^{-1}$). This rate would correspond to k_{-2} in scheme 5.2 i.e the reverse rate of the GAP-accelerated isomerisation reaction.

Figure 8.2 : Reaction of Pro 12 $p21^{Ki\text{-}ras}$.mantGTP with excess GAP_{344}.

Panel A: 1 μM Pro 12 $p21^{Ki\text{-}ras}$.mantGTP in buffer C at 30^{o}C was mixed with increasing concentrations of GAP_{344} and fluorescence intensity (excitation = 366 nm, emission through a KV399 filter) monitored with time. The fluorescence intensity immediately after mixing is defined as 100 % relative fluorescence. Three representative traces are shown in the Figure, corresponding to 6, 20 and 60 μM GAP_{344}, all of which could be fitted by single exponential decays. All of the reactions were performed over a sufficient period of time to define the end points of the reactions (typically $\geq$ 5 half times), and the data is plotted on this scale solely for clarity.

Panel B: The observed rate of the fluorescence change (k_{obs}) from experiments such as those described in Panel A is plotted as a function of the final GAP_{344} concentration. The solid line is a best fit of the data to a hyperbola. Assuming a similar mechanism to that shown in equation 5.1 for wild type $p21^{N\text{-}ras}$, the hyperbolic fit gives a K_d of 24 μM, the maximal rate of the fluorescence change ($k_{+2} + k_{-2}$ in equation 5.2) of 19 x 10^{-3} s^{-1} and an intercept (k_{-2}) of 1 x 10^{-3} s^{-1}.

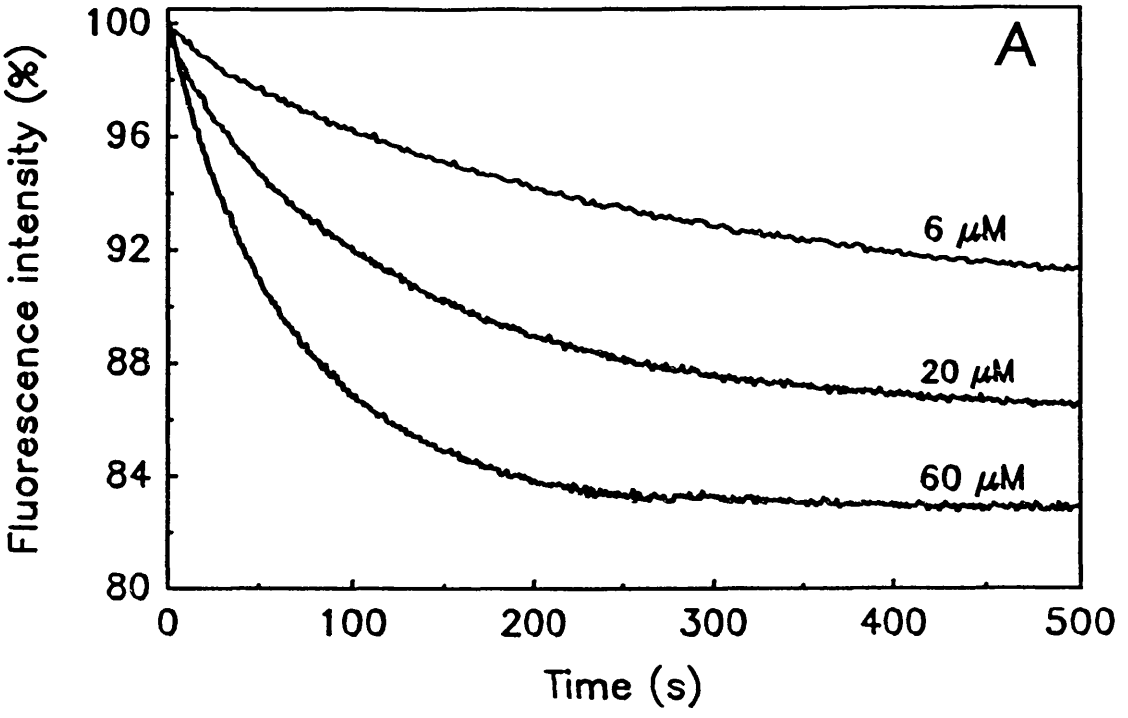
A
Fluorescence intensity (%)
100
96
92
88
84
80
0
100
200
300
400
500
Time (s)
6 μM
20 μM
60 μM

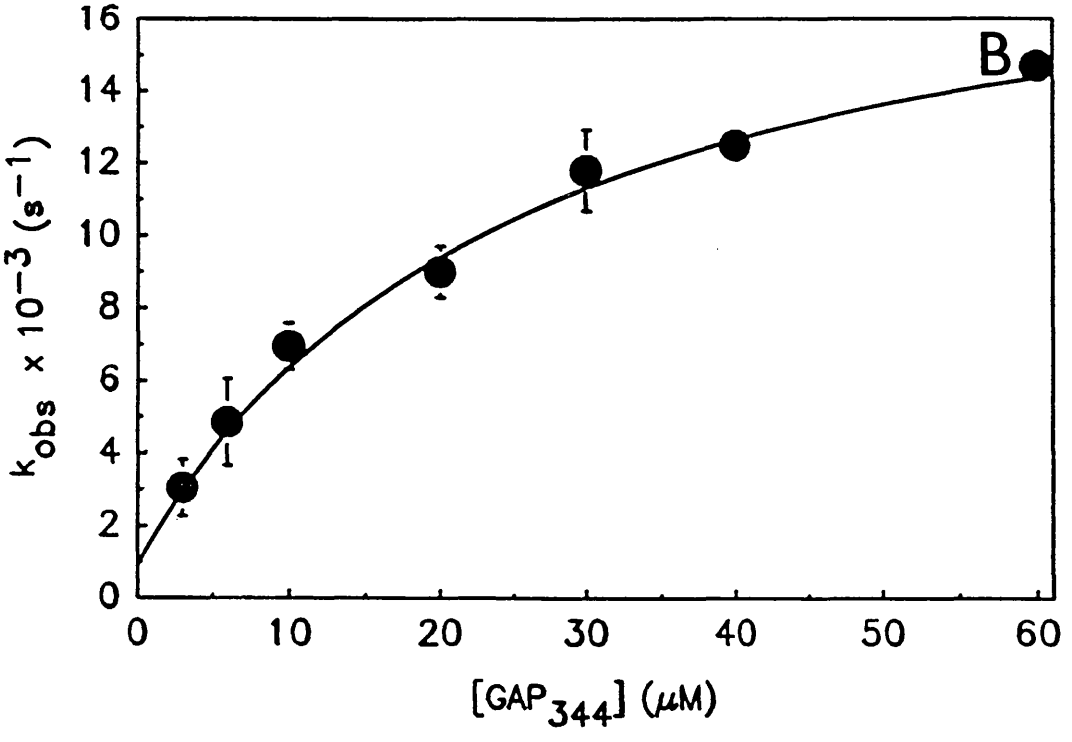
B
k_{obs} x 10^{-3} (s^{-1})
16
14
12
10
8
6
4
2
0
0
10
20
30
40
50
60
[GAP_{344}] (μM)

Thus, the maximal rate of the fluorescence change is 750-fold lower than with wild type $p21^{N\text{-}ras}$ and the equilibrium dissociation constant is increased by 1.4-fold. This data is consistent with the reduced activity of the Pro 12 mutant determined from the multiple turnover studies described above.

8.4.3 *NF1-Activated Pro 12 mantGTPase Mechanism.*

Similar experiments to those described immediately above for GAP_{344} have been performed with the catalytic domain of NF1. Preliminary experiments however demonstrated that the activation of the intrinsic rate of the fluorescence change with NF1 was significantly greater than with GAP_{344}. Thus, mixing 1 μM Pro 12 $p21^{Ki\text{-}ras}$.mantGTP in buffer C at 30°C with 1 μM NF1 lead to a reduction in fluorescence intensity of $\approx$ 13 % occurring with a first order rate constant of 0.035 s^{-1} (Figure 8.3.a). As the concentration of NF1 was increased, these reactions became too fast to measure accurately by manual mixing techniques, and therefore mixing was achieved in a stopped flow apparatus. The decrease in fluorescence intensity observed after rapidly mixing 1 μM Pro 12 $p21^{Ki\text{-}ras}$.mantGTP with 7 μM NF1 could be fitted to a single exponential decay in fluorescence intensity of 9.2 x 10^{-2} s^{-1} with an amplitude of 19.1 %. Neither the rate nor the amplitude of the fluorescence changes were dependent on [NF1] over the range 4 - 12 μM suggesting that the equilibrium constant for the formation of the ternary complex is $\leq$ 2 μM. These experiments therefore demonstrate that the maximal rate of the fluorescence change with NF1 (9 $\pm$ 0.3 x 10^{-2} s^{-1}) is $\approx$ 70-fold lower than the equivalent rate with wild type $p21^{N\text{-}ras}$.mantGTP (6 - 7 s^{-1}).

In order to determine the equilibrium dissociation constant for NF1 with Pro 12 $p21^{Ki\text{-}ras}$ more accurately, the change in steady state anisotropy of the Pro 12 $p21^{Ki\text{-}ras}$.mantGppNHp complex was determined as a function of the [NF1] (chapter 6, Figure 8.3.b). The starting anisotropy was lower than that of full length *N-ras* or *H-ras* complexes, presumably due to the removal of the C-terminal 20 amino acids in *Ki-ras*. However, the increase in anisotropy (0.086) and the calculated equilibrium dissociation constant (1.0 ($\pm$ 0.1) μM) are not significantly different from the equivalent values obtained with wild type $p21^{N\text{-}ras}$.mantGppNHp (K_d = 0.8 $\pm$ 0.1 μM, and change in anisotropy = 0.082).

Figure 8.3 : Interaction of Pro 12 $p21^{Ki\text{-}ras}$ with NF1.

Panel A: The reaction of 1 μM Pro 12 $p21^{Ki\text{-}ras}$.mantGTP with 1 μM NF1. The reaction was performed exactly as for Figure 8.2.a except that 1 μM NF1 was used. The data could be fitted to a single exponential decrease in fluorescence intensity of 13 % occurring with a rate constant of 0.035 s^{-1}. The rate of the fluorescence change observed with higher concentrations of NF1 was determined by stopped flow techniques and saturated at 0.09 s^{-1} as described in the text.

Panel B: Binding of NF1 to Pro 12 $p21^{Ki\text{-}ras}$.mantGppNHp followed by fluorescence anisotropy. Titrations were performed using 1 μM Pro 12 $p21^{Ki\text{-}ras}$ .mantGppNHp in buffer C at 30^{o}C with excitation at 366 nm. Fluorescence emission was observed through a KV399 filter. The solid line is the best fit to a modified hyperbola (Appendix 6.1) yielding an equilibrium constant of 1.0 ($\pm$0.1) μM and a change in anisotropy of 0.082.

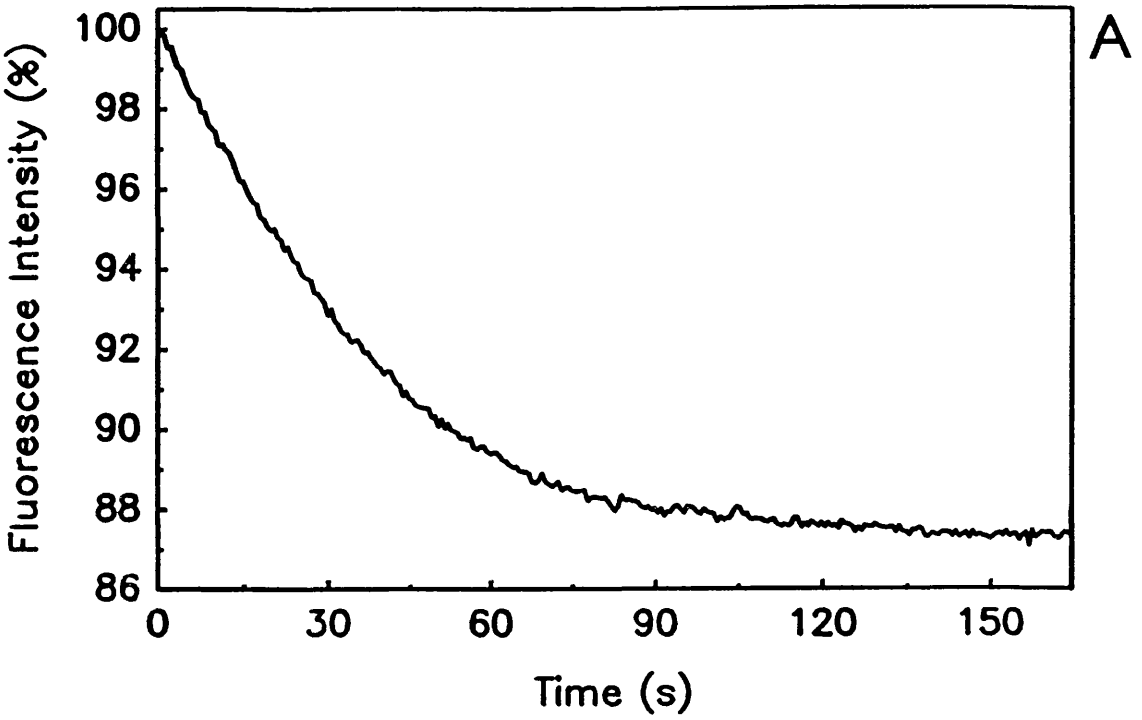
A
Fluorescence Intensity (%)
100
98
96
94
92
90
88
86
0
30
60
90
120
150
Time (s)

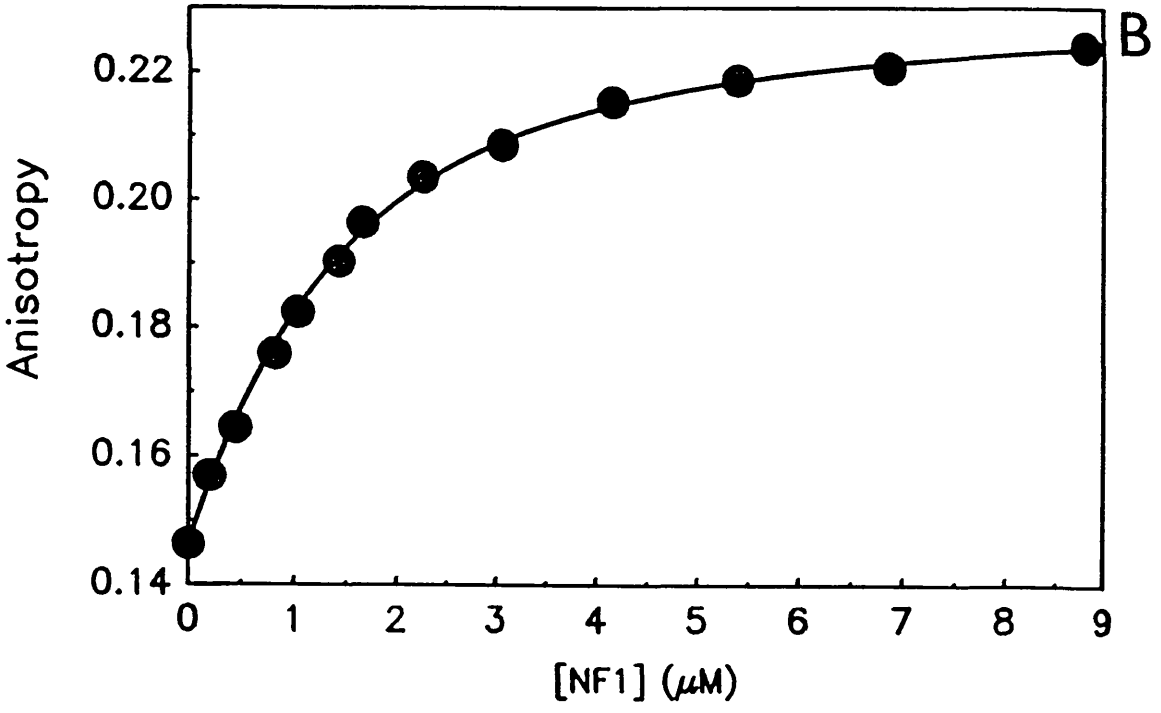
B
Anisotropy
0.22
0.20
0.18
0.16
0.14
0
1
2
3
4
5
6
7
8
9
[NF1] (μM)

Finally, the ionic strength dependence of the NF1 : Pro 12 $p21^{ras}$ interaction was investigated. The addition of NaCl into a solution of 1 μM Pro 12 $p21^{ras}$.mantGppNHp and 1 μM NF1, lead to a reduction in the observed anisotropy (from 0.180 to 0.145) with an IC_{50} of 50 ($\pm$ 9) mM NaCl. This value corresponds to a K_I (chapter 7) of $\approx$ 20 mM NaCl, which is not significantly different from the K_I values obtained for wild type $p21^{N\text{-}ras}$.

8.4.4 *Discussion*

The substitution of Pro for Gly at position 12 in $p21^{ras}$ is unusual in that this mutant is only weakly oncogenic compared to all other codon 12 mutants (Seeburg et al., 1984). All mutations at position 12 that have been tested have a GTPase activity which has been reported to be insensitive to stimulation by GAP (Gibbs et al., 1988). The lack of the strong transforming effect of the Pro 12 ras gene was attributed to the two-fold elevation of the intrinsic rate of GTP hydrolysis compared to wild type $p21^{ras}$. If the intrinsic rate of hydrolysis is important for Pro 12, then it is possible that the effect of GAP on the $p21^{ras}$.GTP / $p21^{ras}$.GDP ratio of the wild type protein might not be as large as expected, and that its intrinsic rate of GTP hydrolysis may be significant. No data on the activation of Pro 12 by NF1 has been published. However, in some cells, NF1 appears to be the main regulatory protein for $p21^{ras}$. Thus, it seemed important to establish how NF1 interacts with Pro 12, and whether it differs compared to GAP. Since techniques were available for measuring the affinity of GAPs for $p21^{ras}$, and the maximal activation of the intrinsic GTP cleavage rate, the interaction between Pro 12 and GAP and NF1 was examined in more detail.

The results of these experiments have demonstrated that the Pro 12 mutant undergoes the same conformational change during the intrinsic , GAP_{344}, and NF1-activated mantGTP hydrolysis reactions as observed in the wild type protein. In contrast, the mantGTP complexes of three oncogenic mutants (Gly 12 → Asp, Gly 12 → Val, and Gln 61 → Leu) show no fluorescence change which correlates with the rate of mantGTP cleavage (data not shown). For these proteins, only the fast phase of the fluorescence change is observed. Several other $p21^{ras}$ mutants will need to be studied before one is able to determine whether or not it is significant that the weakly oncogenic Pro 12 mutant shows the same fluorescence change

observed for wild type $p21^{ras}$ and which is absent with oncogenic mutants.

The equilibrium parameters (K_d and salt sensitivity) that define the interaction of Pro 12 $p21^{Ki\text{-}ras}$ with GAP_{344} and NF1 are not significantly altered by the Gly 12 → Pro mutation. The rates of GDP dissociation from $p21^{ras}$.GDP complexes of wild type and Pro 12 were very similar (P.Lowe, pers. comm, and see Mistou et al., 1992). Furthermore, the SDC25 exchange factor increased the rate of nucleotide exchange with Pro 12 and Gly 12 proteins equally (Mistou et al., 1992). Assuming that any other exchange factor also interacts equally well with both proteins, the surprisingly weak oncogenic activity of the Pro 12 mutant cannot be attributed to a decreased GDP dissociation rate.

The only significant effect that this mutation has on the interaction of the $p21^{ras}$ protein with NF1 and GAP_{344} is that the maximally activated rate of hydrolysis is reduced by a factor of 1000-fold for GAP_{344} and 70-fold for NF1. There is at present no reasonable explanation for the very low activation of the intrinsic mantGTP hydrolysis rate of this mutant given the observation that during the intrinsic mantGTP cleavage reaction this mutant undergoes the same conformational change identified in the wild type protein. Furthermore, the X-ray structure of Pro 12 shows that the region around the gamma-phosphate of GTP is very similar to that of the normal protein. In particular, the conformational change of loop 4 (residues 60 - 65) that has been postulated to be required to reach the catalytically active constellation of these residues (Pai et al., 1990) is unaffected by the mutation (Wittinghofer and Pai, 1991).

One explanation for the catalytic impairment of the Pro 12 mutant might be that the increased size of the Pro 12 residue reduces the ability of GAP to *promote* the rate limiting isomerisation reaction. According to this argument, the mutation would not affect the intrinsic rate of isomerisation of the $p21^{ras}$.GTP complex, rather it would reduce the ability of GAP to accelerate this process. The other extreme case is that the Pro 12 mutation prevents the correct orientation of catalytic residues donated from GAP which *directly* promote the hydrolysis of GTP. However based on the results of chapter 4, potential catalytic residues donated by GAP would only accelerate the rate of the cleavage step occurring after the

isomerisation reaction. Either interpretation must account for the observation that GAP_{344} accelerates the GTP cleavage rate of the wild type protein to a 2-fold greater extent than NF1 whilst with Pro 12, NF1 is 5-fold more active than GAP_{344} (based on V_{max} values).

On the basis of this data, it might be expected that the Pro 12 mutant would be barely activated by either GAP or NF1 *in vivo* ($\approx$ 1 % activation by NF1 compared to wild type $p21^{ras}$) and hence would behave similarly to other codon 12 mutants. If the Pro 12 mutant is less salt sensitive than wild type $p21^{ras}$ this would increase the *in vivo* rate of GAP stimulated GTP hydrolysis. However, with Pro 12, ionic strength was found to reduce the extent of ternary complex formation with GAP_{344} to a similar extent as for wild type $p21^{ras}$ (K_I = 20 mM NaCl).

The data presented in this chapter suggest that within the cell, the ability of GAP or NF1 to activate the GTP hydrolysis rate might be much lower than measured under *in vitro* conditions of low ionic strength. This provides the basis for one explanation as to why the Pro 12 mutation is so weakly oncogenic. If cellular GAPs only have a modest effect *in vivo*, then the higher intrinsic GTP hydrolysis rate of Pro 12 might be sufficient to maintain the protein in a relatively high proportion of the GDP bound form. The ability of GAPs to activate the normal protein would more than compensate for the lower intrinsic GTPase activity of the wild type protein so that a still higher proportion would be in the GDP bound form. This would explain why the Pro 12 mutant is slightly more transforming than the wild type protein, but considerably less transforming than the Val 12 mutant whose intrinsic GTPase rate is 10-fold lower than wild type $p21^{ras}$ and also insensitive to GAP or NF1. A Gly 13 → Ser mutant, which is reported not to be oncogenic (Barbacid, 1987), has an $\approx$ 80-fold lower GAP-activated GTPase rate (Gideon et al., 1992). Interestingly, this mutant has a slightly *higher* intrinsic GTPase activity than the wild type protein. Therefore, the kinetic and biological properties of this mutant are similar to those of Pro 12, and a similar explanation may be afforded for the low oncogenicity of this mutant although its interactions with NF1 have not been reported.

A consequence of this interpretation of the Pro 12 data is that to maintain the protein predominately in the GDP-bound form, the *in vivo* exchange rate must not be significantly higher than the Pro 12 *intrinsic* GTPase rate because neither GAP nor NF1 dramatically accelerate this reaction. Since exchange factors for $p21^{ras}$ may have similar activities with both Pro 12 and wild type proteins, one might speculate that the basal exchange rate for normal $p21^{ras}$ in unstimulated cells must also be similar. This argument only applies to within those cells which were used for measuring the transforming ability of Pro 12. In other cells, e.g activated T-lymphocytes or mitogen-activated cells, the exchange rate might be much greater.

Ideally, one would like to be able to place numerical values for these rate constants although this is dependent to some extent on the accuracy of the quantitative *in vivo* data. In unstimulated cell lines, the majority of $p21^{ras}$ ($\approx$ 90 - 95 %) exists in the GDP-bound state (Trahey and McCormick, 1987 ; Gibbs et al., 1990 ; Satoh et al., 1990) suggesting that the cleavage to exchange rate ratio is $\approx$ 10 - 20. This value is estimated by immunoprecipitation of $p21^{ras}$ from ^{32}P-labelled cells with the monoclonal antibody Y13-259. It is unknown how much the GTP / GDP ratio changes during the isolation of $p21^{ras}$ from broken cells. It would be of interest to determine what this ratio is for cell lines expressing the Pro 12 mutant, and as controls, also for the wild type, Leu 61 or Val 12 protein. An extension of these *in vivo* studies with Pro 12 would be to perform similar studies with a cell line which was deficient in either p120-GAP or NF1 (e.g Basu et al., 1992 ; DeClue et al., 1992). The combination of such *in vivo* studies with the *in vitro* experiments described here may provide additional information as to the mechanism of regulation of $p21^{ras}$ by GTPase activating proteins.

8.5 The Interaction of Thr 35 → Trp and Ile 36 → Trp Mutants of $p21^{H\text{-}ras}$ With Guanine Nucleotides, GAP_{344} and NF1.

The residues surrounding codons 35 and 36 in $p21^{ras}$ have been proposed to be involved in a number of biochemical and biological functions. Thus, residues 32 - 40 form the effector loop, which may also be the binding site for GAP and/or NF1. The threonine residue at position 35 is thought to form interactions with the Mg^{2+} ion bound at the active site of $p21^{ras}$ in the

triphosphate complex and has been proposed to participate in the mechanism of GTP hydrolysis (Pai et al., 1990). This residue may therefore be involved in the processes comprising three elements of the $p21^{ras}$ GTPase cycle: effector binding, Mg^{2+} co-ordination, and GTP hydrolysis.

8.3.1 *Intrinsic and GAP_{344} Activated Rates of mantGTP Cleavage.*

The rate constants for the intrinsic and GAP_{344} - activated mantGTP cleavage reactions with Trp 35 and Trp 36 are shown in Table 8.2. Both mutations has a relatively small effect on the intrinsic rate of mantGTP cleavage (4-fold lower for Trp 35 and 2-fold lower for Trp 36). The addition of GAP_{344} to a final concentration of 1 μM accelerated the rate of Trp 36 p21.mantGTP cleavage by 40 % whilst with Trp 35, no acceleration was detectable. Under these conditions (buffer C, 30°C) the rate of wild type $p21^{H\text{-}ras}$ mant GTP cleavage is estimated to be accelerated some 5000-fold.

8.3.2 *Preliminary Equilibrium Binding Studies of the Interaction of GAP_{344} and NF1 with Trp 36 $p21^{H\text{-}ras}$.*

Since the intrinsic mantGTP cleavae rate of the Trp 36 mutant was not significantly stimulated by GAP_{344}, the equilibrium constant for GAP_{344} could not be measured by stopped flow techniques (chapter 5). Consequently, equilibrium binding studies were initiated (chapter 6) which do not rely on the catalytic activity of either Trp 36 $p21^{ras}$, GAP_{344} or NF1. These preliminary studies have been only partially successful and future work will be required before one can quantitatively define the equilibrium dissociation constants for the binding of GAP_{344} and NF1 to this mutant with confidence.

Unfortunately, the large fluorescence intensity and anisotropy changes which occur on formation of the ternary complex of wild type $p21^{N\text{-}ras}$ with GAP_{344} (chapter 6) were not observed with the Ile 36 → Trp mutant. The starting anisotropy (0.14) of the mantGppNHp complex was similar to that of truncated Pro 12 $p21^{Ki\text{-}ras}$ but neither anisotropy or intensity were affected by addition of GAP_{344} or NF1. Control experiments with wild type $p21^{H\text{-}}$

Table 8.2 Rate Constants for the Intrinsic and GAP_{344} Activated $p21^{ras}$.mantGTPase Activity of Wild Type, Trp 35 and Trp 36 Truncated $p21^{H\text{-}ras}$.

Protein	Rate Constant ($\times 10^{-4} s^{-1}$)			
	GTP Cleavage		GTP Dissociation	GDP Dissociation
	- GAP	+ GAP	- GAP	- GAP
Wild Type[a]	0.88	$\approx$ 5000[b]	N.D	0.61
Thr 35 → Trp	0.37	0.37	1.6	1.5
Ile 36 → Trp	0.70	0.98	1.5	N.D

Notes:.

All reactions performed in buffer C at 30°C. Final $p21^{ras}$.mantGTP concentration was 15 μM and where indicated 1 μM GAP_{344} was added.

(a) Data for full length $p21^{H\text{-}ras}$. The mantGTP cleavage rate with truncated $p21^{H\text{-}ras}$ is 1.4 x 10^{-4} s^{-1} under these conditions.

(b) Estimated from the K_m and V_{max} values for $p21^{N\text{-}ras}$.mantGTP under these conditions (chapter 5). To a first approximation, both N-ras and H-ras are activated to the same extent by GAP_{344}.

^{ras}.mantGppNHp gave the expected increase in both fluorescence anisotropy and intensity using either GAP_{344} or NF1. In an attempt to overcome these problems, a competition experiment was performed where Trp 36 $p21^{H\text{-}ras}$.GppNHp was used to displace wild type $p21^{H\text{-}ras}$.mantGppNHp (1 μM) from a complex with GAP_{344} (15 μM). Sequential addition of Trp 36 $p21^{H\text{-}ras}$.GppNHp into this solution lead to the reduction in anisotropy shown in Figure 8.4.a. The data could be fitted to a hyperbola with an IC_{50} of 12 ($\pm$ 1) μM and an end point of 0.177. The equivalent experiment with NF1 (Figure 8.4.b) was performed under conditions where [wild type $p21^{H\text{-}ras}$.mantGppNHp] = 1 μM, [NF1] = 0.5 μM and [Trp 36 $p21^{H\text{-}ras}$.GppNHp] = 0 - 27 μM. The IC_{50} under these conditions was 38 ($\pm$ 14) μM and the estimated end point was 0.177.

8.5 *Discussion.*

Previous studies of the interaction of GAP with $p21^{ras}$ mutants which have alterations in effector loop (residues 32 - 40) indicated that these mutations destroy the stimulation of the intrinsic GTPase (Adari et al., 1988 ; Cales et al., 1988). The main chain carbonyl of Thr 35 hydrogen bonds to the water molecule at the active site (WAT 175 from Pai et al., 1990) which is thought to be involved in the in-line GTP hydrolysis reaction. The mutation of Thr 35 → Trp is likely to have only a limited effect on the conformation of the main chain at this position since only a minimal effect on the intrinsic rate of mantGTP hydrolysis (4-fold reduction) is observed. In the $p21^{ras}$.GTP complex, the side chain hydroxyl of Thr 35 is proposed to be one of the six ligands for the Mg^{2+} ion bound at the active site. Using the Phe 28 → Leu $p21^{ras}$.mantGppNHp complex (which shows an increase in fluorescence intensity on binding Mg^{2+}, Reinstein et al., 1991), the affinity of $p21^{H\text{-}ras}$.GTP for Mg^{2+} has been estimated to be 28 nM.

Preliminary results have been obtained performing similar experiments on the Trp 35 $p21^{ras}$.GTP complex, where the binding of Mg^{2+} is associated with a 15 % enhancement in intrinsic Trp fluorescence. The estimated value of the equilibrium constant from these titrations is $\approx$ 0.5 μM - some 20-fold higher than for the (Thr 35 Leu 28) mutant. These results are consistent with the crystal structure data discussed above which suggests an important

Figure 8.4: Binding of Trp 36 $p21^{H\text{-}ras}$.GppNHp to GAP_{344} and NF1 Using a Competition Fluorescence Anisotropy Procedure..

Panel A: 1 μM wild type (full length) $p21^{H\text{-}ras}$.mantGppNHp in buffer C at 30°C was mixed with 15 μM GAP_{344} and the fluorescence anisotropy measured (excitation = 366 nm , emission through a KV399 filter). Trp 35 $p21^{Ki\text{-}ras}$.GppNHp in the same buffer was added and the anisotropy re-determined. The concentration of $p21^{H\text{-}ras}$.mantGppNHp and GAP_{344} were maintained at 1 μM and 15 μM final concentrations respectively throughout the titration experiment. The solid line is the best fit of the anisotropy data to a hyperbola yielding a $K_{0.5}$ of 12 ($\pm$1) μM and an end point anisotropy of 0.177.

Panel B: As for panel A except that NF1 was used instead of GAP_{344} using a final [NF1] = 0.5 μM. The solid line is a best fit of the data to a hyperbola with a $K_{0.5}$ of 38 ($\pm$ 14) μM and an end point of 0.177.

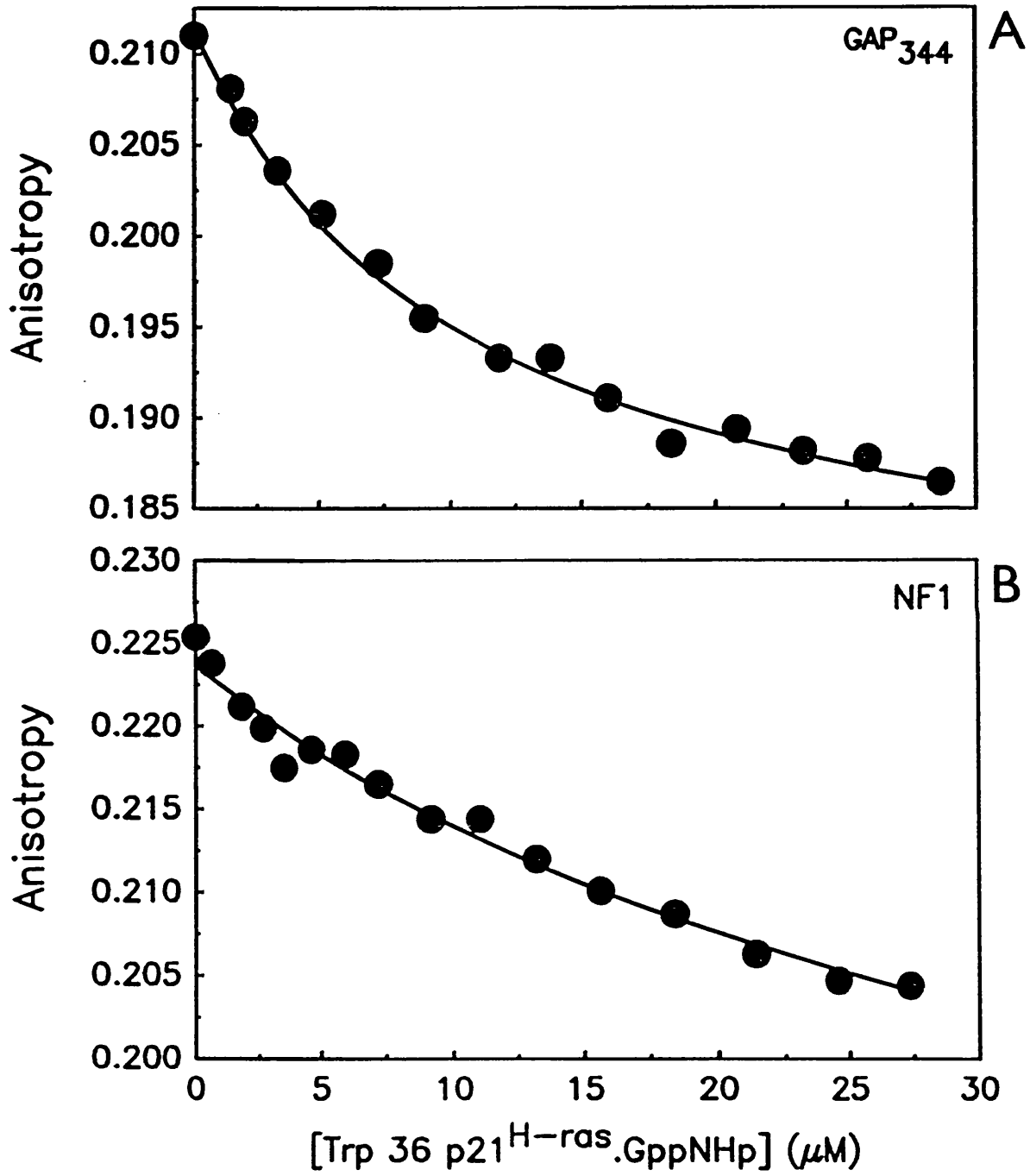
A
GAP344
Anisotropy
0.210
0.205
0.200
0.195
0.190
0.185
B
NF1
Anisotropy
0.230
0.225
0.220
0.215
0.210
0.205
0.200
0
5
10
15
20
25
30
[Trp 36 p21H−ras.GppNHp] (μM)

role for Thr 35 in the co-ordination of Mg^{2+} in these complexes. In future, these experiments could be extended to investigate the affinity of Mg^{2+} for the GDP complex, and for the di- and triphosphate complexes of (Thr 35 Trp 36). Furthermore, the binding of Mg^{2+} to the Trp 28 mutant of $p21^{Ki\text{-}ras}$ is associated with a 30 % reduction in protein fluorescence intensity.

The importance of the Trp 36 mutant of $p21^{H\text{-}ras}$ is that it may be useful to determine whether GAP or NF1 are the effectors of $p21^{ras}$. Since this mutant is inherently oncogenic, and does not negate the transforming ability of the Gln 61 → Leu mutation (C.J Der, pers. comm.), it must bind to the true effector. *In vitro* studies have therefore been performed to determine if either GAP or NF1 bind to this mutant protein. Stopped flow studies were unsuitable due to the low stimulation of the intrinsic GTPase activity whilst direct fluorescence anisotropy and intensity titrations were inconclusive. The competition experiments with wild type $p21^{H\text{-}ras}$.mantGppNHp were however more successful. These experiments demonstrate, qualitatively, that both GAP_{344} and NF1 bind to this mutant. Therefore, it is not possible to unambiguously reject the hypothesis that either of these proteins are the effector for $p21^{ras}$. The titration experiments can be analysed in terms of the Trp 36 $p21^{ras}$.GppNHp acting as a competitive inhibitor of wild type $p21^{ras}$.mantGppNHp. Based on the concentration of Trp 36 $p21^{ras}$.GppNHp required to reduce the anisotropy to 50 % of the initial value in the absence of inhibitor (the IC_{50} value), we can calculate a K_I (see chapter 7) for both GAP_{344} and NF1 of 7.5 ($\pm$ 2.5) μM. Thus, based on these preliminary results, GAP_{344} binds to the GppNHp complex of Trp 36 with an affinity comparable to (or slightly higher than) the wild type $p21^{ras}$.mantGppNHp complex (18 μM) whilst NF1 binds some 30-fold more weakly than to the wild type protein (0.25 μM). If these data are valid, then the results of these experiments would suggest that GAP is more likely to be the effector for $p21^{ras}$ than NF1 (at least in the cell line used for the biological assay for the Trp 36 mutant). Further studies, combining both equilibrium binding and kinetic approaches, will be required before one is able to be confident of this interpretation. In addition, it would be of interest to determine whether the Trp 35 mutant binds to GAP or NF1 since unlike wild type $p21^{H\text{-}ras}$, this mutant is not transforming even when over-expressed *in vivo*. In addition, the double mutant (Trp 35 Leu 61) $p21^{H\text{-}ras}$ is non-transforming, suggesting that this protein cannot bind the true effector (C.J Der, pers. comm.).

CHAPTER NINE

TIME RESOLVED FLUORESCENCE MEASUREMENTS OF $p21^{ras}$ COMPLEXED WITH FLUORESCENT GUANINE NUCLEOTIDE ANALOGUES.

"Ras proteins are monomeric while (classical) G proteins are trimeric"

Kaziro et al., (1991)

9.1 Introduction.

X-ray crystallography studies have provided an enormous amount of structural information concerning the tertiary structure of $p21^{ras}$ (section 1.4.1). However, the native structure may be, in part, constrained by the crystal lattice. In contrast, there is only a limited amount of experimental data concerning the quaternary structure of $p21^{ras}$ (section 1.4.2), and it has often been assumed to be monomeric (see above). It is the aim of the experiments described in this chapter to address this problem. Time resolved fluorescence measurements are particularly suited to evaluate the hydrodynamic properties of $p21^{ras}$ complexed with fluorescent guanine nucleotide analogues. The results of these experiments are compared to those obtained from analytical gel filtration studies.

An additional series of experiments were performed which address questions raised by the steady state fluorescence experiments described in the preceding chapters. Firstly, the fluorescence lifetimes of the individual 2' and 3' isomers of mantGDP were determined in an attempt to explain the observation that the fluorescence intensity of the 3' isomer is greater than that of the 2' isomer (chapter 4). Secondly, the change in lifetime of the $p21^{ras}$.mantGTP complex during the fast and slow phases of the fluorescence intensity change were

characterised in order to provide more information concerning the nature of the process giving rise to these processes.

Previous time resolved fluorescence studies of $p21^{N\text{-}ras}$ complexed with mant-nucleotides (Hazlett et al., 1990) were performed in collaboration with Drs Hazlett and Jameson (see below). The results of these experiments indicated an increase in lifetime (τ_L) of the mant-fluorophore upon binding to $p21^{ras}$, although there was only a 1 - 2 % difference in the life-times of the mantGTP and mantGDP complexes at 5^oC. This latter result was surprising given that the fluorescence intensity of the two complexes differs by 8 - 10 %. The rotational correlation time (τ_C) obtained at both 5^oC and 20^oC were however higher than the theoretical values predicted from the crystal structure dimensions of $p21^{ras}$ (section 1.4.2), and were nearer those for a dimeric structure.

9.2 Principles of Time Resolved Phase and Modulation Spectrofluorimetry.

Time resolved fluorescence measurements were made in the laboratory of, and in collaboration with Drs D.M Jameson (Dept. of Biochemistry and Biophysics, John A. Burns School of Medicine, University of Hawaii (!) at Manoa, Hawaii, USA) and T.L Hazlett (present address: Laboratory for Fluorescence Dynamics, Department of Physics, University of Illinois at Urbana-Champaign, Urbana, Illinois, USA). The measurement of fluorescence lifetimes and time resolved anisotropy decays was achieved using the harmonic response method (for reviews, see Jameson et al., 1984; Jameson and Hazlett, 1990). A brief discussion of the principle of the technique is given here, whilst the instrumental design and data analysis is given in Appendix 9.1. The excited light is sinusoidally modulated at high frequency (typically in the megahertz range) and consequently the fluorescence emission intensity is similarly modulated. However, due to the finite persistence of the excited state of the fluorophore, the emitted light is delayed by a phase angle, ϕ. In addition, the effective amplitude of the emitted sine function (the modulation, M, or AC/DC ratio) will be less than that of the exciting light - a process called demodulation. Using these two parameters (ϕ and M), the lifetime of the fluorophore can be calculated using a knowledge of the excitation frequency. To measure time resolved fluorescence anisotropy decays, the phase and modulation difference between

the parallel and perpendicular components of the emitted light are measured as a function of excitation frequency. In these experiments, the experimental parameters obtained (M and ϕ) were determined over a range of excitation frequencies. Under certain circumstances, the lifetime can be calculated from the data obtained at only one frequency. For anisotropy decays, a range of frequencies allows one to differentiate between the local motion of the fluorophore and the global motion of the protein as a whole.

9.3 Fluorescence Properties of the 2' and 3' Isomers of mantGDP.

Previous studies (chapter 4) indicated that the fluorescence intensity of the 3' isomer of mantGDP and mantGTP is $\approx$ 2-fold higher than that of the 2' isomer. Circular dichroism data (J.F.E & S.R Martin, unpublished results) suggest that the mant-fluorophore interacts with the guanine ring when on the 2' position but not on the 3' hydroxyl. This interaction may quench the fluorescence intensity, either by static or dynamic (collisional) mechanisms. These two possible mechanisms of quenching can be distinguished since the lifetimes of the 2' and 3' isomers will be identical for the case of static quenching whilst dynamic quenching will reduce the lifetime of the 2' isomer (formally equivalent to Stern-Volmer quenching, see Eftink and Ghiron, 1981).

Separation of the isomers of mantGDP was achieved by reverse phase H.P.L.C (section 2.5.1) on a Resolvex C18 column eluting isocratically with 100 mM potassium phosphate, pH 5.5, containing 8 % v/v acetonitrile. Each sample contained $\approx$ 5 - 10 % impurity of the other isomer. The fluorescence lifetime of each isomer was determined at 10^{o}C in the HPLC buffer immediately after purification and could be fitted to a single exponential decay (see Appendix 9). The results of these experiments indicated that the τ_L of the 3' isomer (5.25 ns) was 1.7-fold greater than the 2' isomer (3.08 ns). When these purified samples were left to equilibrate (overnight at room temperature, 28^{o}C), the τ_L for both samples was 4.1 ns. The change in fluorescence intensity occurring during the re-equilibration of these isomers (k_{obs} = 9 ($\pm$ 0.5) x 10^{-4} s^{-1} for either isomer at 37^{o}C) was also determined under the same buffer conditions. The fluorescence intensity changes (either 3' $\rightarrow$ equilibrium, or 2' $\rightarrow$ equilibrium) were consistent with the 3' : 2' fluorescence intensity ratio of 1.8. Since the difference in fluores-

cence intensity (1.8-fold) is similar to the difference in lifetime (1.7-fold), these results suggest that the quenching mechanism is not static in nature. For mant-nucleotides, the observed lifetime is likely to be dependent on more than one structural feature since the lifetime of (2'mant)-3'5'cyclic GMP under these conditions (4.7 ns) is nearer to that of 3'mantGDP rather than 2' mantGDP.

9.4 Lifetimes of $p21^{ras}$ Complexed with Fluorescent Nucleotide Analogues.

All of the fluorescence data were performed at 5 ^{o}C in 50 mM TrisHCl, pH 7.5, 100 mM NaCl, 10 mM $MgCl_2$, 10 mM DTT (buffer B) unless otherwise stated. The concentration of $p21^{ras}$ was 15 μM. A knowledge of the fluorescence lifetime is required before the anisotropy decays can be analysed since the rotational correlation time is related to the extent of depolarisation occurring during the lifetime of the excited state (chapter 6, and Appendix 9.1).

The observed values of ϕ and M vary sigmoidally with the $\log_{10}$ of the frequency (see below). Ideally, the complete curve would be defined using a wide range of frequencies. However, below 5 MHz, then the phase and modulation values are too low and too high (respectively) to be determined with accuracy. In contrast, above 100 - 150 MHz, the data generally become very noisy, although this is dependent to some extent on the performance of the instrument used, particularly with respect to the efficiency of the Pockels cells (see Appendix 9.1). However, the majority of the information which define the fluorescence lifetime is contained when ϕ = 20^{o} - 70^{o} and when M = 20 % - 70 %. Thus, it can be shown that for two fluorophores with significantly different (2-fold) lifetimes, then the values of ϕ and M outside the ranges defined above are essentially identical (within the limits of experimental error inherent in this technique).

9.4.1 *Changes In Fluorescence Lifetime of Nucleotides On Binding to $p21^{ras}$.*

The structures of the mant- and coumarin-derivative of guanine nucleotides are shown in Figure 9.1.a and b. Similar studies to those reported here have also been performed with the fluorescein-derivative of GDP (see section 9.7) whose structure is also shown (Figure 9.1.c)

Figure 9.1 Chemical Structures of the Nucleotide Analogues.

(a) mantGTP

(b) coumarinGTP

(c) fluoresceinGTP

A more detailed description of their synthesis and nomenclature is given in section 2.5.

A

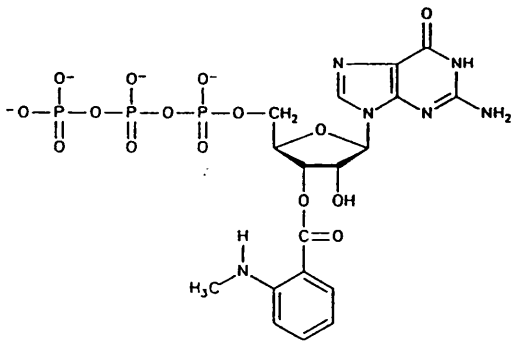

B

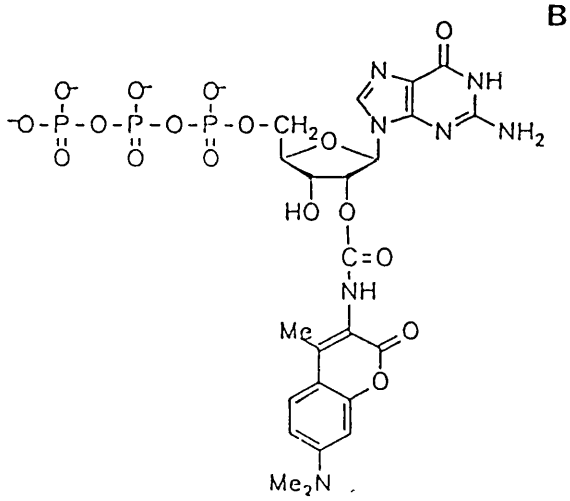

C

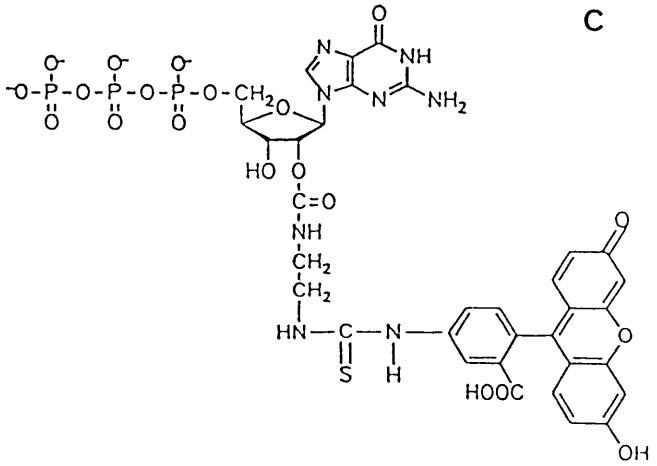

Representative phase and modulation data and the associated best fit curves using the equations described in Appendix 9.1 are shown in Figure 9.2. Figure 9.2.a shows the data for aqueous mantGDP whilst the data shown in Figure 9.2.b were obtained with the $p21^{N\text{-}ras}$.mantGDP complex. The increase in lifetime (4.0 ns for aqueous mantGDP compared to 9.1 ns for the $p21^{ras}$.mantGDP complex) shifts the change in phase and modulation to lower frequencies. For very short fluorescence lifetimes, such as those observed with aqueous coumarin-GDP at 20°C (2.5 ns), then frequencies of >> 100 MHz are required to define the complete phase and modulation curve (Figure 9.2.c). Fluorescence lifetimes for the free and bound fluorophores are given in Table 9.1. A scattering component, treated as 1 ps fluorescence lifetime, was routinely fixed in the analysis to correct for scattered light (Rayleigh or Raman) incompletely removed by the cut on filters used. For most experiments, this scattering component accounted for $\leq$ 2 % of the apparent fluorescence intensity.

For all of the $p21^{ras}$ proteins studied, the lifetime of the mant-fluorophore when bound to $p21^{ras}$ was higher than for the free nucleotide. For $p21^{N\text{-}ras}$, the increase in lifetime was $\approx$ 2.25 fold whilst for $p21^{H\text{-}ras}$ and $p21^{K\text{-}ras}$, a 2.1-fold increase was observed. Since there is no change in extinction coefficient of the mant-nucleotides on binding to $p21^{ras}$ (chapter 2), one would expect the increase in lifetime to parallel the increase in intensity (2.7-2.8 fold for all $p21^{ras}$ proteins). However, these latter experiments were performed at 30°C, and it is entirely possible that the fluorescence intensity of the mant-nucleotide complexed with $p21^{ras}$ shows a differing temperature sensitivity to the free probe (and see below). The lifetime of coumarin-GDP is slightly shorter than that of mantGDP, and does not change appreciably upon binding to $p21^{N\text{-}ras}$. This result is consistent with steady state fluorescence measurements which show only a 2 % increase in intensity upon complex formation.

9.4.2 *Changes In Fluorescence Lifetime Associated with the Hydrolysis of mantGTP..*

Since the intrinsic hydrolysis of mantGTP by $p21^{N\text{-}ras}$ is associated with a biphasic decrease in fluorescence intensity, it was of interest to determine whether a similar reduction in lifetime was observed. The wild type $p21^{N\text{-}ras}$.mantGTP complex was prepared by direct exchange (section 2.6) and rapidly warmed to 30°C by dilution into buffer B at the final work-

Table 9.1 Fluorescence Lifetimes and Rotational Correlation Times of mant- and coumarin-Nucleotide Analogues Complexed to $p21^{ras}$.

Nucleotides Analogue	Lifetime (ns)	Correlation time (ns)
At 5°C:		
$mantGDP_{(aq)}$	4.0	0.4[a]
$p21^{N\text{-}ras}$.mantGDP	9.1	28
$p21^{N\text{-}ras}$.mantGTP	9.2	27
Val 12 $p21^{N\text{-}ras}$.mantGDP	9.0	27
Val 12 $p21^{N\text{-}ras}$.mantGTP	9.0	28
$p21^{H\text{-}ras}$.mantGDP	8.4	26
$p21^{Ki\text{-}ras}$.mantGDP	8.4	26
$coumarinGDP_{(aq)}$	3.4	N.D
$p21^{N\text{-}ras}$.coumarinGDP	3.4	29
$p21^{N\text{-}ras}$.coumarinGTP	3.2	28
Predicted rotational correlation time[(b)] (ns):		
Monomer		14.5
Dimer		29.0
Trimer		43.5
At 20°C:		
$p21^{N\text{-}ras}$.coumarinGTP	2.5	16
$p21^{N\text{-}ras}$.mantGDP[(a)]	8.7	16
Predicted rotational correlation time[(b)] (ns):		
Monomer		8.9
Dimer		17.8
Trimer		26.7

Notes:
(a) From Hazlett et al., (1990)

(b) Calculated assuming a molecular weight of 21,000 daltons, a specific volume of 0.73 mL g^{-1}, a hydration state of 0.3 mL water g^{-1} protein and a temperature of either 5°C or 20°C.

Figure 9.2 Representative Lifetime Phase and Modulation Data.

(A) Phase (x) and modulation (▪) data for mantGDP in solution is plotted as a function of the modulation frequency. The curved lines represent the linear least squares best fit of the data to an exponential decay. The resolved lifetime value was 4.0 ns. Data were taken at $5^{o}C$ excting at 351 nm and measuring emission at wavelengths greater than 415 nm using Schott GG-435 and KV399 filters.

(B) As for (A) except that the $p21^{N\text{-}ras}$.mantGDP complex was used. The resolved lifetime was 9.1 ns.

(C) As for (B) except that the fluorescence lifetime of the $p21^{N\text{-}ras}$.coumarinGTP complex was determined at $20^{o}C$. The resolved lifetime was 2.5 ns.

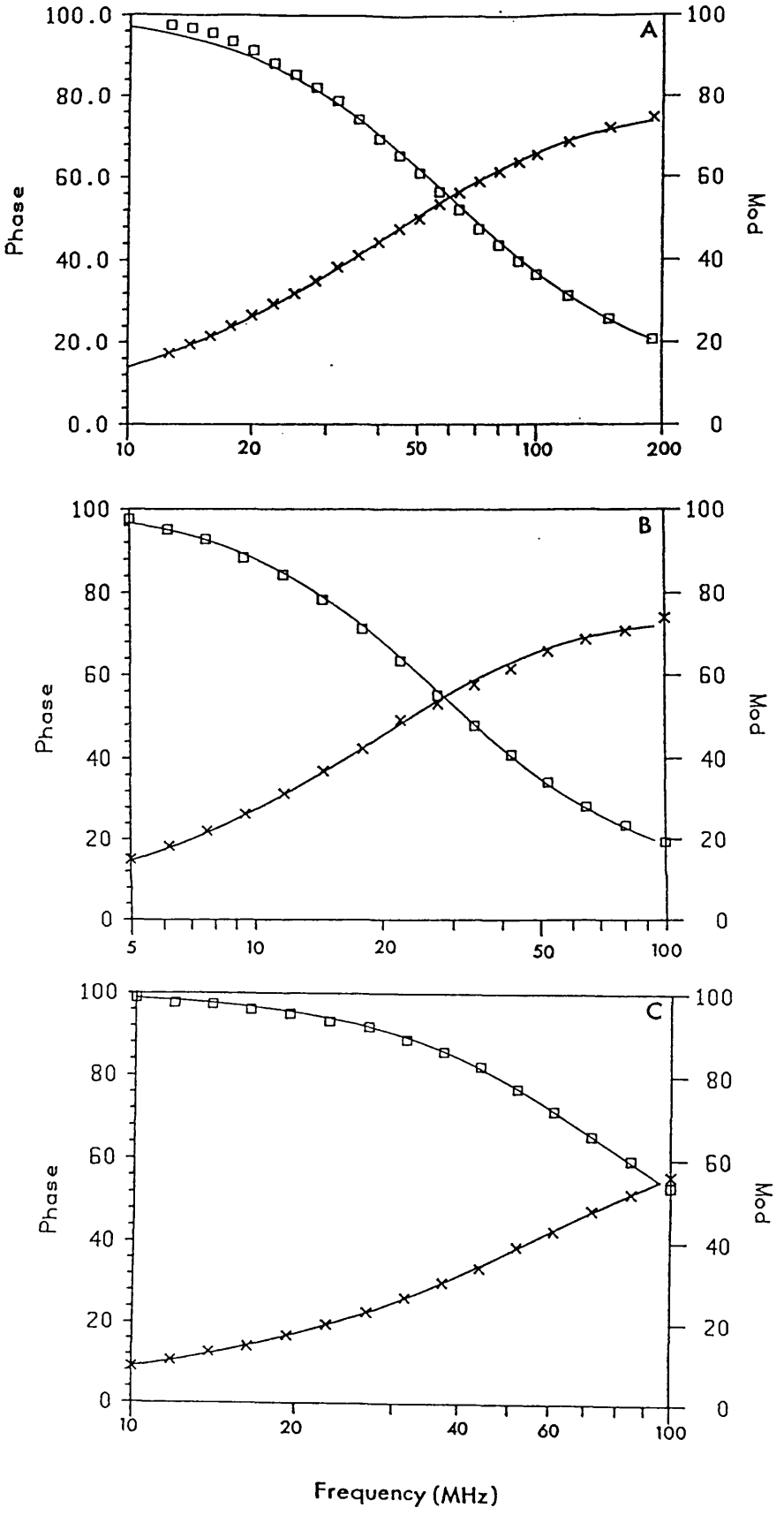
A
B
C
Phase
Mod
100.0
80.0
60.0
40.0
20.0
0.0
100
80
60
40
20
0
10
20
50
100
200
5
Frequency (MHz)

ing temperature. The lifetime was determined as a function of time using a single frequency (25 MHz, Figure 9.3). The solid line through the data is the best fit to 2 exponentials with rate constants of 3.2 x 10^{-3} s^{-1} and 1.8 x 10^{-4} s^{-1} for the fast and slow phases of the lifetime change respectively. The amplitudes and rates of the lifetime changes are comparable with the changes in fluorescence intensity observed previously (chapter 4). These data demonstrate that the fast phase of the fluorescence intensity and anisotropy change observed in chapter 4 is also associated with a decrease in fluorescence lifetime.

9.5 Rotational Correlation Time of $p21^{ras}$-Nucleotide Complexes.

The lifetime values obtained for the $p21^{ras}$ nucleotide complexes (Table 9.1) were used as fixed constants in the analysis of the rotational correlation times (τ_c). Differential phase and modulation measurements were performed to determine the rotational correlation times of the nucleotide complexes (Table 9.1). A two component exponential decay model was used to fit the differential phase and modulation data. For both complexes, two correlation times were observed ; a slow correlation time ($\tau_{c,1}$) consistent with the slow global rotation of the protein.nucleotide complex (Table 9.1), and a second faster correlation time ($\tau_{c,2)}$ which is usually ascribed to the independent local motion of the probe or the structural motion of the surrounding domain. The total amplitude of the anisotropy decay is the sum of the amplitudes of the fast (r_1) and slow (r_2) anisotropy decays. The fast motion is unlikely to be due to the presence of free probe since all the available data (gel filtration and steady state anisotropy measurements, chapter 4) suggests that 1:1 protein.nucleotide complexes are obtained. At low modulation frequencies, the value of ϕ provides information concerning the slower global rotational rate whilst the data at high frequencies allow one to estimate the extent of local motion (see Jameson, 1984 ; Jameson and Hazlett, 1991).

Global correlation times are quoted in the table to the nearest 1 ns. Whilst repetitive analysis of the same sample usually gave τ_c values within 0.5 ns, when different samples of the same complex were analysed, the variation was $\pm$ 1 - 2 ns. Representative differential phase data for the complex of wild type $p21^{N\text{-}ras}$ with mantGDP and coumarinGDP are shown in Figure 9.4.a. The lower phase difference with the coumarinGDP complex compared to

Figure 9.3 Changes in Fluorescence Lifetime Associated with the Hydrolysis of mantGTP by $p21^{N\text{-}ras}$ at 30°C.

A stock solution of wild type $p21^{N\text{-}ras}$.mantGTP on ice was rapidly warmed to 30°C bu dilution into buffer B already at 30°C (see chapter 4). Phase and modulation data were taken at 25 MHz modulation frequency, typically using 3 x 10 sec integration times. The fluorescence lifetimes, τ_M and τ_P, were within 50 ps of each other throughout the time course of the experiment. Data points are shown as the mean of τ_M and τ_P. Lifetime data have been fitted to a double exponential decay with rate constants of 3.2×10^{-3} s^{-1} (0.34 ns amplitude) and 1.8×10^{-4} s^{-1} (1.0 ns amplitude). Fluorescence parameters were set as for Figure 9.2.

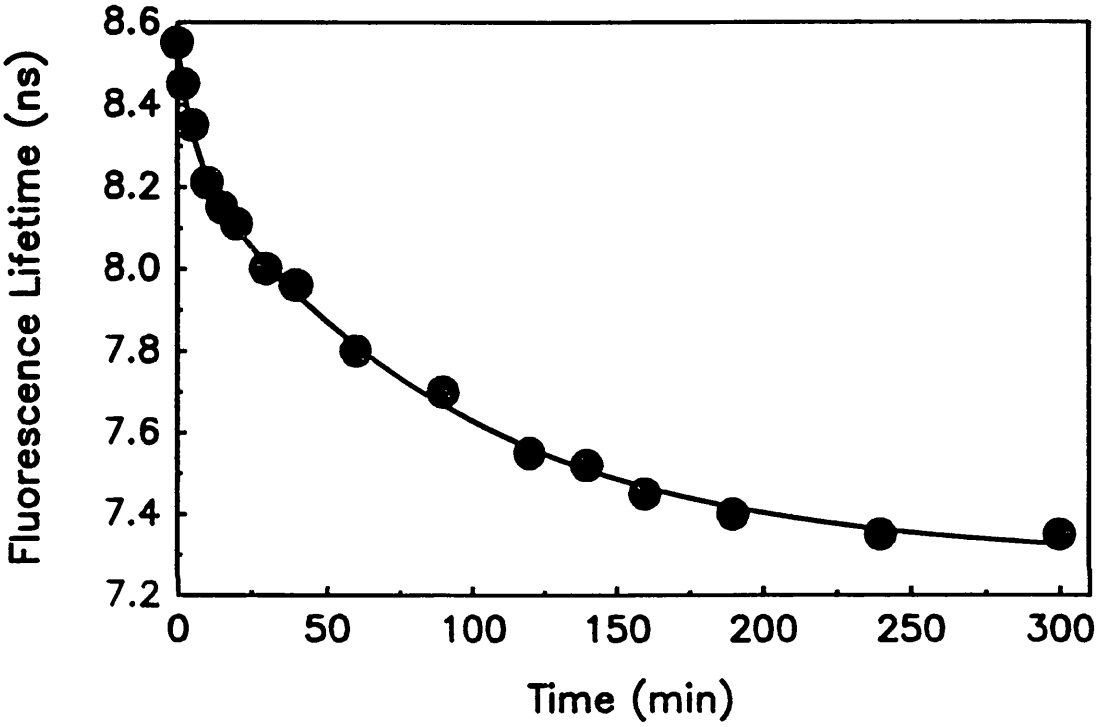
Fluorescence Lifetime (ns)
8.6
8.4
8.2
8.0
7.8
7.6
7.4
7.2
0
50
100
150
200
250
300
Time (min)

Figure 9.4 Representative Differential Phase Data and the Linked Global Correlation Time Analysis.

Panel A: Differential phase data for the complexes of mantGDP (▪) and coumarinGDP (+) with wild type $p21^{N\text{-}ras}$ are plotted as a function of modulation frequency. The curved lines represent the least squares best fit to the data with a single rotational species having two associated rotational correlation times. Although not plotted, relative modulation data (Y) were simultaneously fitted along with the differential phase data to calculate τ_c. The slower global correlation time for the mantGDP and coumarinGDP complexes is 28 ns and 29 ns respectively. Data was taken at 5^0C with the fluorescence parameters described above.

Panel B : The time resolved fluorescence anisotropy data with mantGDP and coumarinGDP complexes of wild type $p21^{N\text{-}ras}$ were co-analysed using the Globals Unlimited^{TM} analysis software. The individual X^2 of the data sets was 5.9 for mantGDP (28 ns) and 0.9 for coumarinGDP (29 ns). Using this data, the resultant X^2 of the data was calculated for various values of $\tau_{c,1}$ fixed in the analysis and plotted as shown in panel B. The observed X^2 when the data are fitted to monomeric, dimeric and trimers models respectively based on the hydrodynamic parameters shown in Table 9.1 are indicated .The globally linked value of $\tau_{c,1}$ for both data sets was 28 ns, with an overall X^2 of 3.4. The sharpness of the global minimum of the X^2 plot, is defined partially by the use of multiple fluorophores with differing lifetimes. An identical global X^2 was obtained for the triple analysis also using the fluoresceinGDP data (T.L Hazlett, pers. comm.).

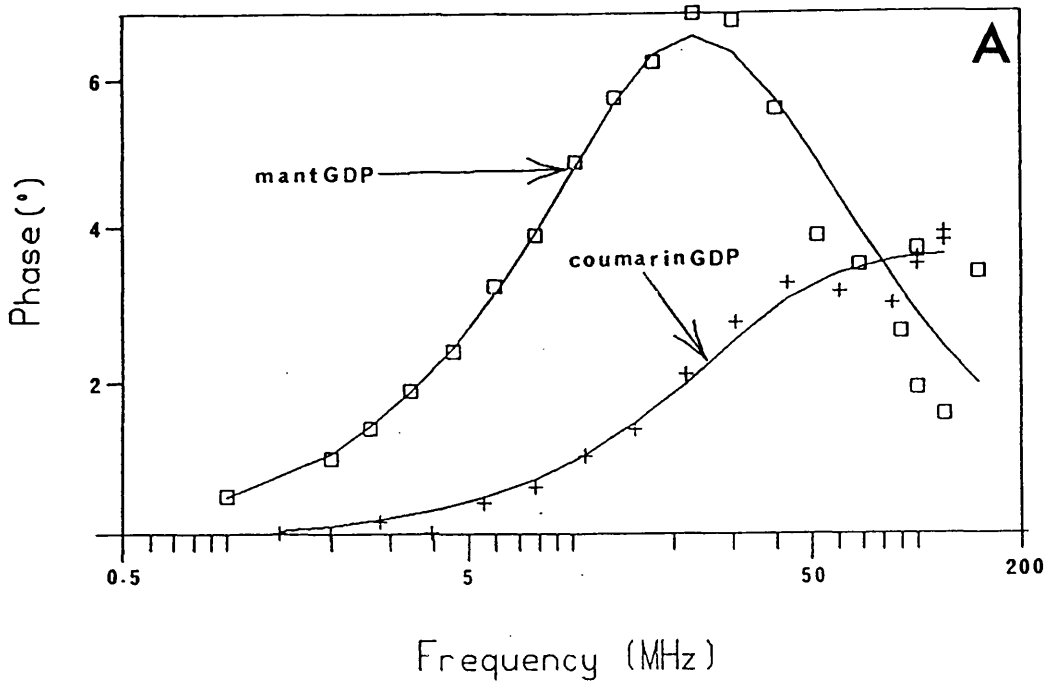
A
mantGDP
coumarinGDP
Phase (°)
6
4
2
0.5
5
50
200
Frequency (MHz)

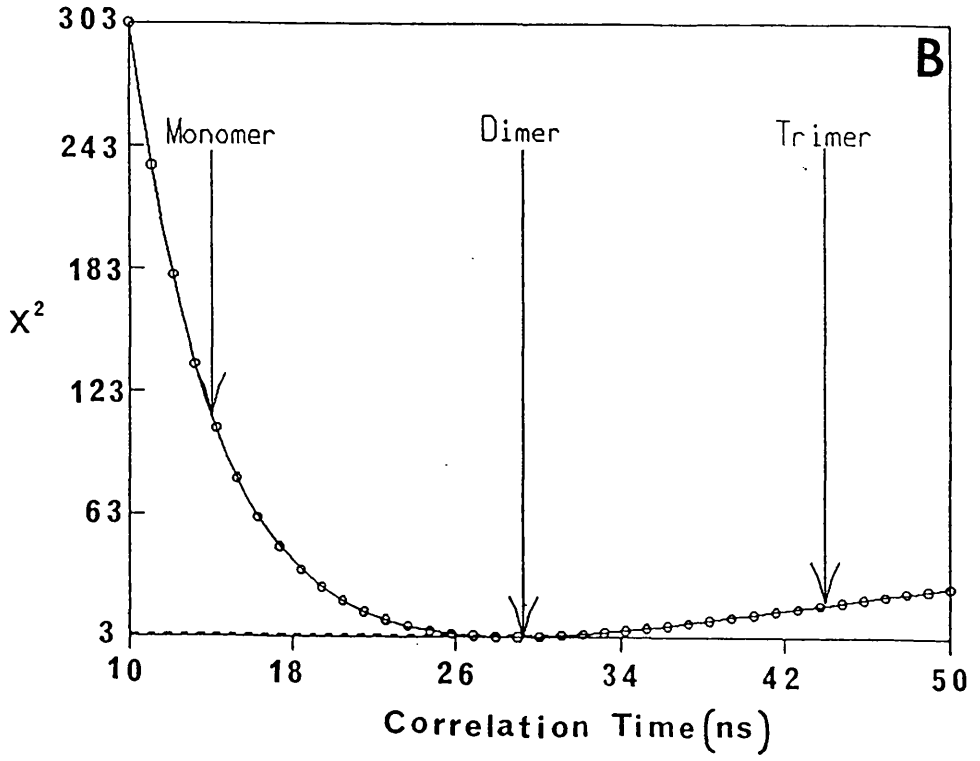
B
Monomer
Dimer
Trimer
303
243
183
123
63
3
X²
10
18
26
34
42
50
Correlation Time (ns)

$p21^{ras}$.mantGDP is due to the shorter lifetime of the coumarin analogue (see above) whilst the greater ϕ at high frequencies for $p21^{ras}$.coumarinGDP is a reflection of the increased amount of local motion for this fluorophore.

Within experimental error, the mant-nucleotide complexes of all three *ras* gene products gave the same global rotational decays with resolved correlation times of between 26 - 28 ns at 5^{o}C. Thus, the global correlation time was independent of the nucleotide state of the complex (mantGTP vs mantGDP) or the residue at codon 12 (Gly 12 or Val 12). In all of these complexes, the amplitude of the global motion, r_1 represented over 92 % of the total anisotropy amplitude, $r_1 + r_2$, indicating very little local motion of the mant-fluorophore in these complexes. This leads to correspondingly high errors ($\pm$ 50 - 100 %) in the absolute values of the $\tau_{c,2}$ (1 - 2 ns) and r_2 (0.01 - 0.02). Only by using higher modulation frequencies than reported here can the (limited) fast motions of the mant-fluorophore be determined with accuracy.

The coumarin-analogues have been used since the orientation of the probes emission and excitation dipoles relative to the rotational axis of the protein may differ from that of the mant-nucleotides. This will change the weighting of the observed correlation time ; in highly asymmetric proteins, the fluorophores orientation along the long or short axis of rotation can have large effects on the observed τ_c. However, the global rotational decays of the coumarin-nucleotides complexed with wild type $p21^{N\text{-}ras}$ (28 - 29 ns) were essentially identical to those obtained with the mant-nucleotide complexes (Table 9.1). One significant difference between the mant- and coumarin-nucleotides was the observation of an increased extent of rapid anisotropy decay with the coumarin complexes ($\tau_{c,2} \approx 0.5$ ns ; $r_2 \approx 0.05$) which may be related to the different chemical structures of the two nucleotides (see below). The global correlation time of the coumarinGTP complex at 20^{o}C (16 ns) is smaller than observed at 5^{o}C and is consistent with the more rapid rotation of the protein at the higher temperature.

The data obtained with both nucleotides were co-analysed using the Global Unlimited^{TM} analysis software in order to link and globally fit the protein rotation, $\tau_{c,1}$. This analysis is based on the concept that whilst the local motions of the fluorophores are likely to differ

between the two complexes, the rotational correlation time of the protein to which these fluorophores are attached must be identical. In this analysis, the values for the r_1, r_2, and $\tau_{c,2}$ of both complexes are allowed to vary independently of each other, whilst the $\tau_{c,1}$ for both complexes must be the same. The final reduced X^2 is that for both sets of data. Such analyses are usually presented in terms of a "X^2 map" which plots the resultant X^2 of the fit to the data for a range of values of $\tau_{c,1}$ fixed in the analysis (Figure 9.4.b). The value of $\tau_{c,1}$ which yields the minimum X^2 is that which fits best to both sets of data. Attempting to fit the experimental data to the value of $\tau_{c,1}$ predicted for a monomeric, dimeric, or trimeric for $p21^{ras}$ (at 5°C, see below) yields the values of X^2 shown in Figure 9.4.b.

9.6 Analytical Gel Filtration Chromatography.

As an alternative to fluorescence spectroscopy, the oligomeric state of $p21^{ras}$ was investigated by analytical gel filtration chromatography using an ACA-54 matrix (Figure 9.5). Both $p21^{N\text{-}ras}$.mantGDP and $p21^{N\text{-}ras}$.GDP ran as a single peak with apparent molecular weights of 28 kDa and 27 kDa respectively - 30 % higher than the molecular weight (21 kDa) calculated from the amino acid sequence. These results are therefore compatible with those obtained by John et al., (1989) using full length $p21^{H\text{-}ras}$.GDP. The fluorescence lifetime and dynamic polarisation data were identical before or after the chromatography procedure (26 ns and 25 ns respectively) and, within experimental error, similar from the values presented in Table 9.1.

9.7 Discussion.

Fluorescence lifetime and dynamic polarisation measurements can probe the solution hydrodynamics of macromolecules under equilibrium conditions. The dynamic polarisation experiments are primarily concerned with the oligomeric state of $p21^{ras}$ in solution. In addition, these time resolved fluorescence studies provide further information concerning the molecular basis for a number of the fluorescence changes observed in previous chapters. These are initially discussed below.

Figure 9.5 Analytical Gel Filtration Chromatography.

The column was calibrated using a range of protein markers of known molecular weight. Elution was performed at room temperature in buffer B at 0.25 mL min^{-1} using an ACA-54 matrix and monitored by absorbance at 280 nm. The total volume of the column was 333 mL whilst the void volume was 49 mL. Standards used were as follows: Bovine serum albumin = 66 kDa ; Horseradish peroxidase = 44 kDa ; Carbonic anhydrase = 29 kDa ; Cytochrome c = 14.3 kDa ; and Aprotinin = 6.5 kDa. The elution volume of each protein is plotted as a function of the $\log_{10}$ of the molecular weight (in Da). The elution volume of $p21^{N\text{-}ras}$.mantGDP and $p21^{N\text{-}ras}$.GDP are shown in the figure, as are the elution positions expected for a protein of M_r = 21 kDa (M) and 42 kDa (D). The calculated apparent molecular of $p21^{N\text{-}ras}$.mant-GDP and $p21^{N\text{-}ras}$.GDP from these experiments is 28 kDa and 27 kDa. Similar experiments with a Sephadex G-50 Superfine matrix also gave an apparent molecular weight of 27 kDa for $p21^{N\text{-}ras}$.GDP.

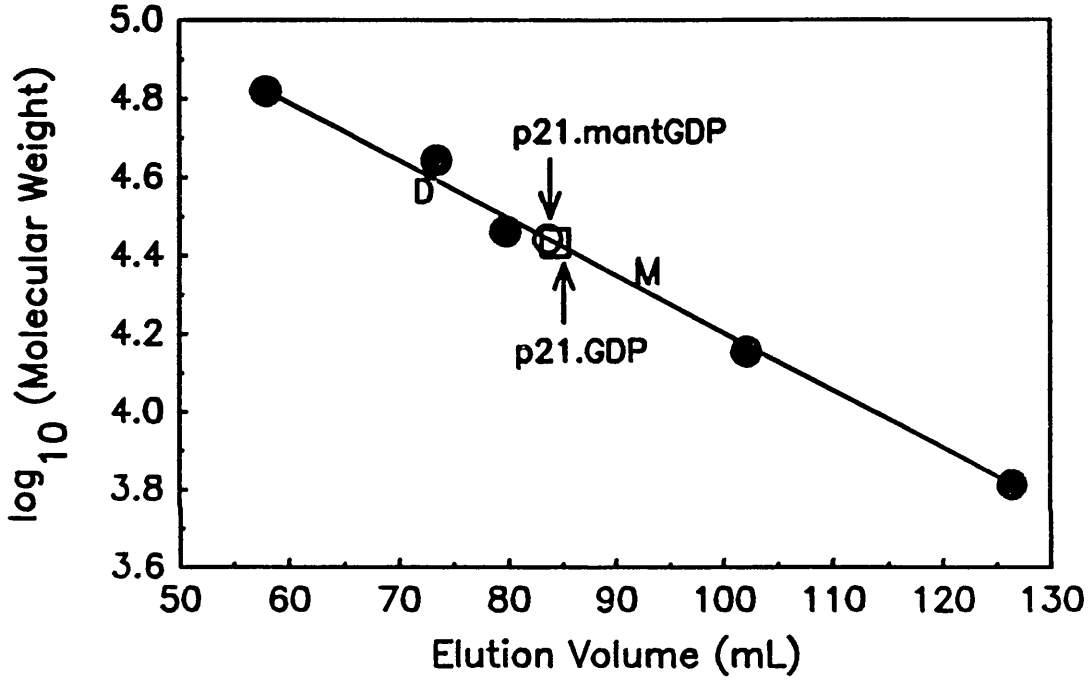
5.0
4.8
4.6
4.4
4.2
4.0
3.8
3.6
log10 (Molecular Weight)
50
60
70
80
90
100
110
120
130
Elution Volume (mL)
p21.mantGDP
p21.GDP
D
M

9.7.1 *Fluorescence Lifetimes.*

Since the lifetimes of the 2' and 3' isomers of mantGDP approximate to their relative fluorescence intensities one can conclude that static quenching of mant-fluorescence in the 2' position is not the cause of the difference in fluorescence intensity. On this basis, one must invoke a collisional quenching mechanism although the molecular basis for this effect is unknown.

A similar mechanism could be proposed for the fast and slow phases of the fluorescence change observed during the hydrolysis of mantGTP by $p21^{N\text{-}ras}$, both of which are associated with a reduction in fluorescence lifetime. In contrast to the results obtained at 30°C, there is no difference in the lifetimes of the mantGTP and mantGDP complexes at 5°C (Table 9.1). Based on these results, one might predict only a very marginal difference in fluorescence intensity at 5°C although this has not yet been investigated. These results may indicate that the probe environment and the protein conformation may be temperature sensitive, or that the temperature-sensitivity of the fluorescence lifetime is different in the two complexes. These effects may also account for the slightly larger fluorescence change observed at 37°C (10 %, Neal et al., 1990) compared to that observed in this work at 30°C (7-8%). A similar mechanism would be one of the possible interpretations of the observation that the increase in fluorescence lifetime on binding mantGDP to $p21^{ras}$ (at 5°C) is smaller than the corresponding increase in fluorescence intensity (at 30°C).

A reduction in fluorescence lifetime during the hydrolysis reaction could also be due to a change in fluorescence resonance energy transfer from Tyr residues in $p21^{ras}$ to the mant-fluorophore (see Valeur, 1991). Whilst this effect is likely to be small due to the low quantum yield of Tyr residues and the low overlap integral, J, (Tyr emission is usually at $\approx$ 305 nm), such a mechanism cannot be excluded. It may be significant in this regard that the crystal structure of $p21^{H\text{-}ras}$.mantGppNHp (Goody et al., 1992) shows the mant-fluorophore stacking on the aromatic side chain of Tyr 32, a residue which has been proposed to undergo a large change in conformation as a result of GTP hydrolysis (Schlichting et al., 1990b). Despite the above, one should be aware of the problems associated with the interpretation of such data,

as expressed by Valeur (1991, chapter 6)

The analysis of fluorescence lifetimes is also required to calculate rotational correlation times (Appendix 9.1). The differential phase and modulation data reveal not only the global correlation time of the protein (see below), but also provide information concerning the extent of local motion of the fluorophore. It is of interest to consider the latter parameter in light of the chemical structures of the fluorescent nucleotide analogues used in this, and other (Hazlett et al., manuscript in preparation) studies. The anisotropy amplitude of the fast motion (r_2) increases according to $p21^{N\text{-}ras}$.mantGDP < $p21^{N\text{-}ras}$.coumarinGDP << $p21^{N\text{-}ras}$.fluoresceinGDP. The length of the "spacer arm" between the ribose and the fluorophore increases in a similar order (Figure 9.1). The increase in local motion may therefore be correlated with the differential interaction of the fluorophore with residues in $p21^{ras}$. The structure of the $p21^{ras}$.mantGppNHp complex proposed by Goody et al., (1992, with the mant-group interacting with Tyr 32) may provide one explanation for the very small extent of local motion observed in these time resolved measurements. For the coumarin- and, to a greater extent, the fluorescein-derivatives, the long spacer arm may prevent this interaction from occurring. For these fluorophores, interactions with other residues distant from Tyr 32 cannot be excluded although based on the increased local motion, such interactions are unlikely to be as restrictive as that with Tyr 32. Since there is no difference in either steady state or time resolved anisotropy between the $p21^{ras}$.mantGTP and $p21^{ras}$.mantGDP complexes, one might expect that the local motion of the mant-fluorophore is restricted by an alternative residue in the mantGDP complex. Structural studies of the coumarinGppNHp, fluorescein-GppNHp, and mantGDP complexes would be informative in this regard.

9.7.2 *Rotational Correlation Times.*

The results presented in this chapter indicate conclusively that the global rotational correlation time of $p21^{ras}$ proteins complexed with fluorescent nucleotide analogues is $\approx$ 28 ns at 5^{o}C. The results with the coumarin-analogue, which has both a different lifetime, structure and extent of local motion than mant-nucleotides, suggests that the observed correlation time is not significantly affected by the nature of the probe. Indeed, a similar value of $\tau_{c,1}$ is

obtained with the fluoresceinGDP complex . Calculations of the rotational correlation time of monomeric, dimeric and trimer structures for $p21^{ras}$ were made using a monomeric molecular weight of 21,000 Da, a specific volume of 0.73 cm^3g^{-1}, a hydration state of 0.3 cm^3 H_2O g^{-1} protein, and assuming a spherical shape (Perrin, 1934 ; Belford et al., 1972 ; Ehrenberg and Rigler, 1972 ; Chuang and Eisenthal, 1972 ; Small and Eisenberg, 1977). At 5°C, these correlation times are 14.5 ns, 29.0 ns and 43.5 ns for a monomer, dimer and trimer respectively (Figure 9.4.b). Based on these calculations, the experimental data with both mant- and coumarin-complexes correspond more closely to the calculated value of a dimeric rather than monomeric structure for $p21^{ras}$. Further calculations using the dimensions of $p21^{ras}$ from the crystal structure (35 Å x 40 Å x 49 Å) show that the rotational correlation time of the monomer due to its non-spherical shape (Small et al., 1988) would be at most 11 % higher than assumed for a sphere. The $\tau_{c,1}$ value obtained for wild type $p21^{N\text{-}ras}$.coumarinGTP at 20°C (16 ns) is identical to that obtained with the mantGDP complex at this temperature (16 ns) T. Hazlett, pers. comm.) and similar to the value predicted for a dimer at this temperature (17.8 ns). Therefore, all of the experimental data suggest that $p21^{ras}$ has a rotational correlation time which is consistent with a dimeric structure for this protein in solution.

One possible explanation for the dimerisation of $p21^{ras}$ would be the formation of a dimer due to intermolecular disulphide linkage. This appears unlikely since 10 mM DTT was added to all the buffers used, and increasing the DTT to 100 mM final concentration had no effect on the correlation times obtained over a period of 6 hours at 30°C. Secondly, the rotational correlation time of truncated (residues 1 - 166) $p21^{Ki\text{-}ras}$.mantGDP (T.L Hazlett, pers. comm) is only marginally lower than that of full length $p21^{Ki\text{-}ras}$.mantGDP, a reduction which is consistent with the loss of the C-terminal 20 amino acids.

An alternative explanation for this result is that the protein is monomeric but the hydration state is significantly greater than used in the calculations (0.3 g H_2O g^{-1} protein). This latter parameter is generally between 0.2 - 0.4 (Jameson and Hazlett, 1991), although changing its value has only a limited effect on the calculated $\tau_{c,1}$ (for a dimer, 29 ns with 0.3 and 31 ns with 0.4). Indeed, to account for the observed value of $\tau_{c,1}$, a hydration state of 1.5 g H_2O g^{-1} would be necessary. A third explanation which cannot be excluded at present would be that

in solution, the $p21^{ras}$ protein adopts an elongated conformation (axial ratio 4:1 - 5:1). Thus, the crystal structure dimensions ($p21^{ras}$ approximates to a sphere) would need to be wildly different from those in solution.

Whilst the fluorescence data are all internally consistent with a dimeric structure for $p21^{ras}$ (M_r = 42 kDa), the gel filtration studies yielded an apparent molecular weight of 27 kDa - between that predicted for a monomer and a dimer. Identical results were obtained with either the mantGDP or GDP complexes, suggesting that the mant-fluorophore does not significantly affect the hydrodynamic properties of $p21^{ras}$. Whilst the results of these gel filtration studies are consistent with those reported previously (John et al., 1989), the cause of the apparent discrepancy between the fluorescence and chromatography data is not immediately obvious. However, it is well known that proteins can elute anomalously from gel filtration columns.

In conclusion, the differential phase and modulation data presented here and elsewhere (Hazlett et al., 1990) indicate a global rotational correlation time for all three $p21^{ras}$ proteins of $\approx$ 28 ns at $5^{o}C$ which is consistent with that expected for a dimeric structure. The reduced X^2 of the data assuming this model is 3.4 compared to 110 and 20 for monomeric and trimeric structures respectively. Alternative explanations would require either an extremely elongated shape in solution or a very high hydration state.

If $p21^{ras}$ is indeed a dimer under these conditions then it raises important questions. What is the K_d for the monomer : dimer equilibrium ? Are the two nucleotide binding sites independent and equivalent ? Does GAP or NF1 bind to the dimer or to the dissociated monomers ? What is the *in vivo* significance of these results ? At present, no answers to these questions are available. However, these results suggest that additional studies, for example using analytical ultracentrifugation, are required in order to address this important issue.

CHAPTER TEN

GENERAL DISCUSSION

"There is something remarkable about science ; one gets such wholesale returns on speculation for such a little input of fact."

Mark Twain.

The experiments described in this thesis have examined the kinetic mechanism of the $p21^{ras}$.GTPase *in vitro*. The effect of the catalytic domains of p120-GAP and NF1-GAP on the intrinsic GTPase mechanism has been investigated, as has the effect of single point mutations in $p21^{ras}$. The overall aim of these studies was to determine how the concentrations of the biologically active $p21^{ras}$.GTP and biologically inactive $p21^{ras}$.GDP complexes are regulated by GTPase activating proteins, and to provide a kinetic explanation for the biological phenotypes of several point mutants.

The major approach that has been used is that of fluorescence spectroscopy, and in particular using the ribose-modified 2'(3') mant-derivatives of guanine nucleotides. Fortunately, these analogues behave kinetically and thermodynamically in a very similar fashion to the parent nucleotides. It is remarkable that this one analogue provides suitable fluorescence intensity (chapters 4 and 5) and anisotropy (chapters 6 & 9) changes with which to monitor all of the elementary steps in the mechanism studied thus far. Thus, the kinetics of nucleotide binding, dissociation, and hydrolysis, and GAP_{344} and NF1 binding and dissociation can be monitored with this analogue. It is apparent from such a consideration that the mant-fluorophore is ideally placed to monitor protein isomerisation and protein : protein interactions occurring during the GTPase mechanism of $p21^{ras}$. Possible explanations for this observation can be considered in light of the extensive structural information available from crystallography studies, and in particular from the three dimensional structure of the $p21^{ras}$.mantGppNHp

complex (Goody et al., 1992).

Whilst potential problems arise with the 2'(3') mant-derivatives due to acyl migration of the fluorophore, it is fortunate that one isomer (3') is preferentially bound to $p21^{ras}$. Whilst the mant-nucleotides have been used almost exclusively in this study, procedures have been developed for the synthesis of a wide range of "designer" analogues with the appropriate fluorescence properties. For these analogues, the fluorescence lifetime, quantum yield, extinction coefficient and chemical structure can be chosen to suit the particular experimental problem. For example, for time resolved fluorescence studies of the interaction of $p21^{ras}$ with GAP proteins, then a fluorophore with a long fluorescence lifetime would be advantageous. An analogue containing the 2,5 DANSYL fluorophore (τ_L = 25 ns) has been synthesised (K.M & J.F.E, unpublished results) and would be suitable for such studies. Alternatively, certain experiments may be required to be performed at sub-micromolar $p21^{ras}$ concentrations and the use of the fluorescein derivative may be appropriate.

Whilst fluorescence spectroscopy is inherently sensitive, relatively large amounts of purified protein are required in order to perform the biochemical and biophysical studies described here. Only as a result of the gift of E.coli expression systems for the proteins (in particular from Drs Hall, Skinner and Lowe) could the experiments be performed. The development of the direct exchange procedure at the outset of these studies has greatly simplified the preparation of protein : nucleotide complexes with high efficiency and rapidity. However, the use of this technique required the protein purification procedure for $p21^{ras}$ to be modified. An improved protocol was developed (chapter 3) achieving both higher yield and purity than previous methods. A major problem encountered during the course of these studies was the low (and often variable) apparent activity of the $p21^{ras}$ preparations obtained using [^{3}H]GDP filter binding assays in comparison to a range of other assays for $p21^{ras}$. The cause of this discrepancy remains elusive despite a considerable effort in exploring potential causes. Fortunately, the concentration of the mant-nucleotide complexes can be readily determined using absorption spectroscopy, albeit with low sensitivity (lower limit at $\approx$ 2 μM).

The first major question to be addressed was the kinetic mechanism of the GAP-accelerated $p21^{ras}$.GTPase using catalytic concentrations of GAP (chapter 4). The results of these experiments, with both the mantGTP and mantGppNHp complexes of $p21^{ras}$, were consistent with the model proposed by Neal et al., (1990, scheme 5.2). In addition to the slow fluorescence change observed by these workers, an additional fast phase of the fluorescence change was observed with $p21^{N\text{-}ras}$ and, less obviously, with $p21^{H\text{-}ras}$, although not with $p21^{Ki\text{-}ras}$. The cause of this initial fluorescence change is unclear ; it is associated with a decrease in both fluorescence lifetime and anisotropy suggesting an increased rotational rate of the fluorophore (global and / or local motion) ; it is not accelerated by GAP, and ; GTPase-stimulation by GAP can occur independently of it. An initial hypothesis, that the lack of this signal with the $p21^{Ki\text{-}ras}$ proteins was due to truncation of these proteins at residue 166, appears unlikely since similar results were observed with either full length or truncated $p21^{H\text{-}ras}$.

The most significant observation from this series of experiments was that GAP accelerated the rate of the slow fluorescence change observed after the binding of both of these nucleotides in a concentration dependent manner. These results therefore provide strong evidence that the overall rate of the GTP hydrolysis reaction catalysed by $p21^{ras}$ is controlled by an isomerisation of the $p21^{ras}$.GTP complex (step 2a, scheme 5.2) and it is this step in the mechanism which is accelerated by GAP. An attractive hypothesis for the structural basis of this mechanism is that proposed by Pai et al., (1990) where a conformational change, related to the re-orientation of residues 60 - 65, is required in order to attain the catalytically active structure with respect to GTP hydrolysis.

It should be noted however that these results are only partially consistent with those reported by other groups. Antonny et al., (1990) introduced a tyrptophan residue at position 56 and showed that the $p21^{ras}$.GTP[gamma]S complex of this mutant underwent a slow fluorescence change (5 % reduction) occurring with the same rate as that of the $p21^{ras}$.GTP complex. This result is therefore in agreement with the model proposed by Neal et al., (1990) using the mantGppNHp complex. However, GAP did not obviously accelerate the rate of this fluorescence change, although an additional slower fluorescence decrease was observed. One problem associated with the interpretation of these data is the lack of information concerning

the chemical state of the nucleotide throughout the time course of these fluorescence changes. Where possible, for the fluorescence experiments described in this thesis, the protein : nucleotide complexes have been extensively characterised by H.P.L.C to determine the ratio of mantGTP to mantGDP or to investigate the stability of the mantGppNHp analogues. Secondly, Rensland et al., (1991) published a similar study to that presented here but using $p21^{H\text{-}ras}$ rather than $p21^{N\text{-}ras}$. Their results with the mantGTP complexes (both in the presence and absence of GAP) are compatible with my data. However, with the $p21^{ras}$.mantGppNHp complex, they only reported a fast 5% fluorescence decrease in intensity but do not show the data after 16 minutes ; a time scale which would not show the slow process that we observe. It seems probable that this fluorescence change merely reflects the fast phase of the fluorescence change (with either mantGTP or mantGppNHp), and in support of this notion, they reported that the rate of this fluorescence change was not accelerated by GAP. It is difficult to determine the reasons for the differing effects of GAP observed in the three sets of experiments. It has been stressed throughout this thesis that fluorescence emission intensity is sensitive to many environmental variables which cannot always be defined or controlled with confidence. Thus differences may occur between $p21^{N\text{-}ras}$ and $p21^{H\text{-}ras}$ or between mantGppNHp or GTP[gamma]S. Furthermore, the introduction of a tryptophan residue may allow the conformational change to occur during the intrinsic GTPase mechanism with the gamma-S analogue, but may prevent the acceleration of this process by GAP. A similar explanation has been afforded in chapter 8 for the Pro 12 mutant. Nevertheless, the data presented here using mant-nucleotides, combined with the characterisation of the protein-nucleotide complexes throughout the time courses of the reactions are proposed to provide strong evidence that GAP accelerates the isomerisation of the $p21^{ras}$.GTP complex and hence the rate of GTP cleavage.

Additional support for the model proposed here comes from oxygen exchange experiments (Webb, 1992b) which demonstrate that the rate of GTP synthesis (k_{-2} in scheme 1) is much faster than calculated from the observed rate of the cleavage step and the equilibrium constant ($[p21^{ras}.GDP]_{\infty}$ / $[p21^{ras}.GTP]_{\infty}$ > 50). One interpretation of this observation is that oxygen exchange is occurring on the reverse rate of step 2b (scheme 2, the cleavage step) which is rapid compared to the rate of the isomerisation reaction (step 2a). Indeed, using GAP

concentrations where the rate of GTP cleavage is accelerated ≈ 200-fold, there was no change in the rate of oxygen exchange suggesting that GAP does not affect the chemical cleavage step directly.

An extension of these fluorescence studies using catalytic concentrations of GAP was to perform similar experiments where GAP is used in molar excess over $p21^{ras}$.mantGTP (chapter 5). From the hyperbolic dependence of the rate of the fluorescence change with $p21^{ras}$.mantGTP on [GAP], it has been proposed that the binding of GAP to $p21^{ras}$.mantGTP is rapidly reversible (K_d = 20 μM) and that the ternary complex subsequently undergoes an isomerisation reaction occurring at 14 s^{-1} at 30°C. This mechanism is also supported by the observation that the transient increase in fluorescence intensity occurring on formation of the ternary complex (chapter 6) is complete within 2 ms after mixing.

This model is entirely inconsistent with that proposed by Antonny et al., (1991, see above) using catalytic concentrations of GAP. In their model, the apparent second order rate of hydrolysis (≈ 7 x 10^5 M^{-1} s^{-1} from this work and 6 x 10^5 M^{-1} s^{-1} from Antonny et al., 1991) is equal to the true bimolecular rate constant, (k_{+1} in scheme 5.1). This model is based on kinetic competition experiments using the GTP, GDP or GTP[gamma]S complexes of wild type $p21^{ras}$ to inhibit the rate of the fluorescence change observed during the GAP-catalysed Trp 56 $p21^{ras}$.GTP hydrolysis reaction. From these experiments, they reported that the GTP complex bound to GAP an order of magnitude more weakly that the GTP[gamma]S complex, but with similar affinity as the GDP complex ! The likely explanation for this effect is that during the time course of the assay the wild type $p21^{ras}$.GTP competitor was hydrolysed to $p21^{ras}$.GDP which would only poorly compete with Trp 56 $p21^{ras}$.GTP. Thus, the concentration of competitor in the GTP-complex was changing and reducing during the time course of the assay. This would explain the lower apparent affinity of the GTP complex (≈ 100 μM) compared to the GTP[gamma]S complex (≈ 10 μM), and also why $p21^{ras}$."GTP" bound with equal affinity as $p21^{ras}$.GDP. From the difference between the two values obtained with GTP and GTP[gamma]S, they proposed that k_{-1} = 6 s^{-1} and k_{+1} >> 6 s^{-1} (using the nomenclature in scheme 5.1). Such a mechanism has been rejected based on the results presented here (see Appendix 5.1). If these rate constants apply to $p21^{ras}$.mantGTP, then the stopped flow

data would not vary hyperbolically with GAP concentration. Furthermore, one can calculate that the observed rate of $p21^{ras}$.mantGTP.GAP formation at 3 μM GAP in the stopped flow experiments should be $\approx 8\ s^{-1}$ at 37°C (half time $\approx$ 0.1 s) and thus the binding reaction would be readily observed (time resolution of the stopped flow $\approx$ 5 ms). However, no such binding reaction was observed over this time course ; indeed, the rate constant for this process has been estimated to be $\geq 1000\ s^{-1}$ (Appendix 5.1). Finally, according to their model, K_m values would not be equal to K_d values - all of the data obtained thus far with GAP suggests that these two values are numerically similar (Webb and Hunter, 1992 ; Gideon et al., 1992 ; this work). Thus, based on several lines of evidence, their model is considered to be untenable.

With NF1, then the binding kinetics are likely to be different from those observed with GAP, and this is probably a reflection of the 20-fold higher affinity with which it binds to $p21^{N\text{-}ras}$.mantGTP (70-fold for $p21^{H\text{-}ras}$.mantGTP). Whilst the approach to equilibrium of the binding step is likely to be significantly slower than with GAP (the reaction with NF1 can be observed on the stopped flow time scale), it is still considerably faster than the rate of the isomerisation reaction ($6\ s^{-1}$). The problems and inconsistencies associated with a comparison between the k_{cat} and K_m values for p120-GAP, GAP_{344} and NF1-GRD based solely on multiple turnover experiments have been addressed in chapter 5 and will not be repeated here. However, it is re-emphasised that such measurements are critically dependent on a knowledge of the molar concentration of active enzyme, which is usually taken to be the total relative concentration of protein based on a dye binding assay (for example, Bradford, 1976). Based on experimental data, it has been argued (chapters 5 and 6) that for our preparations of GAP_{344} and NF1, a similar assumption is valid.

The experiments described in chapter 6 were initiated in order to provide a test of the hypothesis that an increase in mant-nucleotide fluorescence and in Trp 884 - mant-nucleotide fluorescence resonance energy transfer occurs upon ternary complex formation. The results of these experiments are entirely compatible with such hypotheses, although it was noted that the extent of FRET is dependent on many variables, not only the donor - acceptor distance. The effect of increasing NaCl concentration on the interaction of $p21^{ras}$.mantGTP, GAP and

NF1 are consistent with the hypothesis that both GTPase activating proteins are similarly salt sensitive (chapter 7). Results of fluorescence anisotropy titrations, and of kinetic competition and stopped flow experiments were consistent with each other. The equilibrium constant is primarily affected by ionic strength where the K_d increases $\approx$ 5 -fold after the addition of 100 mM NaCl. Different results have been reported by Wiesmuller and Wittinghofer, (1992) although it has been argued that their conclusions are based on a method of data analysis which does not account for the differing affinities with which GAP and NF1 bind to $p21^{ras}$.GTP. The extreme sensitivity of both proteins to ionic strength suggests that *in vivo*, the stimulation of the intrinsic GTPase by GAPs may be significantly less than observed *in vitro*.

Of all of the mutant $p21^{ras}$ proteins studied, the Pro 12 and Trp 35 / 36 mutants are probably the most interesting. The results reported here with Pro 12 $p21^{ras}$ represent the first detailed characterisation of the kinetic properties of this mutant. This is somewhat surprising given the particular biological interest in this mutant. Whilst both GAP and NF1 were found to stimulate the GTPase of the Pro 12 mutant, the activation was between 0.1 % and 1 % that of wild type $p21^{ras}$. NF1 is likely to be the major negative regulator of Pro 12 *in vivo*. These results, combined with the biological assays for Pro 12, have led to the proposal that the *in vivo* stimulation of the intrinsic GTPase of $p21^{ras}$ may be sufficiently small for the absolute value of the intrinsic GTP cleavage rate to become significant. If this is indeed correct, then opinion will have reversed back to that prevalent in the mid 1980's. The second interesting effect of this interpretation is that the rate of nucleotide exchange in fibroblasts or PC12 cells (catalysed by exchange factors) must be significantly slower than that observed in T-lymphocytes. Further *in vivo* studies are required in order to test these hypotheses, although it does demonstrate that the combined use of enzyme kinetics, molecular biology and cell biology can be useful for interpreting the *in vivo* effect of a point mutation in mechanistic terms.

Preliminary results of the Trp 35 mutant has indicated that Thr 35 appears to be important not for the intrinsic GTP cleavage rate but for the GAP-accelerated reaction and for the binding of Mg^{2+}, at least in the GTP-bound form. Based on preliminary data, it appears that

Trp 36 binds to GAP with slightly higher affinity than does wild type $p21^{ras}$. This may be related to the presence of a hydrophobic side chain in the effector / GAP binding loop since the phenyl ring of mant-nucleotides produced a 3-fold reduction in K_d. In contrast, NF1 binds some 30-fold more weakly to Trp 36 $p21^{ras}$.GppNHp than does wild type $p21^{ras}$. Since Trp 36 is an oncogenic mutant, these results would imply that GAP may be more likely to be the effector than NF1. Further spectroscopic and kinetic approaches will be required in order to determine if these preliminary conclusions are valid.

The $p21^{ras}$ proteins have been extensively studied over the last 10 years or so, primarily because of their ability to lead to cell transformation. The literature on these proteins is vast and changes rapidly - the discovery of a wide range of ras-related proteins, each with their own function and possibly GAP protein, increases both the interest in, and the complexity of, the ras signal transduction system. Future experiments, similar to those described here, on the kinetic mechanism of the ras related proteins are no doubt underway in several laboratories. It will be of interest to determine which features of the kinetic mechanism of the $p21^{ras}$.GTPase and of structure are conserved in other small GTP binding proteins. However, there is still a considerable amount of future work that needs to be performed to define the kinetic mechanism of the $p21^{ras}$.GTPase *in vitro*, and in particular for the NF1-activated mechanism. Thus far, most interest has concentrated on the mechanism of the GTP hydrolysis reactions, i.e the de-activation of $p21^{ras}$. With the recent identification of guanine nucleotide exchange factors for $p21^{ras}$, the over-expression of these proteins may allow a detailed kinetic analysis of the exchange reaction to be performed. Finally, a parallel series of experiments are required to investigate the kinetic mechanism of the GTPase cycle of C-terminally modified $p21^{ras}$ in lipid bilayers or detergents.

There is a long way to go before we are able to describe the kinetic, structural and biological properties of $p21^{ras}$ in detail. The approaches used in this thesis may find widespread use in other systems, particularly if the structures of other ras - related proteins allow modification of the ribose moiety of the guanine nucleotide with fluorophores. It is sobering to realise that despite 25 years of detailed investigations of the actin - catalysed myosin ATPase, we are far from achieving a complete understanding of this mechanism. However, if the advances that

have been made with $p21^{ras}$ over the past decade are continued, we may be more optimistic that rationally designed anticancer drugs based on the selective inhibition of oncogenic $p21^{ras}$ proteins will become available in the near future.

ACKNOWLEDGEMENTS

My stay at N.I.M.R has been most enjoyable and there are many people who have contributed to this. Dr John Eccleston (N.I.M.R) has been a constant source of information and advice on all aspects of this project, and I am grateful to him for introducing me to the field of nucleoside triphosphatases. I would like to thank Professor Bastain Gomperts (U.C.L) for agreeing to be my London University supervisor, and for allowing me to attend (and speak at !) the 36th Biochemical Society Harden Conference which he organised. My industrial supervisor, Dr Peter Lowe (Wellcome Research Laboratories, Beckenham, Kent), has provided me with a myriad of p21^{ras} proteins and also the expression systems for GAP_{344}. His pleasant and informative discussions have been of enormous value over the last three years. Thanks are also extended to Dr Richard Skinner for the help with the NF1 purification, and to the other collaborators who provided other expression systems.

The help of Drs David Jameson and Theodore Hazlett (University of Hawaii) with respect to the time resolved measurements is gratefully acknowledged. In addition, Dr Martin Webb (N.I.M.R) provided many useful discussions, particularly with respect to the use of the P_i release assay. Finally, I would like to thank Dr David Trentham for his general support during my stay at N.I.M.R.

Mr Colin Davis taught me how to make up H.P.L.C buffers and Mr Peter Browne provided a valuable lesson in how to express displeasure in experimental results using words of only 4 letters. Apologies are extended to all of those people for whom my disorganisation caused them problems. Socially, thanks go to Drs Steve Martin and Mike Anson and Messrs Alin and Sloane. Finally, I would like to thank the members of my football teams for their constant "advice" on the art of goalkeeping - I wish my successor well !.

The support of the MRC and Wellcome Research Laboratories is gratefully acknowledged. Finally, I would like to apologise in advance to my thesis examiners for the length of this document ; numerous ($\geq$ 6) attempts to reduce it in size proved largely unsuccessful. Most importantly, I would like to thank my family, and in particular my wife, for her constant love and support during the past three years. This thesis is dedicated to them.

REFERENCES

Abo, A., Pick, E., Hall, A., Totty, N., Teahan, CG., and Segal, AW (1991) Nature (London) **353**, 668-670.

Adam-Vizi, V., Knight, D., and Hall, A (1987) Nature (London) **328**, 581.

Adari, H., Lowy, DR., Willumsen, BM., Der, CJ., and McCormick, F (1988) Science **240**, 518-521.

Anderson, D., Koch, CA., Grey, L., Ellis, C., Moran, MF and Pawson, T. (1990) Science **250**, 979 - 982.

Antonny,B., Chardin,P., Roux,M., Chabre,M (1991) Biochemistry **30**, 8287-8295.

Ballester, R., Marchuk, D., Boguski, M., Saulino, A., Letcher, R., Wigler, M., and Collins, F (1990) Cell **63**, 851-859.

Bagshaw, CR., Eccleston, JF., Eckstein, F., Goody, RS., Gutfreund, H., amd Trentham, DR. (1974) Biochem. J. **141**, 351 - 364.

Banik, U. and Roy, S (1990) Biochem. J. **266**, 611-614.

Barbacid, M (1987) Ann. Rev. Biochem. **56**, 779-827.

Bar-Sagi D., and Feramisco, JR., (1986) Science **233**, 1061 - 1068.

Basu, TN., Gutmann, DH., Fletcher, JA., Glover, TW., Collins, FS., and Downward, J (1992) Nature (London) **356**, 713-715.

Becker, J., Tan, TJ., Trepte, H-H., and Gallwitz, D (1991) EMBO J. **10**, 785-792.

Beckner, SK., Hattori, S., and Shih, TY. (1985) Nature (London) **317**, 71 - 72.

Belford, CG., Belford, RL., and Weber, G (1972) Proc. Natl. Acad. Sci. USA **69**, 1392 - 1393.

Bender, A., and Pringle, JR. (1989) Proc. Natl. Acad. Sci. USA **86**, 9976 - 9980.

Birchmeier, C., Broek, D., and Wigler, M. (1985) Cell, **43**, 615 - 621.

Bizub, D., Blair, D., Alvord, G., and Skalka, A. (1988) Oncogene, **3**, 443 - 448.

Bollag, G. and McCormick, F (1991a) Nature (London) **351**, 576-579.

Bollag, G. and McCormick, F (1991b) Annu. Rev. Cell Biol. **7**, 601-632.

Bradford, MM. (1976) Anal. Biochem. **72**, 248 - 254.

Brownbridge, GG., Lowe, PN., Moore, KJM., Skinner, RH., and Webb, MR. (1992) J. Biol. Chem. submitted for publication.

Bos, JL., Tokoz, D., Marshall, CJ., Verlaan-De Vries, M., Veeneman, GH., Van der Eb, AJ., Van Boom, JH., Janssen, JWG., and Steenvoorden, ACM. (1985) Nature (London) **315**, 726 - 730.

Bos, JL., Fearon, ER., Hamilton, SR., Verlaan-De Vries, M., Van Boom, JH., Van der Eb, AJ., and Vogelstein, B (1987) Nature (London) **327**, 293-297.

Bos, JL. (1988) Mutation Res. **195**, 225 - 271.

Bos, JL. (1989) Cancer Res. **49**, 4682 - 4689.

Bourne, HR., Sanders, DA., and McCormick, F (1990) Nature (London) **348**, 125-132.

Bourne, HR., Sanders, DA., and McCormick, F (1991) Nature (London) **349**, 117-127.

Bouton, AH., Kanner, SB., Vines, RR., Wang, HC., Gibbs, JB., and Parsons, JT (1991) Mol. Cell. Biol. **11**, 945-953.

Broach, JR., and Deschenes, RJ. (1990) Adv. Cancer Res. **54**, 79 - 139.

Buchberg, AM., Cleveland, LS., Jenkins, NA., and Copeland., NG. (1990) Nature (London) **347**, 291 - 294.

Burgering, BMT., Medema, RH., Maassen, JA., van de Wetering, ML., van de Eb, AJ., McCormick, F., and Bos, JL (1991) EMBO J. **10**, 1103-1109.

Burstein, ES., Linko-Stentz, K., Lu, Z., and Macara, IG (1991) J. Biol. Chem. **266**, 2689-2692.

Buss, JE., Quilliam, LA., Kato, K., Casey, PJ., Solski, PA., Wong, G., Clark, R., McCormick, F., Bokoch, GM., and Der, CJ (1991) Mol. Cell. Biol. **11**, 1523-1530.

Cabot, MC., Welsh, CJ., Cao, H., and Chabbot, H (1988) FEBS Lett. **233**, 153 - 157.

Cai, H., Szeberenyi, J., and Cooper, GM. (1990) Mol. Cell Biol. **10**, 5314 - 5323.

Cales, C., Hancock, JF., Marshall, CJ., and Hall, A (1988) Nature (London) **332**, 548-551.

Casey, PJ., Solski, PA., Der, CJ., and Buss, JE (1989) Proc. Natl. Acad. Sci. USA U.S.A. **86**, 8323-8327.

Chardin, P., and Tavitian, A., (1986) EMBO. J. **5**, 2203 - 2208.

Chardin, P. (1988) Biochimie **70**, 865 - 868.

Chardin, P., Madaule, P., and Tavitian, A. (1988) Nucleic Acid Res. **16**, 2717.

Chardin, P., Boquet, P., Madaule, P., Popoff, MR., Rubin, EJ and Gill, DM. (1989) EMBO. J. **8**, 1087 - 1092.

Charvier, P., Parton, RG., Hauri, HP., Simons, K., and Zerial, M. (1990) Cell, **62**, 317 - 329.

Chuang, TJ., and Eisenthal, KB. (1972) J. Chem. Phys. **57**, 5094 - 5097.

Clanton, DJ., Hattori, S., and Shih, TY (1986) Proc. Natl. Acad. Sci. USA U.S.A. **83**, 5076-5080.

Clarke, S., Vogel, JP., Deschenes, RJ., and Stock, J. (1988) Proc. Natl. Acad. Sci. USA. **85**, 4643 - 4647.

Colby, WW., Hayflick, JS., Clark, SG., and Levinson., AD (1986) Mol. Cell. Biol. **6**, 730 - 734.

Crechet, J-B., Poullet, P., Mistou, M-Y., Parmeggiani, A., Camonis, J., Boy-Marcotte, E.,

Damak, F., and Jacquet, M (1990) Science **248**, 866-868.

Cremo, CR., Neuron, JM., and Yount, RG (1990) Biochemistry **29**, 3309-3319.

Damak, F., Boy-Marcotte, E., Le-Roscouet, D., Guilbaud, R., and Jacquet, M. (1991) Mol. Cell. Biol. **11**, 202 - 212.

DeClue, JE., Papageorge, AG., Fletcher, JA., Diehl, SR., Ratner, N., Vass, WC., and Lowy, DR (1992) Cell **69**, 265-273.

DeFeo, D., Gonda, MA., Young, HA., Chang, EH., Lowry, DR., Scolnick, EM., and Ellis, RW. (1981) Proc. Natl. Acad. Sci. USA USA **78**, 3328 - 3332.

DeFeo-Jones, D., Tatchell, K., Robinson, LC., Sigal, IS., Vass, WC., Lowy, DR., and Scolnick, EM. (1985) Science **228**, 179 - 184.

De Groot, H., De Groot, H., and Noll, T (1985) Biochem. J. **229**, 255-260.

Deshpande, AK., and Kung, J-F. (1987) Mol. Cell. Biol. **7**, 1285 - 1288.

Der, CJ., Krontiris, TG., and Cooper, GM. (1982) Proc. Natl. Acad. SCi. USA, **79**, 3637 - 3640.

Der, CJ., Finkel, T., and Cooper, GM (1986a) Cell **44**, 167-176.

Der, CJ., Pan, B-T., and Cooper, GM (1986b) Mol. Cell. Biol. **6**, 3291-3294.

de Vos, AM., Tong, L., Milburn, MV., Matias, PM., Jancarik, J., Noguchi, S., Nishimura, S., Miura, K., Ohtsuka, E., and Kim, SH (1988) Science **239**, 888-893.

Dexter, DL. (1964) J. Chem. Phys. **21**, 836.

Didsbury, J., Weber, RF., Bokoch, GM., Evans, T., and Snyderman, R (1989) J. Biol. Chem. **264**, 16378-16382.

Didsbury, JR., Uhing, RJ., and Snyderman, R (1990) Biochem. Biophys. Res. Commun. **171**, 804-812.

Diekmann, D., Brill, S., Garrett, MD., Totty, N., Hsuan, J., Monfries, C., Hall, C., Lim, L., and Hall, A (1991) Nature (London) **351**, 400-402.

Downward, J., Graves, JD., Warne, PH., Rayter, S., and Cantrell, DA. (1990a) Nature (London) **346**, 719 - 723.

Downward, J., Riehl, R., Wu, L., and Weinberg, RA. (1990b) Proc. Natl. Acad. Sci. USA **87**, 5998 - 6002.

Downward, J (1990) Trends Biochem. Sci. **15**, 469-472.

Downward, J. (1992) Bioessays. **14**, 177 - 184.

Eccleston, JF (1981) Biochemistry **20**, 6265-6272.

Eccleston, JF (1984) J. Biol. Chem. **259**, 12997-13003.

Eccleston, JF., Dix, DB., and Thompson, RC (1985) J. Biol. Chem. **260**, 16237-16241.

Eccleston, JF. (1987) In Spectrophotometry and Spectrofluorimetry: A Practical Approach. (DA Harris and CL Bashford, Eds) pp137 - 164. ICR Press, Oxford, U.K.

Eccleston, JF., Moore, KJM., Brownbridge, GG., Webb, MR., and Lowe, PN (1991) Biochem. Soc. Trans. **19**, 432-437.

Edsall, JT and Gutfreund, H. (1983) Biothermodynamics ., the study of biochemical processes at equilibrium, J. Wiley and Sons, NY, pp228 - 237.

Eftink, MR., and Ghiron, CA (1976). Anal. Biochem. **114**, 199.

Ellis, RW., DeFeo, D., Shih, TY., Gonda, MA., Young, HA., Tsuchida, N., Lowy, DR., and Scholnick, EM. (1981) Nature (London) **292**, 506 - 511

Ellis, C., Moran, M., McCormick, F., and Pawson, T (1990) Nature (London) **343**, 377-381.

Ellman, GL (1959) Arch. Biochem. Biophys. **82**, 70 - 77.

Emkey, R., Freedman, S., and Feig, LA (1991) J. Biol. Chem. **266**, 9703-9706.

Ehrenbery, M and Rigler, R (1972) Chem. Phys. Lett. **14**, 539 - 544.

Engelberg, D., Simchen, G., and Levitzki, A. (1990) EMBO J. **9**, 641 - 651.

Fasano, O., Aldrich, T., Tamanoi, F., Taparawsky, E., Furth, M. and Wigler, M. (1984) Proc. Natl. Acad. Sci. USA **81**, 4008 - 4012.

Feig, LA., and Cooper, GM (1988) Mol. Cell. Biol. **8**, 2472-2478.

Feig, LA., Pan, B-T., Roberts, TM., and Cooper, GM (1986) Proc. Natl. Acad. Sci. USA U.S.A. **83**, 4607-4611.

Feramisco, JR., Gross, M., Kamata, T., Rosenberg, M., and Sweet, RW. (1984) Cell **38**, 109 - 117.

Feuerstein, J., Goody, RS., and Wittinghofer, A (1987) J. Biol. Chem. **262**, 8455-8458.

Fiske, CH. and SubbaRow, Y (1925) J. Biol. Chem. **66**, 375-400.

Fleischman, LF., Chahwala, SB., and Chantley, L. (1986) Sciencde **231**, 407 - 410.

Forster, TH. (1948) Ann. Phys. (Leipzig) **2**, 55.

Forster, TH. (1949) Z. Naturf. **4a**, 321.

Frech, M., John, J., Pizon, V., Chardin, P., Tavitian, A., Clark, R., McCormick, F., and Wittinghofer, A (1990) Science **249**, 169-171.

Galwitz, D., Donath, C., and Sander, C. (1983) Nature (London) **306**, 704 - 707.

Garreau, H., Camonis, JH., Guitton, C and Jacquet, M. (1990) FEBS Lett. **269** 53 - 59.

Garrett, MD., Self, A., Van Oers, C., and Hall, A. (1989) J. Biol. Chem. **264**, 10 - 13.

Garrett, MD., Major, GN., Totty, N., and Hall, A (1991) Biochem. J. **276**, 833-836.

Gibbs, JB., Marshall, MS., Scolnick, EM., Dixon, RA., and Vogel, US (1990) J. Biol. Chem. **265**, 20437-20442.

Gibbs, JB., Sigal, IS., Poe, M., and Scolnick, EM (1984) Proc. Natl. Acad. Sci. USA U.S.A. **81**, 5704-5708.

Gibbs, JB., Schaber, MD., Allard, WJ., and Sigal, IS (1988) Proc. Nat'l Acad. Sci. USA **85**, 5026 - 5030.

Gideon, P., John, J., Frech, M., Lautwein, A., Clarck, R., Scheffler, J., and Wittinghofer, A. (1992) Mol. Cell. Biol. **12**, 2050 - 2056.

Gill, SC. and von Hippel, PH (1989) Anal. Biochem. **182**, 319-326.

Goody, RS., Frech, M., and Wittinghofer, A (1991) Trends Biochem. Sci. **16**, 327-328.

Grand, RJA. and Owen, D (1991) Biochem. J. **279**, 609-631.

Gross M., Sweet, RW., Sathe, G., Yokoyama, S., Fasano, O., Goldfarb, M., Wigler, M., and Rosenburg, M. (1985) Mol. Cell. Biol. **5**, 1015 - 1024.

Gutierrez, L., Magee, AI., Marshall, CJ., and Hancock, JF (1989) EMBO J. **8**, 1093-1098.

Hagag, N., Halegoua, S., and Viola, M. (1986) Nature (London) **319**, 680 - 682.

Halenbeck, R., Crosier, WJ., Clark, R., McCormick, F., and Koths, K (1990) J. Biol. Chem. **265**, 21922-21928.

Halford, SE., Bennett, NG., Trentham, DR., and Gutfreund, H (1969) Biochem. J. **114**, 243 - 251.

Halford, SE. (1971) Biochem. J. **125**, 319 - 327.

Halford, SE. (1972) Biochem. J. **126**, 727 - 738.

Hall, A (1984) Oxford Surveys of Eukaryotic Genes. Vol. 1. (Ed: Maclean, N) Oxford University Press, Oxford, 111-144.

Hall, A (1990) Science **249**, 635-640.

Hall, A (1992a) Molec. Biol. Cell **3**, 475-479.

Hall, A (1992b) Cell **69**, 389-391.

Hall, A. and Brown, R (1985) Nucl. Acids Res. **13**, 5255-5269.

Hall, A., Marshall, CJ., Spurr, NK., and Weiss, RA (1983) Nature (London) **303**, 396-400.

Hall, A. and Self, AJ (1986) J. Biol. Chem. 261, 10963-10965.

Han, J-W., McCormick, F., and Macara, IG (1991) Science **252**, 576-579.

Hancock, JF., Marshall, CJ., McKay, I., Gardener, S., Housley, MD., Hall, A., and Wakelam, MJO. (1988) Oncogene **3**, 187 - 193.

Hancock, JF., Magee, AI., Childs, JE., and Marshall, CJ (1989) Cell **57**, 1167-1177.

Hancock, JF., Paterson, H., and Marshall, CJ (1990) Cell **63**, 133-139.

Hart, PA., and Marshall, CJ (1990) Oncogene **5**, 1099-1101.

Harvey, J.J. (1964) Nature (London) **204**, 1104 - 1105

Hata, Y., Kikuchi, A., Sasaki, T., Schaber, MD., Gibbs, JB., and Takai, Y (1990) J. Biol. Chem. **265**, 7104-7107.

Hattori, S., Ulsh, LS., Halliday, K., and Shih, TY (1985) Mol. Cell. Biol. **5**, 1449-1455.

Hazlett,TL., Jameson,DM., Neal,SE., Webb,MR., Eccleston,JF (1990), Biophys. J. **57**, 289a.

Hiratsuka, T (1983) Biochim. Biophys. Acta. **742**, 496-508.

Hiromi, K. (1979). **Kinetics of Fast Enzyme Reactions.** John Wiley. NY. USA.

Hori, Y., Kikuchi, A., Isomura, M., Katayama, M., Miura, Y., Fujioka, H., Kaibuchi, K., and Takai, Y (1991) Oncogene **6**, 515-522.

Hoshino, M., Clanton, DJ., Shih, TY., Kawakita, M., and Hattori, S (1987) J. Biochem. **102**, 503-511.

Huang, YK., Kung, H-F., and Kamata, T (1990) Proc. Natl. Acad. Sci. USA U.S.A. **87**, 8008-8012.

Hrycyna, CA., and Clarke, S. (1990) Mol. Cell Biol. **10**, 5071 - 5076.

Isomura, M., Kikuchi, A., Ohga, N., and Takai, Y (1991) Oncogene **6**, 119-124.

Jablonski, A. (1965) Acta. Phys. Polon. **38**, 717.

Jackson, JH., Cochrane, CG., Bourne, JR., Solski, PA., Buss, JE., and Der, CJ. (1990) Proc. Natl. Acad. Sci. USA **87**, 3042 - 3046.

Jameson,DM (1984): Fluorescence: principles, methodologies, and applications. In: Fluorescein Hapten: an immunological probe. (Ed: Voss,EW) CRC Press, Boca Raton,Florida, 23-48.

Jameson, DM., Gratton, E., and Eccleston, JF. (1987) Biochemistry **26**, 3894 - 3901.

Jameson, DM and Hazlett, TL. (1991) **Time Resolved Fluorescence in Biology and Biochemistry** in "Biophysical and Biochemical Aspects of Fluorescence Spectroscopy" (TG Dewey, Ed). Plenum Publishing Corporation.

John, J., Frech, M., and Wittinghofer, A (1988) J. Biol. Chem. **263**, 11792-11799.

John, J., Schlichting, I., Schiltz, E., Rosch, P., and Wittinghofer, A (1989) J. Biol. Chem. **264**, 13086-13092.

John, J., Sohmen, R., Feuerstein, J., Linke, R., Wittinghofer, A., and Goody, RS (1990) Biochemistry **29**, 6058-6065.

Jones, S., Vignais, M-L., and Broach, JR. (1991) Mol. Cell Biol. **11**, 2641 - 2646.

Kaibuchi, K., Mizuno, T., Fujioka, H., Yamamoto, T., Kishi, K., Fukumoto, Y., Hori, Y., and Takai, Y (1991) Mol. Cell. Biol. **11**, 2873-2880.

Kataoka, T., Broek, D., and Wigler, M. (1985) Cell **43**, 493 - 505.

Kaplan, DR., Morrison, DK., Wong, G., McCormick, F., and Williams, LT (1990) Cell **61**, 125-133.

Kaziro, Y., Itoh, H., Kozasa, T., Nakafuku, M., and Satoh, T. (1991) Ann. Rev. Biochem. **60**, 349 - 400.

Kikuchi, A., Sasaki, T., Araki, S., Hata, Y., and Takai, Y (1989) J. Biol. Chem. **264**, 9133-9136.

Kilmartin, JV., Wright, B., and Milstein, C. (1982) J. Cell. Biol. **93**, 576 - 582.

Kirsten, WH., and Meyer, LA. (1967) J. Natl. Cancer Inst. **39**, 311 - 335

Kitayama, H., Sugimoto, Y., Matsuzaki, T., Ikawa, Y., and Noda, M (1989) Cell **56**, 77-84.

Kitayama, H., Matsuzaki, T., Ikawa, Y., and Noda, M. (1990) Proc. Natl. Acad. Sci. USA, **87**, 4284 - 4288.

Koch, CA., Anderson, D., Moran, MF., Ellis, C., and Pawson, T (1991) Science **252**, 668-674.

Krengel, U., Schlichting, I., Scherer, A., Schumann, R., Frech, M., John, J., Kabsch, W., Pai, E., and Wittinghofer, A (1990) Cell **62**, 539-548.

Lacal, JC., Moscat, J., and Aaronson, SA (1987a) Nature (London) **330**, 269 - 272.

Lacal, JC., Fleming, TP., Warren, BS., Blumberg, PM., and Aaronson, SA (187b) Mol. Cell. Biol. **7**, 4146 - 4149.

Laemmli, UK., (1970) Nature (London) **277**, 680 - 685.

Latwesen, DG., Poe, M., Leigh, JS., and Reed, GH (1992) Biochemistry **31**, 4946-4950.

Ledwith, BJ., Manam, S., Kraynak, AR., Nichols, WW., and Bradley, MO. (1990) Mol. Cell Biol. **10**, 1545 - 1555.

Lloyd, AC., Davies, SA., Crossley, I., Whitaker, M., Housley, MD., Hall, A., Marshall, CJ., and Wavelam, MJO. (1989a) Biochem. J. **260**, 813 - 819.

Lloyd, AC., Paterson, HF., Morris, JDH., Hall, A., and Marshall, CJ. (1989b) EMBO J. **8**, 1099 - 1104.

Lohman, TM. (1984a) Biochemistry 23, 4656 - 4665.

Lohman, TM. (1984b) Biochemistry 23, 4665 - 4675.

Longworth, JW. (1983) **"Intrinsic Fluorescence of Proteins"** in Time Resolved Fluorescence Spectroscopy in Biochemistry and Biology (Cundall and Dale Eds) pp 651 - 725. NATO ASI Series (series A : Life Sciences) Plenum Press.

Lowe, DG., and Goeddel, DV., (1987) Mol. Cell. Biol. **7**, 2845 - 2856.

Lowe, PN., Page, MJ., Bradley, S., Rhodes, S., Sydenham, M., Paterson, H., and Skinner, RH (1991) J. Biol. Chem. **266**, 1672-1678.

Mach, H., Middaugh, CR., and Lewis, RV (1992) Anal. Biochem. **200**, 74-80.

Marchuk, DA., Saulino, AM., Tavakkol, R., Swaroop, M., Wallace, MR., Andersen, LB., Mitchell, AL., Gutmann, DH., Boguski, M., and Collins, FS (1991). Genomics, **11**, 931 - 940.

Maeda, M., Patel, AD., and Hampton, A (1977) Nucl. Acids Res. **4**, 2843-2853.

Magee, AI., Gutierrez, L., McKay, IA., Marshall, CJ., and Hall, A (1987) EMBO J. **6**, 3353-3357.

Manchester (1951) "Biochemistry Today" in Science News. Penguin. (out of print).

Manne, V., Bekesi, E., and Kung, HF (1985) Proc. Natl. Acad. Sci. USA U.S.A. **82**, 376-380.

Manne, V., Yamazaki, S., and Kung, H-F (1984) Proc. Natl. Acad. Sci. USA U.S.A. **81**, 6953-6957.

Manne, V., Roberts, D., Tobin, A., O'Rourke, E., de De Virgilio, M., Meyers, C., Ahmed, N., Kurz, B., Resh, M., Kung, H-F., and Barbacid, M. (1990) Proc. Natl. Acad. Sci. USA. **87**, 7541 - 7545.

Margolis, B., Li, N., Koch, A., Mohammadi, M., Hurwitz, DR., Zilberstein, A., Ullrich, A., Pawson, T., and Schlessinger, J (1990) EMBO J. **9**, 4375-4380.

Marshall, CJ (1986) J. Cell. Sci. Suppl. **4**, 417-430.

Marshall, MS., Hill, WS., Ng, AS., Vogel, US., Schaber, MD., Scolnick, EM., Dixon, RA., Sigal, IS., and Gibbs, JB (1989) EMBO J. **8**, 1105-1110.

Martin, GA., Viskochil, D., Bollag, G., McCabe, PC., Crosier, WJ., Haubruck, H., Conroy, L., Clark, R., O, Connell, P., Cawthon, RM., Innis, MA., and McCormick, F (1990) Cell. **63**, 843-849.

McCormick, F (1992) Phil. Trans. R. Soc. Lond. B **336**, 43-48.

McGrath, JP., Capon, DJ., Goeddel, DV., and Levinson, AD (1984) Nature (London) **310**, 644-649.

Menard, L., Tomhave, E., Casey, PJ., Uhing, RJ., Snyderman, R., and Didsbury, JR (1992) Eur. J. Biochem. **206**, 537-546.

Milburn, MV., Tong, L., deVos, AM., Brunger, A., Yamaizumi, Z., Nishimura, S., and Kim, S-H (1990) Science **247**, 939-945.

Mitchell, RH (1992) on p54 of Moore et al., (1992) Phil Trans. R. Soc. Lond. B (1992) **336**, 49 - 54.

Mistou, M-Y., Jacquet, E., Poullet, P., Rensland, H., Gideon, P., Schlichting, I., Wittinghofer, A., and Parmeggiani, A. (1992) EMBO J. 11, 2391 - 2397.

Mizunu, T., Kaibuchi, K., Yamamoto, T., Kawamura, M., Sakoda, T., Fujioka, H., Matsuura, Y., and Takai, Y (1991) Proc. Natl. Acad. Sci. USA U.S.A. **88**, 6442-6446.

Molloy, CJ., Bottaro, DP., Fleming, TP., Marshall, MS., Gibbs, JB., and Aaronson, SA (1989) Nature (London) **342**, 711-714.

Moore,KJM., Lowe,PN., Eccleston,JF (1992) Phil. Trans. R. Soc. Lond. B **336**, 49-54.

Moore, KJM., Webb, MR., and Eccleston, JF. (1992) Biochemistry, submitted for publication.

Moore and Stein (1948) J. Biol. Chem. **176**, 367 - 371.

Moore and Stein (1954) J. Biol. Chem. **211**, 907 - 915.

Morris, JD., Price, B., Lloyd, AC., Self, AJ., Marshall, CJ., and Hall, A (1989) Oncogene **4**, 27-31.

Mulcahy, LS., Smith, MR., and Stacey, DW. (1985) **313**, 241 - 243.

Neal, SE., Eccleston, JF., Hall, A., and Webb, MR (1988) J. Biol. Chem. **263**, 19718-19722.

Neal, SE. (1989) University of London, PhD Thesis.

Neal, SE., Eccleston, JF., and Webb, MR (1990) Proc. Natl. Acad. Sci. USA U.S.A. **87**, 3562-3565.

Ohga, N., Kikuchi, A., Ueda, T., Yamamoto, J., and Takai, Y (1989) Biochem. Biophys. Res. Commun. **163**, 1523-1533.

O'Brien, SJ., Nash, WG., Goodwin, JL., Lowy, DR., and Chang, EH. (1983) Nature (London). **302**, 839 - 842.

Pai, EF., Kabsch, W., Krengel, U., Holmes, KC., John, J., and Wittinghofer, A (1989) Nature (London) **341**, 209-214.

Pai, EF., Krengel, U., Petsko, GA., Goody, RS., Kabsch, W., and Wittinghofer, A (1990) EMBO J. **9**, 2351-2359.

Paterson, HF., Self, AJ., Garrett, MD., Just, I., Aktones, K., and Hall, A. (1990) J. Cell. Biol. **111**, 1001 - 1007.

Perrin, F. (1934) J. Phys. Radium. **5**, 487 - 511.

Poe, M., Scolnick, EM., and Stein, RB (1985) J. Biol. Chem. **260**, 3906-3909.

Polakis, PG., Rubinfeld, B., Evans, T., and McCormick, F (1990) Proc. Natl. Acad. Sci. USA U.S.A. **88**, 239-243.

Price, BD., Morris, JDH., Marshall, CJ., and Hall, A (1989) Biochem. J. **260**, 157-161.

Prive, GG., Milburn, MV., Tong, L., de Vos, AM., Yamaizumi, Z., Nishimura, S., and Kim, S-H. (1992) **89**, 3649 - 3653.

Raines, RT., Straus, DR., Gilbert, W, and Knowles, J. (1986) Phil. Trans. Roy. Soc. Lond. **317**, 371 - 380.

Reedijk, M., Lui, XQ., and Pawson, T. (1990) Mol. Cell Biol. **10**, 5601 - 5608.

Reinstein, J., Schlichting, I., Frech, M., Goody, RS., and Wittinghofer, A (1991) J. Biol. Chem. **266**, 17700-17706.

Reiss, Y., Goldstein, JL., Seabra, MC., Casey, PJ., and Brown, MS (1990) Cell **62**, 81-88.

Rensland, H., Lautwein, A., Wittinghofer, A., and Goody, RS. (1991) Biochemistry **30-**, 11181 - 11185.

Rey, I., Soubigou, P., Debussche, L., David, C., Morgat, A., Bost, PE., Mayaux, JF., and Tocque, B. (1989) Mol. Cell Biol. **9**, 3904 - 3910.

Ricketts, MH., and Levinson, AD (1988) Mol. Cell. Biol. **8**, 1460 - 1468.

Ridley, AJ., and Hall, A (1992) Cell **70**, 401-410.

Rubinfeld, B., Munemitsu, S., Clark, R., Conroy, L., Watt, K., Crosier, WJ., McCormick, F., and Polakis, P (1991) Cell **65**, 1033-1042.

Sadler, SE., and Maller, JL. (1989) J. Biol. Chem. **264**, 856 - 861.

Sadler, SE., Maller, JL., and Gibbs, JB. (1990) Mol. Cell Biol. **10**, 1689 - 1696.

Salminen, A. and Novick, PJ. (1987) Cell **49**, 527 - 538.

Santos, E., and Nebreda, AR (1989) Faseb. J. **3**, 2151-2163.

Santos, E., Nebreda, AR., Bryan, T., and Kempner, ES (1988) J. Biol. Chem. **263**, 9853-9858.

Satoh, T., Endo, M., Nakamura, S., and Kaziro, Y (1988) FEBS Lett. **236**, 185-189.

Satoh, T., Endo, M., Nakafuku, M., Nakamura, S and Kaziro, Y. (1990) Proc. Natl. Acad. Sci. USA **87**, 5993 - 5997.

Schaber, MD., Garsky, VM., Boylan, D., Hill, WS., Scolnick, EM., Marshall, MS., Sigal, IS., and Gibbs, JB (1989) Prot. Struct. Funct. Gen. **6**, 306-315.

Schafer, WR., Kim, R., Sterne, R., Thorner, J., Kim, S-H., and Rine, J. (1989) Science, **245**, 379 - 385.

Schlichting,I., Wittinghofer,A., Rosch,P (1988) Biochem. Biophys. Res. Commun. **150**, 444-448.

Schlichting, I., Almo, SC., Rapp, G., Wilson, K., Petratos, K., Lentfer, A., Wittinghofer, A., Kabsch, W., Pai, EF., Petsko, GA., and Goody, RS (1990) Nature (London) **345**, 309-315.

Schlichting, I., Rapp, G., John, J., Wittinghofer, A., Pai, EF., and Goody, RS (1989) Proc. Natl. Acad. Sci. U.S.A. **86**, 7687-7690.

Schmitt, HD., Puzicha, M., and Gallwitz, D. (1988) Cell **53**, 635 - 647.

Sedmark, JJ., and Grossberg, SE. (1977) Anal. Biochem. **79**, 544 - 552.

Seeburg, PH., Colby, WW., Capon, DJ., Goeddel, DV., and Levinson, AD (1984) Nature (London) **312**, 71-75.

Segev, N., Mulholland, J., and Botstein, D. (1988) EMBO. J. **7**, 161 - 168.

Seuwen, K., Lagarde, A., and Pouysseger, J. (1988) EMBO. J. **7**, 161 - 168.

Shih, C., Shilo, B., Goldfarb, MP., Dannenburg, A., and Weinberg, RA. (1979) Proc. Natl. Acad. Sci. USA. **76**, 5714 - 5718.

Sigal, IS., Gibbs, JB., D, Alonzo, JS., and Scolnick, EM (1986) Proc. Natl. Acad. Sci. USA U.S.A. **83**, 4725-4729.

Sigal, IS., Gibbs, JB., D, Alonzo, JS., Temeles, GL., Wolanski, BS., Socher, SH., and Scolnick, EM (1986) Proc. Natl. Acad. Sci. USA U.S.A. **83**, 952-956.

Skinner, RH., Bradley, S., Brown, AL., Johnson, NJE., Rhodes, S., Stammers, DK., and Lowe, PN (1991) J. Biol. Chem. **266**, 14163-14166.

Small, EW and Eisenberg, I. (1977) Biopolymers, **16**, 1907 - 1928.

Small, EW., Libertini, LJ., and Small, JR. (1988) Proc. SPIE **909**, 97 - 107.

Smith, PK., Krohn, RI., Hermanson, GT., Mallia, AK., Gartner, FH., Provenzano, MD., Fujimoto, EK., Goeke, NM., Olson, BJ., and Klenk, DC (1985) Anal. Biochem. **150**, 76-85.

Smith, MR., Rya, S-H., Suh, P-G., Rhee, S-G., and Kung, H-F. (1989) Proc. Natl. Acad. Sci. USA **86**, 3659 - 3663.

Smith, MR., Liu, Y-L., Kim, H., Rhee, SG., and Kung, H-F. (1990) Science **247**, 1074 - 1077.

Smithers, GW., Poe, M., Latwesen, DG., and Reed, GH (1990) Arch. Biochem. Biophys. **280**, 416-420.

Srivastava, SK., di Donato, A., and Lacal, JC. (1989) Mol. Cell Biol. **9**, 1779 - 1783.

Stacey, DW., and Kung, H-F. (1984) Nature (London) **310**, 508 - 511.

Stacey, SW., Watson, T., Jung, H-F., and Curran, T. (1987) Mol. Cell Biol. **7**, 523 - 527.

Stammers, DK., Tisdale, M., Court, S., Parmar, V., Bradley, C., and Ross, CK (1991) FEBS Lett. **283**, 298-302.

Takai, Y., Kaibuchi, K., Kikuchi, A., and Kawata, M (1992) Int. Rev. Cytol. **133**, 187-230.

Tamir, A., Fawzi, AB., and Northup, JK (1990) Biochemistry **29**, 6947-6954.

Tanaka, K., Matsumoto, K., and Toh-e, A. (1989) Mol. Cell. Biol. **9**, 757 - 768.

Tanaka, K., Nakafuku, M., Satoh, T., Marshall, MS., Gibbs, JB., Matsumoto, K., Kaziro, Y., and Tole, A. (1990) Cell **60**, 803 - 807.

Tanaka, K., Lin, BK., Wood, DR., and Tamanoi, F (1991) Proc. Natl. Acad. Sci. USA U.S.A. **88**, 468-472.

Temeles, GL., Gibbs, JB., D, Alonzo, JS., Sigal, IS., and Scolnick, EM (1985) Nature (London) **313**, 700-703.

Teng, DHF., Engele, CM., and Venkatesh, TR (1991) Nature (London) **353**, 437-439.

Toda, T., Uno, I., Ishikawa, T., Powers, S., Katoda, T., Broek, D., Cameron, S., Broach, J., Matsumoto, K., and Wigler, M. (1985) Cell **40**, 27 - 36.

Touchot, N., Chardin, P., and Tavitian, A. (1987) Proc. Natl. Acad. Sci. USA **84**, 8210 - 8214.

Tong, L., de Vos, AM., Miburn, MV., and Kim, S-H (1991) J. Mol. Biol. **217**, 503-516.

Tong, L., Milburn, MV., de Vos, AM., and Kim, SH (1989b) Science **245**, 244.

Tong, L., de Vos, AM., Milburn, MV., Jancarik, J., Noguchi, S., Nishimura, S., Miura, K., Ohtsuka, E., and Kim, SH (1989a) Nature (London) **337**, 90-93.

Trahey, M., and McCormick, F (1987) Science **238**, 542-545.

Trahey, M., Milley, RJ., Cole, GE., Innis, M., Paterson, H., Marshall, CJ., Hall, A., and McCormick, F (1987) Mol. Cell. Biol. **7**, 541-544.

Trentham, DR., Bardsley, RG., Eccleston, JF., and Weeds, AG (1972) Biochem. J. **126**, 635-644.

Trentham, DR., Eccleston, JF., and Bagshaw, CR (1976) Quart. Rev. Biophys. **9**, 217-281

Tsai, M-H., Hall, A., and Stacey, DW (1989a) Mol. Cell. Biol. **9**, 5260-5264.

Tsai, M-H., Yu, C-L., Wei, S-F., and stacey, DW. (1989b) Science **243**, 522 - 525.

Tsai, M-H., Roudebush, M., Dobrowolski, S., Yu, C-L., Gibbs, JB., and Stacey, DW (1991) Mol. Cell. Biol. **11**, 2785-2793.

Tsai, M-H., Yu, C-L., and Stacey, DW (1990) Science **250**, 982-985.

Tucker, J., Sczakiel, G., Feuerstein, J., John, J., Goody, RS., and Wittinghofer, A (1986) EMBO J. **6**, 1351-1358.

Ueda, T., Kikuchi, A., Ohga, N., Yamamoto, J., and Takai, Y (1989) Biochem. Biophys. Res. Commun. **159**, 1411-1419.

Ueda, T., Kikuchi, A., Ohga, N., Yamamoto, J., and Takai, Y (1990) J. Biol. Chem. **265**, 9373-9380.

Vogel, US., Dixon, RA., Schaber, MD., Diehl, RE., Marshall, MS., Scolnick, EM., Sigal, IS., and Gibbs, JB (1988) Nature (London) **335**, 90-93.

Vousden, KH., Bos, JL., Marshall, CJ., and Phillips, DH (1986) Proc. Natl. Acad. Sci. USA U.S.A. **83**, 1222-1226.

Walter, M., Clark, SG., and Levinson, AD (1986) Science **233**, 649-652.

Walworth, NC., Brennwald, P., Kabcenell, AK., Garrett, M., and Novick, P (1992) Mol. Cell. Biol. **12**, 2017-2028.

Weber, G (1952) Biochem. J. **51**, 145 - 155.

Webb, MR (1992a) Proc. Natl. Acad. Sci. USA U.S.A. **89**, 4884-4887.

Webb, MR (1992b) Phil. Trans. R. Soc. Lond. B **336**, 19-24.

Webb, MR., and Eccleston, JF (1981) J. Biol. Chem. **256**, 7734 - 7737.

Webb, MR. and Hunter, JL (1992) Biochem. J. in press, .

West, M., Kung, H-F., and Kamata, T (1990) FEBS Lett. **259**, 245-248.

Wheeler, JA. (1956) American Scientist, 44, 360.

Wiesmuller, L., and Wittinghofer, A. (1992) J. Biol. Chem. **267**, 10207 - 10210.

Willingham, MC., Pastan, I., Shih, TY., and Scolnick, EM. (1980) Cell, **19**, 1005 - 1014.

Willumsen, BM., Norris, K., Papageorge, AG., Hubbert, NL., and Lowy, DR (1984) EMBO J. **3**, 2581 2585.

Wittinghofer, A., and Pai, EF (1991) Trends Biochem. Sci. **16**, 382-387.

Wolfman, A., and Macara, A (1990) Science **248**, 67-69.

Xu, G., Lin, B., Tanaka, K., Dunn, D., Wood, D., Gesteland, R., White, R., Weiss, R., and Tamanoi, F (1990) Cell **63**, 835-841.

Yamamoto, J., Kikuchi, A., Ueda, T., Ohga, N., and Takai, Y (1990) Brain. Res. Mol. Brain. Res. **8**, 105-111.

Yatani, A., Okabe, K., Polakis, P., Halenbeck, R., McCormick, F., and Brown, AM (1990) Cell **61**, 769-776.

Yeramian, P., Chardin, P., Madaule, P., and Tavitian, A. (1987) Nuc. Acid. Res. **15**, 1869.

Zhang, K., DeClue, JE., Vass, WC., Papageorge, AG., McCormick, F., and Lowy, DR (1990) Nature (London) **346**, 754-756.

Zhang, K., Papageorge, AG., and Lowy, DR (1992) Science **257**, 671-674.

Appendix 5.1 : Alternative Explanations for the Hyperbolic Dependence of the Observed Rate of the Fluorescence Change (k_{obs}) on [GAP_{344}].

Two step reactions of $p21^{ras}$.mantGTP (R) with GAP_{344} (G) could involve isomerisations of either R or G in addition to, or instead of, those of the ternary complex (RG), as described in the text. An isomerisation of reactive and inactive forms of GAP_{344} would reveal itself as a rate limiting phenomenon at low, rather than high, GAP concentrations where the reactive form becomes deficient (Gutfreund, 1972). Since this is in contrast to what is observed here, such an explanation appears unlikely.

Isomerisation of $p21^{ras}$ on the other hand cannot be excluded based on the available evidence. Thus, equation 5.5 is a plausible mechanism for equation 5.1.

$$R \underset{k_{-1}}{\overset{k_{+1}}{\rightleftharpoons}} R^* + G \underset{k_{-2}}{\overset{k_{+2}}{\rightleftharpoons}} RG^* \qquad (5.5)$$

Whilst equation 5.5 leads formally to different kinetics from equation 5.1 (Halford, 1971), the experiments described here are insufficient to make the distinction. A second alternative, shown in equation 5.6, involves 2 distinct binding modes for GAP:

$$\begin{array}{ccc} R + G & \underset{k_{-2}}{\overset{k_{+2}}{\rightleftharpoons}} & RG^* \\ k_{+1} \uparrow\downarrow k_{-1} & & \\ RG & & \end{array} \qquad (5.6)$$

In this mechanism, a plateau in the rate of RG^* formation will be observed at high $[G]_o$ when the equilibrium constant (K_c) for step 1 is much less than that for step 2 and when $k_{+1} >> k_{+2}$. Under these conditions, the initial phase leads predominantly to RG formation, and the observed saturation rate represents the transformation of RG to RG^* in a flux through R.

As a third alternative, it is possible to postulate the same two step mechanism of reaction proposed in equation 5.1, but with the observed second order rate constant (7×10^5 M^{-1} s^{-1}) being equal to k_{+1} (in equation 5.1) rather than k_{+2} / K_d. This would arise if k_{-1} was less than k_{+2}. This would lead initially to deviation of the plot of k_{obs} against $[G]_o$ from a hyperbola. However, the experimental data fit well to a hyperbola, which is only obtained when $k_{-1} >> k_{+2}$, as they do to the linearised form of equation 5.1 (Bagshaw et al., 1974). In addition, experimental evidence for the rejection of this latter possibility has been obtained. The bimolecular formation of the $p21^{ras}$.mantGTP.GAP ternary complex is associated with an increase in fluorescence intensity compared to the fluorescence intensity of $p21^{ras}$.mantGTP alone (chapter 6). The approach to equilibrium for the binding reaction is achieved within the dead time of the stopped flow apparatus based on the result that no time dependence of this process is observed with GAP_{344}. The observed rate of RG formation, $k_{RG} = (k_{+1} \times [G]_o) + k_{-1} + k_{+2} + k_{-2} \geq 1000s^{-1}$ even at the lowest concentration of GAP used (3 μM, Appendix 6.2). Thus, the 3 components R, G, RG can be treated kinetically as one species on the stopped flow time scale. This result provides direct evidence for the rejection of the hypothesis that $k_{-1} < k_{+2}$ and hence rules out the possibility that the apparent second order rate constant (7×10^5 M^{-1} s^{-1}) is equal to k_{+1} rather than k_{+2} / K_d in a 2-step mechanism (section 5.5.5).

A feature of equations 5.5 and 5.6 (but not of 5.1) is that the apparent second order rate constant at low $[G]_o$ (7×10^5 M^{-1} s^{-1}) is equal to the bimolecular association rate constant (k_{+1} in equation 5.8 and k_{+2} in equation 5.9). The argument used in the previous paragraph does not exclude this possibility for other reaction mechanisms, such as those shown in equations 5.5 and 5.6 The value of k_{+1} or k_{+2} in equations 5.5 and 5.6 respectively is 1-2 orders of magnitude lower than typical protein : protein association rate constants ($\approx 10^7 - 10^8$ M^{-1} s^{-1}, Gutfreund, 1971). Whilst this observation does not exclude the mechanisms shown in

equations 5.5 or 5.6, it does provide circumstantial evidence against these hypotheses. Based on these considerations, the two step mechanism for the binding of GAP_{344} to $p21^{ras}$.mantGTP shown in equation 5.1 is preferred to the other possibilities.

Appendix 6.1 : Fluorescence Intensity and Anisotropy Changes on Formation of the Complex Between $p21^{ras}$.mant-nucleotides and GAPs.

A change in fluorescence intensity and anisotropy occurs on formation of the $p21^{ras}$.mant-nucleotide.GAP ternary complex. In a solution of mixed fluorescent species, the total fluorescence intensity, F_t, and observed anisotropy, r_{obs} are given by:

$$F_t = \Sigma c_i F_i \quad (1)$$

$$r_{obs} = \Sigma (c_i F_i r_i) \div F_t \quad (2)$$

where c_i is the concentration of component i, F_i is the fluorescence intensity of i per unit concentration, and r_i is its anisotropy. Rigorously, the ratio F_i / F_t is the fractional contribution of species i to the observed photocurrent. For a mixture of $p21^{ras}$.mantGTP (R) and GAP (G) in equilibrium, there are two fluorescent species (R and RG). Equation (2) can be re-written in terms of the equilibrium constant for the RG complex, K_d.

$$r_{obs} = \{r_R ([R]_0 - [RG]) + Q [RG] r_{RG}\} \div \{[R]_0 - [RG] + Q [RG]\} \quad (3)$$

$$[RG] = \{K_d + [G]_0 + [R]_0 - \sqrt{((K_d + [G]_0 + [R]_0)^2 - 4 [G]_0 [R]_0)}\} \div 2 \quad (4)$$

where $[R]_0$ and $[G]_0$ are the total $p21^{ras}$ and GAP concentrations respectively, and Q is the relative fluorescence of the ternary complex compared to $p21^{ras}$.mantGTP alone (i.e F_{RG} / F_R). The total fluorescence intensity is given by:

$$F_T = F_R (Q [RG]_0 + [R]_0 - [RG]_0) \quad (5)$$

Non-linear regression data fitting programmes (Enzfitter) were used to fit the anisotropy data to equations 3 and 4, and the intensity data to equations 4 and 5.

Appendix 6.2 : Simulations of the GAP-Activated $p21^{ras}$.mantGTPase Mechanism.

The variation in fluorescence intensity with time during the GAP-activated $p21^{ras}$.mant-GTPase mechanism was simulated using the programme "KSIM" (from Dr N Millar, Kings College, London). The model described is an extension of equation 5.2, where the dissociation of GAP has been included as an additional step (step3). It is assumed that both steps 2 and 3 are irreversible ($k_{-2} = k_{-3} = 0$) since the value of k_{-2} (in equation 5.4) is approximately zero. The variation in fluorescence intensity has been calculated assuming that the relative fluorescence intensities of the intermediates is as follows: R = 100 % ; RG = 125 % ; RG^* = 117 % ; R + G products = 92 %. These values correspond to the fluorescence changes of 25 % on binding and dissociation of GAP and 8 % on the isomerisation reaction as discussed in the text. The conclusions drawn from these simulations is, however, not dependent critically on the absolute values of these fluorescence changes. For example, if all of the amplitudes are reduced to 50% of the values used here by scattered or extraneous light, then similar results are obtained. The only requirement is that there is a significant fluorescence change on both steps 2 and 3. For each plot, time zero corresponds to an infinitely short period of time after mixing R with G (e.g dead time = zero).

The simulations were performed in order to try to distinguish between different models for the GAP-activated mechanism. These simulations concentrate on two experimental observations; (i) that the kinetics of the fluorescence changes are single exponentials over the complete time course of the reactions and (ii) that the rate of the fluorescence change at saturating concentrations of GAP is 14 s^{-1} and varies hyperbolically with GAP concentration. The time courses under a given set of rate constants have only been assumed to be different from single exponential behaviour where such deviations would occur over a time period of $\geq$ 50

ms. Thus, the estimates of the rate constants that would fit to single exponential kinetics are conservative.

(A) *Simulations of the Binding Kinetics (step 1).*

Since no time dependence of the association reaction was observed with 3 μM GAP, then the approach to equilibrium must complete within 1.5 - 2 ms after mixing (the dead time of the stopped flow). The time course of the fluorescence changes associated with the binding reactions have been simulated by varying the values of k_{+1} and k_{-1} whilst maintaining k_{-1} / k_{+1} = 20 x 10^{-6} M (the equilibrium dissociation constant for this step). Values for k_{+2} and k_{+3} were 14 s^{-1} and 100 s^{-1} respectively (see below). The reaction profiles are shown in Figure 1 where the values of k_{+1} (x 10^7 M^{-1} s^{-1}) are (1) = 2.0, (2) = 3.0, (3) = 4.0, (4) = 6.0, and (5) = 8.0. Given the dead time of the stopped flow = 1.5 - 2 ms, this demonstrates that $k_{+1} \geq 5 \times 10^7$ M^{-1} s^{-1} and $k_{-1} \geq 1000$ s^{-1}.

(B) *Simulations of the Kinetics of Steps 2 and 3.*

(i) [GAP] = 20 μM and Step 2 = 14 s^{-1}.

In this series of simulations (Figure 2), k_{+2} has been fixed at 14 s^{-1} and the concentration of GAP at 20 μM (the K_d for the binding step). The values of k_{+1} and k_{-1} have been set at 10^8 M^{-1} s^{-1} and 2000 s^{-1} respectively to represent a rapid equilibration of this step. k_{+3} is varied from 5 s^{-1} to 100 s^{-1}. The lower limit of either k_{+2} or k_{+3} in all of these simulations must be 5 s^{-1} since this is the k_{cat} for the GAP. The values of k_{+3} are (1) = 5 s^{-1}, (2) = 15 s^{-1}, (3) = 25 s^{-1}, (4) = 50 s^{-1}, and (5) = 100 s^{-1}. Only when $k_{+3} \geq 50$ s^{-1} do the kinetics of the fluorescence change approximate to a single exponential where the observed rate = 14 / 2 = 7 s^{-1} ($[G]_o = K_d$).

(ii) [GAP] = 20 μM and Step 3 = 14 s^{-1}.

As above (i) except that k_{+3} has been fixed at 14 s^{-1} and k_{+2} varied from 5 - 200 s^{-1} where (1) = 5 s^{-1}, (2) = 10 s^{-1}, (3) = 15 s^{-1}, (4) = 25 s^{-1}, (5) = 50 s^{-1}, (6) = 100 s^{-1} and (7) = 200 s^{-1} (Figure 3). Over the entire range of values for k_{+2} the kinetics of the fluorescence change are non-exponential, either with lag phases or initial increases in fluorescence intensity during the first 50 - 100 ms of the reaction. Furthermore, when $k_{+2} >>> k_{+3}$, then the observed rate of the second phase plateaus at 14 s^{-1} and is independent of $[G]_o$ over the range 20 - 60 μM.

(iii) [GAP] = 60 μM and Step 2 = 14 s^{-1}.

As above for (i) except that [GAP] = 60 μM (Figure 4). The value of k_{+3} was varied where (1) = 5 s^{-1}, (2) = 10 s^{-1}, (3) = 20 s^{-1}, (4) = 30 s^{-1}, (5) = 50 s^{-1}, (6) = 100 s^{-1} and (7) = 200 s^{-1}. Only when $k_{+3} \geq 50$ s^{-1} does the fluorescence change show single exponential kinetics. Under these conditions, then the observed rate varies hyperbolically with $[G]_o$ such that at 60 μM GAP k_{obs} (= 10.5 s^{-1}) approximates to the experimentally observed rate constant at this $[G]_o$.

(iv) [GAP] = 60 μM and Step 3 = 14 s^{-1}.

As above for (ii) except that [GAP] = 60 μM (Figure 5). The value of k_{+2} was varied where (1) = 5 s^{-1}, (2) = 10 s^{-1}, (3) = 20 s^{-1}, (4) = 30 s^{-1}, (5) = 50 s^{-1} and (6) = 100 s^{-1}. Thus, when $k_{+2} \leq 30$ s^{-1}, then lag phase kinetics are observed. When $k_{+2} \geq 50$ s^{-1} then single exponential kinetics are observed where k_{obs} = 13.8 s^{-1}. Such a mechanism could be discounted at very high $[G]_o$ (166 μM) since an initial rapid decrease in intensity corresponding to k_{+2} would be observed followed by a slow decrease in intensity corresponding to k_{+3} = 14 s^{-1}. However, since such high GAP concentrations were not used, there is no experimental evidence for the rejection of this hypothesis based on such simulations.

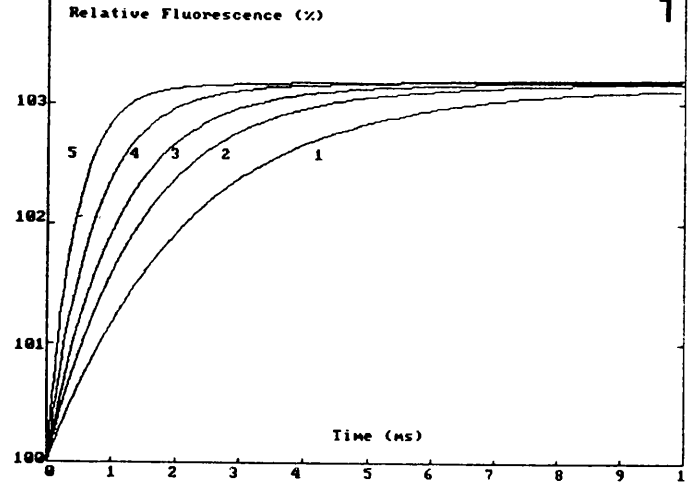
Relative Fluorescence (%)
1
103
102
101
100
5
4
3
2
1
Time (ms)
0
1
2
3
4
5
6
7
8
9
1

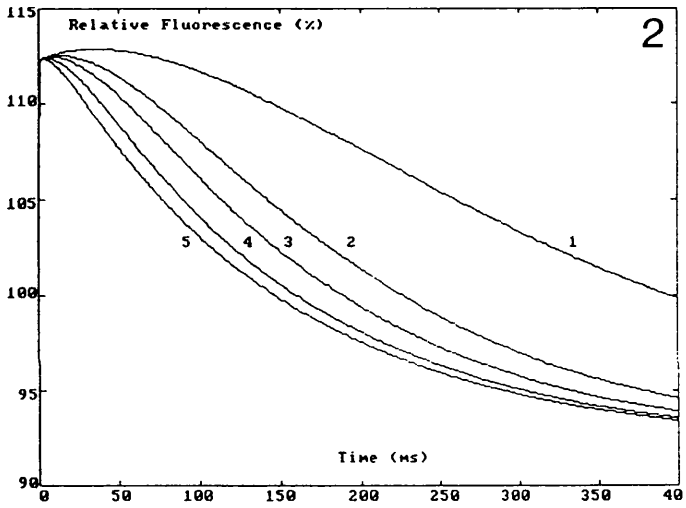
Relative Fluorescence (%)
2
115
110
105
100
95
90
5
4
3
2
1
Time (ms)
0
50
100
150
200
250
300
350
40

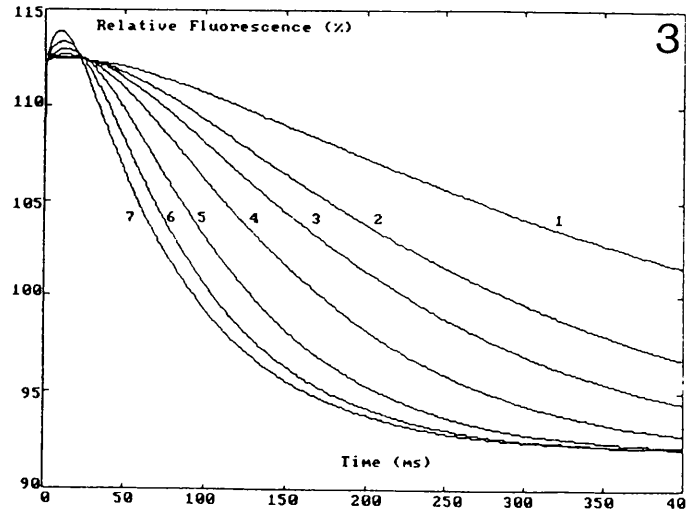
Relative Fluorescence (%)
3
115
110
105
100
95
90
7
6
5
4
3
2
1
Time (ms)
0
50
100
150
200
250
300
350
40

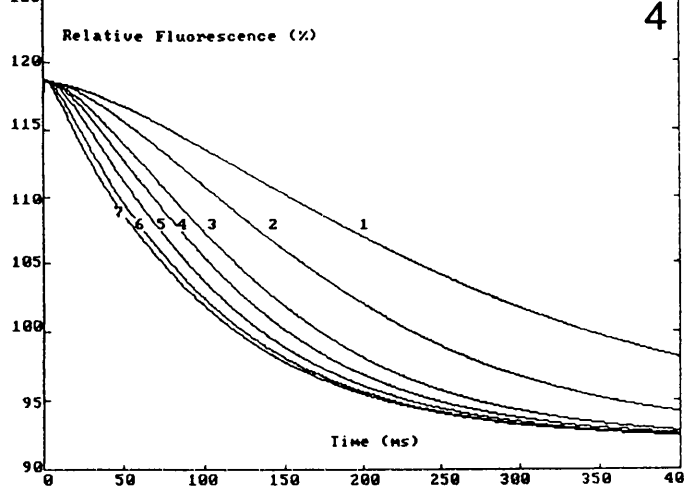
4
Relative Fluorescence (%)
120
115
110
105
100
95
90
7 6 5 4 3 2 1
Time (ms)
0 50 100 150 200 250 300 350 40

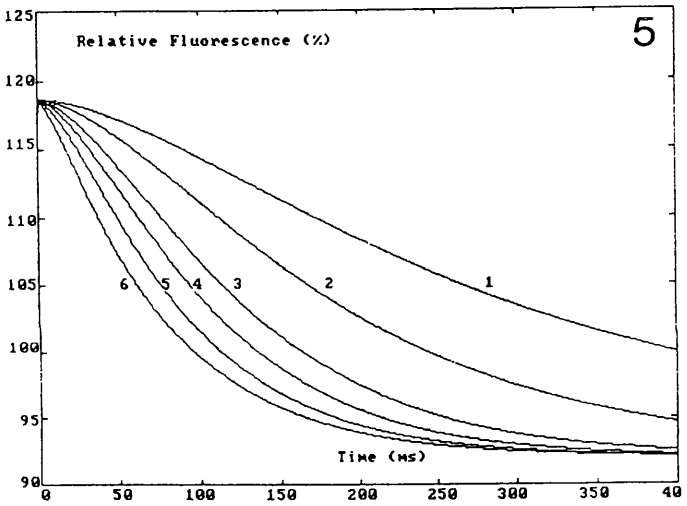
5
Relative Fluorescence (%)
125
120
115
110
105
100
95
90
6 5 4 3 2 1
Time (ms)
0 50 100 150 200 250 300 350 40

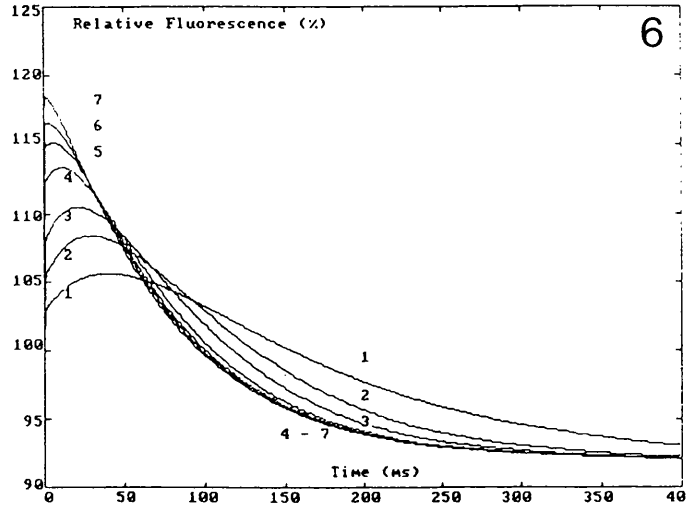
6
Relative Fluorescence (%)
125
120
115
110
105
100
95
90
7
6
5
4
3
2
1
1
2
3
4 - 7
Time (ms)
0 50 100 150 200 250 300 350 40

(v) Step 2 = 100 s^{-1} and step 3 = 14 s^{-1} - Vary [GAP] 3 - 60 μM.

As above in (iv) where k_{+2} = 100 s^{-1} and k_{+3} = 14 s^{-1} except that $[G]_0$ is varied from 3 - 60 μM where (1) = 3 μM, (2) = 6 μM, (3) = 10 μM, (4) = 20 μM, (5) = 30 μM, (6) = 40 μM, and (7) = 60 μM (Figure 6). These simulations show that this particular combination of rate constants only approximates to the experimentally observed data when [G] $\geq$ 40 μM. The rate constant of the second phase of the fluorescence change does not vary hyperbolically with GAP concentration and is essentially constant at 13.5 - 14 s^{-1} over the range $[G]_0$ = 20 - 60 μM. Therefore, this combination of rate constants can be rejected.

Conclusion.

Only when k_{+2} = 14 s^{-1} and $k_{+3} \geq$ 50 - 100 s^{-1} do the simulated time courses for the fluorescence changes correspond with the experimentally obtained traces over the range of GAP concentrations used. This implies that (i) the fluorescence change being monitored on the stopped flow time scale is limited by step 2 and (ii) step 3, which represents the dissociation of GAP, is rapid compared to the rate constant of step 2.

Appendix 7.1 - Competitive Inhibitor Model for the Effect of NaCl on the Rate of GAP-Catalysed Hydrolysis of GTP by $p21^{ras}$.

This model treats NaCl as an competitive inhibitor (I) of the substrate ($p21^{ras}$mantGTP, R) and prevents binding of R to the GAP protein (G). The dissociation constants for the two equilibria shown in equations (1) and (2) below are defined as K_d and K_I respectively.

$$R + G \rightleftharpoons RG \quad (1) \qquad\qquad R + I \rightleftharpoons RI \quad (2)$$

Assume that $[I]_{total}$ $(I_0) \approx [I]_{free}$ (I), and define R_0 and G_0 to be the total concentrations of R and G respectively, and the free concentrations of R and G as R and G respectively.

$$K_d = (G_0 - RG]\,[R]) \div [RG] \quad (3) \qquad\qquad K_I = (R]\,[I_0]) \div [RI] \quad (4)$$

but since $[R_{0]} = [R] + [RG] + [RI]$, re-write equation (4) in terms of [R] to obtain equation (5).

$$[R]\,I_0 = K_I\,[R_0] - K_i\,[R] - K_I\,[RG] \quad (5)$$

$$[R]\,([I_0] + K_I = K_I\,[R_0] - K_I\,[RG] \quad (6)$$

Re-write equation (3) in terms of [R]:

$$K_d\,[RG] = ([G_0] - [RG])\,\{(K_I\,[R_0] - K_I\,[RG]) \div ([I_0] + K_I)\} \quad (7)$$

$$K_d\,([I_0] + K_I)\,[RG] = (G_0] - [RG])\,(K_I\,[R_0] - K_I\,[RG]) \quad (8)$$

Expand equation (8), and re-arrange to solve as a quadratic equation (9).

$$K_I\,[RG]^2 - (K_I\,[R_0] + K_I\,[G_0] + K_d\,([I_0] + K_I))\,[RG] + [R_0]\,[G_0]\,K_I = 0 \quad (9)$$

$$[RG] = \{-b \pm \sqrt{(b^2 - 4\,a\,c)}\} \div 2a \quad (10)$$

Re-arrange equation (9) substituting $X = K_i.[R_0] + K_I.[G_0] + K_d([I_0] + K_I)$ (11)

$$[RG] = \{X - (\sqrt{\{X^2 - 4\,K_I^2.[R_0].[G_0]\}})\} \div 2\,K_I \qquad (12)$$

This treatment accounts for substrate depletion on forming the RI complex but does not account for the depletion of inhibitor. However, in this case, then the total concentration of NaCl added (in the mM concentration range) is not significantly affected by binding to R (in the μM concentration range). Equation (12) describes the variation in [RG] as a function of $[I_0]$. If the subsequent rate of the hydrolysis reaction is unaffected by I_0 as implied from the stopped flow studies, then the dependence of the rate of reaction on $[I_0]$ should also be described by equation (12).

Appendix 8.1 : Rate Constants for the Intrinsic and GAP-Activated $p21^{ras}$.GTPase Mechanism of Asp 12, Val 12 and Leu 61 Mutants of $p21^{ras}$.

Rate Constants for Wild Type, Asp 12 and Val 12 $p21^{N\text{-}ras}$.GTPase Activities.

Protein	Rate Constant ($\times 10^{-4}$ s^{-1})			
	mantGTP Cleavage		mantGDP Dissociation	
	- GAP	+ GAP_{365}[a]	- GAP	+ GAP_{365}
Wild Type	2.1	98	3.4	3.4
Gly 12 →Asp	1.1	1.1	1.7	1.7
Gly 12 →Val	1.0	1.0	0.59	0.59
	0.21[b]		0.78[c]	

Notes:

(i) All reactions were performed in buffer B at 30°C with a final [$p21^{ras}$.mantGTP] = 15 μM. Elementary rate constants were determinerd using the procedures outlined in section 2.9 and chapter 4.

(a) Final concentration of GAP_{365} in these experiments was 3 μM (based on hte Pierce BCA assay).

(b) Rate constant for the cleavage of GTP rather than mantGTP followed by the release of $^{32}P_i$ from the gamma-labelled [^{32}P]GTP complex.

(c) Rate constant for the dissociation of GDP rather than mantGDP followed by nitrocellulose filtration with the [^{3}H]GDP Complex.

Rate Constants for the Intrinsic, GAP_{344} and NF1 Activated $p21^{Ras}$.GTPase of the Full Length Wild Type and Leu 61 $p21^{H\text{-}ras}$ Proteins.

(A) *Intrinsic mantGTPase Rate Constants.*

Protein	Rate Constant (x 10^{-4} s^{-1})	
	mantGTP Cleavage	mantGDP Dissociation
Wild Type (1-186)[a]	0.88	0.61
Wild type (1-166)[b]	1.4	N.D[c]
Gln 61 → Leu (1-186)	0.12	1.0

(B) *Maximally Activated Rate Constants for Leu 61 $p21^{H\text{-}ras}$ with GAP_{344} and NF1.*

Elementary Step	Rate Constant (x 10^{-4} s^{-1})		
	- GAP_{344} or NF1	+ excess GAP_{344}	+ excess NF1
mantGTP Cleavage	0.12	2.4	0.76
mantGTP Dissociation	2.4	0.68	0.57

Notes:

(A) All reactions performed in buffer B at 30°C. (a) and (b) : wild type (Gly 12) $p21^{H\text{-}ras}$ encoding either residues 1 - 186 (full length) or 1 - 166 (truncated) proteins respectively. (c) not determined.

(B) All reactions performed in buffer C at 30°C. Concentrations of GAP_{344} or NF1 were added sufficient to give ≥ 90 % saturation of the Leu 61 $p21^{H\text{-}ras}$.

Appendix 9: Instrumental Design and Data Analysis Used For Time Resolved Differential Phase and Modulation Fluorescence Measurements.

Time resolved fluorescence measurements were performed on a multifrequency K2 lifetime and dynamic polarisation instrument (ISS instruments, Urbana, Illinois, USA) which is based on the design of Gratton and Limkeman (1983). This instrument operates over a wide frequency range (typically 1 - 200 MHz) with a time resolution of 10 - 100 picoseconds. The light source used was an argon ion laser (Spectra Physics, Model 164/9) equipped with selective prism wavelength and UV optics. Fluorescence excitation was achieved at 351 nm line of the argon ion laser. Fluorescence emission was monitored at wavelengths greater than 415 nm using Schott 99.435 and KV399 cut off filters. An extra-cavity electrooptical element (Pockels cell, Lasermetrics Model LM1) driven by an rf power amplifier (Electronic Navigation Industries Model 411AL 10W) allows the sinusoidal modulation of the light intensity (see below). Two frequency synthesisers (Rockland Model 5600 and Fluke Model 6160 A, range 1 - 200 MHz, resolution 1 Hz) were used to generate the sinusoidal signals to drive the Pockels cells and modulate the output of the photomultipliers (see "cross correlation" below).

Before entering the Pockels cell, the light from the laser beam was passed through a rotating calcite prism polariser which, for lifetime measurements, was set at 55^0 to the vertical laboratory axis. This eliminates errors in the measured lifetime due to Brownian diffusion (Spencer and Weber (1970). After the Pockels cell, a second polariser was set at 90^0 to the first polariser. Application of voltage across the Pockels cell leads to rotation of the plane of polarised incident light which in turn is able to be passed by the second polariser. By adjusting the voltage across the Pockels cell sinusoidally, the intensity of light emerging from the second polariser is similarly modulated (the AC signal). This component ensures that the light modulation frequency is equal to the rf driving frequency. The efficient working of the Pockels cell is essential for accurate time resolved measurements. If, for example, this component is poorly aligned optically then low modulation values (AC / DC ratios) are obtained. This is equivalent to a low signal to noise ratio for steady state measurements. Indeed, for a considerable proportion of the experiments described here, the laser beam had "burnt out" the Pockels cell, leading to modulation values considerably less than that expected for such a system ($M \approx 0.05 - 0.1$, compared to the expected value $M \approx 0.3 - 0.5$).

The sample compartment and optical path is similar to that of the Model DP450, (SLM-AMINCO, Urbana, Illinois). The incident light was split by a quartz plate and a fraction of the light was sent to a cuvette (1 cm pathlength) containing a scattering solution which was monitored by a reference photomultiplier (Hamamatsu R928). The fluorescent sample (whose lifetime is to be determined) and a reference fluorescent compound (of known lifetime) were placed in a thermostatically controlled rotating turret assembly.

The emission photomultiplier (Hamamatsu, R928) was used because it shows no sensible colour error and a modest voltage requirement for rf modulation ($\approx$ 10 volts provides a 90% change in photomultiplier output). Whilst the modulation of the photomultiplier is not required in principle (the phase delay and demodulation data can be obtained with the photomultiplier voltage at a constant value), this technique, called cross-correlation, was used since it offers advantages over direct rf measurements in terms of accuracy and noise considerations. In this procedure, the frequency of the voltage sent to the photomultiplier is set at a small value (typically 31 Hz) above the frequency sent to the Pockels cells. Essentially, the phase and modulation information of the signal is transposed to a lower frequency range where digital averaging techniques can be implemented.

Two identical detection electronic systems are used to analyse the outputs of the sample and reference photomultipliers. Each channel consists of an AC and a DC amplifier. The former has one output (tuned at 31 Hz) used for the cross-correlation technique and another is the rectified value of the AC signal (the AC voltage). The DC output provides an integrated signal proportional to the average intensity (the DC signal). An integrating digital voltmeter displays the DC signal, the AC signal and the AC / DC ratio which represents the modulation of the signal.

In a typical measurement, the phase and modulation values for the fluorescent sample are obtained relative to an internal reference signal (from the beam splitter described above)

obtained relative to an internal reference signal (from the beam splitter described above) which has a phase delay assumed to be zero. In this case, the light path from the beam splitter is negligible. The cuvette turret is then rotated and the same measurements are made on a fluorescent standard of known lifetime (glycogen light scattering τ_L = 0.001 ns ; dimethyl-p-Bis(2-(5-phenyloxazolyl))benzene (DMPOPOP) τ_L = 1.4 ns). The absolute phase delay of the fluorescence, ϕ, is then given by equation 9.1:

$$\phi = (\phi_R - \phi_F) - (\phi_R - \phi_S) \qquad 9.1$$

where ϕ_R represents the phase of the internal electronic (R)eference signal and ϕ_F and ϕ_S are the measured phase readings for the (F)luorescent sample and (S)tandard compound respectively. The phase angle is measured in degrees with a resolution of 0.01 - 0.05 ^{o} over the complete frequency range. Typically an integration period of 10 sec is used and, when necessary, several integration times are averaged. The modulation of the fluorescence, M, is defined as:

$$M = (AC/DC)_F \div (AC/DC)_S \qquad 9.2$$

The frequency may be changed rapidly merely by entering the desired frequency into the synthesisers. The phase and modulation data over a range of frequencies (typically 10 - 15 data points from 5 - 100 MHz) are entered into an IBM computer and analysed for lifetimes and dynamic polarisation using the programme ISS187 (ISS Instruments, Urbana, Illinois).

The data are analysed using the equations devised by Dushinsky (1933, see Jameson et al., 1987, Eccleston et al., 1987). In the case of fluorescence due to a single population decaying according to a single exponential, $e^{-t/\tau}$, then the lifetime, τ, is related to M and ϕ by the following equations:

1. Phase $\qquad \tan\phi = w\tau \qquad 9.3$

2. Modulation $\qquad \cos\phi = M = \sqrt{(1 + (w\tau)^2)} \qquad 9.4$

3. Minimising Function $\qquad X^2 = \{\Sigma([P] + [M])\} \div (2n - f - 1) \qquad 9.5$

where w is the modulation frequency is radians per second, X^2 is the reduced chi-squared, f is the degrees of freedom, and n is the number of modulation frequencies. M is the relative modulation and corresponds to the modulation of the fluorescence emission to that of the excitation intensity. The functions [P] and [M] are defined as:

$$[P] = (P_c - P_o)^2 \div \sigma^2_P \qquad 9.6$$

$$[M] = (M_c - M_o)^2 \div \sigma^2_M \qquad 9.7$$

where the subscripts c and o stand for the calculated and observed values respectively, while the subscripts P and M indicate the phase or modulation data.

Thus, each frequency data point yields to values, both of which can be used to measure the fluorescence lifetime. For a homogeneous emitting population, the value of the lifetime determined by these two methods must be the same and independent of the modulation frequency of the measurement. When this relationship does not hold, then a multi-exponential decay and a heterogeneous population of fluorophores must be considered. Since the fluorescence decays reported in this thesis were almost exclusively single homogeneous populations, the data analysis for multiexponential decays is not given here, but are discussed in detail by Jameson et al. (1984).

The numerical treatment of time resolved fluorescence anisotropy decays are discussed briefly below (see Jameson and Hazlett, 1991). Consider the case when the global motion of the probe during the excited state lifetime is negligible. In the presence of a single restrained

anisotropy decay of the probe, the anisotropy will not decay from the limiting anisotropy, r_0, to zero but to a steady value, r_∞. For an unrestrained anisotropy decay then $r_\infty = 0$. The rate of the anisotropy decay is defined by a sum of exponentials which approximates to :

$$r(t) / r_0 = A_\infty + (1 - A_\infty) e^{-Dt/Z} \qquad 9.8$$

where $$A_\infty = r_\infty / r_0 = \tfrac{1}{2} \cos \Theta_{max} (1 + \cos \Theta_{max})^2.$$

The rotational correlation time of the restricted local motion is σ (= Z / D) which is restricted about a cone angle of Θ_{max}. D is the wobbling diffusion constant, and Z is an approximate relation determined from Θ_{max}.

Restrained anisotropy decays in which the global motion of the protein : fluorophore complex cannot be neglected is a more complicated case of the above equations. In this case, a second exponential is added conveying the global rotational rate, and the decay in anisotropy is approximated by:

$$r(t) / r_0 = A_\infty e^{(-t/\sigma 1)} + (1 - A_\infty) e^{-(t/\sigma 1 + t/\sigma 2)} \qquad 9.9$$

where $\sigma 1$ and $\sigma 2$ are the global and local rotational correlation times respectively. For a case where both global and local motions occur, the data will fit to a two-exponential decay, one of which can be treated as the global rate, $\sigma 1$, but the other is a combination of both $\sigma 1$ and $\sigma 2$. When $\sigma 1 >>> \sigma 2$, then equation 9.9 approximates to equation 9.8.

Anisotropy data analysis for differential phase and modulation fluorimetry uses the exponential decays given above which have been transformed into the frequency domain. For a single spherical rotor the phase and modulation data are treated as follows:

1. Phase Difference ($\delta\phi$)

$$\delta\phi = \tan^{-1} \{[18\, w r_0 R]/[(k^2 + w^2)(1 + r_0 - 2r_0^2) + 6R\,(6R + 2k + k r_0)]\}$$

2. Relative Modulation (Y)

$$Y^2 = \{[(1-r_0)k + 6R)^2] + (1 - r_0)^2 w^2\} / \{[1+2r_0 k + 6R]^2 + (1 + 2r_0)^2 w^2\}$$

where $\delta\phi$ is the phase difference ($\phi_{\parallel} - \phi_{\perp}$), Y is the modulation ratio of the AC components ($M_{\parallel} - M_{\perp}$), w is the angular modulation frequency (radians per second), r_0 is the limiting anisotropy, k is the radiative rate constant (s^{-1}, = 1 / τ_L), and R is the rotational diffusion coefficient. For a system with global and local rotational rates, the above equation is modified to account for the second motion in a manner similar to that used for equations 9.8 and 9.9 above.

Differential phase data plotted as a function of modulation frequency for a simple rotor show a smooth bell shaped curve having a peak magnitude and peak frequency determined by the rotational rate, fluorescence lifetime and limiting anisotropy (see Jameson and Hazlett, 1991 for a graphical description of these phenomena). As the motions become slower or the lifetime is reduced, the differential phase peak shifts to lower frequencies and decreases in amplitude.

For more complex systems, the appearance of multiple peaks or shoulders indicate multiple relaxation times. For the case where the local motion of the probe accounts for the majority of the anisotropy decay, then the phase data at high frequencies will predominate and thus to provide an accurate estimate of the rate and amplitude of these processes, very high modulation frequencies are required. A good example of how changes in local motion of the probe will affect the shape of the differential phase plots is given by Jameson et al., (1987) studying

the fluorescence anisotropy of Trp 184 in elongation factor Tu during its interactions with elongation factor Ts. Though not as visually descriptive as the differential phase data, the modulation ratio, Y, is equally sensitive to the sample rotational parameters. In this study, both types of data were collected and analysed simultaneously to increase the accuracy and precision of the recovered rotational parameters.

The kinetic mechanism of the GAP-activated GTPase of p21ras

KEITH J. M. MOORE[1], PETER N. LOWE[2] AND JOHN F. ECCLESTON[1]

[1]*National Institute for Medical Research, Mill Hill, London NW7 1AA, U.K.*
[2]*Wellcome Research Laboratories, Beckenham, Kent BR3 3BS, U.K.*

SUMMARY

Guanine nucleotides modified by acetylation of the ribose moiety with the small fluorophore *N*-methylanthranilic acid(mant) have been shown to bind to p21ras with similar equilibrium and kinetic rate constants as the parent nucleotides. Hydrolysis of p21.mantGTP to p21.mantGDP results in a 10% decrease in fluorescence intensity occurring at the same rate as the cleavage step. A similar process occurs with the non-hydrolysable analogue mantGMP.PNP, and this has led to the proposal that a conformational change of p21.mantGTP precedes and controls the rate of the cleavage step. The fluorescence change with p21.mantGMP.PNP is accelerated in the presence of the C-terminal catalytic domain of GAP, which is consistent with this mechanism. The same conformational change does not occur with oncogenic mutants of p21ras, Asp-12 and Val-12, but does occur with the weakly oncogenic Pro-12 mutant. Stopped flow measurements of the interaction of GAP with p21.mantGTP show an exponential decrease in fluorescence, the rate of which does not vary linearly with GAP concentration. These data imply a rapidly reversible formation of the p21.mantGTP complex with GAP followed by the isomerization of this complex. This is at least 10^5-fold faster than the same process in the absence of GAP.

1. INTRODUCTION

The products of the N-ras, H-ras, and K-ras genes, termed p21 proteins, are low molecular mass proteins (21 kDa) which bind GTP and GDP and have a low intrinsic GTPase activity. The three proteins are highly homologous, mainly differing in the C-terminal 20 amino acids where post-translational modification occurs, enabling them to become associated with a membrane. Single point mutations at certain sites in the proteins lead to oncogenic properties. As with other guanine nucleotide-binding proteins, they exist in a biologically active state when GTP is bound, and hydrolysis to the GDP bound form results in the formation of an inactive state. Dissociation of GDP from the protein is followed by the reformation of the active GTP-bound species. The relative concentrations of p21.GTP and p21.GDP in the cell are therefore governed by the relative rate constants of the hydrolysis of p21.GTP and of the dissociation of GDP from p21.GDP. With purified recombinant proteins, these are both very slow processes with rate constants of about $3 \times 10^{-4}\,s^{-1}$ at 37°C, giving half-times of about 40 min for both processes. However, other proteins have been identified which accelerate these processes and so can control the ratio of p21.GTP and p21.GDP in the cell. Two GTPase activating proteins (GAPs) have been isolated, p120-GAP and NF1-GAP, both of which accelerate the rate of conversion of p21.GTP to p21.GDP. The factors which accelerate the rate of release of GDP from p21.GDP, and hence the rate of conversion of p21.GDP to p21.GTP, are much less well defined, although a factor for the related smgp21 has been characterized (Takai 1992). The properties of p21ras, GAP, and nucleotide exchange factors summarized above have been reviewed by, amongst others, Barbacid (1987), Bourne *et al.* (1991), Grand & Owen (1991), Goody *et al.* (this symposium) and McCormick (this symposium).

To understand how the ratio of p21.GTP to p21.GDP is controlled in the cell, and how single point mutations cause this to be disrupted, we have investigated the kinetic mechanism of the p21ras GTPase activity. We have defined the important intermediates in the GTPase cycle, measured the rate constants of their interconversion, and identified a structural change occurring between p21.GTP and p21.GDP which may be related to its biological function. The main approach used is to design experiments in which the process of interest only occurs once on any given p21 molecule (i.e. single turnover conditions) combined with the use of well-defined complexes of p21 with guanine nucleotide. These methods have proven successful with other GTPase and ATPase mechanisms, such as the myosin ATPase (Trentham *et al.* 1974), the elongation factor Tu GTPase (Eccleston *et al.* 1985) and the mechanism of release of GDP from elongation factor Tu catalysed by elongation factor Ts (Eccleston 1984). They are complementary to the X-ray diffraction studies of complexes of p21 with guanine nucleotides reported by Goody *et al.* (this symposium). The advantage of